The When and How of Rapid Quenching At Intermediate-Redshift

by

David J. Setton

B.S. University of Arizona, 2017

M.S. University of Pittsburgh, 2019

Submitted to the Graduate Faculty of

the Dietrich School of Arts and Sciences in partial fulfillment

of the requirements for the degree of

Doctor of Philosophy

University of Pittsburgh

2023

UNIVERSITY OF PITTSBURGH

DIETRICH SCHOOL OF ARTS AND SCIENCES

This dissertation was presented

by

David J. Setton

It was defended on

July 17, 2023

and approved by

Rachel Bezanson, Department of Physics and Astronomy and PITT PACC, University of Pittsburgh

Jenny E. Greene, Department of Astrophysical Sciences, Princeton University

Jeffrey A. Newman, Department of Physics and Astronomy and PITT PACC, University of Pittsburgh

Evan Schneider, Department of Physics and Astronomy and PITT PACC, University of Pittsburgh

Ayres Freitas, Department of Physics and Astronomy and PITT PACC, University of Pittsburgh

The When and How of Rapid Quenching At Intermediate-Redshift

David J. Setton, PhD

University of Pittsburgh, 2023

One of the most fundamental observations that underpins the study of galaxy evolution is the bimodality between star forming and quiescent galaxies. In the local universe and beyond, the most massive galaxies in tend to be "red-and-dead." Despite the clear evidence for this "quenching" of star formation at early cosmic times, the physical mechanism that drives this transformation is still undetermined. Models invoke a wide range of prescriptions for feedback that vary wildly due to the lack of constraints from data. In this thesis, I provide such constraints by studying samples of young quiescent, or post-starburst, galaxies, with spectroscopy that allows for the precise measurement of their star formation histories.

First, I present work studying the spatially resolved spectroscopy of 6 of the bright post-starburst galaxies using Gemini/GMOS. I find that the majority of the galaxies studied exhibit flat gradients in $H_{\delta,A}$, indicating that their stellar populations are roughly uniform and young out to ~ 5 kpc. The second study in this work focuses on the structures of post-starburst galaxies as traced by rest-frame optical imaging. I find that post-starburst galaxies have compact sizes, in line with previous work, and that they show very little evolution in their size as a function of the time since quenching. Taken together, these two results paint a picture where post-starburst galaxies have compact star forming progenitors that shut off their star formation uniformly. In the final work of this thesis, I place constraints on the rate of quenching. Using deep spectroscopy from the Dark Energy Spectroscopic Instrument Survey Validation sample, I measure star formation histories for $\sim$ 17000 luminous red galaxies. I find a significant increase in the number density of post-starburst samples between $z = 0.4$ and $z = 0.8$. However, I find that true rapid quenchers–galaxies that formed $> 50\%$ of their stellar mass in the Gyr before quenching–are essentially absent at $z < 1$ and only were a significant part of the galaxy population at earlier cosmic times. This motivates the push of spectroscopic surveys to higher redshift, where complete surveys will have the chance to quantify the rate of rapid quenching when it is occurring.

Table of Contents

List of Tables

List of Figures

Preface

It is a common adage that scientific progress is built on the shoulders of giants, and that is certainly true in the grand buildup of the base of knowledge that underscores this thesis. But in my experience, the day-to-day power source to complete this work was the care and support of my family, friends, and colleagues, to whom I am in immense debt.

First and foremost, this work could not have been completed without the unending support of Rachel Bezanson. Your tireless enthusiasm, patience, and detailed advising has been above and beyond what I ever could have expected, and I am so fortunate to have you in my corner. I would not have gotten into graduate school without you, I would not have succeeded in graduate school without you, and I would not feel confident going into my postdoc without you. I have constantly felt empowered by our collaboration, and even at the most frustrating moments of proposal writing and re-writing and re-re-writing, you have made sure that the scientific process is fun and rewarding. I am proud to be your first graduate student and I will carry the lessons I have learned from you throughout for my entire career.

I am also grateful for the work of the many other mentors who guided me. For Jenny Greene, who treated me as a competent scientist from day one and who has always read my work with the utmost care; I am so thrilled that I have the opportunity to work with you and Andy next year at Princeton. For Justin Spilker, for whom no question is too basic and whose guidance in proposal writing has been essential to my success. For Wren Suess, who was the senior grad student I never had; thank you so much for letting me ride on the coattails of your thesis project to start carving my own scientific path. For Brett Andrews, who read all my papers, even the ones he wasn't on, and whose curiosity I will model forever. For Jeff Newman, whose door is never closed for technical questions. And last but not least, to Christopher Willmer and Gurtina Besla, who launched my research career and set me on the path I am on today.

I am thankful for the many other collaborators with whom I have had the pleasure of working. I am grateful for Andy, Mariska, Desika, Gourav, Sedona, Robert, Biprateep,

Jacqueline, Ekta, and Alan: science is fun with you, and I hope that we can continue working together in the future. For Maggie, Anika, and Erin, the (former and current) undergrads who I have had the pleasure of playing a role in advising: you have been a joy to work with and your enthusiasm has kept science fresh for me. And for all my astronomy cohort in Allen 300: thank you for the lively environment and for making coming to work a pleasure every day.

To all my friends in Pittsburgh, thank you for making these six years some of the best of my life and for keeping me sane outside of work. Alan, Rachel, Maria, Malcolm, Anna, Nick, Jared, Lorena, and Ava: you were the best physics cohort (and extended universe) I could have ever asked for, and I am so grateful our sub-group chat had the chance to thrive when we keyed in on ourselves as the people who wanted to go get a drink on Fridays. Neal, Heather: thank you for living with me and dealing with me through some of the silliest and stupidest periods of my life; I cherish our board game nights and the laughs we have. Dylan, Cody, Alex, and Nathan: thank you for seeing movies, going to concerts, grabbing drinks, and for being my friends in Pittsburgh who will never ask me about work unprompted. To the members of the Pittsburgh Movie Club, the Humongous Mellonheads, and Goodbye Gavrilo: thank you for letting me express my love of movies, sports, and music. To Mario's East End Saloon, Nico's Recovery Room, Two Frays Brewery, Soju, Senyai Thai House, Kelly's Bar and Lounge, Spirit, Gene's Place, Belvedere's Ultra Dive, the Squirrel Cage, the Squirrel Hill Sports Bar, PNC Park, Stage AE, Mr. Smalls Fun House, the Manor Theatre, AMC Waterfront 22, Row House Cinema, the Harris Theatre, Friendship Park, Frick Park, Flagstaff Hill, Mellon Park, the Allegheny Cemetery, and all the other third places I've occupied in this wonderful city: thank you for making my time here a pleasure. And to Pittsburgh Rapid Transit: thanks for all the free rides.

To all my friends from before this trip, thank you for sticking with me through it all. Phil, Rod, Jeff, Gus, and Parth: I earnestly think what we have in that group chat is special, and getting to feel sustained contact with you all through this process has made everything feel easier. Juanita, for making Philly my home away from home and for your endless love and care and talk of movies. Carter, Terra, Brenna, Caitlin, Corey, and Phil again: thank you for making every trip home to Phoenix feel so special and full of life. To the members

of U of A Degenerates, thank you for letting me be a petty tyrant running our league all these years and for the continuity in friendship we've had all these years; you can call me Doctor Commissioner now. And to Jonathan and Julian, thank you for being some of my oldest friends and for making me into the musician I am today. I love and cherish each and every one of you and I feel so blessed to have you in my life.

Finally, this work would not have been possible without the love and support of my entire family. Jackie and Eli, thank you for raising me to be curious about the world and for all the sacrifices you made to get me to this point. Jessica and Sophie, thank you for being the most supportive little sisters I ever could have asked for and for laughing with me through it all. To Bubbie Lola, Zaida Norm (z"l), my aunts, uncles, and cousins, and my entire extended family: thank you for shaping me into the person who I am today. And last but certainly not least, to Stephanie: your love and care and the laughter you bring to my life has lit up my heart since you entered my life. I am so thankful to you for everything you do for me and for all the care you have provided. Every adventure we have had has enriched my life and I can't wait to continue this journey with you. And of course, thank you for bringing Maru into my life; this thesis could not have been completed without the two braincells she brought to the table.

This thesis is dedicated to the memory of Michael Pawer (z"l). Your curiosity is sorely missed, and this pale blue dot is sadder without your laughter on it.

1.0 Introduction

At the time of the discovery that the Milky Way was but one of countless galaxies in a universe that is teeming with stars, the study of galaxy evolution was a game of classification. However, the fundamental insights of those classifications have persisted to the present day. Our understanding of the growth of galaxies from the big bang to present is studied through the lens of two fundamental properties that underpin the Astronomy 101 picture of galaxies: shape and color. While initial classification schemes focused on morphology alone [104], the nascent field of galaxy evolution quickly became aware of the intrinsic correlations between these two properties that demarcated a bimodal galaxy population, with spiral galaxies tending to be blue and elliptical galaxies tending to be red [54]. In many ways the story of the last 50 years of astronomy has been applying more sophisticated tools and methods of analysis to explain this fundamental correlation.

As galaxies are composed of stars, an understanding of stellar evolution underpins an understanding of the color bimodality in the galaxy population. The youngest, brightest, and bluest stars in a stellar population die the most quickly [106], so for a galaxy to remain blue it must continually be repopulating its young stellar population by converting dense gas into new stars. With this insight, the bimodality can be mapped from color to physical properties: blue galaxies are star forming by virtue of their young stellar populations, and red galaxies are quiescent due to their lack of such young stars. Thus, the Hubble tuning fork can be thought of as a sequence of evolution, where blue spiral galaxies evolve into red elliptical galaxies when their star formation turns off.

But what makes star formation turn off in these galaxies? And why does morphological transformation observationally appear to be so closely tied to the shutdown of star formation? In this thesis, I will contribute to solving this mystery by focusing on two key questions: *when* do galaxies shut off, and *how* does this transformation occur? I will do so by utilizing spectroscopic samples of quiescent galaxies in conjunction with excellent ancillary data to study the time immediately after the shutdown of star formation–when these young galaxies are "post-starburst"–to understand what physical process is driving their transformation.

1.1 When does quenching occur?

Before delving into the physical drivers of the quenching of massive galaxies, one must first identify the moment in cosmic time that quenching is occurring. The approach to answering such a question that is employed by observational astronomers is to study statistical samples of galaxies across cosmic time to connect the dots between present day populations and their progenitors. In this section, I will first describe the primary methodology that is used in the study of the history of star formation in galaxies: spectral energy distribution fitting. I will then describe the astronomical surveys that have been utilized to answer the question of quenching. Finally, I will summarize the state of the knowledge in the field and point to where my work will fill a gap in knowledge.

1.1.1 Measuring galaxy star formation histories

The spectral energy distribution (SED) of a galaxy is the sum of all the components of light that are emitting in a galaxy–coming from stars, gas, dust, active galactic nuclei, etc.–as a function of the wavelength. The shape and normalization of a galaxy's SED contains an immense amount of information about those sources of light. It follows then that one can infer information about the physical properties of a galaxy by iterating over the possible combinations of those sources of light to infer what combinations can produce the observed SED shape of the galaxy. This technique, known as SED fitting, was employed as far back as the 1970s with early stellar population models [77], became a staple in the archaeological study of star formation histories with measured spectroscopic indices by the early 2000s [113, 114, 205], and has evolved into an industry as samples of galaxies with broadband SEDs have exploded with the advent of all-sky surveys.

There are now countless software packages that employ varying prescriptions for the SED fitting of galaxies (for an excellent review of their comparative capabilities, see [149]), but the general method remains the same across codes [41]: a galaxy is the sum of some set of stellar populations that formed between the start of the universe and the time of the galaxy's observation. All of these stellar populations themselves evolve with time as massive

stars move off the main sequence and die off. The light from these stellar populations is attenuated by dust, and the stellar populations may have some variable or fixed assumptions about their metallicities. There may be some additional contributions from emission from gas (often tied to the current star formation rate of the galaxy), active galactic nuclei (both in the rest optical and the infrared), and warm dust, depending on the sophistication of the models, the wavelength range of the data being fit, and the type of galaxy that is being fit for. Finally, the source must be placed at multiple possible redshifts in the absence of spectroscopic data. In the end, one can marginalize over all possible solutions that match the observed SED shape to constrain basic parameters about the galaxy such as the mean stellar age, the stellar mass, and the current star formation rate.

However, the application of this method to photometric data is not without limitations. Because all information about the stellar population is coming from the shape of the SED, these methods are extremely prone to degenerate combinations of parameters that can produce similar shapes. The first and most obvious issue is that of photometric redshift uncertainties. Because broadband photometry is by definition lacking in lines that anchor the redshift of an object, the shape of the spectral energy distribution is often compatible with a range of redshift solutions, adding significant uncertainty to the stellar mass. Thankfully, massive galaxies, which tend to have strong Balmer/4000 Å breaks, are significantly less susceptible to photometric redshift failures due to the presence of a strong continuum feature that reduces this uncertainty considerably. Far more damning for the study of massive, red galaxies is the age-dust degeneracy, which results from the fact that dusty star forming galaxies and old quiescent populations share extremely similar rest-optical SED shapes [166, 151]. This degeneracy can be broken with the addition of rest-frame near infrared (NIR) data, but it is often the case at high-redshift that photometry at the long wavelengths that map to the rest-frame NIR is hard to come by, and thus, galaxy ages in the largest samples can be highly uncertain.

An even more robust method of breaking these degeneracies is the addition of spectroscopic data to fits. Broadband fluxes measure the average flux density in large ($\Delta\lambda \sim 2000$Å) wavelength ranges, and as such they essentially completely insensitive to the individual spectral features (in both emission and absorption) that contain valuable information about the

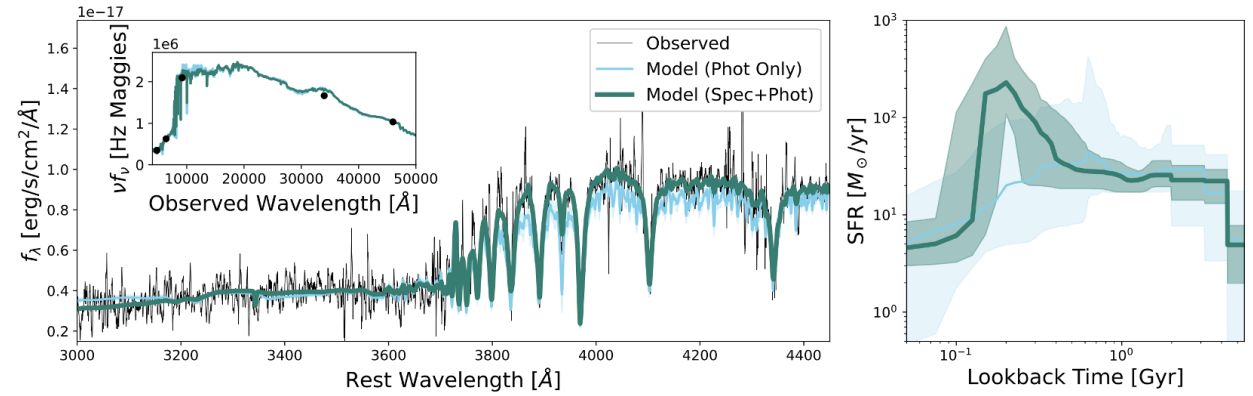

Figure 1: SED fits using `Prospector` [110, 125, 109] to the photometry only (blue) and photometry+spectrum (green) of a young quiescent galaxy from the DESI survey [175]. The derived star formation histories with 68% confidence intervals are shown in the right panel. In a perfect world, broadband photometry from the Legacy Survey [60] alone can confirm the quiescence of this system, but only spectroscopy can precisely date when star formation shut off.

current and past star formation in a galaxy. Take, for example, the galaxy presented in Figure 1. In the work presented in Chapter 4, I fit the combined photometry and spectroscopy of this galaxy from the DESI survey with `Prospector`, a state-of-the-art SED fitting code that implements non-parametric star formation histories in a fully Bayesian manner to measure galaxy properties and their associated covariant uncertainties [110, 125, 109], using a flexible star formation history optimized for young quiescent galaxies [196]. I found that it is consistent with having quenched $\sim$ 100 Myr in the past (see the green star formation history). However, even in a perfect world where the redshift was determined (removing any uncertainty about the location of key SED features), a fit of this same star formation history to the photometry alone yields a much more uncertain star formation history (blue), where it is clear that the galaxy is quiescent and fairly young, but significantly less can be said about precisely when the quenching occurred. In this galaxy in particular, the constraints on the precise time of quenching come from the relative strength of the Balmer absorption

features, in addition to the lack of emission line infill of those features, and the asymmetric Ca H+K doublet just blueward of 4000 Å. The addition of spectroscopy to SED fits significantly improves the fidelity of star formation histories, but the downside is that obtaining spectra for large samples of galaxies is significantly more difficult than obtaining broadband photometry.

In conclusion, SED fitting of broadband photometry is an excellent tool for unlocking the star formation histories of galaxies, and the addition of spectroscopy to these fits improves these fits considerably. I will now summarize the insights gleaned from more local and higher redshift surveys of galaxy evolution as to when quenching occurred.

1.1.2 Galaxy Surveys

Unlike many other physicists, astronomers are not able to conduct controlled experiments to understand the root cause of a physical process (though theorists certainly try their best with simulations). Instead, observers are given the view of the night sky from the earth as a dataset and left to mine it for insights, leveraging the finite speed of light to look back in time at more distant galaxies to trace the fossil record of the universe. However, as telescope resources are not infinite, choices obviously have to be made in the selection of which galaxies are observed with which instruments, with significant trade offs between survey area, depth, and the competing needs of galaxy evolution scientists and the other astronomers with whom they share these resources (most often, cosmologists). In this section, I will give a brief overview of some of the most important astronomical surveys as they relate to quenching in both the local and more distant universe.

1.1.2.1 Low-redshift

Even before the discovery that galaxies were indeed galaxies, works such as the New General Catalog [71] identified and compiled bright sources in the local volume. Much of the early science on the bimodality came from dedicated follow-up of such sources. Spectroscopically confirmed redshifts in conjunction with broadband colors allowed for the construction of early color-magnitude diagrams that illustrated the correlation between color and mor-

phology in nearby galaxies [54]. However, it was not until the advent of "redshift surveys" with the joint goal of understanding cosmology (as at the time, settled questions such as the isotropic nature of the universe were still up to debate) and galaxy evolution that the diversity of the galaxy population was truly captured. The advent of multi-slit spectroscopy allowed for significantly more galaxies to be observed in a single observing run, and early works such as [67] utilized this technique to observe spectra in clusters at then-distant redshifts of ~ 0.5. Dressler and Gunn observed a small but non-negligible number of galaxies with strong Balmer absorption that was extremely rare in existing samples in the more-local universe. They correctly concluded that such galaxies must represent systems that formed a significant amount of stars in a recent burst and then shut off, as such strong Balmer absorption can only come from an A type stellar population (a population with a characteristic age of ∼100 Myr-1 Gyr). While many of these galaxies also showed signatures of an older K population (indicating that this burst may have occurred over an already older stellar population; such galaxies are now commonly referred to as "E+A", "K+A", or "post-starburst" to indicate an elliptical/old stellar population in addition to a younger A type population), their presence indicated that at earlier epochs of the universe, the quenching of bursts of star formation was still ongoing–a seminal observation in the field of quenching. Follow up on "Butcher-Oemler" clusters with the vastly improved resolution and sensitivity of the Hubble Space Telescope suggested that post-starburst galaxies, identified by their strong Balmer line equivalent widths, are associated with mergers in cluster environments [46, 45].

More progress in this field came with the advent of the Las Campanas Redshift Survey (LCRS), which marked a huge leap from the detailed study of small samples (100s-1000s of galaxies) to much more complete samples of 10s of thousands of galaxies in the nearby universe ($z \lesssim 0.2$) [177]. Illustrating the rarity of these recently quenched systems locally, [246] identified only 21 galaxies with deep Balmer absorption and limited [OII] emission in the LCRS sample, and perhaps surprisingly found that $\sim 75\%$ of these galaxies do not live in clusters but are instead in the field. This study also established a clear link between mergers and the "E+A" phase due to the detection of many tidal features, but the small number of detections left a very open question as to how common this phase of evolution was, given that the vast majority of red galaxies in LCRS do not exhibit significant Balmer absorption.

Studies of the star formation histories of quiescent systems yielded similar conclusions that the bulk of the star formation in massive quiescent galaxies occurred long before the present day [205, 206].

The true sea change moment for the study of post-starburst galaxies, and galaxy evolution generally, came with the advent of the Sloan Digital Sky Survey (SDSS) [243]. Using 5 band *ugriz* imaging in conjunction with spectroscopy of $> 10^6$ sources in the initial data release, SDSS revolutionized the census of the universe both by observing unprecedented wealth of data and by democratizing the science via the public distribution of data. Early SDSS papers utilized the combination of the D_n4000 ($\propto$ the light-weighted age of a stellar population) $H\delta_A$ ($\propto$ the dominance of an A type stellar population, though this measurement is notably not monotonic with age) indices to calculate stellar masses, ages, and rudimentary star formation histories at an industrial scale [113, 114]. These seminal works highlighted the true extent of the bimodality in the local universe, and strongly suggested that the most-massive low-redshift galaxies are quiescent and have been quiescent for a very long time. Crucially to the study of post-starburst galaxies, these studies accounted for the presence of recent bursts in these galaxies and found that at the massive end, bursts are essentially negligible, and locally post-starburst galaxies are largely a low mass phenomenon.

This work was further fleshed at low redshift by combining the stellar masses and colors of galaxies with morphological classifications from Galaxy Zoo, a large program that leveraged the general public's interest in astronomy to visually classify huge amounts of SDSS data [131, 130]. [168] approached the question of the galaxy bimodality at $z < 0.05$ by studying in detail the so called "green valley," the region in color space where the high mass quiescent and lower-mass star forming galaxies are sparsely populated in color-magnitude space. They found that in the low-redshift universe, the green valley is *not* populated by proto-quiescent ellipticals that are transitioning into quiescence rapidly; instead, it is largely fading stellar disks that are slowly transitioning through this boundary in color space. The rarity of spheroidal galaxies in the green valley indicates that galaxies that experience morphological transformation cross quickly, and that the rapid quenching process that produces the most massive quiescent galaxies has long since stopped happening to significant portions of the galaxy population.

The work at low-redshift suggests a fairly definitive answer to the question posed in the title of this section in the form of a negative: the quenching of massive galaxies is not occurring commonly in the local universe. The formation of the red sequence occurred at far earlier cosmic times, and as such, any work seeking to study the quenching process at this epoch will necessarily be archaeological, with little chance of catching quenching in-the-act in large statistical samples.

1.1.2.2 Intermediate-redshift

The definition of intermediate-redshift has always been a moving target based on the depth and reach of the world's most powerful telescopes. Even over the course of this thesis work, the definition has been creeping to higher and higher redshift, especially with the advent of JWST. Here, I will arbitrarily define it to mean galaxies at $0.2 \lesssim z \lesssim 2$, where a significant amount of work has been done in recent years to study the incidence and properties of galaxies that are undergoing the rapid quenching process that should result in quiescent elliptical descendants [168].

The large spectroscopic coverage of the SDSS has been a goldmine for identifying statistical samples of post-starburst galaxies even outside of the more local samples where targeting is complete. While most of this work has focused on cataloging the source properties of such samples in the way of structures [39, 162, 174, 176], molecular gas content [89, 90, 88, 190, 20], and star formation histories [90, 191] (including work in the SQuIGG$\vec{L}$E sample in Chapter 2 and 3 in this thesis), work that took on the difficult task of quantifying the color-completeness of SDSS samples like CMASS found that out to $z \sim 0.8$, rapidly quenching post-starburst galaxies account for a very small amount of the decline in star formation in the universe [156]. Similar conclusions have been reached using other more complete spectroscopic surveys such as IMACS and GAMA; while the number density of post-starburst galaxies is rising with lookback time, they still represent a fairly small portion of the quiescent population [154, 163]. This too is consistent with the archaeological study of intermediate-z quiescent galaxies with SED fitting, which reveals that quiescent galaxies at this epoch have formation redshifts of 2-3 [92, 150, 91, 36, 35, 76, 63, 221, 119].

These conclusions have been similarly supported by photometric studies that have leveraged the insights of spectroscopic studies to make photometric selections that are robust on samples that are complete to higher-redshift. The first attempt at this using the NEWFIRM Medium Band Survey (NMBS) was able to quantify the growth in the population of young quiescent galaxies out to $z \sim 2$, and found that the number density increases dramatically at $z > 1$ such that the majority of the growth in the quiescent sequence could be driven by this channel, though photometric fitting left significant uncertainty on how rapid the quenching in this young sample was [226]. Further studies have used more granular photometric definitions that separate out young and old quiescent galaxies to quantify the rate of rapid quenching, and a consensus is growing that rapid quenching is significantly more common at higher redshift [230, 19, 231, 152], though there is some debate from star formation history as to whether there is a real binary between rapid and slower channels [199]. In either case, galaxies are quenching at $z \sim 2$ and it is clear from studies of the mass function and star formation rate density that the star formation rate of the universe declined steeply after this point [145, 133, 64, 126, 127, 220], but large representative spectroscopic samples of these galaxies in transition have yet to be observed. Whatever the mechanism is that is driving rapid quenching in this epoch is the mechanism that is responsible for the formation of the majority of the quiescent galaxies in the universe.

1.1.2.3 High-redshift

While the consensus is that the decline in the star formation rate of the universe and the quenching of massive galaxies occurred after $z \sim 2$, there is a growing body of spectroscopic and robust photometric observations of massive quiescent systems as far back as $z = 3 - 4$ [189, 49, 94, 85, 141, 212, 58, 112, 34, 37]. For these galaxies to have formed $\gtrsim 10^{11} M_{\odot}$ in the ~ 2 Gyr after the big bang *and* for their star formation to have essentially completely shut off, their quenching by definition must have been extremely rapid. Similar to how it is unclear whether the low-redshift galaxies that have quenched rapidly are clear analogues to the representative quiescent galaxies quenching at $z \sim 2$, it is also unclear whether these galaxies are higher redshift analogues to those same galaxies. As they represent some of

the most massive galaxies in the universe at their epoch, they will be intensely studied in the coming years as the infrared instrumentation on JWST unlocks their full SEDs and structures.

1.1.3 We know when, but how quickly remains an open question

The growing body of evidence has indicated strongly that the star formation history of the universe peaks at cosmic noon, $z \sim 2$, and declines thereafter. Studies of the star formation histories of galaxies have given strong evidence toward a rapid quenching channel, but questions of exactly how common this channel is remain open due the fundamental limitations of photometric data to address timescales. In Chapter 4 of this thesis, I present work that directly contributes to addressing this dearth of data by using the early Dark Energy Spectroscopic Instrument (DESI) survey to constrain the incidence of rapidly quenching galaxies with robustly constrained star formation histories out to $z \sim 1.3$ with the largest spectroscopic sample of post-starburst galaxies to date. While the DESI sample still falls short of comprehensively cataloging the quenching at its peak epoch, the work showcases the methodology that will, in the next generation of surveys, make immense strides in completing our census of the decline of star formation in the universe.

1.2 How does quenching occur?

In the previous section, I described the observational evidence for quenching and the consensus view that the star formation history of the universe peaked at $z = 2$ and declined via the rapid quenching of galaxies after that. However, the focus there was entirely on the *when* of quenching. Here, I turn my focus to the *how*, with an emphasis of the physical observables that can constrain theories. The molecular gas surface density and star formation rate surface density are strongly correlated in galaxies (as formulated in the now-ubiquitous Kennicutt-Schmidt law [171, 117, 164, 201]). As such, it is clear that the mechanism that is quenching galaxies must do something to either remove gas, halt the accretion of additional

gas, or stop existing gas reservoirs from collapsing to form new stars [136]. Many of these mechanisms are distinguishable via the study of the molecular gas content itself in these galaxies; for example, the absence of molecular gas is strong evidence for a channel that results in the removal of gas. However, in the example of gas removal, there are a plethora physical processes that have been proposed to remove gas, and the absence of cold gas detections would not alone be able to distinguish between them.

Thankfully, direct measurements of the molecular gas in recently quenched systems are not the only way that observers can provide evidence in favor or contradicting theoretical predictions of the rapid quenching mechanism. Instead, a more holistic set of observations that ties together the star formation histories, AGN signatures, structures, and molecular gas contents in recently quenched galaxies can paint a more clear picture of the conditions under which the galaxy stopped forming new stars. In this section, I will outline some of these key observations of recently quenched systems across cosmic time and the implications for the physical drivers of quenching.

1.2.1 The role of gas and AGN in maintaining massive galaxy quiescence

Observations in both in the local universe [244, 51] and at higher-redshift [184, 234, 228] show that the majority of massive quiescent galaxies are gas poor relative to their star forming counterparts, with gas fractions ($M_{\rm H_2}/M_\star$) at or below $\sim 1\%$ in the local universe and generally constrained to below $\sim 5\%$ near cosmic noon. As such, any model that accounts for the quenching of massive galaxies must both use up or remove the majority of the gas in a galaxy *and* halt the future accretion of gas. In simulations, these observations can essentially only be reproduced via the inclusion of feedback from active galactic nuclei [188, 61, 118, 47, 102], which can serve to both remove the gas in galaxies, and perhaps more importantly, to significantly reduce the inflow of gas from the hot halo via the maintenance mode of feedback driven by hot gas accretion.

There is significant indirect evidence for the activity maintenance mode in massive galaxies. The bulge mass of a galaxy is strongly correlated with the mass of the supermassive black hole [82], which should in turn be proportional to the magnitude of the radio feedback

in galaxies. In turn, the bulge mass of a galaxy is the single best predictor of quiescence in observational samples of galaxies [24]. Together, these correlations indicate that the co-evolution of central black holes and galaxies themselves drives the transformation to quiescence, at least in halting the accretion of additional gas after the interstellar medium of the galaxy is used up or removed.

However, the story of the removal of the interstellar medium, and more broadly the connection between AGN and rapid quenching, is significantly less clear than the maintenance of quiescence. CO observations of post-starburst galaxies in the local universe [89, 88] and intermediate-z [190, 18, 20] have shown that galaxies can maintain significant (10-20%) molecular gas fractions for $\sim$ 100 Myr after quenching; after that, galaxies tend to be undetected with upper limits that constrain them to typical quiescent molecular gas fractions. While there is significant evidence for the increased presence of AGN in the youngest post-starburst systems [97, 88], they tend to be weak and this correlation could simply be due to the presence of gas that is fueling rather than the AGN itself impacting the gas. Furthermore, direct observations of outflowing gas driven by AGN have yet to be seen in post-starburst systems, so even if AGN can explain the maintenance of feedback, their presence does not include smoking gun evidence of gas removal. Finally, the AGN themselves still do not provide any evidence for why a burst of star formation seems to precede the rapid quenching of galaxies.

1.2.2 Clues from structural measurements

The growing body of evidence for the quenching process in massive galaxies appears to be that galaxies undergo a process of rapid truncation in their star formation rate that results in a quiescent galaxy with a early-type morphology, a distinct physical process from the slower quenching mode that populates the green valley with red disks [168, 230, 239, 19, 235]. The question remains however as to what the cause of this rapid truncation is. It is here that detailed structural studies of the descendants of rapid quenching, post-starburst galaxies, can provide evidence as to the cause of this truncation.

From this body of evidence, a clear consensus is emerging as well; galaxies that quench

rapidly at intermediate-high redshift have compact, early-type morphologies in the period immediately after quenching as borne out in their compact sizes and high Sérsic indices [226, 241, 9, 135, 239, 194, 238, 195]. This implies that the galaxies experienced compact and rapid star formation in the period immediately prior to quenching, and that either morphological transformation accompanies the quenching process via a compaction event that funnels gas inward, inducing a burst of star formation and triggering an AGN [101, 55, 250, 200], or that the galaxies were already compact prior to reaching the necessary threshold in density for quiescence [217]. This points to submillimeter galaxies [209, 210] or compact star forming galaxies [15, 14] as a likely progenitor population to post-starburst galaxies, as they are compact and have intense star formation rates that could, if rapidly quenched, result in galaxies that look very similar to post-starburst galaxies

One potential pathway that could lead to a compaction type event is gas rich major mergers, which can effectively funnel gas toward the center of a galaxy and induce centralized star formation [17, 101, 222]. There is significant evidence that post-starburst galaxies at low- and intermediate-redshift are associated with mergers due to their over-abundance of tidal features relative to field quiescent and star forming galaxies [157, 167, 219, 75, 233], but at higher redshift the picture remains less clear due to the resolution and depth limits of existing surveys of young, massive quiescent galaxies; there are some predictions that violent disk instabilities or other secular processes may dominate at these epochs [222, 250].

Spatially resolved studies of galaxies have the ability to distinguish between different pathways. At low-z, IFU surveys like SDSS MaNGA [29] have enabled the study of local post-starburst systems that exhibit a variety of radial structures [162, 39], but outside the local universe resolved studies of young quiescent systems have been sparse due to the observational difficulty of obtaining resolved spectroscopy. One-dimensional slit experiments have shown some evidence of positive age gradients, pointing to a central burst quenching mechanism [59], while HST/GRISM observations have been more varied but have shown some evidence for more flat age gradients [107, 5, 6], potentially indicating that rapid quenching is a more galaxy wide event. However, dust gradients complicate all these interpretations significantly, as the flat color gradients observed in photometric studies can also point to compaction in the case where dust is obscuring the central region of the galaxy where a

burst is occurring [194, 195]. There is significant room for new discoveries in this space by studying spectroscopic samples of young quiescent galaxies with ground based observatories at intermediate-z, and it is likely that the advent of JWST will provide ample opportunities to extend this work to high redshift to directly probe the spatially varying stellar populations in young quiescent galaxies.

1.3 Thesis outline

In this thesis, I will utilize two spectroscopic samples of young quiescent galaxies to address gaps in the knowledge of the how and why of quenching. The first of these is the SQuIGG$\vec{L}$E sample, which was selected from the Sloan Digital Sky Survey at $z > 0.5$ using a rest frame UBV color cut that is optimized for the selection of galaxies with stellar populations dominated by A-type stars [123, 191]. The pure selection of a population from $z = 0.5 - 0.9$ provides an excellent laboratory to study quenching, and in this redshift range it is one of the largest samples of recently quenched galaxies with robust measured star formation histories. Our team has been active in acquiring ancillary data to study the molecular gas content [190, 20], structures [105], merger signatures [219, 187], and AGN [97] in this post-starburst sample.

In Chapter 2 of this thesis, I conduct a follow-up of the pilot study conducted by [105], who observed a flat $H_{\delta,A}$ gradient in a single $z \sim 0.7$ massive post-starburst galaxy using spatially resolved Gemini/GMOS spectroscopy, indicating that the galaxy quenched on ~ 5 kpc spatial scales simultaneously. Using additional follow-up GMOS spectroscopy of five additional galaxies, I perform additional analysis constraining the rotational motion and age gradients in a larger sample to test predictions of models of quenching described in Section 1.2.

The SQuIGG$\vec{L}$E sample was selected from the SDSS with spectroscopy that is sufficiently deep to perform robust star formation history fitting [191]. However, the imaging from SDSS is not up to the task of measuring structures at intermediate-z due to the lack of depth and resolution. In Chapter 3, I analyze a subsample of SQuIGG$\vec{L}$E that overlaps with the

Hyper-Suprime Cam imaging survey [3], utilizing the increased depth and resolution of that imaging to study the structures of this unique post-starburst sample.

SQuIGG$\vec{L}$E was largely selected from the highest-redshift end of the SDSS BOSS sample where targeting is very incomplete, limiting the ability to constrain number densities [53]. However, the in-progress DESI Luminous Red Galaxy (LRG) survey is mass-complete to significantly higher redshift than SDSS [248], and as such, it provides novel samples to study the incidence of rapid quenching. In Chapter 4, I use early, deep spectroscopy from the DESI LRG Survey Validation sample to fit star formation histories to $\sim$ 20000 massive quiescent galaxies, constraining the evolving number density of recently quenched galaxies at $z = 0.4 - 1.3$ [249, 248].

Finally, in Chapter 5, I provide a summary of my work and my thoughts on the path forward toward a better understanding of the when and how of rapid quenching as novel surveys begin to unlock the spectroscopy of complete samples near cosmic noon.

2.0 SQuIGG$\vec{L}$E Survey: Massive z$\sim$0.6 Post-Starburst Galaxies Exhibit Flat Age Gradients

2.1 Introduction

Modern astronomical surveys have confirmed that the population of galaxies is bimodal, dividing fairly neatly into star-forming and quiescent populations. This bimodality is present in galaxy colors [23, 108], sizes and structures [178, 214], and star formation rates [148], although some studies suggest that the quiescent galaxies represent a long tail in star-formation rates as opposed to a distinct population and that the existence of a "green valley" may be the result of optical sample selection [72, 50]. Nevertheless, at some point, all quiescent galaxies must have been star-forming; therefore, they are the descendants of a past star forming population that has turned off its star formation, or quenched. Whether the star forming progenitors of today's elliptical galaxies resembled their counterparts today remains to be seen [202]. Despite this uncertainty, the existence of massive quiescent galaxies as early as $z \sim 4$ [189, 49, 204, 85, 141] implies that many galaxies transition from star-forming to quiescent via a rapid channel that shuts off star formation quickly and efficiently.

In order to empirically understand this rapid channel of quenching, one can study galaxies which have recently ended an intense episode of star formation. These galaxies, often called post-starburst (PSB) galaxies, can be identified by their spectral energy distributions (SEDs) which exhibit spectral shapes and features characteristic of A stars, indicating that star formation shut down in the last $\sim$ 1 Gyr [67, 245]. Post-starburst galaxies can be selected by their strong Balmer absorption features and low star-formation rates [89]. While some post-starbursts appear to be galaxies in transition from star-forming to quiescent for the first time [7], others may be older "K+A" quiescent galaxies with composite SEDs that include light from K-giants along with A stars formed in a frosting of recent star formation [90].

Many physical models have been proposed for shutting off star formation and the relative efficiency of different physical mechanisms can vary throughout a galaxy. Therefore, the distribution of stellar ages in a galaxy, which themselves hold a record of the star formation

history, can be used to distinguish among models. For example, mergers can drive gas to the center of a galaxy, triggering a strong burst of star-formation, after which the galaxy quenches [101, 182, 222]. This quenching pathway would produce a positive age gradient, where the stellar population at the center of the galaxy is younger than the population on the outskirts. In contrast, simulations of quenching via wet compaction, where gas migrates inward in a way which compacts a galaxy, suggest that galaxies may experience extended star formation outside their core after the central gas is depleted, resulting in negative radial age gradients [198, 250].

Spatially resolved studies of the stellar populations of post-starburst galaxies at low-redshift have found a range of stellar age profiles traced by spectral indicators like $H\delta_A$ and D_n4000 [240, 160, 39], and local starburst galaxies appear to be experiencing centrally concentrated bursts [74]. However, these galaxies may not be representative of the evolutionary path that quenches galaxies for the first time. While low-mass local post-starburst galaxies can be extremely burst-dominated, at higher mass where the aforementioned bimodalities are the most extreme, post-starbursts are predominantly "K+A" post-starbursts in which a small burst has occurred in a quiescent galaxy that formed at high redshift [99, 90]. This indicates that while massive post-starbursts do exist in the local universe, they do not tend to be galaxies that are quenching their primary epoch of star formation, which is unsurprising given that local massive galaxies are almost exclusively old [140]. Furthermore, post-starbursts constitute a negligible part of the $z < 1$ luminous galaxy population [156] and while massive post-starbursts exist at intermediate redshift ($0.5 < z < 1$), it is not until $z = 2$ that they start to represent a significant fraction of the population of massive, quenched galaxies [226, 230]. Thus, in order to understand the galaxies which are quenching their primary epoch of star formation, we must look to earlier cosmic time.

While $z = 2$ quenched galaxies are still beyond the reach of spatially resolved spectroscopic studies outside of extreme lensed systems [107, 5], intermediate-redshift post-starbursts are more accessible. Post-starburst galaxies have been studied in the Large Extra Galactic Astrophysics Census (LEGA-C) survey, which consists of deep (∼20 hours/galaxy) spectra of galaxies at $z \sim 0.8$ in the COSMOS field [215]. These intermediate mass ($10^{10}\ M_\odot < M_\star < 10^{11}\ M_\odot$) post-starbursts have positive age gradients [59] and com-

pact sizes [239, 238] consistent with formation via a recent central starburst. However, these galaxies, like their counterparts at low redshift, are observed following a frosting of recent star formation; the strong, but not extreme, $H\delta_A$ in their sample indicates that K-giant stars are contributing significantly to the optical light of these galaxies. LEGA-C's pencil beam survey design does not allow it to find the rare but crucial A-star dominated post-starbursts that are in the stage of rapid transition from star forming to quiescent. By leveraging the wide-area of the Sloan Digital Sky Survey (SDSS), one can identify rare galaxies at intermediate redshift that have recently shut off their primary epoch of star formation. In a pilot program, [105] found a flat age gradient in a single z=0.747 galaxy, indicating that the most extreme post-starbursts may quench differently than their less extreme "K+A" counterparts.

In this work, we build on that study of J0912+1523 and present five additional IFU observations of massive ($M_\star \geq 10^{11} M_\odot$), burst-dominated post-starburst galaxies at z $\sim$ 0.6. In Section 2.2, we describe the parent SQuIGG$\vec{L}$E sample, as well as our spectroscopic analysis of the follow-up GMOS observations presented in this work. In Section 2.3, we discuss the spatially resolved stellar populations of the sample. Finally, in Section 2.4, we highlight the implications of our study on the quenching of massive galaxies in this epoch. Throughout this paper we assume a concordance ΛCDM cosmology with $\Omega_\Lambda = 0.7$, $\Omega_m = 0.3$ and $H_0 = 70$ km s^{-1} Mpc^{-1}, and quote AB magnitudes.

2.2 Data

2.2.1 The SQuIGG$\vec{L}$E Sample

For this study, we target a subsample of galaxies from the SQuIGG$\vec{L}$E (Studying Quenching in Intermediate-z Galaxies: Gas, Angu$\vec{L}$ar Momentum, and Evolution) Survey (K. Suess et. al in preparation). SQuIGG$\vec{L}$E is designed to identify post-starburst galaxies that have recently quenched their primary epoch of star formation. The survey identifies all galaxies at $z > 0.5$ with integrated signal-to-noise of 6 in synthetic rest-frame U, B, and V filters from spectroscopic data in SDSS DR14 [1]. We use the rest-frame color cuts

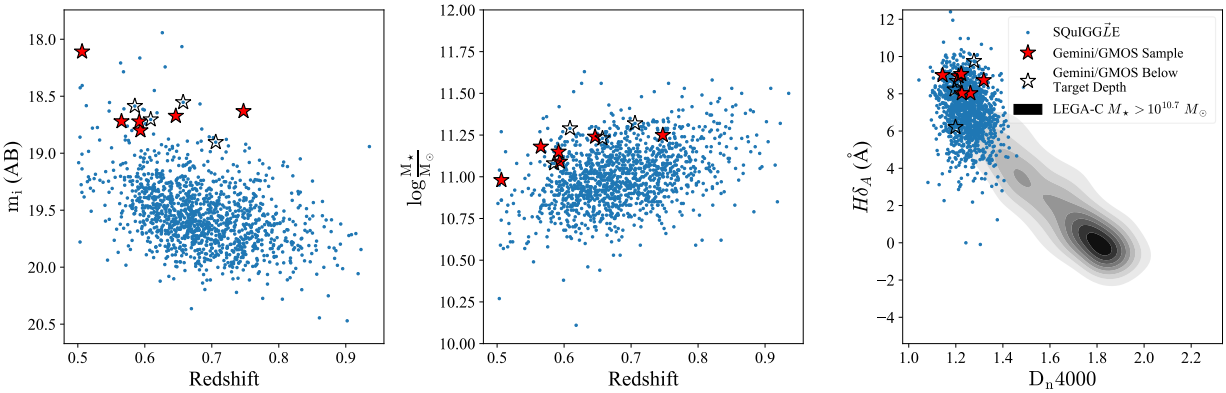

Figure 2: SDSS observed i-band magnitude versus redshift (left), stellar mass versus redshift (center), and $H\delta_A$ versus D_n4000 (right) for the entire SQuIGG$\vec{L}$E sample. In each panel, the Gemini/GMOS targets are shown as stars, where filled stars are those that are included in this sample. The Gemini/GMOS targets are among the brightest galaxies in the parent sample by selection. In the right panel, the distribution of similarly massive ($M_\star > 10^{10.7}\ M_\odot$) galaxies at $0.6 < z < 0.8$ from the LEGA-C survey are indicated by the grey shaded region. The SQuIGG$\vec{L}$E galaxies are all significantly offset in $H\delta_A$ versus D_n4000 from the LEGA-C quiescent galaxies at this redshift. The Gemini/GMOS targets span the SQuIGG$\vec{L}$E range of D_n4000 and are higher on average in $H\delta_A$.

Table 1: Properties of the GMOS observations

ID	Name	RA	Dec	z	Stellar Mass	i	GMOS Program	Integration[1] Time	Image[2] Quality
		(degrees)	(degrees)		($\log\frac{M_\star}{M_\odot}$)	(AB Mag)		(s)	
SDSS J110932.14-004003.8	J1109-0040	167.384	-0.6678	0.593	11.09	18.8	GN-2019A-Q-234	9720	20
SDSS J023359.33+005238.4	J0233+0052	38.4972	0.8774	0.592	11.15	18.72	GN-2017B-Q-37	7560 (6480)	20
SDSS J091242.76+152305.1	J0912+1523	138.1782	15.3848	0.747	11.25	18.63	GN-2016A-FT-6	9802	20
SDSS J083547.08+312144.5	J0835+3121	128.9462	31.3624	0.506	10.98	18.11	GN-2017B-Q-37	6300	70
SDSS J075344.17+240336.1	J0753+2403	118.4341	24.0601	0.565	11.18	18.72	GN-2017B-Q-37	8640 (5400)	70
SDSS J144845.91+101010.5	J1448+1010	222.1913	10.1696	0.646	11.24	18.67	GS-2018A-FT-112	11880 (8640)	70

[1]Integration time that was considered useful are shown in parentheses if they differ from the total integration time. Useful frames of data are those which do not have visible issues after scattered light subtraction of significant noise spikes in the $H\delta_A$ bandpass.

[2] The Image Quality quoted is the worst case conditions under which the majority of frames were observed. IQ20 corresponds to FWHM$\leq$0.5" seeing and IQ70 corresponds to FWHM$\leq$0.75" seeing at zenith.

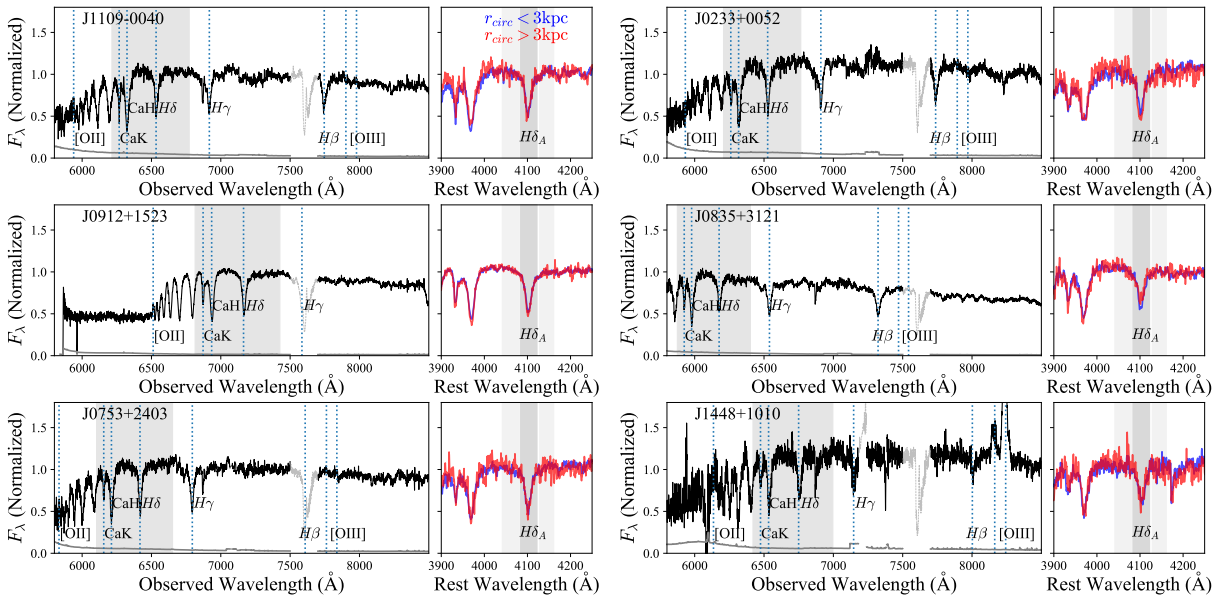

Figure 3: The Gemini/GMOS spectra integrated within a 2" circular aperture for each target are shown on the left. The grey line is the error on the flux and relevant lines are labeled. The spectra are plotted as transparent where they are masked due to strong telluric features. The luminosity-weighted inner (r_{circ} <3 kpc, blue) and outer (r_{circ} >3 kpc, red) spectra are shown in the right panel, highlighting the Lick $H\delta_A$ bandpass (dark gray) and continuum (light gray). Absorption features are remarkably uniform in the inner and outer spectra, with strong Balmer absorption throughout. All spectra are normalized to the flux at 4000 Å in the rest-frame.

$(U - B > 0.975; -0.25 < B - V < 0.45)$ in [122] to identify post-starburst galaxies with strong Balmer breaks and blue colors redward of the break, thereby selecting A-star dominated spectral energy distributions (SEDs). This selection identifies 1318 unique galaxies with $0.5 < z < 0.94$ and $17.94 < i < 20.47$. To characterize the stellar populations and measure stellar masses, we perform stellar population synthesis modeling of the SDSS spectra and *ugriz* photometry using `FAST++`[1], an implementation of the popular `FAST` program [123]. We assume a delayed exponential star formation history, BC03 stellar population libraries [28], a [38] initial mass function, and a [30] dust law. The galaxy masses span $10^{10.11} M_\odot < M_\star < 10^{11.63} M_\odot$ with mean $M_\star = 10^{11.0} M_\odot$. Although SQuIGG$\vec{L}$E galaxies are not explicitly selected based on their $H\delta_A$ absorption, the sample exclusively exhibits strong Balmer absorption consistent with the common post-starburst selection: 98% of the sample meets a $H\delta_A > 4$ Å criterion sometimes used to select post-starburst galaxies [89, 239]. The extremely strong Balmer absorption in this sample (median $H\delta_A$=7.12 Å) reflects a recently burst of star formation is dominating both the mass and light of these galaxies [113].

2.2.2 Gemini/GMOS Observations

From the 1318 SQuIGG$\vec{L}$E galaxies, we conducted follow-up observations of ten optically-bright SQuIGG$\vec{L}$E galaxies using the GMOS IFU instruments on Gemini North and South. In Figure 2, we show the Gemini/GMOS targets (large stars) and the parent SQuIGG$\vec{L}$E sample (small symbols) in SDSS i magnitude versus redshift, mass versus redshift, and $H\delta_A$ versus D_n4000. Comparing to massive galaxies in the LEGA-C survey, the high $H\delta_A$ and low D_n4000 of SQuIGG$\vec{L}$E indicate that the post-starburst galaxies we select are indeed significantly younger than typical $z \sim 0.7$ quiescent galaxies. Objects that fall short of target depths are indicated by open symbols. The integration times ($\sim$ 2.5 hours/galaxy) were chosen to measure the stellar continuum in spatially resolved spaxels and annuli to probe the kinematics and ages of the stellar populations of each galaxy. Each galaxy was observed using the R400 grating (5500Å $< \lambda <$ 10500Å). The observations were collected between 2016 and 2019. Each exposure was bias subtracted, scattered light corrected, cosmic ray

[1] https://github.com/cschreib/fastpp

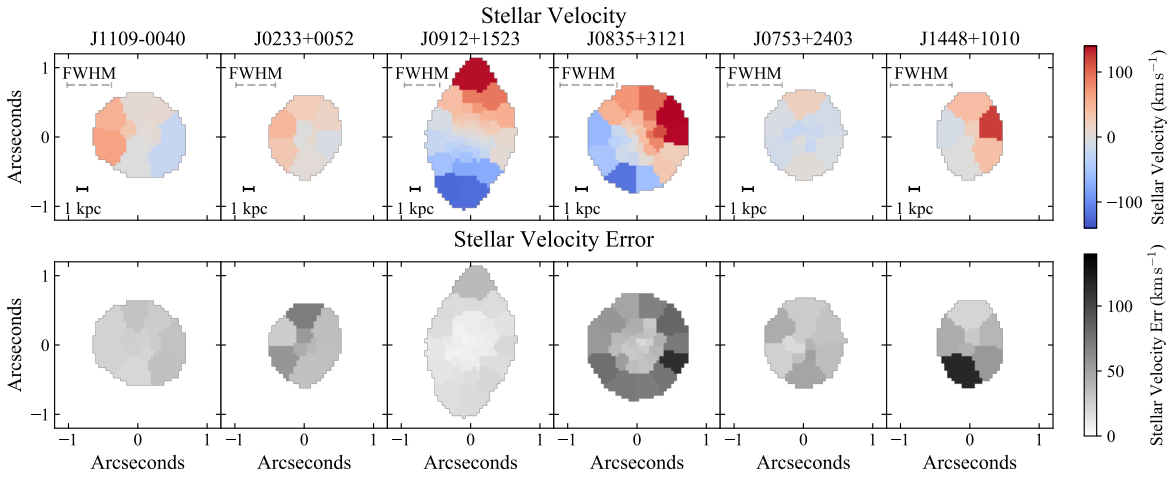

Figure 4: Measured stellar velocity (top) and velocity error (bottom) maps for the massive post-starburst galaxies in this sample. In J1109+0040, J0912+1523, and J0835+3121, unambiguous velocity gradients are detected, despite very different seeing conditions. For the rest of the sample, ordered motion is either ambiguous or non-existent. Effective point spread functions are not well-constrained for these observations, but worst-case FWHM limits are indicated by gray dashed lines.

rejected, flat field corrected, wavelength calibrated, response corrected (using a standard star which was not observed on the same night as the observations), and sky subtracted using the gfreduce and related IRAF packages following [128]. All individual datacubes were constructed using the gfcube package at a resolution of 0.05 "/pixel. Each spatial pixel was then iteratively sigma clipped using `astropy` sigma_clip to remove noise spikes at the 5-σ level [11, 10]. We performed an additional sky subtraction using a spline fit to the median of the outer pixels to account for any catastrophic over- or under-subtraction of the continuum in the GMOS pipeline.

We combined all individual reduced datacubes for each object using an inverse variance weighted average. We truncate the spectra above 8500 Å because the data quality drops off severely and there are no useful spectral features present. Because the standard stars were

not observed under the same viewing conditions and orientation as the science frames, the initial response correction is uncertain. We use the SDSS spectra to improve the response correction, using the luminosity weighted average of each cube within the 2" or 3" SDSS fiber aperture to obtain a 1D integrated galaxy spectrum. We fit a 10th order polynomial to models of the SDSS continuum generated by `FAST`, and do the same with the integrated GMOS spectra. We use the ratio of these polynomials to rectify the spectral shape of each individual spaxel.

Individual spaxels in the datacubes generally have insufficient signal-to-noise to facilitate robust measurement of stellar absorption features (median S/N$\sim$0.8 Å^{-1} in the outer spaxels), so some binning is required. We Voronoi bin [32, 31] the data to a signal-to-noise of 6 Å^{-1} at $\sim$ 4100 Å. In addition, we bin the spaxels using elliptical isophotes with an axis ratio and orientation we fit with the `photutils` python package [27]. We adopt an adaptive binning scheme, expanding the semi-major axis of the isophotal ellipses until we reach a target uncertainty in the Lick $H\delta_A$ index less than 1.5 Å. These annular measurements sacrifice spatial resolution to gain signal to noise and provide a natural comparison to radial models by use of the circularized radius, defined as $r_{circ} \equiv \sqrt{ab}$, where a and b are the semi-major and semi-minor axes of the ellipse that intersects the center of the bin

Unfortunately, the signal-to-noise in the stellar continuum in several datacubes were insufficient for this analysis. Three were not observed to a depth where we could resolve six Voronoi bins, so we exclude them from all additional analysis. We also exclude one other galaxy due to issues with strong residual sky features that overlap with $H\delta_A$ spectral feature. The details of the remaining six galaxies, including integration times and approximate seeing conditions, are presented in Table 1. The integrated spectra of the sample are shown in the left panels of Figure 3. In the right panels, we highlight the $H\delta_A$ bandpass and show luminosity weighted spectra from inner ($r_{circ} < 3$ kpc, blue) and outer ($r_{circ} > 3$ kpc, red) annuli. In all galaxies except for J0835+3121, the Balmer absorption is similarly strong in both the inner and outer bins.

We use Penalized Pixel Fitting (`pPXF`) [33] to measure the stellar line-of-sight velocities in each Voronoi bin. We fit the spectra using theoretical stellar spectral libraries to match the spectral resolution of the observations, which are $\sim$ 0.5 Å pixel^{-1} in the rest frame [21].

We fit the spatially binned spectra using a 1st order multiplicative polynomial and 5th order additive polynomial to account for uncertainty in the continuum shape. We measure the Lick $H\delta_A$ index using `pyphot`[2], fitting the continuum with a 1st order polynomial. We estimate the uncertainty in this index via a 1000-iteration Monte Carlo resampling of the error vector.

Due to the limited field of view of GMOS (3.5"x5"), our observations never include nearby stars, and as such, cannot exactly constrain the effective point spread function (PSF). However, due to the small angular sizes of the sample galaxies, we expect the impact of beam smearing to be strong, and must account for it in our analysis. Gemini provides seeing information in their RAW-IQ scores for the observations that measure an upper limit for the FWHM of the PSF at zenith. For galaxies observed in IQ-20, the seeing at zenith should be no greater than 0.5". For galaxies observed in IQ-70, the seeing at zenith should be no greater than 0.75". These values can be corrected for airmass effects as:

$$\mathrm{FWHM}_{corr} = \mathrm{FWHM}_{zenith} * (\mathrm{airmass})^{0.6} \tag{1}$$

We treat $\mathrm{FWHM}_{\mathrm{corr}}$ as the FWHM of a Moffat profile and consider it to be a conservative upper limit on the seeing that we use in our analysis of these galaxies.

2.3 Analysis

2.3.1 Stellar Velocities and $H\delta_A$ Profiles

Using the Voronoi bins and elliptical annuli discussed in Section 2.2.2, we can study the ordered motion and spatially-resolved age sensitive features in this sample of massive post-starbursts. In Figure 4, we present stellar velocity maps of the sample. Two galaxies (J0912+1523 and J0835+3121) show clear signs of strong ordered motion, with a third (J1109-0040) showing weaker but still significant velocity gradient. The other three galaxies do not exhibit statistically significant velocity gradients. Detailed analysis of the intrinsic velocity structures of these galaxies would require a more precise model of the point spread

[2]https://github.com/mfouesneau/pyphot

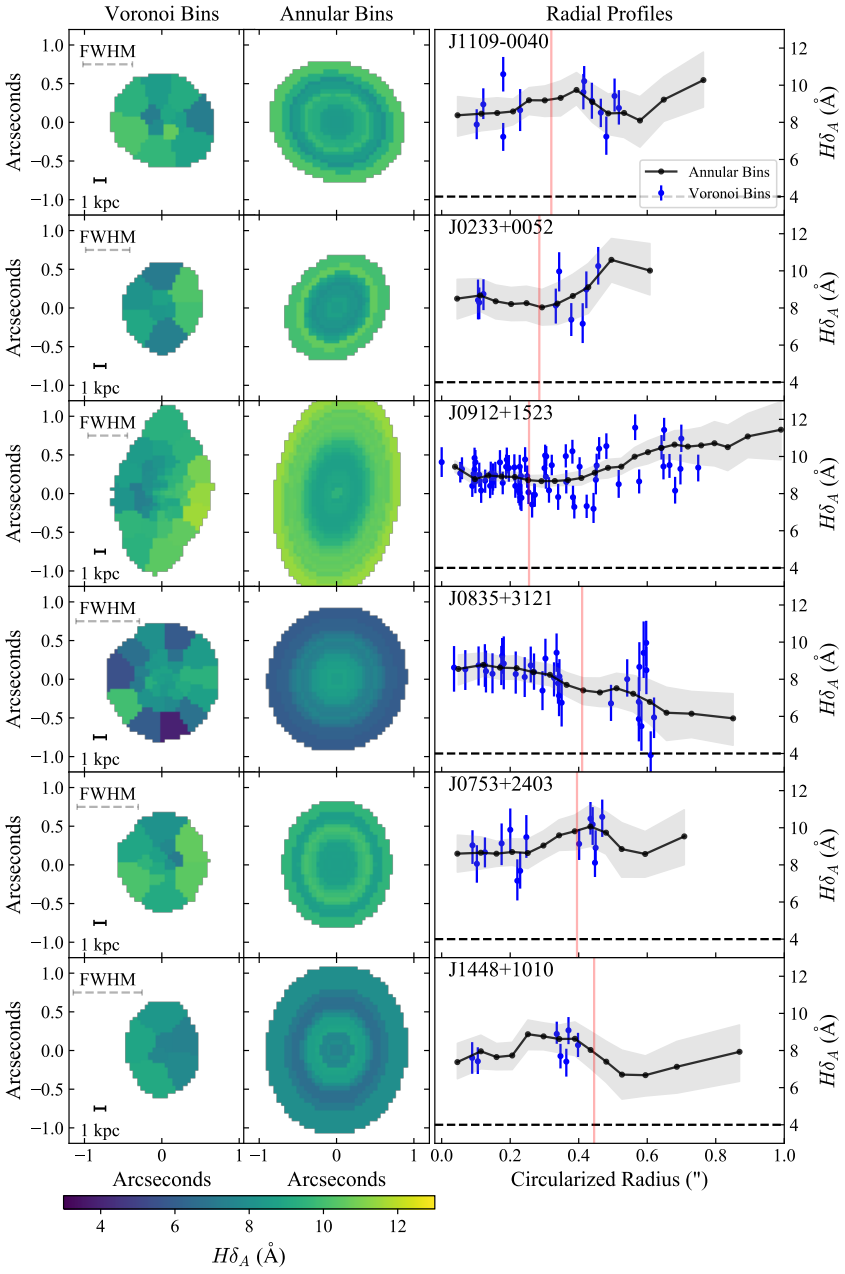

Figure 5: $H\delta_A$ maps for the final sample in Voronoi (left) and annular bins (center). The dashed error bars represents the FWHM of the worst case seeing conditions. (Right): $H\delta_A$ profiles versus circularized radius for Voronoi bins (blue symbols) and annular bins (black line with gray band). The red vertical lines represent the worst-case half-width half maximum of the point spread function. The dashed horizontal line at 4 Å indicates the common threshold to spectroscopically identify post-starburst galaxies. The entire sample is consistent with PSB-like absorption at all radii.

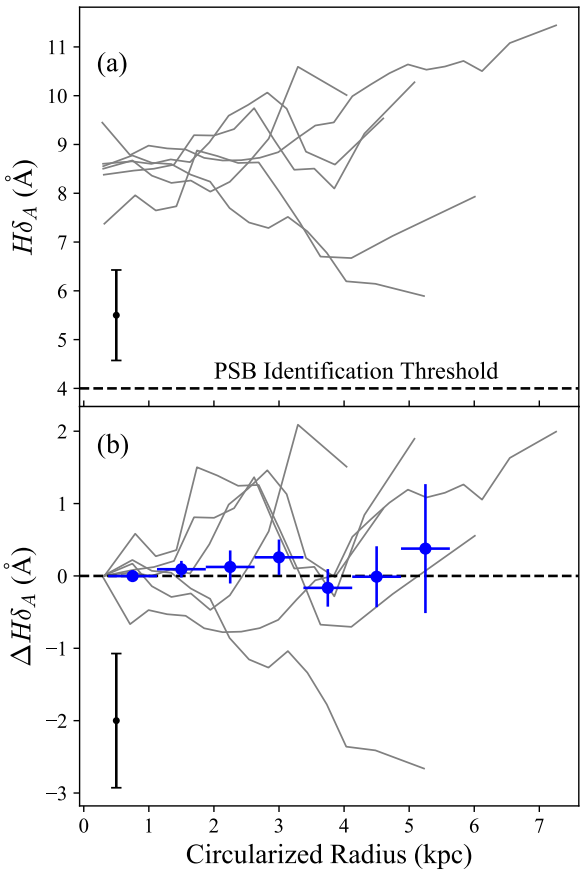

Figure 6: (a) Annular $H\delta_A$ profiles (a) and gradients (b) for the sample as a function of physical radius. The error bar represents the average error in the measurements of $H\delta_A$. (b) Radial $H\delta_A$ trends relative to the central measurement. The blue points show the running mean and error on the mean in 0.75 kpc bins. The average profile is flat to 5.5 kpc.

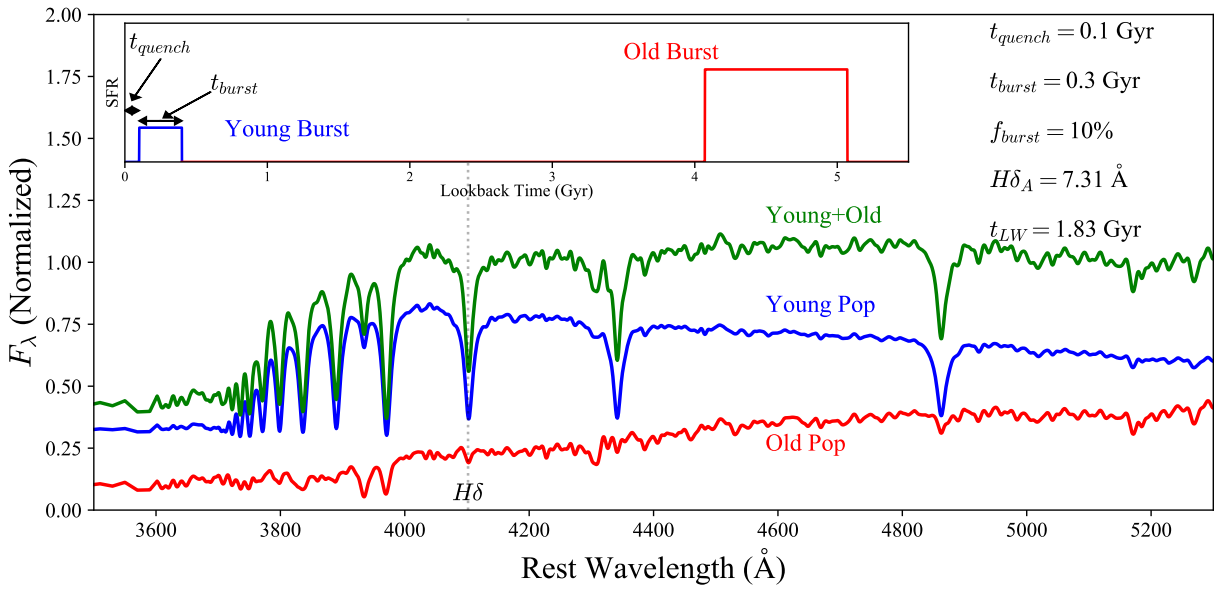

Figure 7: An example of the model spectra that can be generated using the two burst toy model. In the main figure, old population that formed 90% of the total mass at z=2, representing a population of older stars which formed at early times (red spectrum), is combined with a recent 300 Myr burst that quenched 100 Myr prior to observation (blue spectrum), to produce a post-starburst integrated spectrum (green). The spectra are normalized to the flux at 4000 Å in the composite spectrum. The inset panel shows the star formation history that produces these SEDs, with the same color scheme as the main figure.

function and is outside the scope of the current paper (see [105] for more in depth discussion about the velocity structure of J0912+1523). However, the fact that we successfully resolve rotation in one of the galaxies that was observed under the worst seeing conditions indicates that all targets are at least marginally spatially resolved.

The $H\delta$ absorption feature at 4100 Å and the D_n4000 ratio of flux redward and blueward of the Balmer/4000 Å break together are very powerful in constraining the age of a stellar population [113]. However, D_n4000 is very sensitive to systematic uncertainties in the sky subtraction and response correction, especially in faint outer spaxels (for more, see [105]).

In contrast, $H\delta_A$ is insensitive to both these uncertainties in addition to dust extinction. Given the extreme $H\delta_A$ exhibited by galaxies in this sample, we elect to use it alone as a tracer of stellar age, as strong absorption is still very constraining (see Section 2.3.2). In Figure 5, we show $H\delta_A$ maps in both Voronoi (left) and annular (center) binning schemes. The right column shows sets of $H\delta_A$ measurements versus the circularized radius. In blue, the Voronoi measurements are plotted with associated errors. The black line and shaded region correspond to the annular measurements and associated errors. All galaxies exhibit PSB-like light ($H\delta_A > 4$ Å, black dashed line) at all radii. In Figure 6, all annular profiles (6a) and gradients (6b) are shown as a function of the physical circularized radius with a characteristic error bar in the bottom corner. The average $\Delta H\delta_A$ is shown as blue points with error bars representing the error in the mean. Out to 5.5 kpc, the average gradient of this sample is flat. If we remove J0835+3121, which is host to the most significant gradient, there is a small signature of stronger absorption at large radii.

In Table 2, we list the measurements of $H\delta_A$ and $H\delta_A$ gradients. The $H\delta_A$ indices measured from spatially integrated spectra in a 2" aperture are listed first with associated errors. We also measure the slope of the annular profiles using the publicly available Markov Chain Monte Carlo (MCMC) fitting code emcee [84] to perform a linear regression. Four of the six galaxies are consistent with a flat $H\delta_A$ gradient at the 2-σ level, while the galaxy J0912+1523 has a slightly increasing $H\delta_A$ profile. Only J0835+3121 exhibits a negative gradient in $H\delta_A$. We also measure the Spearman correlation coefficients for each $H\delta_A$ profile and reach similar conclusions to those in the linear regressions.

2.3.2 Flat Age Gradients in SQuIGG$\vec{L}$E Post-Starbursts

In most stellar populations, $H\delta_A$ is insufficient to constrain age because it does not monotonically increase or decrease with time and therefore cannot be inverted [113]. However, for very high values, $H\delta_A$ has significant constraining power because the light-weighted spectrum of a galaxy must be dominated by short-lived A-type stars to result in such extreme absorption. In this section, we utilize a simple two-burst star formation history model to constrain the radial age profiles in these galaxies. We implement this modeling in two ways. First,

Table 2: Properties of radial $H\delta_A$ profiles

Name	Integrated $H\delta_A$ [1] (Å)	$\frac{dH\delta_A}{dr}$ (Å kpc^{-1})	Spearman ρ^2
J1109-0040	8.94 ± 0.15	0.21 ± 0.21	0.371
J0233+0052	8.73 ± 0.17	0.47 ± 0.32	0.482
J0912+1523	9.0 ± 0.04	0.25 ± 0.06	0.834
J0835+3121	8.03 ± 0.13	-0.66 ± 0.17	-0.968
J0753+2403	9.06 ± 0.15	0.3 ± 0.24	0.401
J1448+1010	8.02 ± 0.25	-0.03 ± 0.22	-0.191

[1]This value is measured on the luminosity weighted combination of spaxels within a 2"-diameter circular aperture.
[2]The Spearman correlation coefficient for the annular measurements of $H\delta_A$ as a function of the circularized radius.

we treat the annular $H\delta_A$ measurements as independent, and use the model to understand the range of light-weighted ages (t_{LW}) that correspond to these measurements. Second, we test the extreme case of a nuclear starburst imposed on an older stellar disk to test whether the flat observed $H\delta_A$ profiles could result from an unresolved central burst. Together, these models will inform the type of intrinsic age profiles and formation mechanisms of the sample.

In order to produce model spectra, we use a simple two top hat star formation history illustrated in Figure 7. This model generates two distinct stellar populations, one of which is representative of a galaxy that formed stars at early times and another that represents a younger, more recently formed population. The model allows for a combination of old and young populations with the flexibility to tune the length and timing of the younger burst in addition to the mass fraction. We use the `FSPS` python package to generate composite stellar population synthesis models with custom star formation histories [43, 42, 83]. We adopt `MIST` isochrones [65, 40] and use `MILES` spectral libraries [165, 78]. For all models, we assume solar metallicity, and we test to ensure that our conclusions are valid for different assumptions. The model depends on 3 parameters: the time since quenching (t_{quench}), the secondary burst fraction (f_{burst}, defined as the ratio of the mass formed in the recent burst to the total mass formed), and the length of the recent burst (t_{burst}). We fix the older burst last for a duration of 1 Gyr centered at $z = 2$ to represent star formation which occurred well before the recent burst. For an old stellar population, both $H\delta_A$ and the luminosity vary weakly with time,

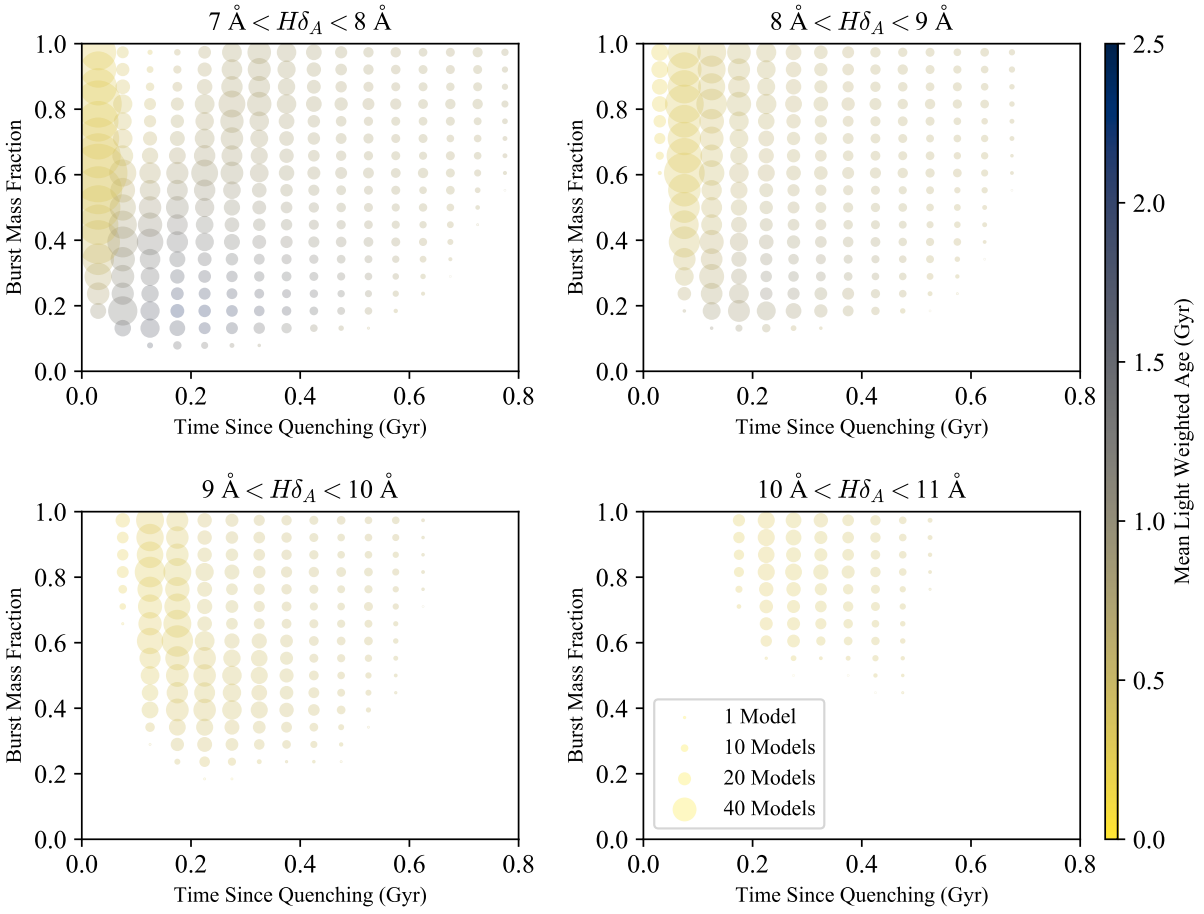

Figure 8: The secondary burst fraction versus time since quenching for our toy models which result in $H\delta_A > 7$ Å. The points are colored by the light-weighted age (at 4000 Å) and the size of the points is proportional to the number of models in the library that meet the $H\delta_A$ criteria in that bin. The plots are divided into the models which have $H\delta_A$ 7-8 Å (top left), 8-9 Å (top right), 9-10 Å (bottom left), and 10-11 Å (bottom right). High values of $H\delta_A$ are only possible for galaxies with light-weighted ages that are on the order of the time since quenching and an A-type stellar population is dominating the light.

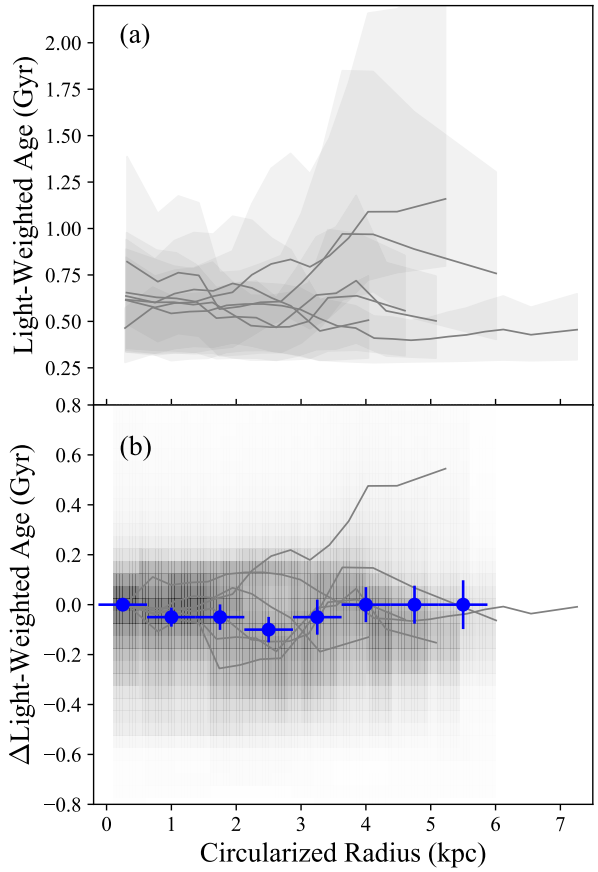

Figure 9: (a) Light-weighted age at 4000Å as a function of the circularized radius, as derived from two-burst star formation histories. The solid lines show the median light-weighted age fit to each measurement and the grey shaded regions bound the 1-σ spread about the median. The galaxies are consistent with being $\sim$ 600 Myr old. (b) Age gradient profiles as a function of the circularized radius. The shaded background represents the sum of the posteriors for the light-weighted age of all 6 galaxies in the sample, divided by the total number of galaxies in the sample. The blue points are the median of the average posterior, along with errors determined via jackknife resampling. The sample exhibits flat age gradients out to 5.5 kpc.

so our results are insensitive to the choice of the old burst's exact age and star formation history. The combination of these parameters allows for a wide range of quenching histories and naturally produces post-starburst SEDs. Example models for a burst fraction of 10%, $t_{quench} = 100$ Gyr, and $t_{burst} = 300$ Myr are shown in Figure 7. Because of the vastly different mass-to-light ratios, a recent burst population (blue) which only contributes a small part of the mass budget of the galaxy can still significantly dominate the light of an older population (red), resulting in a composite spectrum (green) which exhibits strong Balmer features. $H\delta_A$ is sensitive to changes in all three of the model parameters.

Using this model, we can probe the parameter space that can produce sufficiently high $H\delta_A$ to match the observations. We generate a model library with 40 linearly spaced points 0.01 Gyr $\leq t_{quench} \leq$ 2 Gyr, 99 linearly spaced points with 1% $\leq f_{burst} \leq$ 99%, and 40 linearly spaced points 0.01 Gyr $\leq t_{burst} \leq$ 2 Gyr, and measure $H\delta_A$ and the light-weighted age (at 4000 Å) for each star formation history. In Figure 8, we show the models collapsed in f_{burst} versus t_{quench} that can result in $H\delta_A > 7$ Å. The symbols are colored by mean light-weighted age and symbol size indicates the number of models that lie in that region of parameter space. Such high $H\delta_A$ values most often result from a high secondary burst fraction and a short time since quenching ($t_{quench} < 0.8$ Gyr), which together result in young light-weighted ages. $H\delta_A > 8$ Å constrains the light-weighted stellar population to be younger than 1 Gyr, while $H\delta_A > 9$ Å can only be produced by a stellar population that is between 200 and 600 Myr old. The star formation rate of the secondary burst is extremely degenerate with the length of the burst and is not well constrained by $H\delta_A$ alone. However, all models which result in $H\delta_A > 7$ Å can at least be constrained to have star formation rates above the [227] star-forming main sequence at z=0.7 in order to form 10^{11} solar masses by the time of observation, indicating that these galaxies likely went through a recent starburst phase.

We use this library of models to fit the observed $H\delta_A$ profiles and convert empirical measurements to light-weighted age profiles and gradients. For each individual $H\delta_A$ measurement, we marginalize over t_{quench}, f_{burst}, and t_{burst} and plot the median light-weighted age as solid lines and the 68% confidence intervals as shaded regions in Figure 9a. The light weighted ages in all cases are young, and in four of the six galaxies are constrained to be

$\lesssim 1$ Gyr at all radii. We run identical fits assuming both sub- and super- solar metallicity (logZ $= [-1.0, -0.5, 0.5, 1.0]$) and find that systematic shifts in the inferred light-weighted ages are $\lesssim 100$ Myr, which are much smaller than the errors in our fits. The shift is such that low metallicity leads to older inferred ages and high metallicity to younger ages. In Figure 9b, we show the trends relative to the central light-weighted age. In addition, we bin the posteriors for the light-weighted age as a function of radius for the sample and show the full posterior as a shaded region in the background, with the median and errors calculated from jackknife resampling in 0.75 kpc bins as blue points and error bars. The sample average is flat, and any deviations in the median of the posterior are ≤ 100 Myr. The gradient of the average sample is flat regardless of our assumptions about metallicity.

Clearly the extreme $H\delta_A$ in these massive post-starbursts necessitates that light from A-type stars dominate at all radii. However, due to the relatively low spatial resolution of our data, it is possible that this is not the result of a spatially extended post-starburst region but instead a secondary and unresolved nuclear burst of star formation. These nuclear starbursts are found in compact galaxies at $z \sim 0.6$ [173], and could wash out any intrinsic age-gradients by dominating the optical light under poor seeing conditions. We employ a toy model of an older, extended population superimposed with a nuclear starburst to test whether the observed $H\delta_A$ profiles could result from an unresolved secondary central burst.

The details of this model and the fits to the galaxies are summarized in Appendix A.1. In short, we fit the radial $H\delta_A$ profiles of each galaxy with a central young burst and a spatially-extended old population (to represent a stellar disk at $z = 2$) and test whether intrinsic positive age gradients could be masquerading as flat gradients under the worst-case seeing conditions outlined in Section 2.2.2. The results of this fitting are shown in Figure 10 as 1000 models drawn from the posterior (left) and a cumulative distribution function for the burst fraction (right). One galaxy, J0835+3121, is well fit by a secondary central burst with $f_{burst} \sim 20\%$, but the flat profiles in the remaining galaxies can only be produced by a central burst if a substantial amount of the mass (median $f_{burst} = 66 - 98\%$, see Table A.1) was formed in the most recent episode of star formation. For these five galaxies, we conclude that the $H\delta_A$ profiles must be the result of either a spatially extended post-starburst region, or that they must have formed the majority of their mass in the last ~ 0.5 Gyr such that

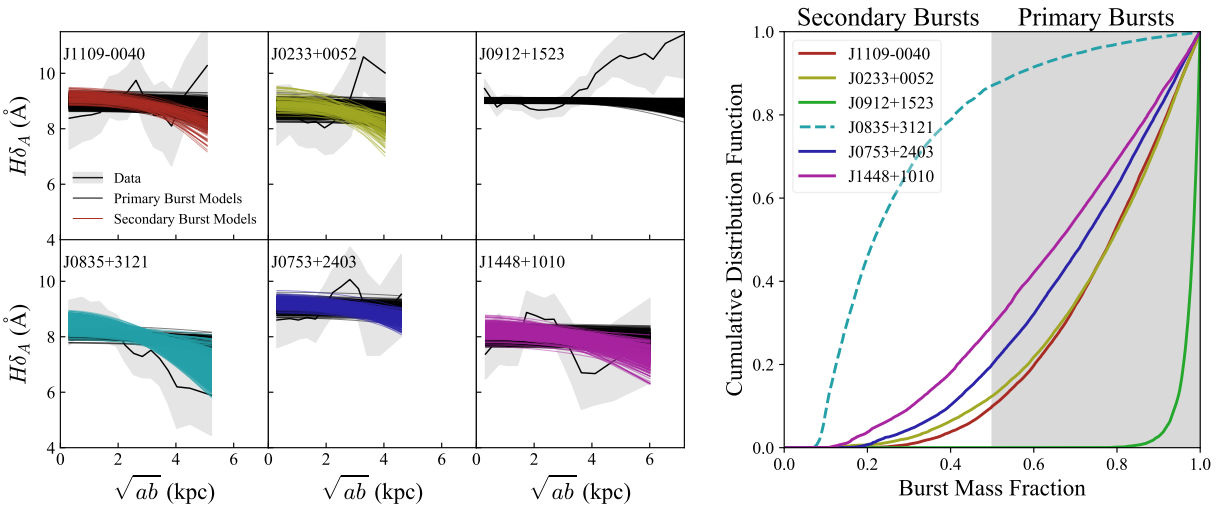

Figure 10: Observed $H\delta_A$ profiles with profiles derived from central burst toy models convolved with pessimistic seeing conditions (left) and cumulative distribution function of burst fractions obtained from those models (right). 1000 models randomly drawn from the posteriors are superimposed on each panel, with colored lines indicating models that form a subdominant secondary burst and black profiles indicating models in which $> 50\%$ of stars were formed in the central burst. The flat $H\delta_A$ profiles exhibited by five galaxies are only consistent with unresolved, central bursts if the majority of stars were formed in the burst. Only J0835+3121 (shown on the cumulative distribution function as a dashed line) is best fit by a secondary central burst that formed $\sim 20\%$ of the total galaxy mass.

the burst is not secondary, but instead is the dominant epoch of the galaxy's star formation. Either way, the optical light at all radii must be dominated by a recent burst which means that star-formation occurred and shut off uniformly throughout the galaxies.

2.4 Discussion

In this work, we find strong evidence that the stellar ages in $z \sim 0.6$ massive post-starburst galaxies are comparable across the face of the galaxy, at least to ~ 5 kpc. In contrast, both star-forming and quiescent galaxies tend to have intrinsically negative color gradients out to $z = 2$ [194], indicating that younger stars dominate the light profiles of these galaxies at large radii while older stars dominate in their cores. In star forming galaxies, these negative age gradients can be ascribed to star formation in disks, which populates the outer regions of galaxies with younger stars [147], and in quiescent galaxies they are likely caused by the addition of ex-situ stars, which puff up the outer regions with younger stars from less massive systems [22, 146, 100, 218]. The lack of radial trends in the stellar ages of this sample indicates that if SQuIGG$\vec{L}$E post-starbursts are galaxies in transition from star-forming to quiescent, the process that quenches them must do so in a way that erases the existing negative age gradient from the progenitor stellar disk. The high $H\delta_A$ that we observe everywhere implies that these galaxies are not typical star-forming galaxies which simply truncated their star-formation, but instead have actually experienced an enhancement in star-formation rate which preceded quenching. Local starburst galaxies have been shown to have flat star-forming surface densities and light weighted ages [25], and such galaxies could indeed evolve into post-starbursts like the ones we observe.

If instead the progenitors are quiescent galaxies experiencing a burst of star-formation that pushes them into the SQuIGG$\vec{L}$E selection, they *also* must form the new stars in such a way that overcomes an age gradient that has been caused by minor mergers, and in A.1, we show that this can only happen if a nuclear starburst formed $\gtrapprox 50\%$ of the total galaxy mass. This indicates that it is unlikely that these galaxies quenched via a halo process that cuts off the gas supply to the galaxy all at once [81], as a uniform shutdown of star formation

that does not include a significant burst would not be able to transform the existing galaxy stellar age profiles. It is also unlikely that any event that preferentially removes gas from the center of the galaxy, like AGN driven outflows [137], could cause the quenching in this sample, as that would likely enhance any existing negative age gradients. Wet compaction events [198, 250] are also unlikely to be responsible, as they predict negative age gradients much stronger than those we observe, which are at most consistent with $|\Delta t_{LW}| \sim 100$ Myr.

One way to erase intrinsically negative age gradients is via a starburst event that is more centrally concentrated than the underlying distribution of older stars. Gas rich mergers could effectively trigger this mode of quenching by driving gas to the center of a galaxy to rapidly form a new generation of stars [101, 182, 222]. There is significant evidence for this mode of quenching, as post-starbursts have been found to lie below the mass-size relation for both star-forming and quiescent galaxies at intermediate redshift [9, 239, 238]. [59] find evidence for positive age-gradients in the stacked $H\delta_A$ and Fe4383 profiles of the LEGA-C post-starburst sample, and [173] identified a population of extreme compact starbursts in the SDSS, which have light profiles that are well-fit by an unresolved nuclear starburst superimposed with an underlying de Vaucouleurs profile. At $z = 2$, star forming galaxies have been found with star forming regions which are a factor of 2 more compact than the older stellar disks, suggesting that ~ 300 Myr depletion times would yield integrated light profiles that are similarly compact to the population of quiescent galaxies [202]. Although one galaxy in this sample could easily be representative of this channel, in some cases the central starbursts in the [202] sample are sufficiently extreme that the new stellar population could outshine any older stellar light, erasing age gradients. Therefore, although these star-forming galaxies are identified at an earlier epoch, we cannot rule out a low-redshift tail of the population as a possible set of progenitors of the SQuIGG$\vec{L}$E galaxies studied herein.

However, in the majority of the sample, only a burst of star formation which forms the majority of the stellar mass of the galaxy or is comparably extended to the older population could result in the observed $H\delta_A$ profiles. There is evidence that photometrically-selected post-starburst galaxies at z$\sim 1-2$ exhibit flat color gradients [135, 194], which is a qualitatively similar result to the flat age gradients we detect. Furthermore, [194] found that the mass-weighted sizes in post-starbursts are actually very similar to those of quiescent

galaxies at a given epoch, and the difference in observed size manifests almost entirely from the accretion of stars at large radii in galaxies in post-quenching minor mergers. Since we are catching these galaxies directly after quenching, it may be that we are observing them before they have acquired their typical negative quiescent age gradient. This seems consistent with the $z \sim 2$ lensed quiescent galaxies studied in [107] and [5], which both exhibit flat age gradients and could have evolved from systems similar to the ones in this sample.

The literature includes objects that exhibit a diversity in age gradients; whether these reflect distinct quenching channels or two quenching modes that smoothly evolve in prevalence over cosmic time remains to be seen. At low-redshift, massive post-starburst galaxies appear to be quiescent galaxies that have just quenched a secondary and sub-dominant episode of star-formation. At earlier cosmic times, an older underlying population of stars does not exist, and post-starburst galaxies are galaxies that have just finished quenching their primary epoch of star formation. We posit that the SQuIGG$\vec{L}$E sample represents an intermediate redshift tail to the high-redshift post-starburst distribution due to their strong absorption ($\langle H\delta_A \rangle \sim 7.12$ Å) and flat age gradients, in contrast to the comparatively weaker absorption ($\langle H\delta_A \rangle \sim 5.5$ Å) and positive age gradients in LEGA-C that more closely resemble local post-starbursts. In this paper, we have demonstrated that quenching in class of post-starburst galaxies identified in SQuIGG$\vec{L}$E happens simultaneously throughout the galaxies or, if centrally concentrated, is dominant in both mass *and* light.

2.5 Summary and Conclusions

In this work, we study a sample of massive post-starburst galaxies at z$\sim$0.6 using spatially resolved spectroscopy. We find the following:

- Three of the six galaxies show unambiguous signs of ordered motion, while the rest of the sample shows weak or unresolved ordered motion (see Figure 4). One rotating galaxy was observed under the worst seeing conditions, indicating that all galaxies are at least marginally resolved in the IFU datacubes.

- Five of the galaxies we observe exhibit $H\delta_A \gtrapprox 7$ Å measured out to $r_{circ} \sim 5$ kpc, indicating that an A-type stellar population dominates their optical light at all radii (see Figures 5 and 6). On average, the sample exhibits flat $H\delta_A$ and light-weighted age profiles, with young ($t_{LW} \sim 600$ Myr) ages throughout (see Figure 9).
- We test whether the observed $H\delta_A$ profiles could be the product of an unresolved nuclear starburst in an older quiescent galaxy. In one galaxy, we find that the observed $H\delta_A$ profile is best fit by a central burst with a secondary burst mass fraction of ∼20%. For the remaining five galaxies, we find that their $H\delta_A$ profiles are not consistent with an unresolved central secondary starburst (see Figure 10).
- The finding of flat age gradients stands in contrast with other studies of less extreme post-starbursts that appear to be the products of central secondary bursts of star formation. This indicates that we have identified a sample of galaxies which have recently ended their primary epoch of star formation in a way that quenches the entire galaxy within ~ 100 Myr.

The fundamental limitation of this study is the seeing, which, from the ground, is comparable to the sizes of the galaxies at this redshift. Future work using adaptive optics or space based IFU such as NIRSPEC on the James Webb Space Telescope could probe galaxies in transition with finer resolution. JWST in particular would have the advantage of pushing out to IR wavelengths where any residual star formation can be spatially resolved with $H\alpha$. Although spectroscopic identification of post-starburst galaxies is optimal, identification of galaxies within SDSS limits the SQuIGG$\vec{L}$E sample to the tail end of a post-starburst distribution that peaks at earlier times [227, 230]. Future large surveys like the Dark Energy Spectroscopic Instrument [56] and Prime Focus Spectrograph [203] surveys will allow for spectroscopic identification of post-starburst galaxies at $z > 1$, when we expect the rapid quenching process to be more dominant. Future studies with these exciting new samples and instruments will continue to improve our understand of the gas, kinematics, and stellar populations of these higher redshift post-starburst galaxies to understand how galaxies transform during the peak epoch of quenching.

3.0 The Compact Structures of Massive $z \sim 0.7$ Post-Starburst Galaxies in the SQuIGG$\vec{L}$E Sample

3.1 Introduction

Broadly speaking, galaxies in the Universe can be divided into star-forming and quiescent populations. These populations of galaxies are distinct in that star-forming galaxies form many stars at a rate which is proportional to their stellar mass [227], whereas quiescent galaxies form few or no stars. In addition, the two populations differ structurally at all epochs; star-forming galaxies as a population are systematically larger and less compact than the coeval quiescent population at fixed stellar mass [214, 144, 116]. This indicates that a structural transformation may be coincident with the shutdown of star formation, a process which is jointly referred to as "quenching".

There is a growing body of evidence that two distinct pathways to quiescence exist: slow quenching that dominates at low redshift as galaxies gradually exhaust their gas supplies and high redshift rapid quenching that often follows a period of significant starburst [239, 19, 195], though there is a significant diversity in quenching times especially among the galaxies which quench more slowly [199]. The existence of quenched galaxies at high redshift [189, 49, 204, 85, 141, 212, 58, 112] indicates that the seeds of the most massive quiescent galaxies in the local Universe formed on very short timescales through this rapid mode. However, it is still unclear what causes massive galaxies to abruptly quench after an intense period of star formation, and simulations need to invoke various forms feedback to actively suppress star formation and prevent the formation of over-massive galaxies [169, 179]. As such, placing empirical constraints on the quenching process, especially in the rapid channel, is essential to understanding the precise process galaxies undergo as they shut off their final epoch of star-forming activity.

Ideally, this process could be studied by finding galaxies at the exact moment preceding the rapid shutdown of their most recent episode of star formation. Unfortunately, rapid shutdown by definition occurs on extremely fast timescales, and it is difficult to identify pop-

ulations in the midst of shutdown, especially given the uncertainty of future star-formation activity in any galaxy experiencing a starburst at the time of observation. However, it is instead possible to identify the immediate descendants of galaxies which went through the rapid channel by looking for galaxies whose spectra are dominated by a stellar population which formed in the last <1 Gyr but which show no evidence of recent star formation. These galaxies are often referred to as post-starburst, or "K+A" galaxies, due to their composite spectral energy distributions (SEDs) which are dominated by late-type B and A type stars [67, 245].

Numerous methods have been developed to select post-starburst galaxies, including Balmer absorption strength in conjunction with a measure of weak nebular emission [240, 160, 89, 239, 39], "K+A" template fitting [156], photometric supercolors [229, 9, 135, 232], or UVJ color space [19, 194]. All these methods have in common the goal of selecting galaxies with light dominated by a young stellar population with no ongoing star formation [87]. Although a dramatic burst of star formation is not strictly required as suggested by the term post-*starburst*–the spectral signatures seen in post-starburst galaxies can be produced by truncation of existing high star formation rate–it is thought that bursts do accompany quenching in high mass galaxies [89, 231, 191]. Post-starburst galaxies serve as a laboratory for understanding the progenitors of the rapid quenching channel and their evolution immediately after star formation shuts off can shed light on the conditions which caused the galaxies to cease forming new stars.

One important empirical probe of the quenching of massive galaxies comes from the study of their structures. Because star-forming galaxies at any given epoch are consistently larger than quiescent galaxies [214, 144, 116], it has been suggested that mergers can drive both the quenching and structural transformation of galaxies by driving gas inwards and rendering a more compact aggregate light profile with the resulting centralized star formation [222, 247, 155]. Mergers appear to be very common in post-starburst galaxies [246, 157, 167], and in simulations mergers have been shown to result in an enhancement in the quiescent fraction in post-merger systems [161]. A number of structural studies of post-starburst populations have found that they are compact relative to both coeval star-forming and quiescent populations [241, 9, 135, 239, 194] and have younger central stellar populations than their outskirts

[39, 59, 237]. However, the evidence for the ubiquity of merger-driven central starbursts as the driver of structural transformation is inconclusive. The most massive post-starburst galaxies at intermediate-to-high redshift have been found to lack color or age gradients [135, 174, 194], disfavoring out purely nuclear starbursts and implying that star formation prior to quenching may have occurred on kiloparsec scales. These field studies are in contrast with observations of post-starburst galaxies in dense clusters, where environmental effects such as ram-pressure stripping have been shown to be the dominant quenching mechanisms [138, 139, 223].

In order to use structures to understand the quenching process, one would ideally like to track the evolution of post-starburst galaxies as a function of their time since quenching. However, precise timing of the time since quenching requires high quality rest-frame optical spectra. Because the post-starburst population does not emerge significantly until $z \sim 1$ [226, 230], those spectra must be obtained at a minimum of intermediate-redshift to catch even the tail end of the rapid quenching that dominates in the early universe. To date, spectroscopic studies of intermediate-redshift post-starburst galaxies have been limited to small samples [239, 231]. However, spectroscopic samples of post-starburst galaxies at intermediate-redshift are accessible in the Sloan Digital Sky Survey (SDSS) thanks in large part to the CMASS BOSS sample [53] which targeted high-mass red galaxies at intermediate-redshift. Leveraging this spectroscopic sample in addition to a handful of ancillary SDSS programs, we have launched the SQuIGG$\vec{L}$E Survey [191], which spectroscopically identified 1318 post-starburst galaxies in the SDSS at $z > 0.5$ with spectral signatures that indicate that they have recently shut off their primary epoch of star formation. Crucially, these spectra allow us to characterize the properties of the burst, to measure the time since star formation quenched, and to track the evolution of the sample in key properties as a function of the time since quenching. This sample has allowed us to study in detail the link between the star formation shutdown and AGN incidence [97], molecular gas content [190, 20], and the incidence of mergers [219].

In this work and its companion letter [219], we match 145 post-starburst galaxies in the SQuIGG$\vec{L}$E Survey to deep imaging in the Hyper Suprime-Cam Survey [4, 3] in order to study their sizes, structures, and merger signatures and connect these properties to

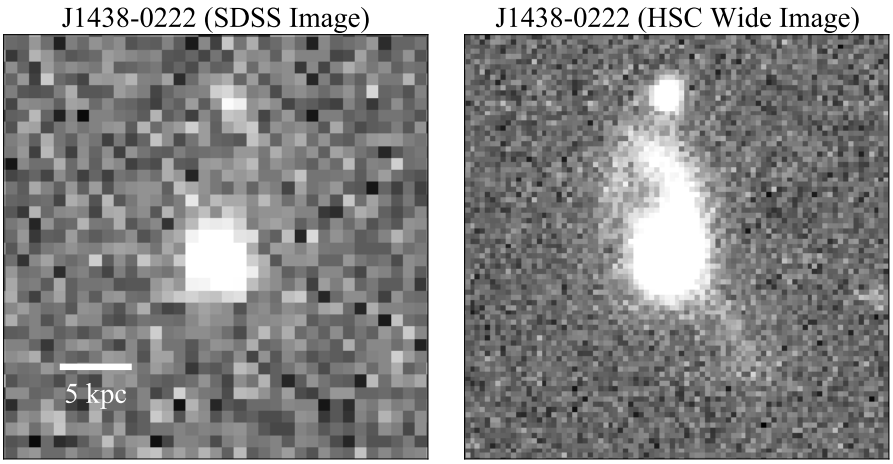

Figure 11: i-band images of J1438-0222, a z=0.698 post-starburst galaxy from the SDSS (left) and the Hyper Suprime-Cam Wide Survey. The cutouts are centered at the same physical location, and the pixel scales are 0.396 and 0.168 "/pixel respectively. The combination of better resolution and deeper images resolves faint, low surface brightness light that was previously inaccessible at this redshift, allowing us to accurately measure sizes and identify merger signatures.

those of the star formation histories as derived from the SDSS spectroscopy. In Section 3.2, we introduce the SQuIGG$\vec{L}$E sample and a mass-matched control sample of quiescent and star-forming galaxies to which we compare. In Section 3.3, we detail our methodology for measuring sizes and structures. In Section 3.4, we present our analysis of the sizes and structures. Finally, in Section 3.5, we discuss our results and their significance to understanding the rapid quenching pathway of galaxy evolution. Throughout this paper we assume a concordance ΛCDM cosmology with $\Omega_\Lambda = 0.7$, $\Omega_m = 0.3$ and $H_0 = 70\ \mathrm{km\,s^{-1}\,Mpc^{-1}}$, and quote AB magnitudes. All reported values of the effective radius ($\mathrm{r_e}$) are measurements of the semi-major axis and are not circularized.

3.2 Data

3.2.1 The SQuIGG$\vec{L}$E Sample

In order to study the descendants of the rapid quenching process, we turn to the SQuIGG$\vec{L}$E Survey. The SQuIGG$\vec{L}$E Sample is selected from the Sloan Digital Sky Survey DR14 spectroscopic sample [1] using the rest-frame U_m, B_m, and V_m medium-band filters from [122] to select galaxies with strong Balmer breaks (indicated by red $U_m - B_m$ colors) and blue slopes redward of the break (indicated by blue $B_m - V_m$ colors). In [191], we show that this method reliably selects post-starburst galaxies which quenched within the last $\sim$ 500 Myr, 75% of which formed $> 25\%$ of their stellar mass in a recent burst, and further discuss the specific selection effects and how they differ from other post-starburst selection techniques. While SDSS imaging exists for the entire sample, the depth and resolution is not sufficient to resolve the galaxies. However, the Hyper Suprime-Cam (HSC) Wide Imaging Survey [4] overlaps with $\sim 10\%$ of the galaxies in SQuIGG$\vec{L}$E and is deep enough to resolve the main galaxies in addition to faint structures, as seen in Figure 11.

In order to characterize the stellar populations of these galaxies, we perform two sets of spectral energy distribution (SED) modelling. The first, described in [174], are performed on the the SDSS spectra and *ugriz* photometry using `FAST++`[1], an implementation of the `FAST` stellar population fitting code [123]. We assume a delayed exponential star formation history (SFR $\sim te^{-t/\tau}$), BC03 stellar population libraries [28], a [38] initial mass function, and a [30] dust law. While these fits are limited to capturing only the recent burst of star formation in post-starburst galaxies due to the imposition of a single rise and fall in the star formation history, the physical measurements derived from this common parameterization can easily be compared to other galaxies in the literature which are fit similarly.

In addition to the traditional parametric fits, we perform non-parametric fits using a custom implementation of `Prospector` [110, 125, 109]. These star formation histories impose their own set of priors on the stellar mass which result in higher stellar masses than those derived with a delayed exponential star formation history [132, 127]. In addition, non-

[1] https://github.com/cschreib/fastpp

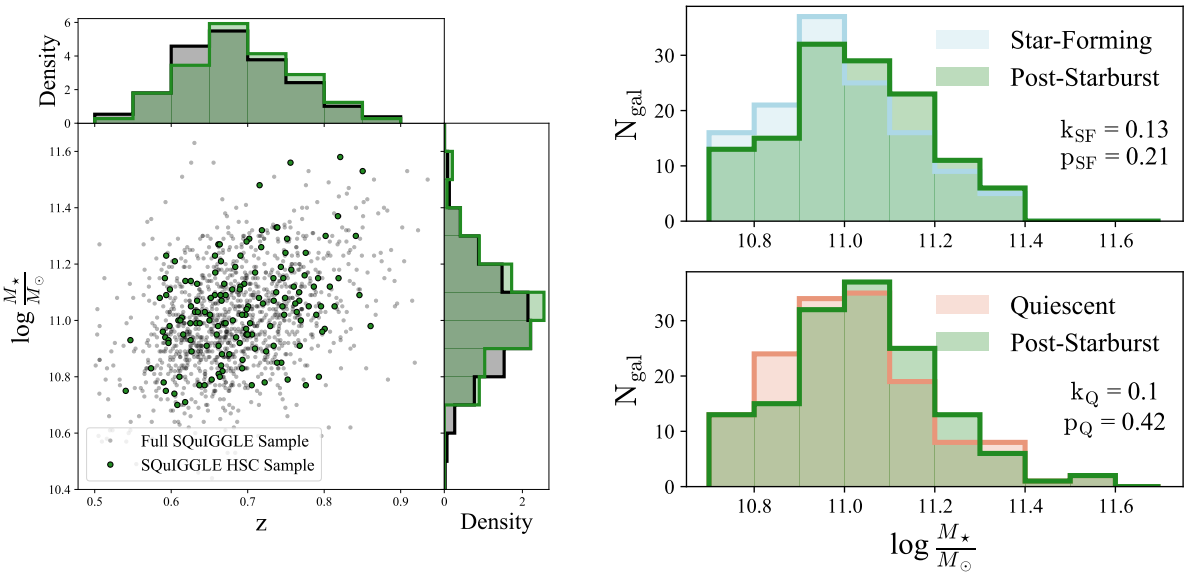

Figure 12: (Left): Stellar mass versus redshift for the full SQuIGG$\vec{L}$E post-starburst sample (grey) and the HSC sample in this work (green). Above the mass-cut of $M_\star > 10^{10.7}$ $M_\odot$, the HSC sample spans the full range of SQuIGG$\vec{L}$E. (Right): The stellar-mass distributions for the mass-matched far-forming (blue) and quiescent (red) matches with the SQuIGG$\vec{L}$E sample. The samples are well matched in stellar mass, as indicated by the results of Kolmogorov–Smirnov tests on the two histograms.

parametric star formation histories are still only weakly constraining on star formation before the recent burst due to the outshining from the recently formed stellar population; as such, the prior chosen for early formation times significantly affects the conclusions about the burst mass fraction. However, these non-parametric fits are very useful for providing lower limits on the burst mass fraction with the conservative priors chosen, for robustly recovering the time since quenching, and for reliably measuring instantaneous star formation rates. For this work, we use the stellar masses derived from the delayed exponential star formation history for consistency in comparisons to other mass-size relations, and employ the non-parametric star formation histories to investigate trends within the SQuIGG$\vec{L}$E post-starburst sample.

3.2.2 Coeval control sample from the LEGA-C Survey

In order to contextualize the sizes and structures of SQuIGG$\vec{L}$E post-starburst galaxies relative to coeval star-forming and quiescent galaxies, we require a sample of $z \sim 0.7$ galaxies with high quality spectra which fully overlaps with HSC. For this, we turn to the LEGA-C Survey DR3 [216]. The LEGA-C Survey consists of deep ($\sim$ 20 hours/galaxy) spectroscopy of galaxies in the COSMOS field. Because the SQuIGG$\vec{L}$E sample was selected from a variety of SDSS target selections with a variety of different color and magnitude cuts, we do not yet have a full understanding of how mass complete or representative the sample of post-starburst galaxies are. As such, we elect to compare to a very conservative subset of LEGA-C galaxies above which completeness correction factors are negligible to ensure that the control population we are comparing to is fully representative of the galaxy population at $z \sim 0.7$. In this work, we use the sub-sample of LEGA-C galaxies with stellar masses (derived similarly to the SQuIGG$\vec{L}$E sample using delayed-exponential star formation histories) above $10^{10.7}$ $M_{\odot}$, slightly higher than the characteristic mass of the sample and well into the regime where completeness corrections are ~ 1 [215]. We divide the LEGA-C sample into quiescent and star-forming by their UVJ colors as in [215] and use those samples as a control group to compare morphology and size measures to the post-starburst galaxies in SQuIGG$\vec{L}$E, using similarly derived delayed exponential star formation history masses.

The LEGA-C sample was selected using a redshift dependent K-band magnitude cut, in contrast with SQuIGG$\vec{L}$E, which was selected using rest-frame colors and a signal-to-noise cut from the whole of SDSS, largely from luminous red galaxies targeted using the CMASS selection criteria [53]. As such, the mass and redshift distributions of the two samples are different, even above the previously discussed stellar-mass threshold. In order to fairly compare structural measurements, we create a mass-matched subsample of LEGA-C following the procedure described in detail in [219]. Briefly, for each galaxy in SQuIGG$\vec{L}$E we select the quiescent and star-forming galaxy in LEGA-C which is within 0.05 dex in stellar mass and is the closest in redshift to our main galaxy without replacement.

We perform this procedure on the full sample of SQuIGG$\vec{L}$E galaxies with high quality HSC imaging (see Section 3.2.3) resulting in a final sample of 144 mass-matched pairs of post-

starburst and quiescent and 129 pairs of post-starburst and star-forming galaxies. For the fifteen most massive galaxies in the SQuIGG$\vec{L}$E sample with high quality HSC imaging, there is no similar-mass star-forming counterpart. This dearth of massive star-forming galaxies could be expected in a pencil-beam survey like LEGA-C given the steep high-mass end of the star-forming stellar mass function [145]. In addition, we are not able to match one of the most massive post-starburst galaxies to a quiescent counterpart. The results of the mass-matching procedure are shown as histograms in Figure 12b. In both cases, a KS test finds that the stellar mass distributions of the post-starburst and control samples are consistent with being drawn from the same distribution ($k_Q = 0.10,\ p_Q = 0.42$; $k_{SF} = 0.13,\ p_{SF} = 0.21$). For testing of size-fitting methodologies and the determination of the mass-size relations for star-forming and quiescent samples, we utilize the entirety of LEGA-C's mass-representative ($\log\frac{M_\star}{M_\odot} > 10.7$) sample. For all other comparisons, we utilize the mass-matched samples, and show the star-forming matched post-starburst sample as dashed histograms for comparison with the star-forming disxtributions. We note that by construction, the redshift distributions of the mass-matched samples, which were a secondary priority, overlap less precisely than those of the stellar masses. The LEGA-C quiescent and star-forming samples are a median 0.038 and 0.058 higher in redshift than SQuIGG$\vec{L}$E. We consider this offset to be acceptable for the secondary parameter, as we are primarily interested in structural parameters of galaxies as they relate to stellar mass and the effects of surface brightness dimming are small over this narrow range in redshift.

In addition to fully overlapping with HSC, the LEGA-C Survey has the added bonus of being fully observed with existing HST/ACS F814 imaging. This allows us to also use the galaxies in LEGA-C as a test to ensure that the inferences we make using ground-based data agree with the higher-resolution space-based data afforded by HST.

3.2.3 Hyper-Suprime Cam Imaging

In Figure 11, we show that the SDSS images of SQuIGG$\vec{L}$E galaxies are insufficient in both depth and resolution to study the structures of post-starburst galaxies at $z \sim 0.7$. However, imaging from the Hyper-Surprime Cam (HSC) Survey [4] can be used to robustly

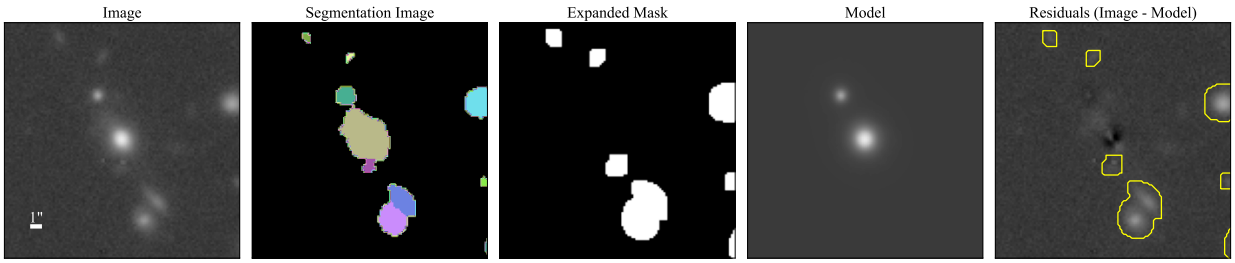

Figure 13: A demonstration of the multi-component fitting procedure on a SQuIGG$\vec{L}$E post-starburst galaxy. We first show the unmasked image centered on the galaxy of interest in a 20"x20" cutout, with nearby interlopers. The second panel demonstrates the source identification procedure described in Section 3.3.1, which successfully detects and deblends all sources in the field of view. The third panel shows the mask that we provide to `GALFIT`, which is the segmentation map for all sources >25 pixels from the galaxy of interest or which are within 25 pixels but are 3 dex fainter than the main source convolved with a 3-pixel tophat kernel. Note that the object to the Northeast of the galaxy of interest is bright and close enough to not be masked. In the fourth panel, we show the best fitting model produced by `GALFIT`, and in the final panel we show the residuals on the same color scale as the image and the model, with the masked regions outlined. The fitting successfully accounts for the majority of the light from both the main galaxy and the neighbor.

obtain sizes from the ground out to $z < 1$ [116]. As of PDR3, the HSC Wide Survey has taken data in at least one *grizy* band [115] of ~ 1300 deg^2 of the sky at depths ~ 3 orders of magnitude deeper than the SDSS [3], making it ideal for the detailed study of SQuIGG$\vec{L}$E post-starburst galaxy images. The survey design is such that the i-band was observed to great depths (26.2 mag point source limit), and, perhaps more importantly, at extremely high resolution (point spread function FWHM $\sim$ 0.6", a factor of ~ 2 improvement over SDSS). As such, we elect to perform all our analysis on the i-band images which provide the best combination of depth and seeing and overlap with $\sim 10\%$ of the SQuIGG$\vec{L}$E sample.

For every galaxy in SQuIGG$\vec{L}$E with i-band imaging in the HSC footprint, we pull a 48x48" coadd cutout and the corresponding point spread function (PSF) model from the PSF Picker[2] [26]. After performing the same mass-cut ($\log\frac{M_\star}{M_\odot} > 10.7$) as on LEGA-C, we find that 150 SQuIGG$\vec{L}$E galaxies have been imaged in the HSC i-band. We visually inspect all galaxies and exclude images with clear visual artifacts (e.g. cosmic rays, image streaks) in the region of the central object, as well as objects with extremely bright nearby sources which significantly alter the sky subtraction. This removes 5/150 galaxies with HSC coverage, leaving us with a total of 145 post-starburst galaxies with clean images. A full gallery of the SQuIGG$\vec{L}$E sample cutouts is shown in [219]. The results of this selection in the mass-redshift plane are shown in Figure 12. The subset of SQuIGG$\vec{L}$E galaxies we study in this work spans the range of the full SQuIGG$\vec{L}$E sample above the mass-completeness cut.

In addition, we pull cutouts using the identical procedure as above for the entirety of the LEGA-C mass-representative sample. The HSC Survey consists of 3 sky layers: wide, deep, and ultra deep, covering 1400 deg^2, 26 deg^2, and 3.5 deg^2 respectively and each ~ 1 dex deeper than the shallower layer [4]. Every galaxy in SQuIGG$\vec{L}$E was observed only at wide depth; however, the LEGA-C field overlaps with the deep layer of HSC. In order to facilitate a fair comparison to the SQuIGG$\vec{L}$E sample, we utilize the wide depth reductions of the LEGA-C galaxies to ensure that the surface brightness limits are similar between the two samples. However, we also pull the full depth HSC Deep cutouts and PSF models for the entire sample, which we use to test the reliability of our fitting procedures for deeper

[2]https://hsc-release.mtk.nao.ac.jp/psf/pdr3/

images.

3.2.4 Tidal Feature Classifications

In [219], we present visual classifications of the incidence of tidal features in the mass-matched SQuIGG$\vec{L}$E and coeval LEGA-C samples. In brief, we instructed eleven members of the SQuIGG$\vec{L}$E team and the Pitt Galaxy Group to assign a binary classification of "Tidally Disturbed" or "Not Disturbed" to postage stamps of the SQuIGG$\vec{L}$E and mass-matched LEGA-C control samples in random order. We divide galaxies into 3 categories: disturbed ($>$ 70% agreement that a tidal feature is present, $N_{gal} = 61$), non-disturbed ($>$ 70% agreement that no tidal features are present, $N_{gal} = 51$), and ambiguous (all galaxies which meet neither of these conditions, often due to the presence of neighbors where the association is unclear and rankers were divided, $N_{gal} = 33$). Throughout this work, we utilize the disturbed and non-disturbed sub-samples of SQuIGG$\vec{L}$E to test whether structural parameters vary based on whether or not a galaxy has clear tidal features.

3.3 Galaxy size and structure fitting

3.3.1 Measuring Sérsic sizes

We utilize `GALFIT` [159] to quantify the structural parameters of SQuIGG$\vec{L}$E post starburst galaxies and the LEGA-C control sample. For each image, we identify and deblend all light sources detected at the 5σ level above the background using the Python `astropy photutils` package [11, 10], using the following settings which were chosen to optimally deblend based on visual inspection of the resultant segmentation maps:

`fwhm_smooth` = 3

`sigma_detect` = 3

`npixels` = 5

`npixels_deblend` = 5

We use the `source_properties` function to extract approximate centroids, axis ratios, position angles, and fluxes of each source. We then mask all sources greater than 25 pixels (4.2 arcseconds) from the center of the image and any objects within the central 25 pixels that are more than three magnitudes fainter than the central object. We smooth the resultant mask with a 3-pixel radius top hat filter in order to ensure that we are accounting for all galaxy light from all interloping sources. These aggressive masking choices were made to ensure that all bright nearby sources are being accounted for with their own models and that the Sérsic profiles are sensitive to the smooth central profiles of the galaxies. To this end, we elect in our deblending parameters to err on the side of classifying spatially distinct tidal features, such as the one to the northwest of the galaxy in Figure 14, as their own objects and to mask them, biasing the sizes of all galaxies we fit towards smaller values.

We then allow `GALFIT` to fit the object of interest and the remaining neighboring galaxies (those within 25 pixels and within 3 magnitudes of the central object) with Sérsic profiles convolved with the PSF. We adopt the bounds on the Sérsic index $0.5 < \mathrm{n} < 6$ following the most recent LEGA-C data release to facilitate comparisons to their fits using HST/ACS F814 images [216]. The centroid, position angle, axis ratio (b/a), and magnitudes measured by `photutils` are used as initial guesses for the parameters in the Sérsic fits for each object. The sky background is initialized at 0 and is a free parameter in the fit. In Figure 13, we demonstrate the full Sérsic fitting procedure on a SQuIGG$\vec{L}$E galaxy which has a nearby source that meets our criteria for simultaneous fitting. The nearby source immediately to the south of the galaxy of interest is too faint to be fit, and as such appears in the mask, but the source to the northeast is bright enough to be fit with its own Sérsic model. The best fitting Sérsic parameters from these fits are detailed in Table 3.

In [97], we find that $\sim 5\%$ of SQuIGG$\vec{L}$E post-starburst galaxies host AGN, which are identified via their strong [OIII]/H_β ratios. However, in all cases the narrow lines indicate that the AGN are strongly obscured, and should not significantly impact the rest-frame optical continuum of the galaxies. As such, we do not elect to fit any additional point-source components to the 6 AGN in our sample. Throughout this work, we report the semi-major effective radius ($\mathrm{r_e}$) as the measure of galaxy size.

Although the LEGA-C control sample is covered by the deeper HSC-Deep imaging,

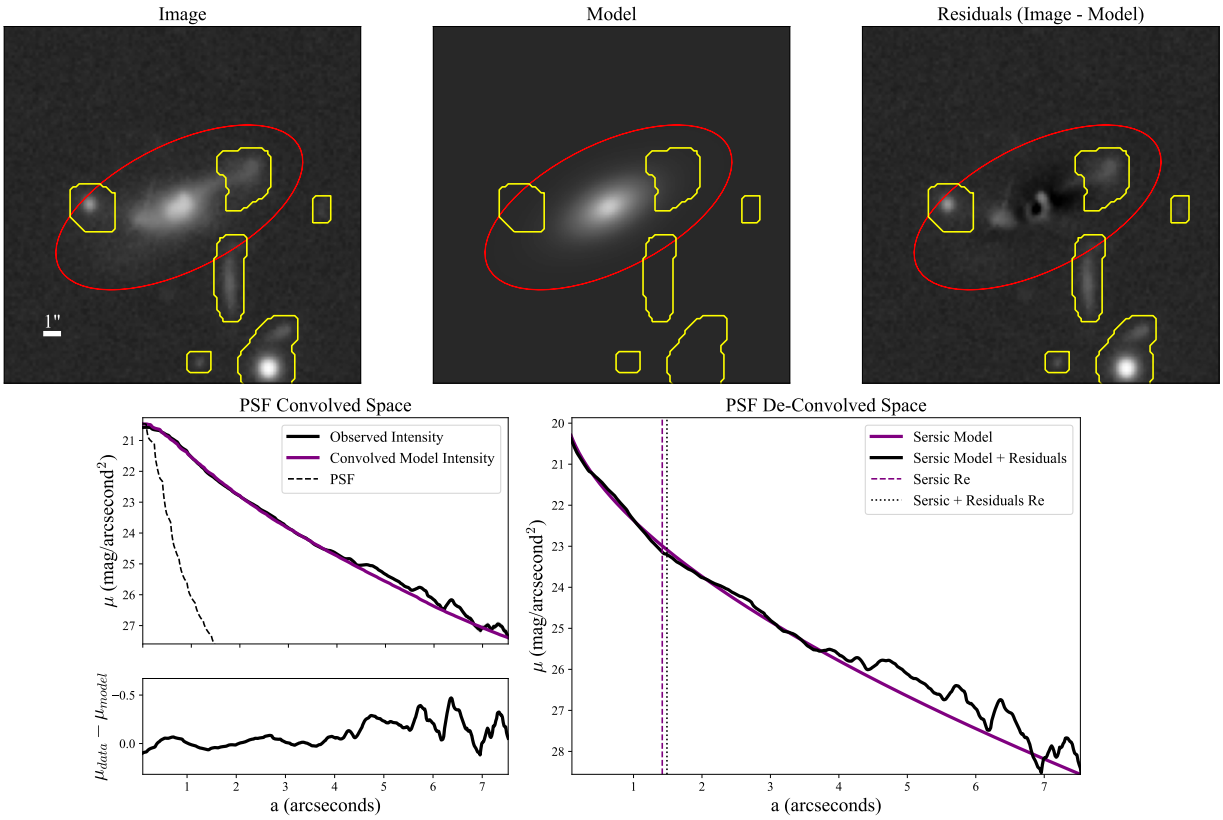

Figure 14: (Top): The image, bests fitting Sérsic model, and resulting residuals of a SQuIGG$\vec{L}$E post-starburst galaxy which exhibits clear merger features, some of which are masked (yellow outlines) in our source identification algorithms. The red aperture indicates the largest annulus used in extracting a 1D surface brightness profile, corresponding to the point where the signal-to-noise drops below 5. (Bottom Left): Observed (black) and model (purple) radially averaged surface brightness profiles as a function of the semi-major axis of the best fitting ellipse, with residuals shown below. The Sérsic model under-estimates the surface brightness at large radius. (Bottom Right): The same model (purple) as the center, now shown without PSF convolution. The same profile is shown with the residuals added to them using the method from [197]. The dashed and dotted lines represent the effective radius of the profile before and after this addition takes place. While the residuals do affect the total shape of the profile, the measurement of effective radius is largely robust to this correction.

Table 3: Structural and selected spectrophotometric properties of post-starburst galaxies

Name	$z_{\rm spec}$	$\log(\frac{M_\star}{M_\odot})^a$	$r_{\rm e,Sersic}$ (kpc)^b	$r_{\rm e,corr}$ (kpc)^c	n^b	mag^b	b/a^b	$\log(\Sigma_{\rm 1kpc})^b$	G^d	GC^d	t_q (Gyr)^e	Burst Fraction^e
J1042+0500	0.6266	$10.89\ ^{+0.01}_{-0.02}$	0.78	0.76	5.98	19.61	0.94	10.16	0.59	2.5	$0.31\ ^{+0.09}_{-0.1}$	$0.52\ ^{+0.21}_{-0.12}$
J0907+0423	0.6635	$11.27\ ^{+0.01}_{-0.02}$	7.03	6.06	3.47	19.25	0.85	9.81	0.5	2.97	$0.11\ ^{+0.08}_{-0.04}$	$0.36\ ^{+0.58}_{-0.2}$
J0226+0018	0.5405	$10.75\ ^{+0.03}_{-0.03}$	2.09	2.09	6.0	19.26	0.89	9.83	0.63	2.67	$0.36\ ^{+0.13}_{-0.13}$	$0.44\ ^{+0.34}_{-0.17}$
J0224-0105	0.5979	$10.98\ ^{+0.01}_{-0.02}$	3.36	3.21	5.76	18.82	0.81	9.97	0.64	2.84	$0.39\ ^{+0.18}_{-0.11}$	$0.88\ ^{+0.12}_{-0.62}$
J0221-0646	0.6613	$10.98\ ^{+0.02}_{-0.02}$	5.58	5.82	5.56	19.46	0.67	9.88	0.51	2.64	$0.22\ ^{+0.08}_{-0.07}$	$0.27\ ^{+0.28}_{-0.08}$
..	..	..	..	..	..	..	..	..	..	..	..	..

[a]Stellar masses were derived using a delayed-exponential star formation history, described in Section 3.2.1.
[b]Sérsic parameters were derived using single-component 2D Sérsic models to fit the galaxies of interest. Uncertainties derived by refitting the galaxies using a range of PSF models from nearby locations on the sky are shown in Table 4. For details, see Section 3.3.1.
[c]The residual-corrected effective radii were derived using the method of [197], described in Section 3.3.3.
[d]The Gini coefficient (G) and the generalized concentration (GC) were measured on the segmentation maps described in Section 3.3.1, for details see Section 3.4.3.
[e]Time since quenching (t_q) and the burst fraction are model parameters derived from non-parametric star formation history fitting of the galaxies, see [191] for details

SQuIGG$\vec{L}$E galaxies fall entirely within the shallower HSC-Wide footprint. In order to compare morphological measurements fairly to SQuIGG$\vec{L}$E, we utilize imaging for the LEGA-C control sample (galaxy postage stamps and PSFs) of the HSC-Deep field that is only stacked to Wide depths. To assess the reliability of our structural measures, we compare the results from HSC fits for the LEGA-C sample to structural parameters measured from HST/ACS F814W imaging in [216] in Appendix B.1. We find that our fits are very reliable despite the images being lower in resolution by a factor of ~ 3 compared to the HST/ACS F814W imaging. In many cases, the increased low-surface brightness sensitivity of HSC better captures the wings of galaxy profiles at large radius. This difference in profiles can explain the systematic offsets in the Sérsic index and the effective radius. We find that we recover the axis ratio with extremely high precision and accuracy (median $\Delta b/a$ =0.005, $\sigma_{\Delta b/a} = 0.11$).

We also test the robustness of our fits by comparing to analysis of HSC Deep imaging for the LEGA-C sample. We find that our measurements of the effective radius between the Deep and Wide are extremely consistent, with a median offset of 0% and a scatter of $\sim 8\%$ in measured size. Axis ratios are similarly well constrained, with a scatter in $\sigma_{b/a} \sim 0.02$. The median Sérsic index fit with the Deep images is found to be slightly lower than with Wide, with $\Delta n = -0.05$, $\Delta n_{16\%} = -0.45$, and $\Delta n_{84\%} = 0.15$. We conclude that the HSC Wide images are sufficient for robustly measuring sizes of massive galaxies at intermediate redshift.

We also use the derived Sérsic profiles to compute the stellar mass surface density within one kiloparsec ($\Sigma_{1\mathrm{kpc}}$). We do so by multiplying the fraction of the flux contained within 1 kpc by the galaxy stellar mass and dividing by the area of the bounding ellipse using the best fitting Sérsic profile parameters, implicitly assuming a flat M/L gradient.

$$\Sigma_{1\mathrm{kpc}} = \frac{M_\star \frac{f_{1\mathrm{kpc}}}{f_{\mathrm{tot}}}}{\pi(1\ \mathrm{kpc})^2(b/a)} \tag{2}$$

3.3.2 Systematic Size Errors Due to PSF Models

The formal uncertainties on the sizes for bright galaxies measured using `GALFIT` are very small because the HSC images are so high in signal-to-noise. However, these formal

uncertainties ignore potentially significant systematic errors. Likely the largest systematic is the assumption that the PSF model used in the Sérsic model fitting is well determined at any point in the sky. As galaxies at intermediate-redshift have intrinsic sizes similar to the full-width-half-maximum of the point spread function, small changes in the shape of the PSF can lead to significantly different measurements of galaxy size and Sérsic index.

In order to account for this, for each galaxy in SQuIGG$\vec{L}$E we sample the PSF from the HSC PSF Picker at 50 locations drawn from a normal distribution surrounding the galaxy with $\sigma = 0.375$ degrees in RA and Dec. This choice of σ ensures that we will be picking PSFs which are distributed throughout the entire 1.5 degree field of view of HSC surrounding the object of interest. At each position, the PSF is estimated based on surrounding stars, and the distribution in the shapes of these PSFs should approximate the uncertainty in the determination of the PSF at the position of the galaxy itself.

We refit each galaxy with each of the 50 randomly drawn PSFs and quantify the error in the measurement of the effective radius. We find that the uncertainties from this PSF shuffling are an order of magnitude larger than the formal uncertainties (median $\sigma_{\rm re,formal} = 0.004$", median $\sigma_{\rm re,PSF} = 0.049$"). We take these systematic errors to be dominant and throughout the rest of the work, all errors reported in the size result from this methodology. For each of the 50 iterations, we also calculate $\log(\Sigma_{\rm 1kpc})$, for which we find a median error of 0.05 dex. The full 1σ confidence intervals in Sérsic properties inferred from the PSF refitting are shown in Table 4.

3.3.3 Accounting for non-Sérsic light

Sérsic profiles can provide average properties of the smooth 2D light distributions of galaxies. [213, 9, 239, 144, 116]. However, the Sérsic model does not fully account for asymmetric light from tidal features, which are present in many galaxies and are very common in the SQuIGG$\vec{L}$E sample of post-starburst galaxies in deep imaging (see [219]) and are not fully masked even in our conservative source identification procedure (see Figure 14). Additionally, single component Sérsic fits need not perfectly describe the profiles of isolated galaxies; for example, the presence of a bright point source component (which we do not

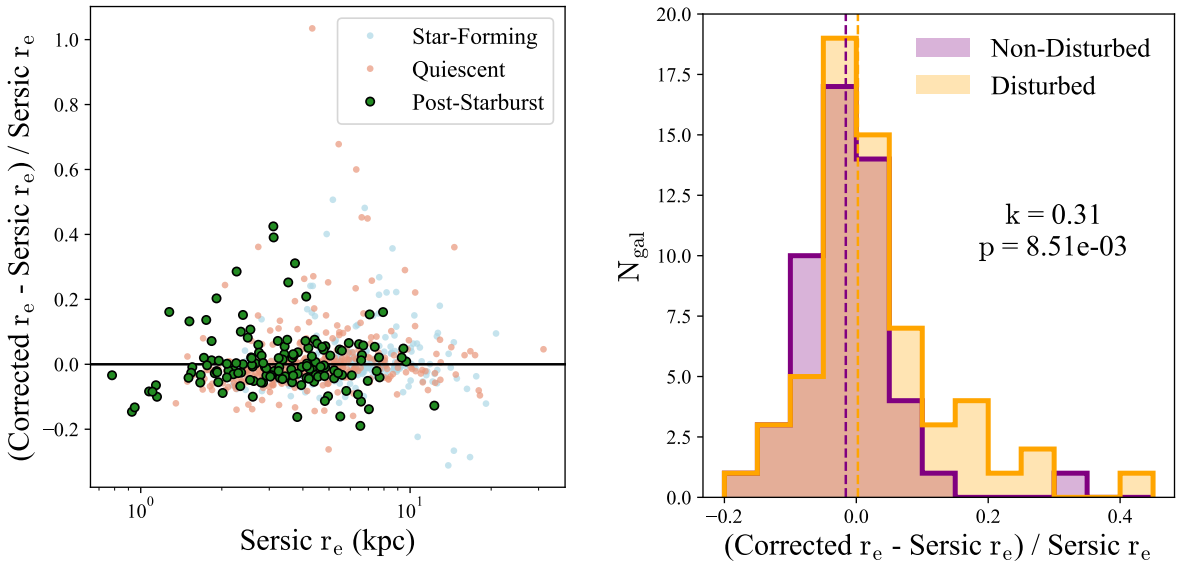

Figure 15: (Left): The measured Sérsic effective semi-major axis radius from `GALFIT` versus the residual-corrected percent error in r_e from the application of the [197] technique to post-starburst galaxies in SQuIGG$\vec{L}$E and quiescent/star-forming galaxies from the LEGA-C survey. Globally, the addition of the residuals only biases measurements to be $\sim$ 1% smaller, and majority of galaxies have measured sizes consistent within $\sim$ 10%. (Right): The distributions of the residual-corrected percent error in r_e for the disturbed and non-disturbed post-starburst samples. The median offsets in measured sizes (vertical lines) for the samples are comparable, but the majority of the galaxies where the corrected sizes are significantly larger are visually flagged as tidally disturbed.

expect from AGN but could potentially result from nuclear star-formation) could drive a fit to be overly peaked, missing light in the wings of the galaxy as a result. These deviations in the Sérsic fits from the true surface brightness profiles of galaxies can bias inferences about the sizes of galaxies; accounting for it is important in accurately comparing to the sizes of coeval galaxies.

We follow [197] to correct for deviations from Sérsic profiles, including asymmetries, while accounting for PSF smearing. To start, we run `GALFIT` on galaxies as described in Section 3.3.1. We begin by performing annular photometry on the residual (galaxy image minus the best fitting Sérsic models of *all* simultaneously fit galaxies multiplied a mask which masks all non-primary sources, including those which were fit simultaneously) using the best fitting position, position angle, and axis ratios derived from the Sérsic fits. We extract the profiles out to the annulus where the signal-to-noise in the galaxy image drops below 5, ~ 28 mag/arcsecond^2 [103]. We add these PSF-convolved residuals to the *deconvolved* best fitting Sérsic profile and re-measure the half-light radius from the residual corrected growth curve. An illustration of this method is shown in Figure 14 for a clearly disturbed galaxy. Even in this extreme case, the tidal features do not contribute significantly to the total galaxy flux and the measured size is only 5% larger than the Sérsic effective radius.

In general, the residual corrected sizes do not deviate significantly from the corresponding Sérsic effective radii. We show this in Figure 15a, comparing the sizes measured with `GALFIT` to the residual-corrected sizes. While we find that in a few cases, the residual-corrected sizes are significantly ($\gtrapprox 25\%$) larger than those measured by Sérsic fits, the median deviation from Sérsic is $\sim -1\%$ for star-forming, quiescent, and post-starburst galaxies, indicating that non-Sérsic and asymmetric light is not significantly affecting galaxy sizes. The majority of the measurements which skew toward significantly larger sizes are due to the presence of tidal features along the semi-major axis (see Figure 15b). We adopt these corrected effective radii as our measure of galaxy sizes for the remainder of this work. However, due to the lack of systematic offsets in any of the samples, all conclusions in this work would not change if we were to use the Sérsic-only half-light sizes.

3.4 The Sizes and Structures of Post-Starburst Galaxies

3.4.1 Post-starburst half-light sizes

Across redshift, star-forming and quiescent galaxies exhibit differing relations in the size-mass plane when size is quantified by the half-light radius [214, 239, 144]. The sizes of galaxies scale with their stellar mass, but quiescent galaxies are generally smaller and follow a steeper relation than star-forming galaxies. In this section, we hope to constrain the rapid path to quiescence by comparing the sizes of coeval post-starburst, quiescent, and star-forming galaxies. In Figure 16, we show the residual corrected effective radius versus mass for the SQuIGG$\vec{L}$E post-starburst galaxies in green, along with the mass-representative ($\log\frac{M_\star}{M_\odot} > 10.7$) LEGA-C star-forming (blue) and quiescent (red) samples. The blue and red solid lines are our best fitting relations for star-forming and quiescent galaxies respectively, and the dashed lines are the best fitting relations from [214]. There is considerable scatter in the sizes of the post-starburst galaxies, but on average they are fairly compact relative to all of the LEGA-C sample.

In order to test the relative compactness of post-starburst galaxies, we define $\Delta\log(\mathrm{r_e})$, the vertical offset with regard to the quiescent mass-size relation, $\hat{\mathrm{r}}_{\mathrm{e,Q}}(\log\frac{M_\star}{M_\odot})$, as follows:

$$\Delta\log(\mathrm{r_e}) = \log(\mathrm{r_e}) - \log(\hat{\mathrm{r}}_{\mathrm{e,Q}}(\log\frac{M_\star}{M_\odot})) \tag{3}$$

In Figure 17a, we show the distributions in $\Delta\log(\mathrm{r_e})$ of the SQuIGG$\vec{L}$E post-starburst galaxies in green in addition to the quiescent (red) and star-forming (blue) mass-complete samples. All three populations show similar scatter (~ 0.2 dex), but the SQuIGG$\vec{L}$E galaxies $\sim$0.1 dex more compact in their light distributions than quiescent galaxies at similar redshift. In order to quantify the uncertainty in the inferred median $\Delta\log(\mathrm{r_e})$, we refit the quiescent mass-size relation using the `emcee` implementation of Markov Chain Monte Carlo [84] and draw randomly from the posterior for the intercept and slope. We find a 1σ confidence interval on the median value of $\Delta\log(\mathrm{r_e})$ of [-0.17, -0.07]. In Figure 17b, we show that the offset from this sequence does not correlate with the mass of the galaxy. We perform a two-sample Kolmogorov–Smirnov test on $\Delta\log(\mathrm{r_e})$ for the post-starburst and quiescent samples

Table 4: Uncertainties on Sersic parameters from PSF model refitting

Name	r_e (kpc)			n			mag			b/a			$\log(\Sigma_{1kpc})$		
	16%	50%	84%	16%	50%	84%	16%	50%	84%	16%	50%	84%	16%	50%	84%
J1042+0500	0.94	1.3	1.62	2.72	3.09	5.82	19.64	19.66	19.67	0.74	0.82	0.94	9.94	10.02	10.1
J0907+0423	6.98	7.3	8.28	3.21	3.51	4.64	19.16	19.24	19.26	0.84	0.86	0.89	9.71	9.73	9.8
J0226+0018	2.25	2.37	2.48	4.02	5.32	6.0	19.25	19.27	19.31	0.82	0.86	0.9	9.69	9.74	9.76
J0224-0105	3.04	3.22	3.29	4.86	5.63	6.0	18.82	18.84	18.87	0.78	0.8	0.83	9.86	9.88	9.91
J0221-0646	5.39	5.58	5.83	5.16	5.6	6.0	19.44	19.45	19.47	0.68	0.71	0.74	9.68	9.7	9.72
..	..	..	..	..	..	..	..	..	..	..	..	..	..	..	..

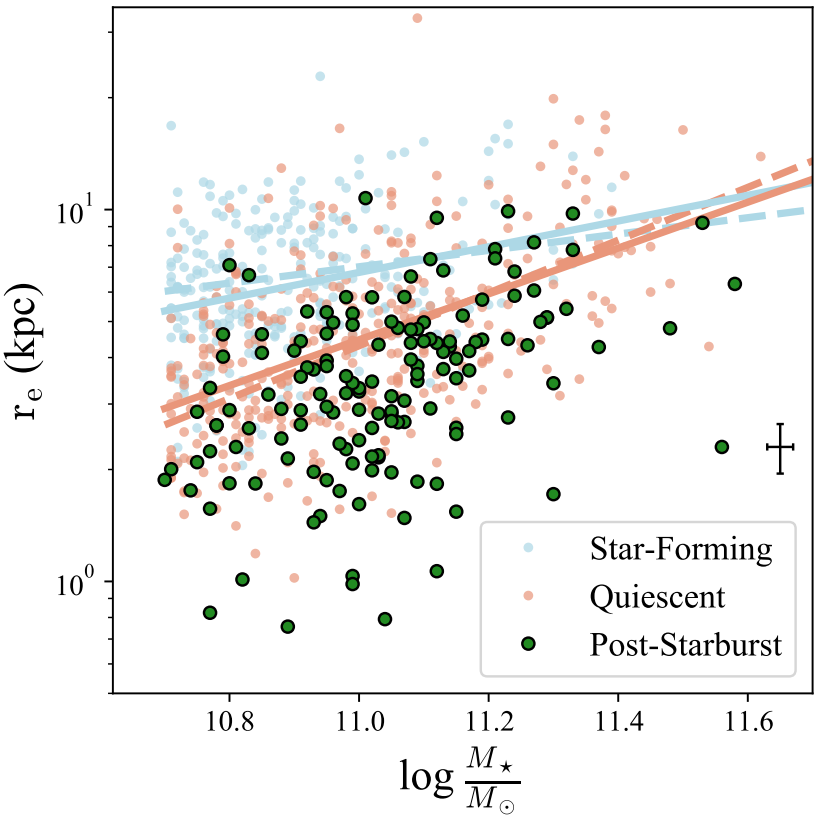

Figure 16: The effective radius versus stellar mass relation for $z \sim 0.7$ post starburst (green), quiescent (red), and star-forming (blue) galaxies. Characteristic error bars in the mass and size are shown in black. The best fitting relations to star-forming and quiescent galaxies (blue and red respectively) are shown as solid lines. Best fits from [214] for $0.5 < z < 1.0$ are shown as dashed lines. SQuIGG$\vec{L}$E post-starburst galaxies are compact on average relative to both star forming and quiescent galaxies, though there is significant scatter within each population.

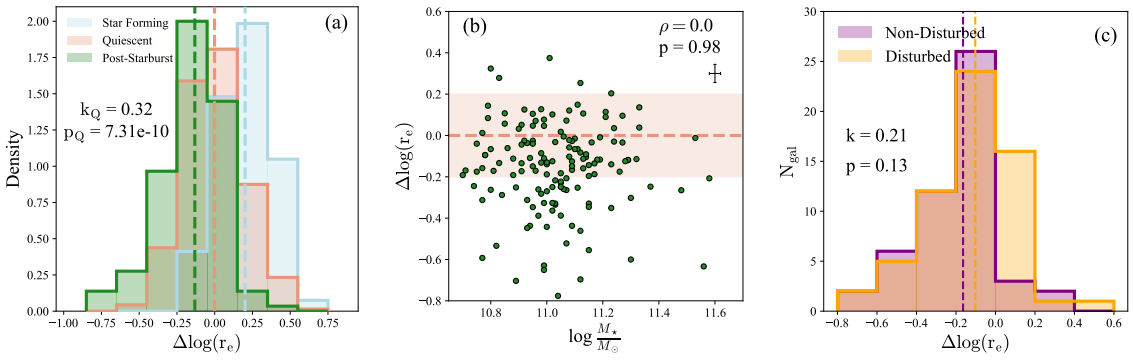

Figure 17: (Left): The distribution of $\Delta\log(r_e)$ from the quiescent mass-size relation for the star-forming (blue), quiescent (red), and post-starburst (green) samples. The medians of the samples are indicated with vertical dashed lines. The star-forming sample is a median ~ 0.2 dex larger than the quiescent sample at a given stellar mass. The post-starburst sample is a median of 0.13 dex below the quiescent population. All 3 samples have similar scatter of ~ 0.2 dex. (Center): $\Delta\log(r_e)$ versus log $M_\star$ for the SQuIGG$\vec{L}$E post-starburst sample (green). The red dashed line and shaded region represent the quiescent mass-size relation. Typical errors are shown as in black. Post-starburst galaxies uniformly scatter below quiescent galaxies, with no trend as a function of the stellar mass as evidenced by the Spearman correlation coefficient (ρ) and associated p-value. (Right): Distributions in $\Delta\log(r_e)$ for the non-disturbed an disturbed samples of post-starburst galaxies as defined in [219]. While the median size at fixed stellar mass is slightly smaller than for the non-disturbed sample, a Kolmogorov–Smirnov test shows that the samples are consistent with being drawn from the same distribution (see associated k and p values).

find that they are not consistent with being drawn from the same distribution (p=2.57e-4). In addition, we perform a 2D Kolmogorov–Smirnov test [158, 80] on the mass-matched mass-size plane to ensure that this conclusion is robust to our definition of $\Delta\log(r_e)$. This test confirms that post-starburst galaxies are not consistent with being drawn from the same 2D distribution as the quiescent galaxies (p=7.95e-4).

The compact sizes we measure for the post-starburst sample relative to coeval quiescent and star-forming populations are broadly consistent with the smaller-than-average coeval post-starburst galaxies selected from the LEGA-C survey [239, 238] in addition to high mass ($M_\star > 10^{10}\ M_\odot$) post-starburst galaxies at $1 < z < 2$ [241, 9, 135]. The light-weighted sizes are also similarly compact to the $M_\star \sim 10^{11}\ M_\odot$ post-starburst galaxies in [194]. In Figure 17c, we show the distributions in $\Delta\log(r_e)$ splitting the sample into disturbed and non-disturbed using the classifications from [219]. While the median size at fixed stellar mass is slightly larger for the disturbed population (owing to the fact that tidal features do influence the effective radius), a Kolmogorov–Smirnov test shows that the distributions do not differ significantly, and the entire post-starburst sample is compact relative to coeval quiescent galaxies.

Crucially, we note that these galaxies are resolved in the HSC imaging. In Appendix B.1, we demonstrate that the sizes we measure using HSC imaging of galaxies at this redshift are almost entirely consistent with the sizes measured on the smallest galaxies in [216], and in Appendix B.2, we demonstrate that the 1D and 2D surface brightness profiles of the smallest galaxies in SQuIGG$\vec{L}$E are significantly different from that of the PSF. In the i-band, the light of the youngest stellar population will almost completely dominate over any older stellar population, and so the sizes we measure are likely to primarily trace the physical extent of that population. This finding indicates that the recent star formation was extended on at least kpc scales past the circumnuclear region in all the galaxies in our sample.

3.4.2 Other parametric measures of structure

In addition to the half-light radius, the Sérsic models also include the Sérsic index (n) and the projected axis ratio (b/a) in the 2D fits to the galaxies. These structural measures

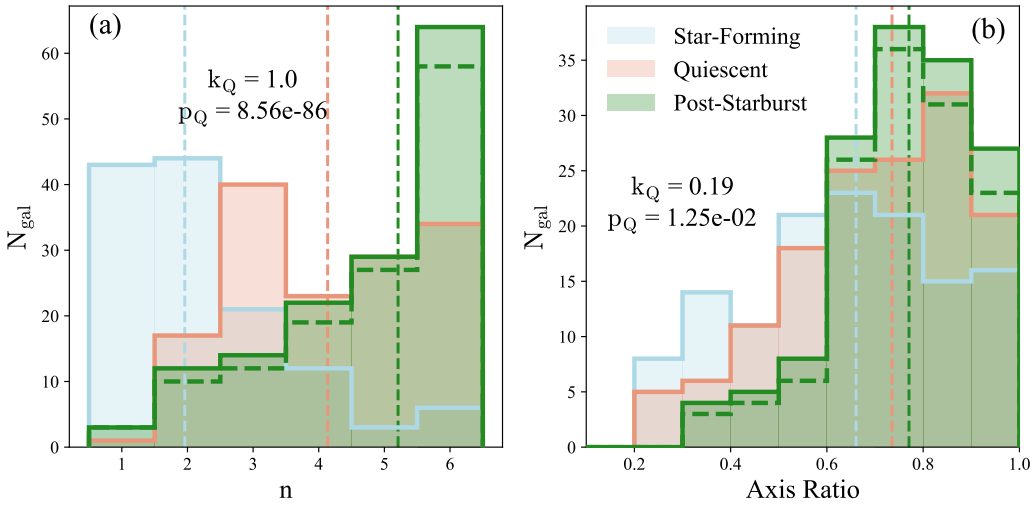

Figure 18: (Left) The distributions of mass-matched post-starburst (green), star-forming (blue), and quiescent (red) galaxies for the Sérsic index n. The dashed post-starburst histogram shows the post-starburst galaxies which are mass-matched to the star-forming sample. Post-starburst galaxies are overwhelming fit with large n, often running up against the $n = 6$ boundary. The Sérsic index distribution is distinct from that of star-forming galaxies, which favor small n. (Right) The distributions of axis ratios, defined as the ratio of the semi-minor axis to the semi-major axis. Star-forming galaxies show the most elongation, followed by quiescent galaxies, and post-starburst galaxies are slightly rounder than both. In both plots, the median of each distribution is shown as a dashed vertical line. The results of a Kolmogorov–Smirnov test between the quiescent and post-starburst distributions are shown on both figures.

encode information about the 3D structures and light profiles of galaxies and show different empirical trends for star-forming and quiescent populations [178, 214]. In Figure 18, we show the distributions in the Sérsic index and the axis ratio for post-starburst galaxies, as well as the mass-matched quiescent and star-forming control samples. As expected, the star forming sample and the quiescent sample are significantly different in their Sérsic index distributions; star forming galaxies are fit with small Sérsic index ($n_{med} \sim 2$) and quiescent galaxies are systematically fit with higher n ($n_{med} \sim 4$). Post-starburst galaxies have higher Sérsic indices than both of these samples, with a median Sérsic index of 5.2. These higher Sérsic indices are likely driven by the concentrated light of these objects, and visual inspection of the median 1D surface brightness profiles of the sample confirms that the majority of the galaxies are being well fit by these high Sérsic indices. We note, however, that many post-starburst and quiescent galaxies run up against the boundary we impose at n=6. We run a number of tests including residual inspection, fitting images with a central point source component in addition to a Sérsic profile, and expanding the threshold Sérsic index to n=8, in order to quantify the effects of the run-up against the boundary to our results. Ultimately, the qualitative results of the paper are insensitive to any changes to our fitting procedure, but we describe these tests below.

For the sample of SQuIGG$\vec{L}$E post-starburst galaxies, 36% galaxies run up against the n=6 boundary, whereas in the mass-matched quiescent sample 20% of the galaxies are best fit with n=6. In general, the Sérsic index is the least well constrained property in our fits, as it is extremely sensitive to the shape of the PSF model we use in fitting. Additionally, these uncertainties grow as a function of the best fitting Sérsic index, such that for galaxies with intrinsically high Sérsic indices (e.g., quiescent and post-starburst galaxies), the Sérsic indices are particularly poorly constrained. Visual inspection of the residual 1D surface brightness profiles of the galaxies which run up to the n=6 boundary show that, in contrast with the rest of the sample, these have median central mismatches of -0.04 mag/arcsecond^2. The models are systematically fainter in the center than the galaxies and brighter than the galaxies on scales of ~ 1". This imperfect agreement between data and model is what we would expect from a mismatch between the model PSF we use in the fitting of the galaxies and the true PSF of the galaxies, where the centrally concentrated light of the galaxies is

smeared by a PSF which is wider than the true PSF. In some cases (e.g. galaxy J0226+0018 in Table 3 and 4), a nearby PSF model is capable of causing the fit to converge to a Sérsic index which is within the range we allow, but in many cases all 50 fits in our rerun with nearby PSF models converge to the same n=6 value.

This issue of high-n pileup cannot be resolved by simply expanding the Sérsic index to higher values. We re-run our fits of the SQuIGG$\vec{L}$E sample with an upper boundary on the Sérsic index of n=8 and find that 20% of the galaxies still converge to the upper boundary and show the same characteristic residual shape as in the n=6 boundary fits, indicating that the light is generally not well fit by a Sérsic profile regardless of the limit we place on n. For the galaxies which were best fit with n=6 in the original fits, these new fits yield residual corrected sizes which are a median of 10% larger than those fit with n=6, which is a significant change but is not one which would significantly alter any of our conclusions about the size of the sample relative to co-eval galaxies. In addition, we also run a set of fits with an additional point source component fixed to the same centroid as the galaxy of interest. $\sim$ 25% of these fits fail to converge, and among those that do converge, the majority are fit with an essentially negligible point-source component (median Sérsic mag - point-source mag = -2.47). Additionally, the galaxies which are fit with significant with point source components tend not to be those which are at the n=6 boundary. We conclude that deviations from Sérsic profiles are likely being driven by PSF models which are not perfectly matched to the intrinsically high Sérsic index galaxies we are fitting. On the whole, all conclusions regarding the size of the galaxies are not strongly influenced by the inability to perfectly determine the Sérsic index, as evidenced by the very good match in the sizes of the LEGA-C quiescent galaxies we measure to those measured using HST/ACS imaging (see Appendix B.1).

The distribution of projected axis ratios for SQuIGG$\vec{L}$E post-starburst galaxies also skews significantly higher star-forming galaxies and slightly higher than quiescent galaxies. Taken together, these parametric measures indicate that post-starburst galaxies structurally appear to be fairly compact spheroids. If these galaxies began their lives as extended disks, any structural transformation must have pre-dated or occurred concurrently with the shut-down of star formation, such that they structurally compact $\sim$ 100 Myr after quenching.

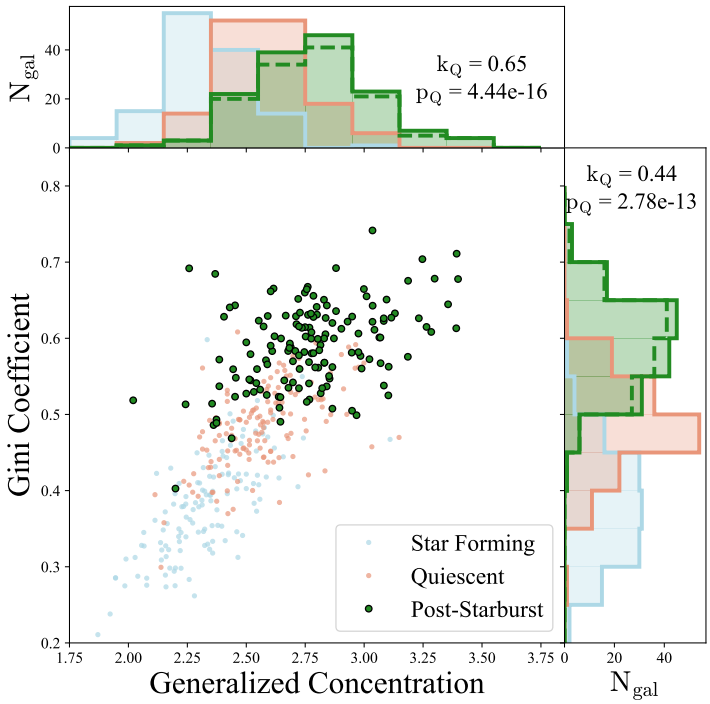

Figure 19: The Gini coefficient versus the generalized concentration for the mass-matched post-starburst (green), quiescent (red), and star-forming (blue) galaxies. The dashed post-starburst histogram shows the post-starburst galaxies which are mass-matched to the star-forming sample. These non-parametric measures of light concentration are strongly correlated. By both measures, the post-starburst population is more concentrated than both the quiescent and star-forming populations, in agreement with Sérsic parameters.

3.4.3 Non-parametric measures of structure

Although we have shown that the light profiles of the post-starburst galaxies and the coeval control sample do not significantly deviate from Sérsic, the assumption of Sérsic profiles, especially those which run up against an artificial barrier in Sérsic index n, may introduce model dependent effects that muddy interpretations of compactness. Therefore, as a parallel test, we turn to non-parametric measures, namely the Gini coefficient and the generalized concentration (GC), which we measure using the `GALMORPH` suite [86]. We use

the standard definition of the Gini coefficient defined in [2]. However, the definition of the generalized concentration differs from the traditional concentration statistic [44] by not using circular apertures but instead by comparing the minimum number of pixels which contain 20% of the galaxy's light (a_{20}) to the minimum number of pixels containing 80% of the galaxy's light (a_{80}) as follows:

$$\mathrm{GC} = 5 \log_{10} \frac{a_{80}}{a_{20}} \tag{4}$$

These measures rely only on the rank ordering of pixels after source identification is performed. Higher values of these parameters indicate a high concentration of light in very few pixels.

In Figure 19, we show the distributions of the post-starburst and control samples in this space for the mass-matched samples. The two measures are indeed correlated, and confirm the compact nature of post-starburst galaxies relative to the quiescent and star forming control samples. The post-starburst galaxies are particularly distinct from star-forming galaxies in Gini-concentration plane, indicating that if these galaxies are the descendants of similarly extended star-forming galaxies, they must have undergone a significant structural transformation. This is the same conclusion we draw from the parametric metrics (see Section 3.4.2).

3.5 The origins of compact post-starburst galaxy structure

In this section, we speculate on the origin of the compact structure and identify possible progenitors to the rapid channel of quenching.

3.5.1 Testing the central starburst scenario

Quenching caused by merger-driven central starbursts resulting in quenched galaxies have been shown to occur in simulations [17, 222], and gas-rich wet compaction events could similarly cause a centrally concentrated starburst which, post-burst, would appear compact

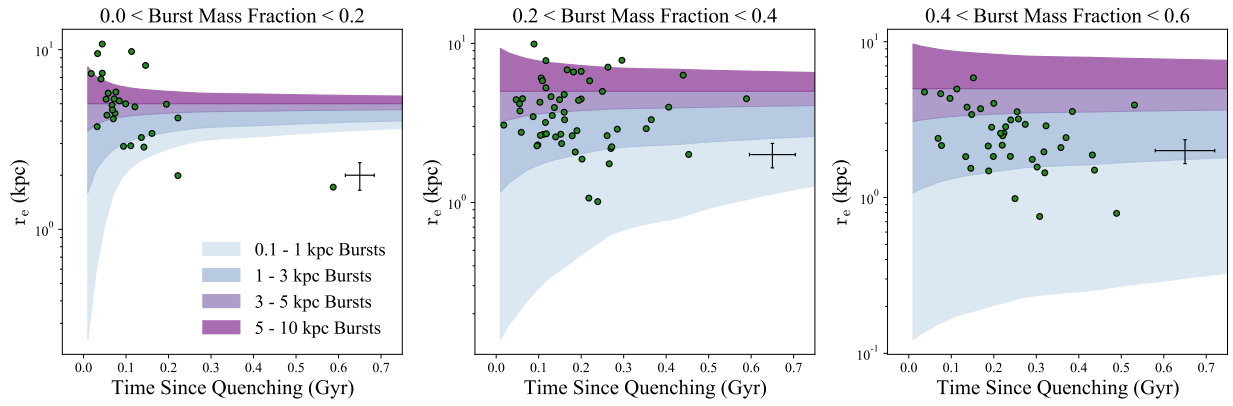

Figure 20: The half-light radius versus the time since quenching for the SQuIGG$\vec{L}$E post-starburst galaxies, divided into three bins of burst mass fraction (as measured in [191]). In the background, we shade the regions of size evolution populated by burst models described in Section 3.5.1 for a range of central burst sizes. We find that the majority of SQuIGG$\vec{L}$E post-starburst galaxies are inconsistent with the models of a sub-kpc scale burst, and can only be well-described by bursts that are extended on 1-10 kpc scales.

[200, 250]. Observations of post-starburst galaxies have suggested that their compact structures are consistent with being the result of a recent central starburst [239, 238, 59]. In addition, at redshifts similar to those of SQuIGG$\vec{L}$E, extremely compact starburst galaxies have been observed with $\sim 25\%$ of the mass of 10^{11} $M_{\odot}$ galaxies existing in the central ~ 100 parsecs [173, 62].

Our previous study of 6 galaxies in the SQuIGG$\vec{L}$E sample using spatially resolved spectroscopy measured flat age gradients, disfavoring formation via a secondary central burst of star formation [174]. However, if the recent burst of star formation totally dominates the light of the galaxy, hiding existing gradients, we would expect those signatures to fade with time. As the SQuIGG$\vec{L}$E sample spans a range of 0-700 Myr since quenching, we can use it to test whether galaxies are consistent with centralized starbursts imposed on older, more extended populations. Because the youngest, brightest stars in newly formed stellar populations die the most quickly, a central starburst's influence on the size of a galaxy would

become weaker with time, leading to size growth as a function of the time since quenching. In Figure 20, we show a subset of the SQuIGG$\vec{L}$E sample divided up into bins of burst mass fraction (as measured in [191]) to show trends for galaxies which formed a similar fraction of their stellar mass in the recent burst of star formation. None of these bins show the predicted positive trend for a central starburst; conversely, the smallest and largest burst fraction bins are consistent with a negative slope (Spearman correlations for the 0-20% bin: $\rho = -0.52, \mathrm{p} = 0.004$; Spearman correlations for the 40-60% bin: $\rho = -0.38, \mathrm{p} = 0.01$), and the central bin is consistent with no slope (Spearman correlation for the 20-40% bin: $\rho = -0.10, \mathrm{p} = 0.45$). We additionally test for correlations between the Gini coefficient and the generalized concentration parameters and find no significant correlation with the time since quenching. The lack of a positive correlation between these measures of concentration and the time since quenching suggests that highly centralized star formation is unlikely to have occurred prior to quenching in post-starburst galaxies.

We further illustrate this result via the use of a toy model of half-light radius evolution. Using `fsps` [43, 42, 83] to track the evolution of the rest frame optical light with time, we simulate the superposition of an instantaneous burst of star formation on an older galaxy population by modeling both the galaxy and the burst as n = 4 Sérsic profiles. We fix the older population to be 1 Gyr old and to have $\mathrm{r_e} = 5$ kpc, the approximate size of a $10^{11} M_\odot$ quiescent galaxy at this redshift. We test 3 burst regimes, 0 - 20% burst fraction (modeled with a 10% burst), 20 - 40% burst fraction (modeled with a 30% burst), and 40 - 60% burst fraction (modeled with a 50% burst), and a range of burst geometries ranging from an extremely centralized 100 parsec burst to an extended 10 kpc burst. We set the central and underlying dust attenuation to 0.5 and 0.1 dex respectively using the `fsps` `dust2` parameter to reflect that the central region may be significantly more attenuated than the older population, but still restricting to the range of best fitting dust values from spectrophotometric modeling (median `dust2` ~ 0.3, see [191]). We note that these assumptions neglect the possibility that heavily obscured star formation is contained in the galaxies. Some post-starburst galaxies have been shown to contain deeply embedded dust reservoirs in the central ~ 100 parsecs with $A_\mathrm{v} \sim 10^4$, which could in principle shield large amounts of central star formation [181]. However, in a previous study of CO(2-1) for a small (13 galaxy)

subsample of SQuIGG$\vec{L}$E, we do not see evidence of centrally concentrated molecular gas or continuum emission in the detected galaxies at $\sim$ 1" resolution. We measure molecular gas effective radii on the order of kiloparsecs and do not detect continuum emission in all but one galaxy [20]. As such, we assume dust obscuration informed by our best fits to OIR spectrophotometric data.

We show the tracks generated by these models as shaded regions on Figure 20. The vast majority of SQuIGG$\vec{L}$E galaxies are inconsistent with a sub-kpc scale burst of star formation. To ensure that these conclusions are not heavily dependent on toy model assumptions about the underlying galaxy age and size, we test for a range of values (r_e = 3 kpc and 10 kpc, age = 0.5 Gyr) and find that the majority of galaxies are too large to ever overlap with the sub-kpc burst tracks. We note that these observed kpc-scale bursts of star formation do not completely eliminate mergers as a possible trigger for inducing the burst and subsequent suppression of star formation, as IFU studies of post-merger galaxies have found evidence for centrally peaked but still global enhancements in star formation rate [207]. The lack of agreement between models for a highly concentrated burst of star formation and the size-age trends we observe only shows that star formation could not have occurred solely in the central regions of recently quenched galaxies.

The negative/inconclusive trends in r_e versus time since quenching indicate that these post-starburst galaxies do not evolve significantly in their $\sim$ 500 Myr after quenching and that the youngest stars in the galaxy are distributed on spatial scales similar to any underlying older population. This is consistent with the finding that a small sample of SQuIGG$\vec{L}$E post-starburst galaxies exhibit flat age gradients [174], which are also seen in young quiescent galaxies closer to cosmic noon [5, 107] and compact local quiescent galaxies that may be the descendants of early universe rapid quenching [172]. As we are still accounting for some unmasked tidal light in the fits to our galaxy sizes (see Figure 14), we propose that any negative trend in time since quenching versus size may be the result of tidal features which are commonly present in the young post-starburst galaxies [167, 219] and which fade on $\sim$ 200 Myr timescales. There is evidence for this when we split the sample into disturbed and non-disturbed using the classifications from [219], as the youngest galaxies in the sample are far more likely than the oldest ones to host visible tidal features. However, we note

that the sizes of the galaxies we fit are not being primarily driven by asymmetric non-Sérsic light, as the corrections for the disturbed and non-disturbed samples are both consistent with no systematic offset in measured half-light radius, and instead are primarily driven by the central light of the galaxy due to our aggressive deblending and masking.

Why, then, do the SQuIGG$\vec{L}$E post-starburst galaxies differ from other populations of post-starburst galaxies whether locally [237] or at intermediate-redshift [239, 59] which do show evidence of centrally concentrated star formation? The answer may lie in selection. High mass galaxies in samples selected using $H_{\delta,A}$ equivalent width techniques like those in [239] have been shown to have very small burst mass fractions, on the order of $\sim 5\%$ [90]. The bursts in these galaxies are weak relative to the $> 20\%$ bursts in SQuIGG$\vec{L}$E galaxies which are completely dominated by A-type populations [191]. The galaxies with small bursts may represent a dusting of central star formation on top of an already quiescent population (which is similar to the toy model which does a poor job of describing SQuIGG$\vec{L}$E post-starburst size evolution) rather than a true quenching of a galaxy's primary epoch of star formation that occurs in the entire galaxy simultaneously. High redshift, massive post-starburst galaxies have been found to lack color gradients, suggesting that galaxies must shut off star-formation such that a young stellar population dominates the light at all radii on kiloparsec scales in the immediate aftermath of quenching [135, 194]. These fundamental differences in the galaxy masses, burst mass fractions, and stellar age distributions between low- and high-redshift post-starburst galaxies may be the result of fundamentally different physical processes (e.g. increased major merger rates or higher gas fractions at earlier cosmic time). We suggest that the SQuIGG$\vec{L}$E post-starburst galaxies are the lower-z extension of that population of rapidly quenching galaxies, and explore in the following section what progenitors could have resulted in the formation of compact post-starburst galaxies without purely central star formation.

3.5.2 Preferential fast quenching in compact star-forming galaxies

The commonly invoked central starburst pathway to quiescence is often proposed as a way to take an extended star-forming galaxy and to produce a more concentrated elliptical galaxy.

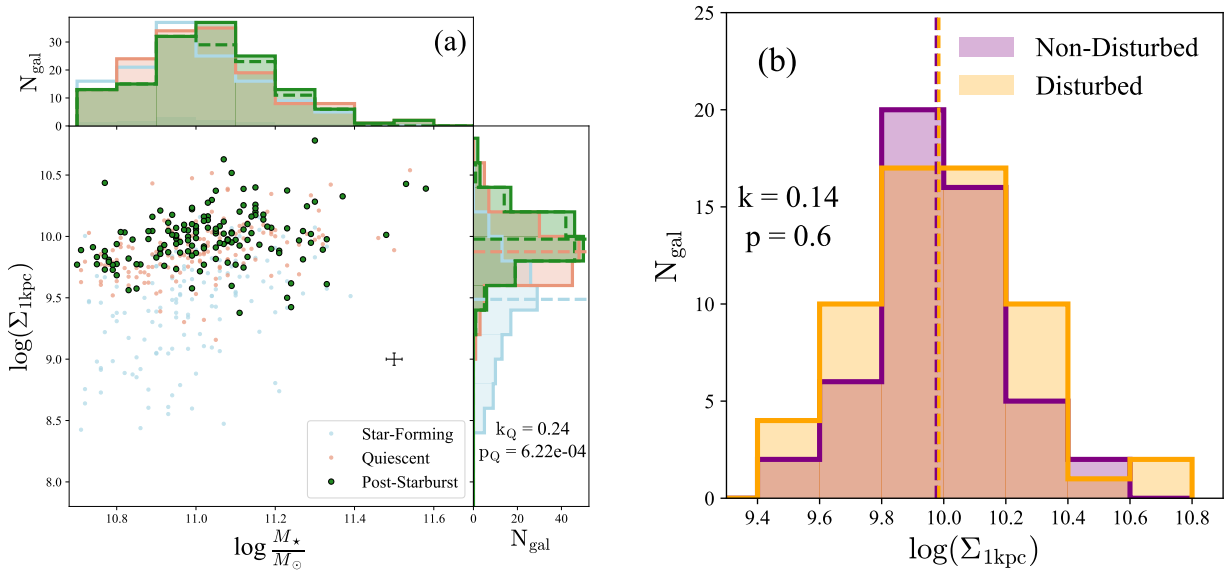

Figure 21: (Left): The stellar mass surface density in the central kpc as a function of the stellar mass for SQuIGG$\vec{L}$E along with the star-forming and quiescent sub-samples. Typical error bars derived from the PSF shuffling procedure are shown in black. The dashed post-starburst histogram shows the post-starburst galaxies which are mass-matched to the star-forming sample. SQuIGG$\vec{L}$E galaxies are only slightly denser than quiescent galaxies, while star-forming galaxies are significantly less dense than both populations. The results of a Kolmogorov–Smirnov test between the quiescent and post-starburst $\log(\Sigma_{1kpc})$ distributions are shown on the verticle histogram. (Right): The distributions of in $\log(\Sigma_{1kpc})$ for the disturbed and non-disturbed post-starburst populations, as defined in [219]. As with the compactness at fixed stellar mass (see Figure 17), a Kolmogorov–Smirnov test shows that the distributions are not significantly different between the two populations. The SQuIGG$\vec{L}$E sample of post-starburst galaxies is uniformly dense in its core regions.

However, galaxies need not shrink down in the size-mass plane. Instead, these galaxies may have small sizes because they are the evolutionary descendants of more compact star-forming galaxies, which quenched rapidly after reaching a stellar density threshold that is correlated with other feedback mechanisms [217].

In Figure 21a we show the relationship between the stellar mass and stellar surface mass density in the central kpc for the galaxies in SQuIGG$\vec{L}$E and LEGA-C. Post-starburst galaxies are only slightly denser than the quiescent galaxies at this redshift (median $\log(\Sigma_{\rm 1kpc,PSB}) - \log(\Sigma_{\rm 1kpc,Q}) = 0.10$). In contrast, the post-starburst and quiescent samples are significantly more dense than star-forming galaxies at fixed stellar mass (median $\log(\Sigma_{\rm 1kpc,PSB}) - \log(\Sigma_{\rm 1kpc,SF}) = 0.48$). The density of the post-starburst galaxies is similar to those found in previous studies of quiescent galaxies at this stellar mass, $\log(\Sigma_{\rm 1kpc}) \sim 10$ [79, 217, 14, 143, 225, 195]. This supports the finding that galaxy structure in the central regions is largely set at the time quenching occurs. In addition, we find that dense central structures are in place for the entirety of the SQuIGG$\vec{L}$E sample, regardless of the presence of tidal features; in Figure 21b, we show that there is no significant difference in $\Sigma_{\rm 1kpc}$ between the disturbed and non-disturbed populations. This does not preclude mergers helping the galaxies reach the central density threshold required for shutdown; simulations which rely on AGN feedback to quench galaxies have shown that only mergers which push galaxies into the regime where their central black holes are massive enough to trigger feedback effectively quench galaxies [161], and more rapid quenching is strongly associated with an increased injection of AGN feedback prior to quenching [153]. However, it does suggest that mergers may not be the smoking gun progenitor of all post-starburst galaxies.

Because the central mass of a galaxy and the black hole mass are strongly correlated [120], it is natural to investigate the incidence of AGN in these dense post-starburst galaxies. The youngest galaxies in SQuIGG$\vec{L}$E host optical AGN at significantly higher rates than the oldest post-starburst galaxies and older quiescent galaxies [97]. If feedback from AGN is connected to density, then it is possible that these galaxies went through a quasar phase which is still turning off in the youngest galaxies in the sample and that the galaxies will remain quenched after the AGN runs out of fuel and shuts down due to radio-mode feedback [47]. After that, minor mergers will contribute to the growth in outer density to grow

galaxies without substantially changing their central density [22, 218]. This ex-situ growth could lead to a better match in the half-light radii of the galaxies as they grow their sizes without significantly changing their central structures.

The similar central densities and discrepant half-light radii of post-starburst and quiescent galaxies implies that the profiles should differ in shape most significantly in the wings if ex-situ growth is the dominant mode of evolution post-quenching. To investigate this, we derive one-dimensional surface mass profiles for the post-starburst and quiescent galaxies by multiplying the observed surface brightness profiles by the mass-to-light ratio, assuming no radial gradients. In Figure 22, we show the median surface mass profiles for the post-starburst and quiescent samples with associated scatter, as well as the difference between the median profiles. The ex-situ growth hypothesis is supported by these stellar-mass profiles, as the differences between the median profiles increases steadily out to $a = 10$ kpc. This profile difference at large radii is likely less extreme in reality due to the empirical color gradients found in quiescent galaxies [192, 193, 194, 116]. Quiescent galaxies tend to be bluer in their outskirts, which would lead to a smaller mass-to-light ratio and would alleviate at least some of the tension between these profile shapes. However, the color gradients present in quiescent samples are likely the result of the minor mergers we suggest are the dominant growth path post-quenching, and this normalization scheme still shows that the shapes of the profiles are most significantly different at $a > 10$ kpc. Taken together, we suggest that in rapid quenching, the seeds of the structure of the quiescent population are formed in the recent burst on kpc scales, after which feedback correlated with density suppresses any additional star formation and minor mergers become the primary form of galaxy mass growth.

One possible class of progenitors could be dusty, extreme starbursts, or "sub-mm galaxies" [209, 210, 231], which have the extremely high star formation rates and feedback necessary to produce galaxies like those in SQuIGG$\vec{L}$E [186, 185]. At high redshift, sub-mm galaxies also lie slightly below quiescent galaxies in the mass-size plane [95]. If they shut off their rapid star formation abruptly and uniformly, sub-mm galaxies would likely result in post-starburst SEDs and flat age gradients similar to those measured in SQuIGG$\vec{L}$E galaxies [174]. While detailed analysis of number densities is beyond the scope of this work, we note that in LEGA-C, star-forming galaxies do exist which are dense enough in $\log(\Sigma_{1\mathrm{kpc}})$ to

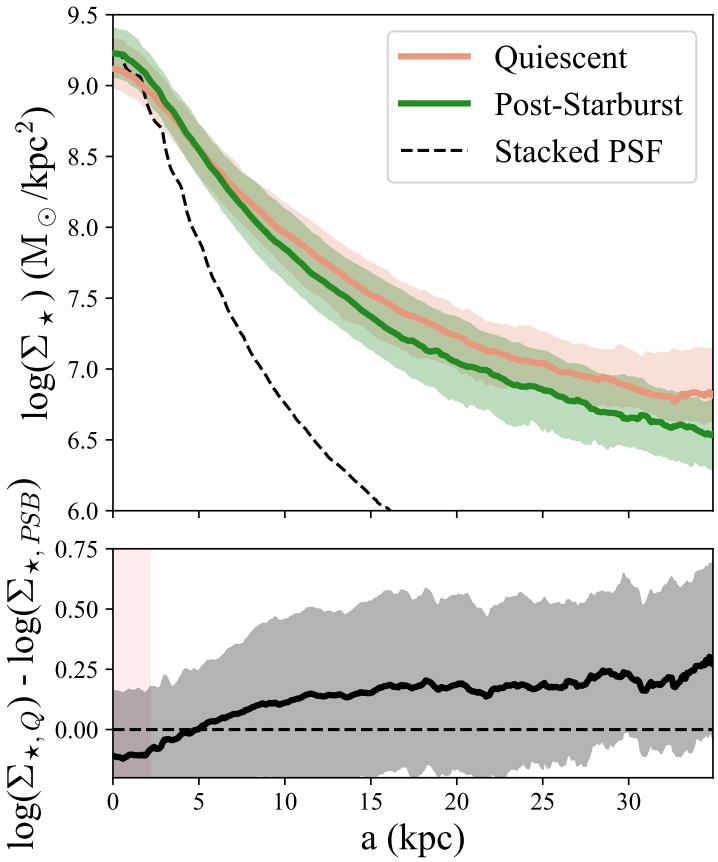

Figure 22: One-dimensional median stacks of the surface mass profiles of SQuIGG$\vec{L}$E post-starburst galaxies (green) and the mass-matched LEGA-C control sample (red) as a function of the semi-major axis of the best-fitting ellipse in kiloparsecs. The profiles are truncated at the radius where the number of galaxies used in the stack drops below 20. Also shown is a stack of the model point-spread functions used in the fits (black dashed line). The bands bound the 16th and 84th percentile surface mass profiles for each sample. In the bottom panel, we show the difference between the quiescent and post-starburst median profiles as a black line with combined scatter indicated as a grey band, with the half-width half maximum seeing (0.3"$\sim$2.1 kpc at z=0.7) indicated by the pink shaded region. The differences in the profiles increases as a function of radius, flattening at $\sim$ 10 kpc.

evolve into SQuIGG$\vec{L}$E post-starburst galaxies without a significant amount of additional compaction. These galaxies do not have star formation rates high enough to be sub-mm galaxies, but it is unlikely that such extremely rare progenitors would be found in a field as small as that of LEGA-C. Future work will focus on more strongly constraining the density of SQuIGG$\vec{L}$E-like post-starburst galaxies as a function of redshift to tie them more concretely to a progenitor population.

Ultimately, we conclude that the recent star formation in post-starburst galaxies must have taken place on spatial scales which are comparable to the size of the galaxy, as we do not see any evidence of the type of fading that would be expected from a centralized starburst. Although galaxy mergers likely play a role in quenching some of the post-starburst galaxies in SQuIGG$\vec{L}$E (see [219]), the finding that $\log(\Sigma_{1\mathrm{kpc}})$ is fully consistent between the disturbed and non-disturbed samples and the lack of positive size evolution suggests that merger driven central starbursts are not the entire story. Instead, the mergers may, in some galaxies, simply be the last push towards a central density high enough to trigger feedback which rapidly shuts off star formation while locking in existing structure and maintains the shutdown. After this, galaxies could passively evolve into red, quiescent galaxies that grow in half-light size via minor mergers but otherwise do not significantly change in their structures.

3.6 Conclusions

Using images from the Hyper-Suprime Cam Survey, we study the sizes and structures of $z \sim 0.7$ post starburst galaxies from the SQuIGG$\vec{L}$E Survey [191] in comparison to coeval massive galaxies in the LEGA-C Survey. By performing single-component Sérsic fitting of the galaxies, we have robustly measured sizes which account for non-Sérsic low surface brightness features and structural measures like the Sérsic index and the axis ratio. In addition, we measure non-parametric indicators of concentration. We conclude the following:

- Post-starburst galaxies have smaller half-light radii than coeval star-forming and quiescent galaxies at similar stellar mass (see Figures 16 and 17). Specifically, they are systematically $\sim$0.1 dex smaller than quiescent galaxies and $\sim$ 0.4 dex smaller than star-

forming galaxies. The compactness at fixed stellar mass does not vary strongly based on whether or not a galaxy is tidally disturbed.

- The sizes and structures of post-starburst galaxies, as measured via parametric (see Figure 18) or non-parametric measures (see Figure 19) also point to concentrated, round galaxies which are more similar to quiescent galaxies than they are to star-forming galaxies.
- Post-starburst galaxies either negative or flat correlation between their sizes and their time since quenching (see Figure 20). This trend stands in constrast with what would be expected for a fading central starburst, indicating that the recent burst of star formation was not limited to the galaxy center, and instead must have occurred on larger ($\gtrapprox$ 1 kpc) spatial scales.
- The central densities of post-starburst galaxies are very similar to those of quiescent galaxies (see Figure 21) and match the common threshold for quiescence, $\log(\Sigma_{1\mathrm{kpc}})$ $\sim$ 10 found in the literature.
- The median shape of the post-starburst and quiescent surface brightness profiles are most significantly different at large radius (a>10 kpc), where the quiescent sample has more light (see Figure 22). This indicates that while the central shapes of galaxies do not change significantly once quiescence is reached, the outer envelopes may indeed grow via minor merging which deposits stellar mass as large radius.

Two competing forces are at play in the detailed study of the rapid mode of quenching. On the one hand, fast quenching dominates at high redshift, so in the ideal case one would hunt for post-starburst galaxies at the highest redshift possible in order to identify candidates for galaxies which have recently shut off their primary epoch of star formation. On the other hand, in order to push to high redshift, deep integration times are required, which makes it difficult to cover the large patches of sky necessary to identify galaxies in this short-lived period of evolution. The ideal situation (deep, red spectroscopic surveys of large areas of the sky), however, is right around the corner with the impending public releases of deep spectroscopic surveys like the Dark Energy Spectroscopic Instrument [56] and the Prime Focus Spectrograph [203] surveys. In the very near future, the high-quality spectra from these surveys will allow for the identification of large samples of post-starburst galaxies out

past $z \sim 1$. Future studies of the galaxies identified in these surveys will significantly bolster our understanding of the rapid mode of quenching by identifying the first statistically large samples of post-starburst galaxies near the era of cosmic noon. The quantification of the number density, size, structure, AGN activity, and gas content of post-starburst galaxies as a function of redshift will place strong constraints on the rapid quenching pathway of galaxy evolution.

4.0 DESI Survey Validation Spectra Reveal an Increasing Fraction of Recently Quenched Galaxies at $z \sim 1$

4.1 Introduction

In the local Universe, the vast majority of massive ($\log(M_\star/M_\odot) \gtrsim 11$) galaxies are completely quiescent and have been so for $5-10$ Gyr [145, 64, 127, 220]. There is a growing consensus that two distinct pathways to quiescence are at play, with a rapid path dominating the buildup of quiescent galaxies at high redshifts and a slower channel that populates the "green valley" at low redshift [168, 239, 135, 19, 195]. While the observational evidence for more rapid early star-formation in the most massive systems at early times is strong [111], the precise details of how the quiescent population grows from the rapid quenching pathway as a function of cosmic time remain very uncertain. Some studies have characterized the rates of rapid quenching as a function of cosmic time using either photometric [226, 230, 19, 152] or shallow spectroscopic [162] samples and have found that recently quenched galaxies, sometimes known as post-starburst galaxies, stopped contributing significantly to the quiescent population by $z \gtrsim 0.5$. However, photometric studies yield weak constraints on timescales and star formation histories. Thus, our picture of precisely when galaxies shut off their star formation and the contribution of late-time star formation remains poorly constrained.

Ideally, one would study the assembly of the red sequence by modeling the star-formation histories of complete samples of massive galaxies and studying how the incidence and characteristics of the population vary as a function of cosmic time. An immense amount of work has been done over the past decades to study that star formation histories of quiescent systems across cosmic time using photometric and spectroscopic data [208, 70, 69, 93, 92, 48, 150, 35, 19, 199]. However, measuring the high-order moments of a star-formation history, such as timescales and burst fractions, requires high signal-to-noise continuum spectroscopy [196]. The limiting factor in performing such modeling has been the availability of sufficiently deep spectra beyond $z \gtrsim 0.5$. The largest existing spectroscopic samples have not

prioritized observing the gamut of quiescent galaxies; the SDSS LRG [73] and BOSS [53] surveys targeted the reddest quiescent galaxies, prioritizing pure, uniform samples at the expense of younger, bluer galaxies, with targeting that steeply drops off at $z \sim 0.5$ where the post-starburst population beings to emerge [230, 19]. In contrast, the EBOSS [52] survey poorly sampled the quiescent population in favor of more accessible emission line sources. Deeper, more targeted surveys such as LEGA-C [216, 239], Carnegie-Spitzer-IMACS [69], and VANDELS [142, 35] have identified samples of ∼1000s of massive quiescent galaxies at $z \gtrsim 0.5$, requiring significant investments on deep fields to reveal spectroscopic information for small samples.

The next generation of large spectroscopic surveys will revolutionize the availability of continuum spectroscopy of massive galaxies. Here, we utilize the Dark Energy Spectroscopic Instrument (DESI), a robotic, fiber-fed, highly multiplexed spectroscopic surveyor that operates on the Mayall 4-meter telescope at Kitt Peak National Observatory [56]. DESI, which can obtain simultaneous spectra of almost 5000 objects over a $\sim 3^\circ$ field [57, 180], is currently over a year into a five-year survey of approximately one-third of the sky [56], and has already observed more galaxies than the entire Sloan Digital Sky Survey. The DESI Luminous Red Galaxy (LRG) target selection is both broader in color and faintness relative to surveys like BOSS, and as a result is complete to higher redshift ($z \sim 0.8$) and observes the Balmer break out to $z \sim 1.3$ [248]. Here we show that even the relatively small ($\sim$ 20000 galaxies) but deep Survey Validation (SV) sample of LRGs within the DESI Survey can be leveraged to identify new and exciting samples of recently quenched galaxies that push well beyond what previous surveys have been capable of.

In this letter, we infer non-parametric star formation histories of LRGs in the DESI SV sample (DESI Collaboration et al. in preparation) and use them to study the growth of the red sequence from recently quenched galaxies. In Section 4.2, we describe the parent sample and demonstrate the use of non-parametric star formation histories to fit the spectrophotometric data with `Prospector` [110, 125, 109]. In Section 4.3, we use the results of this fitting to identify recently quenched galaxies and characterize their evolving number densities as a function of cosmic time. Finally, in Section 4.4, we discuss the implications of these findings on our understanding of the physical mechanisms that are driving the production of massive,

quiescent galaxies through the rapid quenching channel.

Throughout this letter, we compare our own selection of "recently quenched galaxies" to literature samples and selection criteria for post-starburst galaxies. We note that many of these post-starburst selections do not explicitly require a burst of star formation, as any dramatic truncation in star formation can produce an A-star dominated SED.. We assume a concordance ΛCDM cosmology with $\Omega_\Lambda = 0.7$, $\Omega_m = 0.3$ and $H_0 = 70$ km s^{-1} Mpc^{-1}, and quote AB magnitudes.

4.2 Data

4.2.1 The DESI LRG SV Sample

In order to characterize the growth of the population of quiescent galaxies at intermediate redshifts, this work relies on the large program of deep spectra that were taken as a part of the DESI SV LRG sample [249, 248]. The primary objective of DESI is to determine the nature of dark energy with precise cosmological measurements [129], but the wealth of spectroscopy provides an excellent sample for studies of galaxy evolution. The data volume of the DESI requires multiple supporting software pipelines and products used in this work. Target selection and photometry, which included forward modeling of the differential effect of the PSF across bands, was performed on imaging from the DESI Legacy Surveys [251, 60]. Fiber assignments, tiling, and target selection were performed with the algorithms outlined in Raichoor et al., Schlafly et al., and Myers et al. (in preparation) respectively. All redshifts were determined with the `Redrock` pipeline (Bailey et al. in preparation). All spectroscopy used was reduced using the "Fuji" internal spectroscopic data release which will be identical to the DESI Early Data Release [98].

There are two primary reasons for the choice to utilize the SV sample. First, the SV selection is more inclusive than subsequent Survey Validation samples and the main DESI sample [248]. While this was intended as a test of the redshift recovery so that targeting could be refined from the main survey, these expanded color cuts mitigate potential bias against

observing young, recently quenched LRGs. Second, the SV observations were an order of magnitude deeper than the observations for the main survey, with ~ 2.5 hours of integration per spectrum, resulting in the high signal-to-noise measurements of the continuum. While the SV sample included fainter targets, we restrict this study to the brightest SV LRGs with an observed fiber z magnitude $z_{\rm fiber} < 21.6$ cut similar to the one that is used in the full LRG sample.

We select all tiles that were observed under the dark time observing conditions in SV. We then select all galaxies which meet the LRG SV cuts outlined in [248] with an additional $z_{\rm fiber} < 21.6$ magnitude constraint, a cut at $z > 0.4$ (above which the SV LRG sample begins to be mass complete), and a cut at $z < 1.3$ (at which point the age-sensitive H_δ absorption feature is no longer covered by DESI spectroscopy). We remove galaxies with poor redshift measurements by applying a cut of `ZWARN` $== 0$ to the DESI catalog. We then remove the 580/17797 galaxies that did not reach target depth (exposure time $t_{\rm exp} > 1$ hour). The median exposure time of this final sample is 2.4 hours, with 16th and 84th percentile exposure times of 1.5 and 4.1 hours respectively. This selection results in a total sample of 17217 galaxies.

4.2.2 Inferring Star Formation Histories with `Prospector`

We model the DESI spectra and photometry using non-parametric star formation histories with the SED fitting code `Prospector` [110, 125, 109] to infer the detailed stellar populations of the sample. Non-parametric star-formation histories (SFHs) are particularly useful for fitting post-starburst galaxies because they do not impose an analytic form on the shape of the SFH, which allows for multiple rises and falls over the course of a galaxy's lifetime. We adopt a flexible bin model that is optimized to model recently quenching galaxies [196]. The model utilizes 3 fixed time bins at early times ($t_{\rm lookback} > 2$ Gyr), 5 flexible bins that each form the same amount of total stellar mass (allowing for greater resolution near periods of intense star-formation), and a final flexible bin that allows a galaxy to remain quenched after star formation is finished. This scheme was extensively tested and is well designed to recover quenching timescales and burst mass fractions [196, 191].

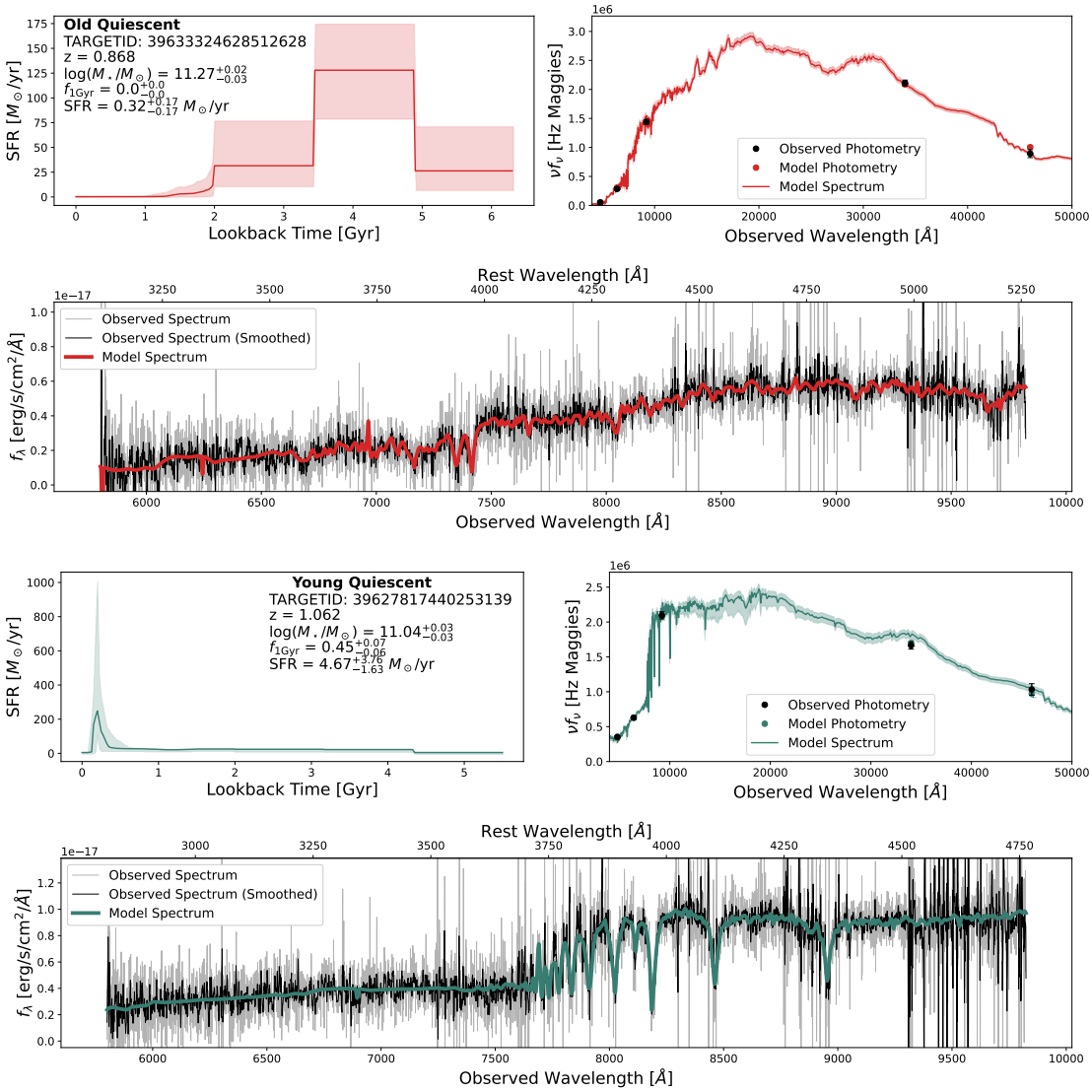

Figure 23: Example old (top, TARGETID=3963332462851262) and recently quenched (bottom, TARGETID=39627817440253139) galaxies from the DESI SV LRG Sample with `Prospector` fits using the star-formation history model from [196]. For each galaxy, we show the median and 68% confidence interval star-formation history (top left) with selected galaxy properties. We also show the best fitting models (color) to the observed photometry ($g/r/z/W1/W2$, black) (top right). Finally, we show the DESI spectrum (observed, grey; 5 pixel boxcar smoothed, black) along with the best fitting model (color) (bottom). From this modeling, we identify quiescent LRGs and infer the dominance of recent star formation and the timescale of quenching.

We use the `dynesty` dynamic nested sampling package [183], the Flexible Stellar Population Synthesis (FSPS) stellar population synthesis models [43, 42], the MILES spectral library [165, 78], and the MIST isochrones [40, 65]. We assume a [38] Initial Mass Function and fix the model redshift to the spectroscopic redshift. In contrast with the [191] prescription for fitting post-starburst galaxies, we elect to fit nebular emission non-physically by marginalizing over Gaussian lines at the locations of emission features in the spectrum. The massive LRG sample likely hosts many active galactic nuclei (AGN) which can contribute strongly to a galaxy's emission line strength [97]. Additionally, the LRG selection allows for the targeting of a small fraction of dusty star-forming galaxies with strong emission lines; we want to be completely agnostic to the source of emission when fitting star formation histories to these galaxies. This procedure subtracts out the emission from the spectrum at each step in the fitting before calculating the likelihood, which allows the fits to utilize continuum information (e.g. $H\beta$ absorption) despite the existence of emission that our models do not generate using information about the current SFR.

We use the mass–metallicity prior described in [124]. We utilize the `PolySpecModel` procedure which accounts for deviations between the shape of the photometry and the spectrum by dividing out a polynomial from the observed and model spectra during fitting, using a `Prospecter`-default 12th order Chebyshev polynomial. We assume the [121] dust law with a free A_v and dust index. Additionally, following [231], we assume that the attenuation is doubled around young ($< 10^7$ yr) stars. We fix the shape of the IR SED following the [66] dust emission templates, with $U_{\rm min} = 1.0$, $\gamma_e = 0.01$, and $q_{\rm PAH} = 2.0$. Finally, we include both a spectroscopic jitter term to account for the possibility of underestimated noise and the `Prospector` pixel outlier model. We center priors on the SFH such that they follow the predicted SFH of a massive quiescent galaxy from the `UNIVERSEMACHINE` catalog [16]; this weakly prefers solutions with early-time star formation in the star formation histories we fit to ensure that outshining of a young stellar population is treated conservatively. The fidelity of this star formation history at recovering mock parameters is illustrated in [196]. Of principle importance to this work, the burst fraction is well recovered when $< 50\%$ of a galaxy's stellar mass is formed in a burst. For greater burst fractions, outshining by the young stellar population becomes so dominant that the relative strength of the oldest stellar

population cannot be constrained by the existing data, and as such, our conservative prior drives the fits to a higher burst fraction solution than the inputs. Thus, burst fractions measured in this work to be $\gtrsim$50% can be thought of as strong lower limits.

We fit all 17217 galaxies in the DESI SV LRG sample ($z_{\rm fiber} < 21.6$) with this procedure, providing the Milky Way extinction corrected $g/r/z/W1/W2$ photometry (using the extinction maps from [170]) and the galaxy spectrum. The scaling of the SED being fit is set by the photometry that captures all galaxy light rather than just the light in the fiber. We expect the total fraction of galaxy light contained in the fiber to vary as a function of redshift but to always be $\gtrsim$ 50% of the total light, as the fiber size is 0.75" in radius (4 kpc at z=0.4, 6.5 kpc at z=1.3). Our fits are constrained by the SED shape of the photometry , and the polynomial correction to the spectrum will account for any color gradients, though we expect those to be minimal given that both the spectrum should be representative of the majority of the galaxy light for most of the sample. Because the signal in the redshift range of interest is concentrated at the red end of the spectrograph, we elect to only fit the spectra from the R and Z arms of the spectrograph (5800Å $< \lambda_{\rm obs} <$ 9824Å) to save on computation time and to avoid any issues with the flux calibration at the fainter end of the spectra. In this wavelength range, the resolution R ($\lambda/\Delta\lambda$) ranges from $\sim 3200 - 5100$. While the 1.5" ($\sim$8 kpc at $z = 0.4$, $\sim$13 kpc at $z = 1.3$) diameter aperture of the DESI fiber is large enough to capture the majority of galaxy light at highest redshift end of our sample, we do note that our modeling approach assumes a lack of color gradients in the galaxies and that the light represented in the spectrum is identical to that of the photometry, which models all galaxy light. Fits failed to converge for 52/17217 galaxies (0.3% of the total sample). Visual inspection of the spectra of these failed fits suggests that they broadly fall into four categories: extremely low signal-to-noise galaxies, spectra with large masked regions, galaxies with incorrect redshift assignment, and broad-line AGN/QSOs (which our models are not equipped to characterize). As such, we omit the unmodeled galaxies and perform all analysis on the 17703 successfully fit galaxies.

Example fits to quiescent (top, red) and recently quenched (bottom, green) galaxies are shown in Figure 23. The quiescent galaxy that is representative of the majority of the DESI LRG sample is fit entirely with early star formation, consistent with a very old stellar

Table 5: Selected Fit Quantities and Errors

z	$\log(M_\star/M_\odot)$	SFR $[M_\odot/\mathrm{yr}]$	ΔSFR	$f_{1\mathrm{Gyr}}$
0.5568	$11.23^{+0.01}_{-0.01}$	$2.31^{+0.47}_{-0.35}$	$-1.16^{+0.08}_{-0.07}$	$0.11^{+0.01}_{-0.01}$
0.6701	$11.22^{+0.01}_{-0.01}$	$1.17^{+0.14}_{-0.14}$	$-1.52^{+0.05}_{-0.06}$	$0.0^{+0.0}_{-0.0}$
0.8976	$11.23^{+0.02}_{-0.1}$	$0.92^{+0.84}_{-0.31}$	$-1.76^{+0.39}_{-0.18}$	$0.0^{+0.07}_{-0.0}$
0.5396	$11.36^{+0.01}_{-0.01}$	$2.98^{+0.4}_{-0.34}$	$-1.16^{+0.06}_{-0.06}$	$0.05^{+0.01}_{-0.02}$
0.4364	$11.12^{+0.01}_{-0.01}$	$2.85^{+0.27}_{-0.24}$	$-0.9^{+0.05}_{-0.04}$	$0.01^{+0.0}_{-0.0}$
0.8807	$11.34^{+0.03}_{-0.03}$	$0.08^{+0.28}_{-0.08}$	$-2.86^{+0.62}_{-1.51}$	$0.0^{+0.0}_{-0.0}$
0.6999	$10.8^{+0.03}_{-0.04}$	$19.39^{+2.56}_{-2.4}$	$0.08^{+0.07}_{-0.09}$	$0.22^{+0.05}_{-0.04}$
0.5415	$11.11^{+0.04}_{-0.03}$	$0.09^{+0.05}_{-0.04}$	$-2.45^{+0.19}_{-0.28}$	$0.01^{+0.01}_{-0.0}$
0.5166	$11.2^{+0.02}_{-0.03}$	$21.25^{+2.17}_{-3.02}$	$-0.15^{+0.06}_{-0.08}$	$0.1^{+0.02}_{-0.02}$
1.0623	$11.04^{+0.03}_{-0.03}$	$4.67^{+3.76}_{-1.63}$	$-0.94^{+0.26}_{-0.18}$	$0.45^{+0.07}_{-0.06}$

Selected median and 68% confidence values of relevant parameters derived from the posteriors of the `Prospector` fits to DESI SV LRGs for a random sample of galaxies.

population, and as such, all the mass was formed in the three fixed-width early-time bins. In contrast, the recently quenched galaxy is clearly fit with a post-starburst SED shape with strong Balmer absorption features and a characteristic lack of emission line infill. This indicates that the post-starburst galaxy has quenched after a period of intense star formation, and the star formation history reflects this. We infer that the galaxy began rapidly forming stars ~ 500 Myr before observation, and quenched ~ 150 Myr ago.

From the posteriors on the star formation histories, we derive a number of model parameters, many of which we directly use to select and characterize the properties of recently quenched galaxies. Stellar masses are calculated accounting for mass loss and have typical 1σ uncertainties of 0.025 dex, and rest absolute magnitudes are calculated directly from the spectra generated from the posterior. We measure the star-formation rate in all galaxies as the star-formation rate in the closest bin to the epoch of observation in the non-parametric star formation history. Above $\sim 1 M_\odot/\mathrm{yr}$, these star-formation rates have been shown to reliably recover the instantaneous star-formation rate of mock galaxies, and our measurements have typical uncertainties of $\sim 15\%$. Below this, they are effectively upper limits [196]. Additionally, we quantify the offset from the star-forming sequence, ΔSFR, as:

$$\Delta\mathrm{SFR} = \log(\mathrm{SFR}) - \log(\mathrm{SFR}_{\mathrm{SFS}}(\mathrm{z})) \tag{5}$$

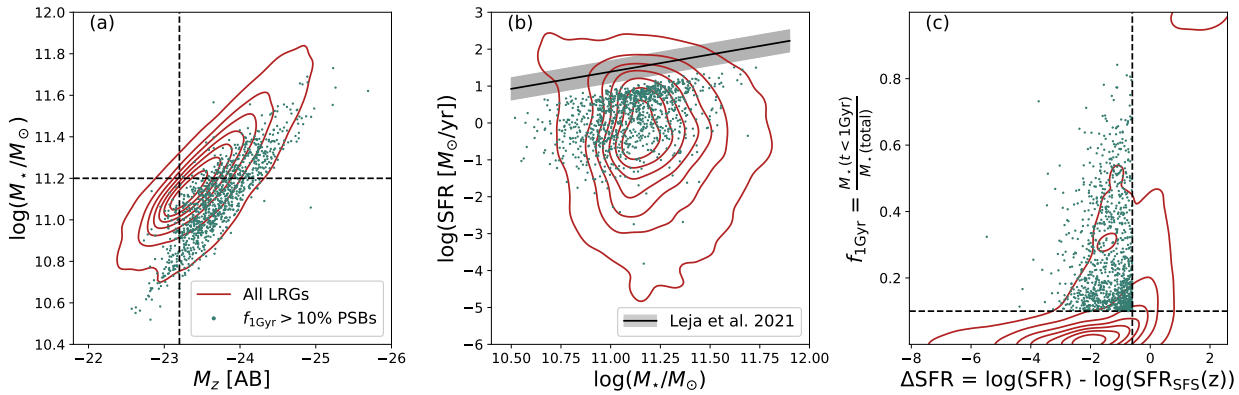

Figure 24: Properties of the full LRG sample (red contours) and a subset of galaxies that recently quenched a significant episode of star formation using our fiducial selection ($f_{1\mathrm{Gyr}} > 0.1$, $\Delta\mathrm{SFR} < -0.6$, green points). All plotted points are the median values from the posterior of the `Prospector` fits. In panel (a), we show the stellar mass versus the absolute magnitude (M_z) along with the magnitude limited threshold ($M_z < -23.2$) and the mass complete threshold ($\log(M_\star/M_\odot > 11.2$) discussed in Section 4.2.3. In panel (b), we show the star-formation rate versus stellar mass, with the star-forming sequence at $z = 0.7$, the median redshift of our sample, shown as a black line with characteristic ~ 0.3 dex 1σ scatter [127]. In panel (c), we show the recently quenched selection plane, $f_{1\mathrm{Gyr}}$ versus ΔSFR, with the fiducial selection cuts illustrated as dashed lines. The sample is significantly brighter than the parent sample at fixed stellar mass and occupies a unique part of parameter space by having formed a significant amount of recent stellar mass despite being fully quenched.

where $\mathrm{SFR_{SFS}(z)}$ is the inferred star formation rate from the star-forming sequence at the observed redshift of the galaxy defined in [127], which is also measured using `Prospector` SED fits. We set a fiducial threshold for quiescence at $\Delta\mathrm{SFR} = -0.6$, $\sim 2\sigma$ below the main sequence at a given redshift. Near the fiducial value, the typical uncertainty in ΔSFR is ~ 0.1 dex. As with the star formation rate, this value is significantly more uncertain for measured values. Finally, we measure the fraction of the total stellar mass formed in the Gyr before observation, $f_{1\mathrm{Gyr}}$. Galaxies with small $f_{1\mathrm{Gyr}}$ are very well constrained to be small, and for

galaxies which formed $10-70\%$ of their stellar mass in the past Gyr, typical uncertainties are $15-30\%$. A sample of constraints on parameters is shown in Table 5.

We show some of the observed and derived characteristics of the full LRG sample as red contours in Figure 24. In the first panel, we show the stellar mass versus the rest frame absolute magnitude, M_z, illustrating the tight correlation between the two parameters. We additionally show lines which correspond to the cuts we make in the two parameters to construct the volume limited samples described in Section 4.2.3. In the next panel, we show the star formation rate versus the stellar mass along with the "star forming sequence" at $z = 0.7$ with 0.3 dex scatter from [127] to illustrate that the sample is largely quiescent. Finally, we show the sample in the selection plane of $f_{1\mathrm{Gyr}}$ versus $\Delta\mathrm{SFR}$ discussed in Section 4.3.1 with our fiducial cuts to select recently quenched galaxies. In all 3 planes, we show the fiducial sample of galaxies as green points.

4.2.3 Selecting Volume Limited Samples

Because the choices made in spectroscopic targeting significantly impact the observed sample, it is necessary to select a volume limited sample to fairly compare galaxies across redshift bins. This is especially true because the $z_{\mathrm{fiber}} < 21.6$ cut in observed magnitude would observe a faint galaxy at low-redshift but not high-redshift. We use the fits to the spectrophometric data to select samples which we can use to infer number densities. Throughout this letter, we utilize three relevant samples: the full LRG sample, the rest absolute Z-magnitude selected "magnitude limited" sample, and the "mass complete" sample to select recently quenched galaxies.

4.2.3.1 The Magnitude Limited Sample

By virtue of being the youngest and brightest galaxies in any given quiescent sample, galaxies have the lowest $M_\star/L$ ratios at fixed stellar mass and therefore are relatively bright compared to the majority of LRGs. As such, in order to get large, complete samples of galaxies to study as a function of redshift, a luminosity cut will maximize the sample size. We define a magnitude limited sample with rest-frame $M_z < -23.2$, at which the entirety

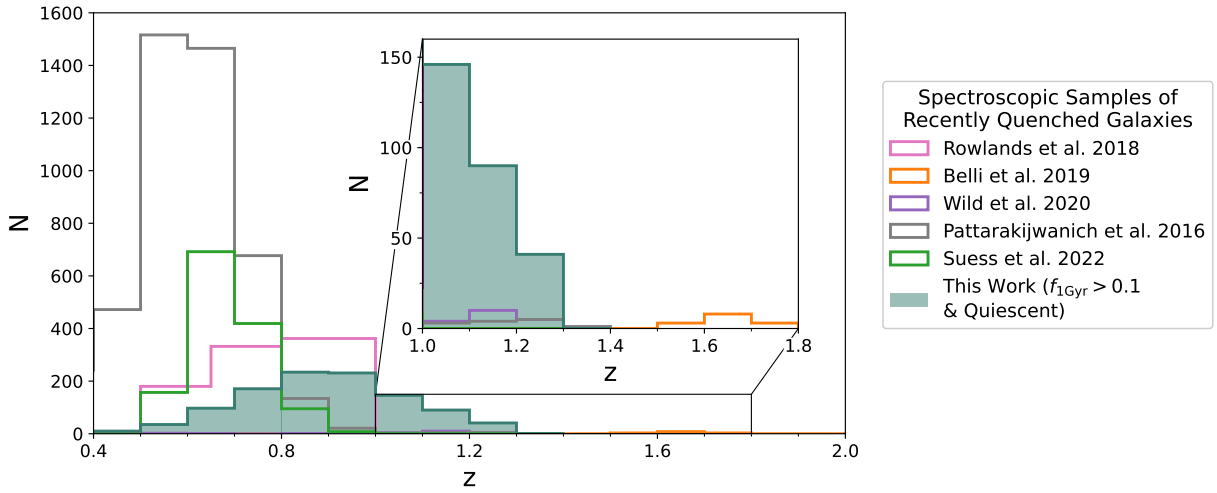

Figure 25: Redshift distributions of spectroscopic samples of recently quenched galaxies from $0.4 < z < 2.0$, with an inset focusing on $z > 1$ where the improvement in sample size from this work is most significant. Our fiducial sample ($f_{1\mathrm{Gyr}} > 0.1$, $\Delta\mathrm{SFR} < -0.6$, selected from the full LRG sample) is shown as a filled green histogram. Other samples shown include PCA-identified post-starburst galaxies from [162] and [231], galaxies with $t_{50} < 1.5$ Gyr from [19], galaxies selected with K+A template fitting from the SDSS [156], and galaxies selected using rest UBV filters from the SQuIGG$\vec{L}$E sample also selected from the SDSS [191].

of the reddest (in rest $g - z$ color, which should map to the highest $M_\star/L$ ratios) 2.5% of the LRG sample is selected at $z = 0.8$. This selection results in the largest volume limited sample we can obtain where we expect to have observed all bright galaxies in DESI out to $z \sim 0.8$, yielding a total of 8683 galaxies.

4.2.3.2 The Mass Complete Sample

While a magnitude limited sample selects the bulk of the galaxies in the SV sample, in order to characterize the growth of the population relative to the fainter (at fixed stellar mass) old quiescent population, we instead require a mass complete sample. In the redshift range $0.4 < z < 0.8$, the DESI LRG targeting only selects a sample which is $\gtrsim 80\%$ mass

complete for very massive galaxies [248]. As such, in situations where we wish to compare to the quiescent population as a whole, we elect to use only galaxies above this stellar mass, regardless of their rest-frame M_z. This sample is significantly smaller than the magnitude limited sample, with only 5375 galaxies above the stellar mass cut at $z < 0.8$.

We show the cuts in rest-frame M_z and stellar mass that result in the two subsamples in Figure 24a, illustrating that the stellar mass cut is significantly more restrictive than the magnitude cut, which lets through galaxies at masses as low as $10^{10.8} M_{\odot}$. At fixed stellar mass, the fiducial sample (see Section 4.3.1) is significantly brighter than a typical LRG (red contours), and we therefore maximize our ability to constrain the number density of recently quenched galaxies as a population by instituting a cut on the absolute magnitude.

4.3 Analysis

4.3.1 Selecting Recently Quenched Galaxies

There are a number of ways of selecting recently quenched/post-starburst galaxies, all of which share the common goal of selecting galaxies that recently quenched after a period of significant star formation [87]. Historically, these galaxies have been selected using a combination of emission line cuts (to select against current star formation) and Balmer absorption depth (to select for a stellar population dominated by A type stars) [67, 246, 12]. Here, we leverage the tightly constrained star formation histories to select a physically motivated sample of recently quenched galaxies. First, we focus on selecting a pure quiescent sample. In Figure 24b+c, it is clear that some galaxies that are dusty and star-forming have been selected due to their red colors and exist in the LRG parent sample. To remove these, we perform a conservative cut in ΔSFR, classifying galaxies as quiescent only if their median ΔSFR is $\sim 2\sigma$ (0.6 dex) below the star-forming sequence at their redshift from [127]. This selection, which is highlighted in Figure 24c, removes 2622 galaxies ($\sim$ 15% of the total sample). All qualitative results in this work are insensitive to the exact definition of quiescence that we adopt, though exact sample sizes and number densities will by definition

differ slightly.

Secondly, we are interested in separating the quiescent galaxy population physically into recent additions to the red sequence and older galaxies. In this work, our definition of recently quenched does not require a burst, as we are interested in classifying all galaxies which rapidly formed a significant amount of stellar mass before quenching as galaxies. To select such a sample, we leverage the inferred star formation histories to measure the fraction of the stellar mass formed within the last Gyr ($f_{1\mathrm{Gyr}}$) for all galaxies [221]. In combination with the cut for quiescence, selecting galaxies with high $f_{1\mathrm{Gyr}}$ identifies a sample that must have rapidly truncated its star formation in order to have formed a large amount of its stellar mass while also reaching quiescence within 1 Gyr. We adopt $f_{1\mathrm{Gyr}} > 0.1$ (also shown in Figure 24c) for our fiducial selection and explore the impact of different thresholds in Section 4.4. The fiducial selection identifies 1089 galaxies from the 15012 quiescent LRGs using the fiducial $f_{1\mathrm{Gyr}} > 0.1$ selection.

This sample of galaxies is unparelled in size beyond $z \gtrsim 1$. In Figure 25, we show the redshift distributions of this sample compared to other large spectroscopic samples of post-starburst galaxies at intermediate redshift. Our sample of 100s of galaxies at $z < 0.8$ is smaller than other samples which select galaxies from the full Sloan Digital Sky Survey [156, 191] or VIPERS Survey [162]. However, at $z > 1$ (shown in the inset), we find that this sample dramatically increases the number of spectroscopically confirmed galaxies at the tail end of cosmic noon.

While our selection of galaxies relies on our inferred star formation histories, there are many other selections that use empirical measures of spectroscopic features to select post-starburst galaxies [87]. We choose a few common post-starburst identification methods and compare the resulting number densities with our fiducial model (see Section 4.3.2). For all literature comparisons, we use the same $\Delta\mathrm{SFR} \leq -0.6$ criterion for quiescence rather than relying on common empirical metrics like EW H_α, which falls out of our spectral window for most of the sample, or EW [OII], which is an uncertain tracer of SFR due to potential contribution from AGN/LINERs. We note that while exact definitions of H_δ spectral indices vary in the literature (e.g., [8] uses H_δ, [89] uses $H_{\delta,A}$, and [13] $H_{\delta,F}$), these differences are subtle. We adopt $H_{\delta,A}$ as our preferred definition, as it is optimized for features from A-

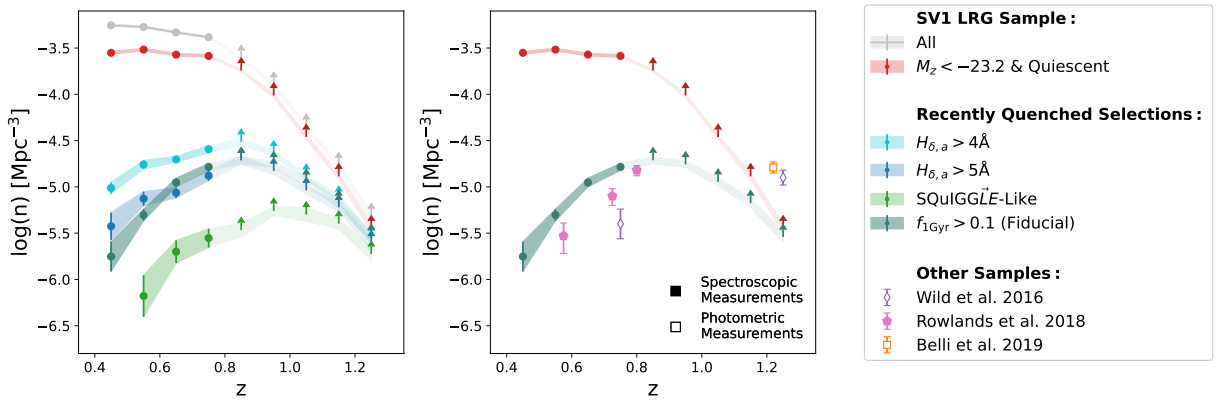

Figure 26: (Left): Number densities within the DESI SV LRG sample (full sample, gray; luminosity-complete and quiescent, red) and a variety of selections from the magnitude limited (see Section 4.2.3.1) quiescent sample ($H_{\delta,a} > 4$, light blue; $H_{\delta,a} > 5$, dark blue; SQuIGG$\vec{L}$E SED selection, light green; and $f_{1\mathrm{Gyr}}$, green). Beyond $z \sim 0.8$, we indicate that the measured number densities are lower limits by plotting as upward facing arrows. All selections show an increasing number density over the redshift range in which we are complete, with varying normalization resulting from the relative restrictiveness of the post-starburst criteria. (Right): The same magnitude limited LRG and $f_{1\mathrm{Gyr}} > 0.1$ samples as the previous panel in addition to literature measurements (photometric: open symbols; spectroscopic: filled symbols). All three of the [230] ($M_\star > 10^{10.8} M_\odot$), [162] ($M_\star > 10^{11} M_\odot$), and [19] ($M_\star > 10^{10.8} M_\odot$) samples show a trend of increasing number density with redshift, but the normalization differs between the different samples as a result of differing stellar mass limits and selection techniques.

type stars [236]. The three selections we compare to our fiducial selection ($f_{1\mathrm{Gyr}} > 0.1$ and $\Delta\mathrm{SFR} < -0.6$) are as follows (all numbers quoted are the raw number of galaxies in the full sample, not in a volume limited sample):

1. $H_{\delta,A} > 4$ Å: After applying the quiescence criteria, we select 1727 galaxies with $H_{\delta,A} >$ 4Å following e.g., [89, 90, 239, 242].
2. $H_{\delta,A} > 5$ Å: We impose a more stringent cut, $H_{\delta,A} >5$ Å, following e.g., [8, 13], selecting 1035 post-starburst galaxies.
3. SQuIGG$\vec{L}$E Selection: Finally, after applying the quiescence criteria, we use medium band synthetic rest-frame UBV filters to identify post-starburst galaxies with $U - B >$ 0.975 and $-0.25 < B - V < 0.45$ following the procedure for selecting galaxies with SEDs dominated by A-type stellar populations [191]. We apply these cuts to the median best-fit models because the spectral coverage is not red enough to consistently overlap with the synthetic V filter. This selection finds only 324 post-starburst galaxies.

4.3.2 The number density of recently quenched galaxies

The DESI SV LRG selection is designed to have a uniform comoving number density of galaxies at $0.4 < z < 0.8$, which enables robust determination of number densities of subsets of the spectroscopic sample [248]. For this selection, we use the target density of 1439 deg^{-2} to calculate the number density in bins of $\Delta z = 0.1$ in redshift from $z = 0.4$ to $z = 1.3$ by measuring the density of targets for a given selection criterion and dividing by the volume of the bin. We measure the number densities only for the magnitude limited or mass complete samples. We utilize jackknife resampling of the 31 SV pointings to calculate the errors on the measured number densities. The errors do not account for catastrophic redshift errors, but those should be very rare ($\leq 0.5\%$, see [248]) and subdominant relative to cosmic variance and Poisson errors.

The comoving number density of each recently quenched subsample of the magnitude limited sample as a function of redshift is shown in Figure 26. The raw number density of the DESI LRG SV sample ($z_{\mathrm{fiber}} < 21.6$) is shown in grey. We show the number density of the rest-frame magnitude limited ($M_z < -23.2$) sample with the fiducial quiescence cut

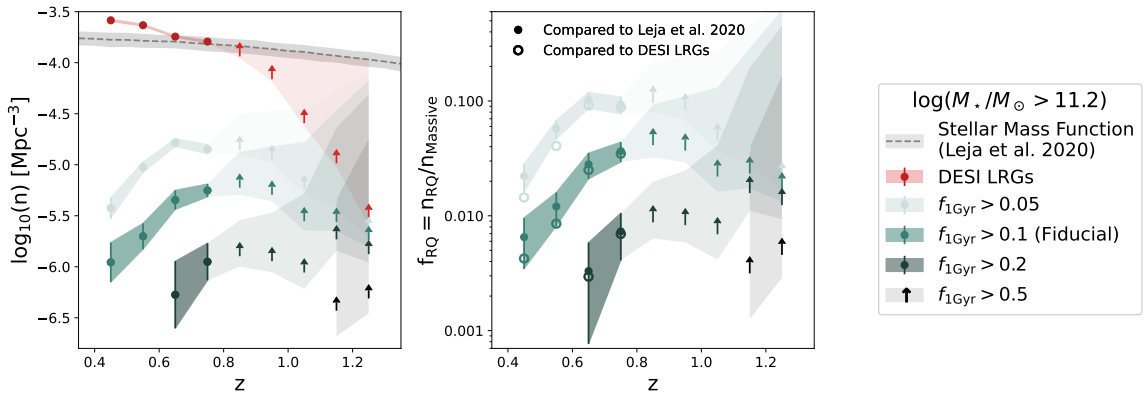

Figure 27: The number densities (left) and fractions (right) of recently quenched galaxies in the mass complete sample ($\log(M_\star/M_\odot) > 11.2$, see Section 4.2.3.2). The dashed line and grey band (left) represent the stellar mass function of similarly mass galaxies [126], and the red points show the number density of all LRGs above the mass limit. The light green, green, dark green, and black points represent the number densities and fractions of recently quenched galaxies with $f_{1\mathrm{Gyr}}$ greater than 0.05, 0.1, 0.2, and 0.5 respectively, as compared to the stellar mass function from [126]. On the right panel, the open points of the same colors show the fraction of galaxies as compared to our own massive galaxy number density measurements. Above $z = 0.8$, measurements are indicated as lower limits with errors inflated to encapsulate the possibility that all galaxies which were not targeted by DESI meet the selection criterion.

($\Delta\mathrm{SFR} < -0.6$) in red. We then apply the post-starburst selections outlined in Section 4.3.1 to the magnitude limited sample. The number densities are shown for $H_{\delta,A} > 4$ Å (light blue), for $H_{\delta,A} > 5$ Å (dark blue), SQuIGG$\vec{L}$E-like (light green), and our fiducial $f_{1\mathrm{Gyr}} > 0.1$ selection (dark green). In all cases, the number density of post-starburst galaxies rises as a function of redshift in the range of redshifts where the parent LRG sample is complete ($z < 0.8$). Above this, we illustrate that our measurements are lower limits.

In the second panel of Figure 26, we compare our fiducial sample of galaxies to several measurements from the literature. We find qualitative agreement with previous studies that observe the number density of recently quenched galaxies increasing with redshift [230, 162, 19]. Additionally, the number density of the galaxies that we measure is very similar to that of compact star forming galaxies at z=0.5, adding credence to the argument that such galaxies may be progenitors to local post-starburst galaxies [211, 62, 224]. However, in detail, this comparison is limited by systematic effects; our sample is systematically more massive than other post-starburst samples, and is selected using a magnitude (not mass) limit. Additionally, as shown in the first panel of Figure 26, differing identification techniques can significantly impact the measured number density of post-starburst galaxies. Still, a clear consensus emerges from this comparison that recently quenched galaxies were increasingly common at greater lookback time.

4.3.3 Exploring the Growth of the Red Sequence by Rapidly Quenched Galaxies

In the previous section, we studied the number density of a magnitude limited sample of galaxies to maximize our sample size. Here, we attempt to explicitly quantify the fraction of massive galaxies that have recently quenched and joined the red sequence as a function of cosmic time. To do so, we utilize the mass complete ($\log(M_\star/M_\odot) > 11.2$, see Section 4.2.3.2) subset of the LRG sample, which we show in the first panel of Figure 27 (red) along with the corresponding stellar mass function from [126]. This measurement over-predicts the stellar mass function by ~ 0.2 dex at $z \sim 0.4$ while matching well at $z \sim 0.7$. This may be due to systematic differences in the stellar mass estimates (e.g., differences in modeled star formation histories, unmodeled contributions from AGN, or spectrophotometric modeling in

our fits versus broadband multiwavelength SEDs), and the mismatch in redshift evolution may be a result of the targeting incompleteness. As such, we adopt the number densities from the stellar mass function as the total abundance of massive ($\log(M_\star/M_\odot) < 11.2$) galaxies and note that the fractions we measure may be systematically lower than reported by ~ 0.2 dex. Above $z = 0.8$ where LRG targeting is known to be incomplete, we inflate the upper error bar on the measured lower limits by assuming that every galaxy we have not targeted meets the selection criteria (quantified by the deviation between the measured number density and the stellar mass function) to capture the possibility that every galaxy we did not measure is a recently quenched galaxy. Since this is unlikely due to the lower $M_\star/L$ ratio of galaxies, this conservative estimates captures the full range of possibility in the number density of galaxies in a given selection at $z > 0.8$.

We show the number densities of four different selections of recently quenched galaxies: $f_{\rm 1Gyr} > 0.05$ (light green), $f_{\rm 1Gyr} > 0.1$ (green), $f_{\rm 1Gyr} > 0.2$ (dark green), and $f_{\rm 1Gyr} > 0.5$ (black). Points that do not appear indicate that the redshift bin contained zero galaxies that met the selection criteria. All four sets of recently quenched galaxies show increasing number densities with redshift. However, even at $z \sim 0.8$, galaxies which formed a large fraction of their stellar mass in the past Gyr are very rare. For example, at $z = 0.8$, galaxies that formed $> 20\%$ of their stellar mass in the past Gyr were significantly (> 1 dex) rarer than those which formed 5% of their stellar mass. We find that the number density of the $f_{\rm 1Gyr} > 20\%$ population cannot be decreasing with lookback time, and in fact, at $z \sim 1.2$ the lower limit number density of this population is higher than the number density at z=0.8. The rarity of such objects at intermediate-z is extremely consistent with the rarity of "late bloomers," galaxies that formed the majority of their stellar mass in the 2 Gyr before quenching [68]. Additionally, we identify a very small population of galaxies which rapidly formed $\geq 50\%$ of their stellar mass in the Gyr before observation at $z = 1.1 - 1.3$, with lower limits that indicate a number density of at least $\log_{10}(\rm n) > -6.5$ Mpc^{-3}. Similar extreme post-starburst galaxies have been found in photometric samples with comparably low number densities and could represent analogs to the formation of massive quiescent galaxies at high-z [152].

In the right panel of Figure 27, we show the same samples as fractions of the total

massive galaxy population (shown with solid points using the stellar mass function from [126] as the denominator and empty points using our own measurements of the LRG number density). We find that galaxies which formed $> 20\%$ of their stellar mass represent $\sim 0.5\%$ of the total galaxy population at z=0.8, but by $z \sim 1.2$ must be at least 1%, with an upper limit that extends to them being $\sim 50\%$ of the quiescent population. Similarly, the most extreme burst-dominated systems ($f_{1\mathrm{Gyr}} > 50\%$) must be at least $\sim 0.5\%$ of the total galaxy population at z=1.2, but this fraction could be as high as 20%. In contrast, galaxies with $f_{1\mathrm{Gyr}} > 5\%$ and $> 10\%$ are significant even at z=0.4, representing $\sim 1.5\%$ and 0.5% of the massive galaxy population, and by $z = 0.8$ they are $\sim 10\%$ and 3% of the total population. Studies of massive quiescent and post-starburst galaxies at similar redshifts have measured similar burst fractions of $\sim 5\%$ in the bulk of their samples, indicating that at the massive end, the vast majority of "post-starburst" galaxies are the evolutionary products of a recent dusting of star formation rather than the truncation of their primary epoch of star formation [154, 90].

The general rarity of extreme massive post-starburst galaxies in this sample is consistent with findings that the formation redshift of $\log(M_\star/M_\odot) = 11.2$ galaxies is $z_{\mathrm{form}} \sim 2-3$ [92, 150, 91, 35, 76, 63, 221, 119]; at the epochs we are probing, the average massive quiescent galaxy quenched long in the past. However, we find that a significant number of massive galaxies are still quenching with very high $f_{1\mathrm{Gyr}}$ well after cosmic noon ($z \sim 2$), and expect that with a more complete sample, at higher redshift the population dominated by recent star formation would become the norm.The sharp observed decline in rapid quenching after cosmic noon suggests a fundamental shift in the evolutionary histories of massive galaxies. By combining this preliminary analysis with similar stellar population synthesis modeling of larger, mass-complete samples and ancillary datasets (e.g., by analyzing galaxy structural evolution and morphological transformation), we hope to illuminate the physical mechanism(s) that are responsible for halting star formation and sustaining quiescence of massive galaxies since $z \sim 1$.

4.4 Discussion and Conclusions

Using the DESI SV sample, we measure non-parametric star formation histories for a novel sample of Luminous Red Galaxies. We select physically motivated samples of galaxies and leverage the well characterized parent sample to characterize the increasing number density of recently quenched galaxies with lookback time. We find the following:

1. The sample of quiescent galaxies which formed $> 10\%$ of its stellar mass in the past Gyr represents a novel spectroscopic sample. The sample of 277 galaxies we identify at $z > 1$ is an order of magnitude larger than previous samples (see Figure 25).
2. The number density of galaxies rises steadily with redshift from $z = 0.4 - 0.8$ based on our model selection and empirical identification methods; post-starburst galaxies were more common at earlier cosmic time (see Figure 26).
3. The fraction of massive ($\log(M_\star/M_\odot) > 11.2$) galaxies which have recently quenched their star formation and which formed $> 10\%$ of their stellar mass in the past Gyr rises in this redshift range from $\lesssim 0.5\%$ at z=0.4 to $\sim 3\%$ in at z=0.8 (see Figure 27). Furthermore, at $z > 1$, we find a significant emerging population that formed $> 20\%$ and $> 50\%$ of its stellar mass in the past Gyr.

As our criteria for selecting recently quenched galaxies simply required a rapid truncation in a galaxy's star formation rate that drove a galaxy into quiescence in $<\lesssim$1 Gyr, there is substantial variety in the star formation histories of galaxies which fall into a given selection for $f_{\rm 1Gyr}$. The simplicity of this selection allows for simple determination of the rate at which galaxies have entered into quiescence, but it does not distinguish between, for example, a secondary starburst in an already quiescent galaxy versus a rapid truncation of the primary epoch of star formation at fixed $f_{\rm 1Gyr}$. Future work will endeavor to combine these star formation histories with ancillary data to paint a holistic picture of the quenching of these galaxies. For now, we use constraints on the fraction of galaxies which recently entered into quiescence to discuss possible physical mechanisms that could be driving the rapid cessation of star formation in this sample of galaxies.

One of the most compelling fast processes that could induce, then shut off, star formation

and produce post-starburst galaxies is major mergers [101]. After cosmic noon, simulations have found that many massive galaxies that quench do so via major mergers [222], which funnel gas inward and induce a burst of star formation that rapidly shuts off. Indeed, many studies of post-starburst galaxies have found that merger features are more common in post-starburst systems [157, 167, 75, 219].

We estimate the relative frequency of major mergers using the `UNIVERSEMACHINE` [16] and find that 15% and 20% of $\log(M_\star/M_\odot) > 11.2$ galaxies, at $z = 0.4$ and $z = 0.8$ respectively, experienced a major merger ($M_{\star,2}/M_{\star,1} > 25\%$ in the progenitor galaxies in the merger tree) in the past Gyr. This rate is significantly higher than the the 0.5% and 3% fractions we find for our fiducial sample of recently quenched galaxies, and the merger fraction increases more slowly than the fraction. Some of this difference may be driven by gas-poor major mergers between already quiescent systems or gas rich mergers that do not quench, and we conclude that it is plausible that every very massive galaxy that rapidly quenches between $0.4 < z < 0.8$ does so as a result of a major merger, and that not every major merger results in a post-starburst galaxy. This is in line with predictions from the Illustris TNG simulation that only $\sim 5\%$ of massive galaxies will quench within $\sim$500 Myr of coalescence after a major merger [161], and indicates that even if major mergers are an essential part of the quenching process, they do not universally produce post-starburst galaxies. However, at high-z, our measured lower limits fall short of placing strong constraints.

Still, the high-z tail of our distribution promises to be a very powerful tool for studying rapid quenching. Prior to DESI, only a small number of spectroscopic continuum observations from surveys could be mined for post-starburst galaxies above $z \gtrsim 1$ [231], and often samples can only be obtained through targeted followup of photometrically identified sources [19]. Even in the smallest (but highest signal-to-noise) subset of DESI LRG spectra, we have identified an order of magnitude more spectroscopically confirmed galaxies than had been measured previously. Future work will leverage these star formation histories further to study trends using parameters such as the time since quenching [191], which has been used in post-starburst populations to constrain the evolution of AGN incidence [97], sizes [176], molecular gas contents [20, 187], and merger fractions [219]. Using the combination of the unique spectroscopically derived moments of the star formation history and ancillary data,

we hope to place strong constraints on the mechanisms that drive the quenching of massive galaxies as close to cosmic noon as is currently possible. Future surveys, such as PFS [96] and MOONRISE [134] will extend wavelength coverage into the NIR, pushing farther in redshift to cosmic noon. In conjunction with this sample, comprehensive studies of the properties of galaxies from $z = 0$ to $z = 2$ will paint a cohesive picture of the rapid quenching process and its role in producing the present-day quiescent population.

5.0 Conclusions

In this thesis, I have investigated the how and when of rapid quenching by studying the structures and number densities of intermediate-redshift recently quenched galaxies. In Chapter 2, I showed that post-starburst galaxies from the SQuIGG$\vec{L}$E sample at $z \sim 0.7$ exhibit flat gradients $H_{\delta,A}$, indicating that the shutdown in star formation occurred in these galaxies on a galaxy-wide scale. In Chapter 3, I used deep imaging from the Hyper-Suprime Cam survey to study the structures of galaxies from SQuIGG$\vec{L}$E and found that they are compact relative to star forming and quiescent galaxies at their same epoch. Taken together, these results suggest an already compact progenitor to the rapid quenching channel. Finally, in Chapter 4, I measured star formation histories of the DESI LRG Survey Validation sample and constrained the incidence of rapid quenching. I found that the number density of recently quenched galaxies declined sharply after $z = 1$, and that at $z < 1$ the population of massive quiescent galaxies that recently formed the majority of its stellar mass is essentially negligible. However, at the highest redshift tail of this sample, that population that is analogous to the rapidly quenching population near cosmic noon begins to emerge in earnest.

Looking forward, there is still significant work to be done in analyzing these intermediate-redshift samples. In particular, the mystery of the molecular gas reservoirs that persist after the cessation of star formation in post-starburst galaxies [190, 20, 187] and its relation to mergers, AGN, and morphological transformation is crucial to understanding the physical drivers that suppress star formation in quiescent systems. I have been involved in follow up ALMA surveys that have quadrupled the sample size of CO observations of SQuIGG$\vec{L}$E post-starburst galaxies from 12 to 52. I look forward to using this sample to study the properties of gas-rich and gas-poor post-starburst systems to identify the physical drivers of the varying gas reservoirs in these systems.

Additionally, the sizeable sample of $z > 1$ post-starburst galaxies that formed a majority of their stellar mass in the Gyr before observation provides an excellent laboratory for testing the physical driver of rapid quenching in systems that should mirror the properties of typical quiescent galaxies near cosmic noon. The importance of mergers in rapid quenching at

$z \sim 0.7$ has been clearly established [219], but is this the case nearer to cosmic noon? My in-progress HST SNAP program (HST-#17110) will test this by obtaining imaging of ∼100 post-starburst galaxies from this sample to measure structures and tidal signatures in this novel sample. These targets will also be excellent candidates for follow up NIR and radio spectroscopy to constrain the incidence of AGN and molecular gas reservoirs respectively, allowing for the direct comparison of the holistic properties of these unique $z \sim 1$ rapid quenchers to their lower-redshift counterparts in SQuIGG$\vec{L}$E.

I have gleaned clear insights by studying the tail end of high redshift rapid quenching at intermediate-z but representative samples of massive galaxies in the epoch of rapid quenching right is just barely out of the reach of the current generation of large spectroscopic surveys. However, the next generation of surveys using novel instrumentation on the largest telescopes in the world is just on the horizon. In the coming years, the Prime Focus Spectrograph [96] and MOONRISE [134] GTO surveys will come online on Subaru and the VLT respectively. These surveys will utilize sensitive NIR instrumentation and the vast improvement in collecting area from 10 meter class telescopes to observe representative samples of massive galaxies from $z \sim 1 - 2$, observing exactly the epoch that is necessary to perform a census of rapid quenching at cosmic noon. In particular, the deep fields of these surveys will drill down for $\gtrsim$ 10 hours on tens of thousands of galaxies, measuring spectroscopy that is deep enough to perform robust star formation history fitting that constrains quenching timescales. As a Brinson Prize Fellow, I am eager to involve myself in the PFS Survey so that when the data comes, we are primed to connect the work that has been done at intermediate-z to the epoch of quenching near cosmic noon to solve the puzzle of what is driving the shutdown of star formation in the universe.

Appendix A Appendix to Chapter 2

A.1 Unresolved Central Burst Toy Model

In order to test whether the observed flat $H\delta_A$ could be the result of an unresolved nuclear starburst, we assume a simple geometry for an underlying stellar population that formed at $z \sim 2$ and superimpose a central burst under the worst case seeing conditions. We distribute the light from the older population following an exponential disk with r_e=3 kpc, the characteristic size of a late type $\sim 10^{10.5} M_\odot$ galaxy at $z \sim 2$. To this underlying profile we add a pointlike central starburst, convolved with a Moffat profile with the conservative FWHM limit (see Section 2.2.2).

The resulting intensity and $H\delta_A$ profiles for the same burst as in Figure 7 are shown in Figure 28 for a galaxy observed under 0.5" seeing conditions. The left panel shows the intensity profile in the B band, which is dominated by an A-type stellar population well past the half-width-half-maximum of the Moffat central burst due to the much smaller mass-to-light ratio of the recently formed stars. The coloring scheme is the same as in Figure 7, where the blue light profile corresponds to the young population, red to the old population, and green to the composite. The labeled bands in the left panel correspond to the 3 sub-panels in the center of the figure, which show the spectral region around $H\delta$ at 1, 3, and 5 kpc. In the outer radii, light from the older population becomes more dominant, and by 5 kpc the older population is contributing more light to the $H\delta_A$ feature than the recent secondary burst. The $H\delta_A$ profile for this model configuration is shown in the right panel and by ~ 5 kpc the absorption has fallen below the common post-starburst selection of $H\delta_A > 4$ Å.

For each galaxy in this sample, we fit the 3-parameter central burst model to the $H\delta_A$ profiles using emcee [84]. We assume the following flat priors on our parameters: 0.001 Gyr $< t_{quench} <$ 2 Gyr and 0$< f_{burst} <$1. We allow the length of the burst, t_{burst}, to be anywhere from 0.001 Gyr to the maximum time between quenching and the end of the old burst. We fit the models to the $H\delta_A$ profile and integrated measurements for each galaxy. We run the fits using 24 walkers and 5000 iterations and exclude the first 500 iterations to ensure burn

Table 6: Constraints on the burst conditions that that reproduce observed $H\delta_A$ profiles

Name	Max FWHM[1]	t_{quench} (Gyr)			Burst Mass Fraction			t_{burst} (Gyr)			
	(")	16%	50%	84%	16%	50%	84%	5%	16%	50%	84%
J1109-0040	0.64	0.06	0.16	0.41	0.57	0.79	0.94	0.43	0.35	0.76	1.03
J0233+0052	0.57	0.05	0.15	0.42	0.54	0.79	0.94	0.37	0.3	0.84	1.17
J0912+1523	0.51	0.06	0.18	0.41	0.96	0.98	1.0	0.92	0.42	0.83	1.05
J0835+3121	0.82	0.09	0.22	0.42	0.12	0.22	0.46	–[2]	0.2	0.57	1.1
J0753+2403	0.79	0.07	0.18	0.41	0.46	0.72	0.92	0.32	0.27	0.68	0.95
J1448+1010	0.89	0.05	0.18	0.43	0.38	0.66	0.9	0.22	0.42	1.13	1.66

[1]See Section 2.2.2 for details on the upper limits on the full-width half maximum of the point spread function

[2]For J0835+3121, we do not quote the 5% value in the burst fraction because the distribution is not single tailed from a burst mass fraction of 1

in. Visual inspection of our walkers confirms that the fits have converged. The resulting best fitting parameters are shown in Table A.1.

In Figure 29, we show the results of the fitting on one of the galaxies with a flat $H\delta_A$ profile, J1109-0040. The left panel shows the corner plot for the 3 model parameters with 68-, 95-, and 99-percent contours bounding the data. The right panel shows the observed $H\delta_A$ profile along with the median and 1-σ bounds in the best fitting model generated from 1000 random draws from the posterior distributions. A central burst can still be hidden by poor seeing conditions, but only if the majority of the mass of the galaxy formed in the later burst. This essentially rules out a central *secondary* burst of star formation; the only solutions that fit the data at the 1-σ level require $f_{burst} \geq 50\%$.

In Figure 30, we show the results of the fitting for for J0835+3121, which prefers a lower secondary burst fraction in contrast to the other 5 galaxies in our sample. For this galaxy, we place a rough upper limit on the fraction of stars that formed in a central burst: above this fraction, we would expect our observed profile to be significantly more flat than the observed profile. It appears that our worst case PSF may over-estimate the true PSF, which is why the models are not able to decline as quickly as the observed profile. Interestingly, we detect ordered motion in this galaxy (see Figure 4), and while we cannot rule out that a merger is the cause of that motion, it is clear that the galaxy is not entirely dispersion-dominated at this stage of its evolution.

The posteriors for the four remaining galaxies are shown in Figure 31. All four of them are similar to J1109-0040 in that the burst fraction can be constrained as a single tailed distribution from a 100% burst, which will result in a perfectly flat profile. The exact constraints vary between the galaxies, with extreme cases like J0912+1523 being entirely inconsistent with an unresolved secondary starburst. Other galaxies are less constrained due to less extended profiles or worse seeing conditions, but they still can only produce the observed profiles if the central burst is comparable in mass to any underlying population.

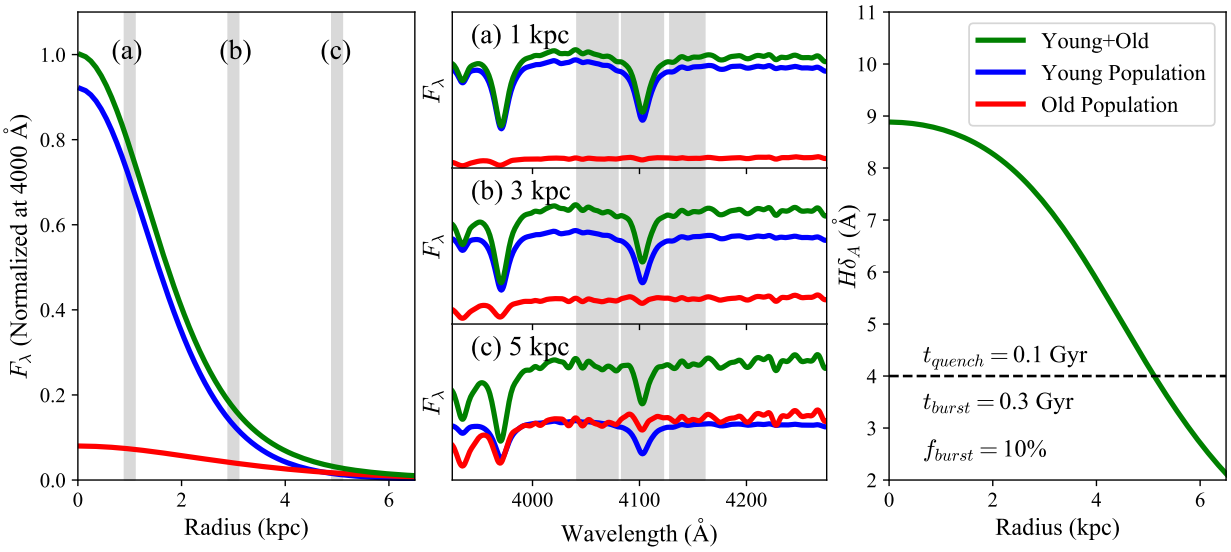

Figure 28: An example of the radial variation in $H\delta_A$ we would see for an unresolved central starburst and an underlying older population in an r_e=3 kpc exponential disk profile, using the same parameters as Figure 7. (Left): The normalized intensity profiles for the populations. The old profile is convolved with the Moffat seeing and is plotted in red. The burst profile is a Moffat profile with FWHM of 0.5" and is plotted in blue, and the green profile is the sum of the two. The grey bands labeled a, b, and c are located at 1, 3, and 5 kpc respectively. (Center): The evolution of the SEDs in the $H\delta_A$ bandpass at 1, 3, and 5 kpc. The coloring convention is the same as the previous figure, where red is the older spectrum, blue is the recent starburst spectrum, and green is the composite spectrum. The spectra are normalized to the flux at 4000 Å in the composite spectra. At low radius, the central burst dominates the light, but at 5 kpc, the older population is contributing non-negligible flux, resulting in weaker $H\delta_A$ absorption. The gray bands indicate the two continua for the $H\delta_A$ Lick index, as well as the line range. (Right): The $H\delta_A$ profile that would result from this model, which falls off at large radii.

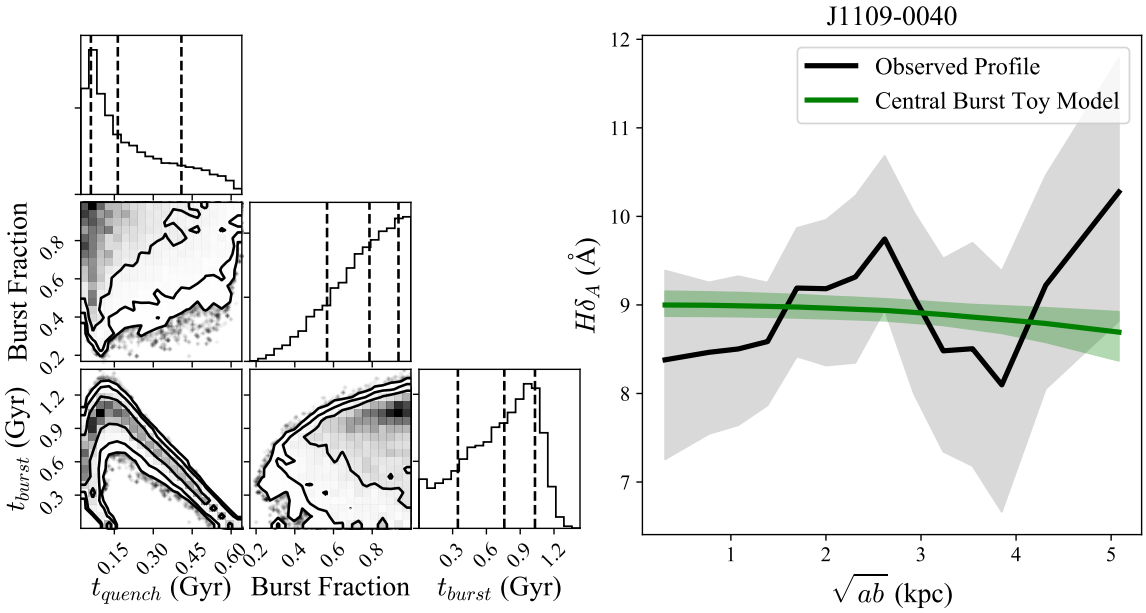

Figure 29: The results of fitting our two-burst model to J1109-0040. (Left): The corner plot resulting from our MCMC run showing the posterior of our 3 parameter model. The contours represent 1, 2, and 3 sigma confidence intervals, and the dashed lines on the 1D histograms are the median and upper and lower 68% regions. Note that the burst fraction 2-D histogram is physically bounded between 0 and 1, so it is not concerning that our fit to a flat profile runs up against that boundary. (Right): The $H\delta_A$ profile for this galaxy with the median and upper and lower 68% models plotted on top, showing that we are able to achieve a good fit to the observed profile. This modeling allows us to place strong constraints on the central burst strength below which we would expect our profile to be distinct from the flat profile we observe.

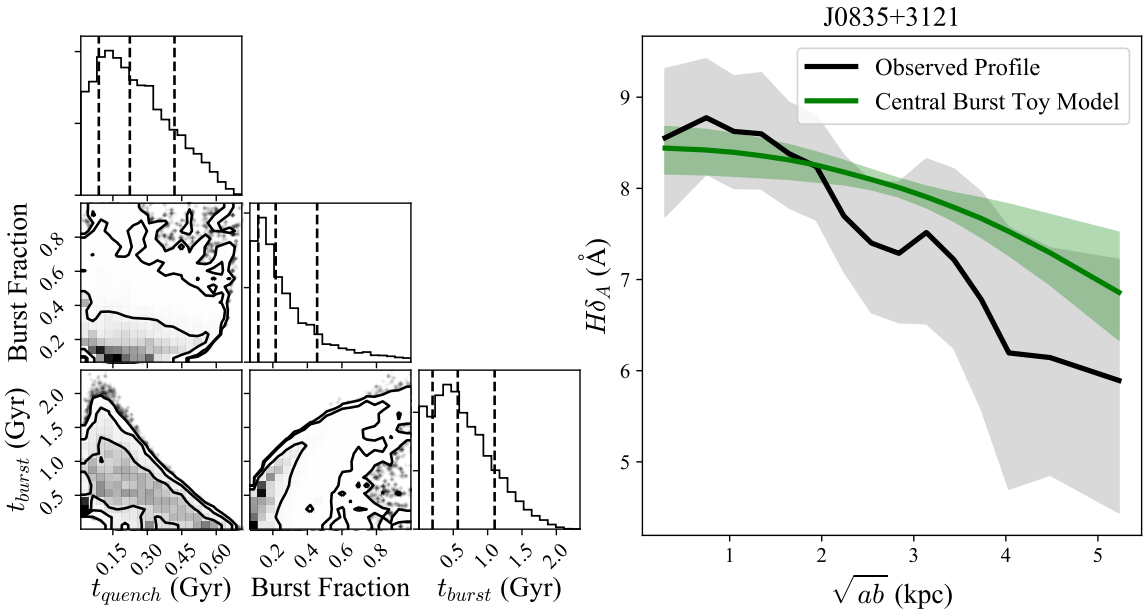

Figure 30: The results of fitting our two-burst model to J0805+3121. (Left): The corner plot resulting from our MCMC run showing the posterior of our 3 parameter model. The contours represent 1, 2, and 3 sigma confidence intervals, and the dashed lines on the 1D histograms are the median and upper and lower 68% regions. (Right): The $H\delta_A$ profile for this galaxy with the median and upper and lower 68% models plotted on top, showing that we are able to achieve a good fit to the observed profile. In contrast to J1109-0040, here the fits allow us to place an upper limit on the central burst fraction that would agree with the observed declining $H\delta_A$ profile.

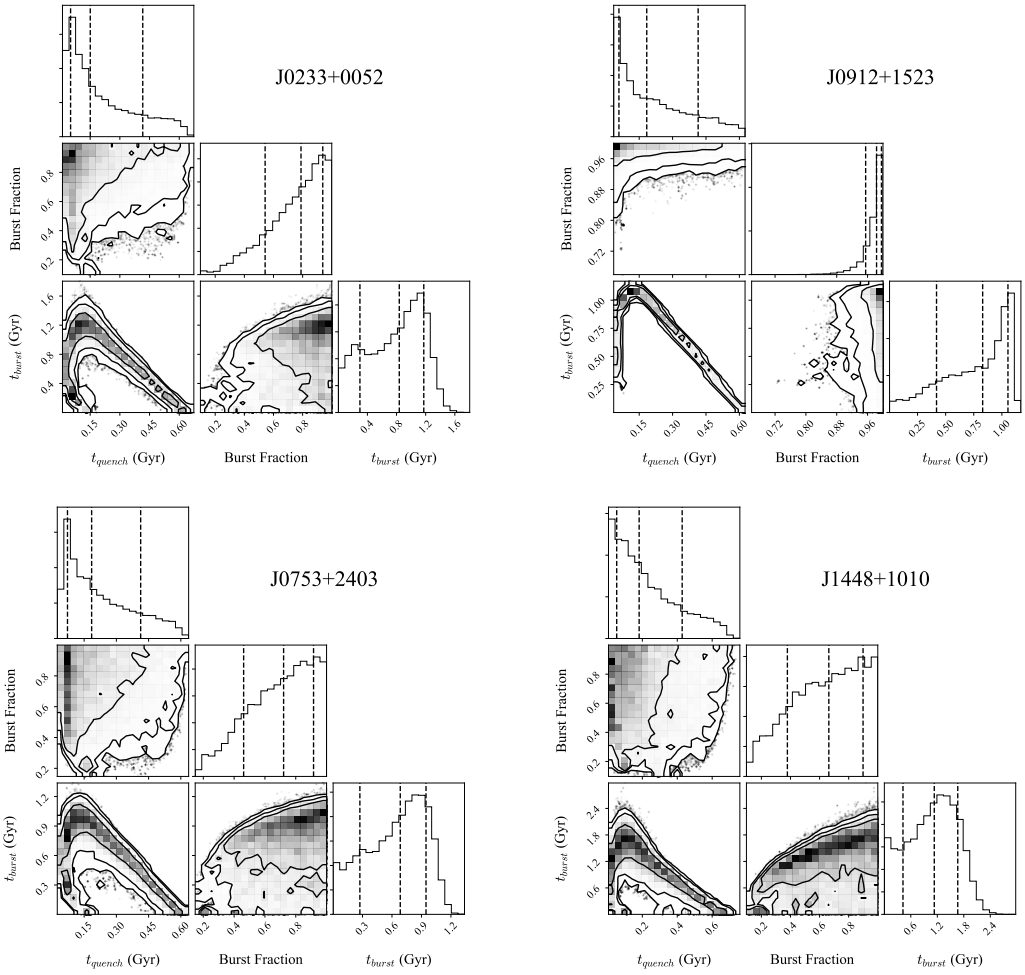

Figure 31: The posteriors for the four galaxies not shown in Figures 29 and 30. The unresolved central starburst model can only match the profiles of these galaxies with very high burst fractions.

Appendix B Appendix to Chapter 3

B.1 Verifying the accuracy of structural measurements using ground-based imaging

The i band galaxy images from the HSC survey are remarkable both for their depths and resolutions from the ground, but their resolution (PSF FWHM $\sim$ 0.6") is still dwarfed by that of space based instruments like the Hubble Space Telescope (PSF FWHM $\sim$ 0.15"). We have turned to the HSC survey because obtaining space based images of the entire SQuIGG$\vec{L}$E post-starburst sample is unfeasible; the galaxies are distributed throughout the entire SDSS footprint and it would require a significant investment to get HST followup imaging of the entire sample. However, the LEGA-C Survey, which we utilize as a coeval comparison sample of galaxies, completely overlaps with HSC and also has existing HST/ACS F814 imaging. This means that we can directly compare the Sérsic sizes and structures we derive for LEGA-C galaxies to those measured in [216] to test how our ground based measurements compare to those from space.

In Figure 32 and Figure 33, we show the comparisons between our measured sizes and Sérsic indices and the values measured from the HST images, split into quiescent (red) and star-forming (blue) populations. For the majority of galaxies, the sizes are fairly well recovered, especially in the quiescent populations where the percent error in the sizes scatters around 0%. However, for star-forming galaxies, there is a systematic offset, where the galaxies are measured in HST to be a median of $\sim$ 8% larger than they are in HSC imaging. This difference is reflected in the Sérsic indices as well; quiescent populations are measured in HST with slightly higher Sérsic indices, but the difference is more pronounced in the star-forming populations.

In Figure 34, we show the covariance between these two offsets. Galaxies which are fit in HST with larger sizes are also fit with larger Sérsic indices, and this tail at the larger-size/higher-Sérsic index end is more pronounced in the star-forming population. Because high Sérsic index corresponds to both a more peaked core and more extended wings, we

turn to 1D surface brightness profiles to understand what is driving this difference. In order to do so, we generate models of the best fitting space-based galaxy parameters from [216] at the pixel scale of HSC and convolved with the same HSC PSF we use to fit the galaxies. In order to avoid systematic differences in source identification and deblending, we restrict this test to galaxies which do not have a bright neighbor within 25 pixels. In Figure 35 and Figure 36, we show residuals in the surface brightness profiles for galaxies as fit in this work (dark blue) and with the best fitting models fit to the HST images of the galaxies under HSC viewing conditions (teal), binned by the offset between the two measurements. We find that the differences in size and Sérsic index are largely driven by a difference in the wings. The HST Sérsic structures overpredict the amount of light that will be present at large radius, and, as a result, measure larger sizes. This is likely due to the sensitivity of HST to the cores of the galaxies; in trying to accurately fit the peaky centers of the galaxies, the HST fits converge to large n, which is compensated for by inflated sky values. In contrast, HSC's remarkable low-surface brightness limits ($\sim$ 28.5 mag/arcsecond^2) allows for well calibrated sky measurements which result in small residuals at large radius. This better allows for the galaxies to be fit with low Sérsic indices, which is more significant in the star-forming galaxies which tend to be more disk-like.

Our fitting does an especially good job at recovering the shapes of galaxies in their axis ratios. We illustrate this in Figure 37, showing the 1:1 relation between the projected axis ratios we measure and those from [215]. The values agree between the ground and space based measurements with a scatter of only $\sim$ 0.07, indicating that even with significantly more PSF smearing, the projected galaxy shapes are still recoverable using `GALFIT`. Perhaps more important, there does not appear to be any trend with the sizes of the galaxies; in the right panel of Figure 37, we show that the difference in axis ratios does not correlate with size for either the star-forming or quiescent control samples. Even at the low size (r_e $\sim$0.1") limit where the sizes of the galaxies are significantly smaller than the PSF, the axis ratios are still robustly recovered. This indicates that the roundness that we measure in SQuIGG$\vec{L}$E galaxies is not just a resolution effect, but a real physical property we can trust in our interpretations.

We conclude that ground-based imaging with low surface brightness limits is extremely

well suited for the task of measuring galaxies sizes and Sérsic structures. While the loss in resolution from HST to HSC does not allow for the centers of galaxies to be resolved, the increase in sensitivity at large radius allows for the total light of the galaxy to be better accounted for, which improves the measurement of r_e . In addition, we find that observing from the ground does not affect measurements of the axis ratio significantly, even for the smallest galaxies.

B.2 Comparing the smallest galaxies to an unresolved point source

Despite the agreement between the sizes fit on the LEGA-C control sample and those in HST, resolution is still a concern. The smallest galaxies in the SQuIGG$\vec{L}$E sample are fit with sizes ∼0.1", whereas the median seeing in the HSC i-band is ∼ 0.6". In order to confirm that all the sizes we report for galaxies are reliable from a ground based survey, we re-run all our fits using an identical algorithm to the one outlined in Section 3.3.1, but this time we force the two-dimensional galaxy profiles to be a point source convolved with the PSF we provide to `GALFIT` from the HSC PSF Picker. We calculate radial χ^2 values both the Sérsic and PSF-only models out to the point where the signal-to-noise in the galaxy profile drops below 5, and find that the PSF-only models have median χ^2 values ∼2.5 orders of magnitude higher than for the Sérsic models convolved with the PSF, indicating that the SQuIGG$\vec{L}$E sample is significantly resolved. Even the best performing PSF models are still significantly worse fits than Sérsic profiles.

To illustrate this, in Figure 38 we show the two smallest galaxies in SQuIGG$\vec{L}$E which do not have bright nearby companions, as well as the 2D and 1D best fitting Sérsic and point source models. The 1D profiles are extracted using the best fitting axis ratio from the Sérsic model. It is clear from the residuals and the 1D profile that the Sérsic model better captures the true shape of the galaxy profiles, both in the centers (where the PSF is far too peaked) and in the wings. In addition, in the case of J2241+0025, there is a clear elongation in the galaxy that that the PSF shape cannot account for. Thus, even though the galaxy sizes we fit are small, we still consider them to be reliable when the PSF is properly

accounted for in the fits.

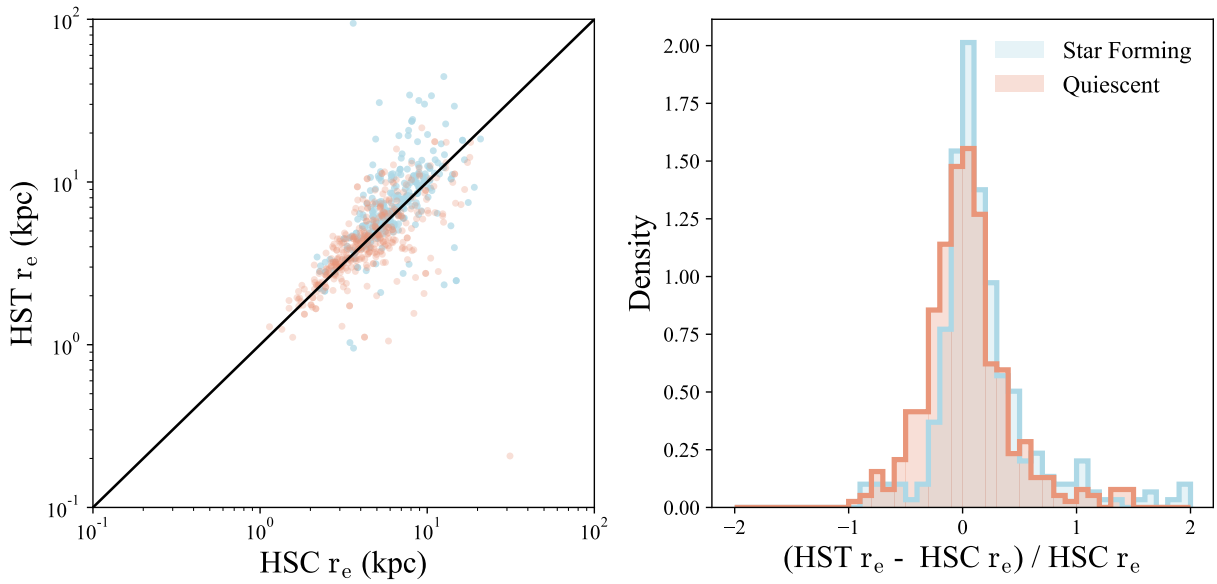

Figure 32: (Left) The one-to-one relation between the Sérsic effective radii we measure on the HSC images and the Sérsic radii from [216] measured from HST/ACS images. Star forming galaxies are colored as blue, and quiescent galaxies are red. (Right) The percent difference in the measurements for the two LEGA-C samples. For quiescent galaxies, the median sizes we measure are extremely close, with a scatter of $\sim$ 20%. For star forming galaxies, the scatter is similar, but there is a systematic offset where the HST sizes are $\sim$ 8% larger than the ones we measure. Both sub-samples have longer tails in the direction of larger HST sizes.

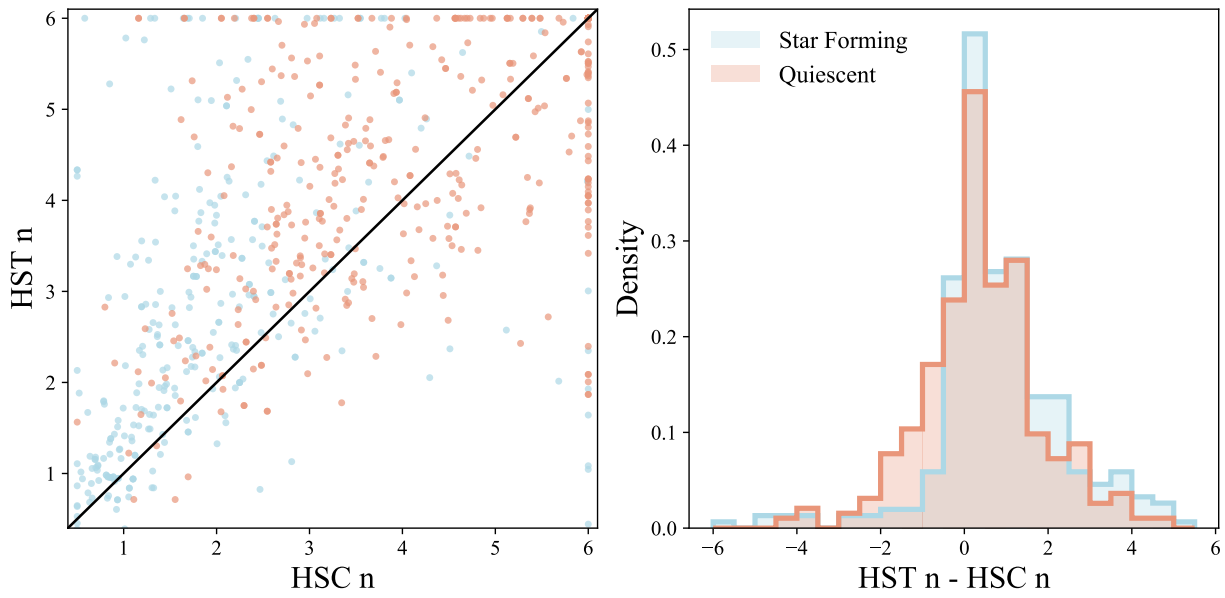

Figure 33: As in Figure 32, but for the Sérsic indices. In both the quiescent and star forming subsamples, the Sérsic indices measured in HST tend to be larger than those we measure with HST, but the trend is more pronounced for the star forming galaxies.

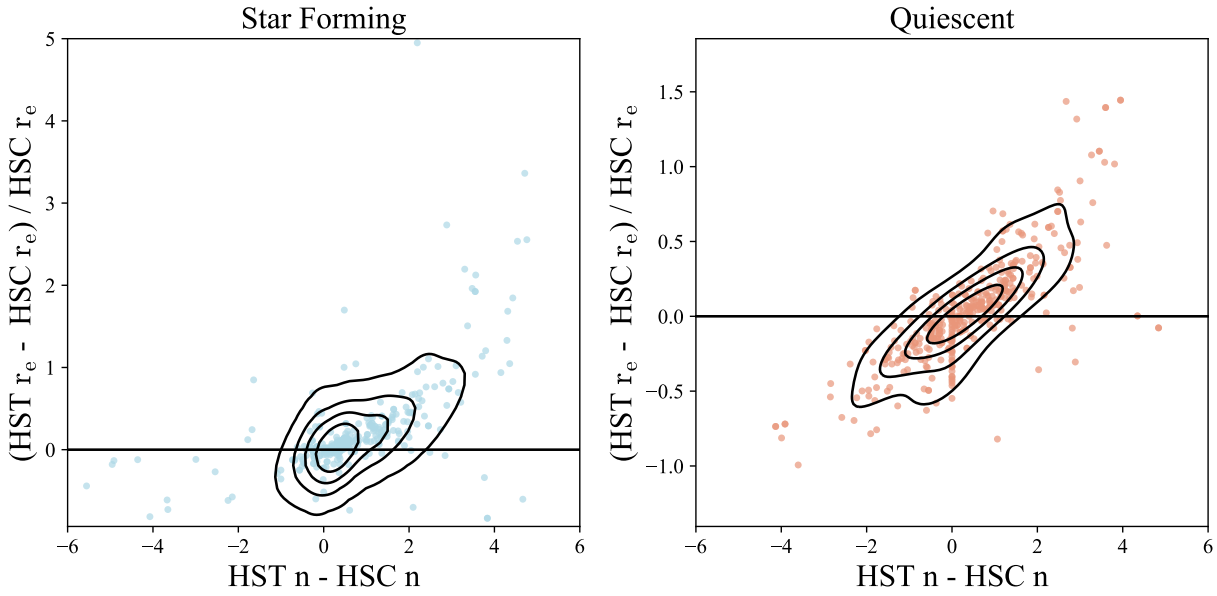

Figure 34: The percent difference in the size vs the difference in Sérsic index for the star forming (left) and quiescent (right) sub-samples, with contours bounding 80% of the galaxies. There is a trend in both samples where a mismatch in Sérsic index correlates with a mismatch in the measured sizes. (Note: We truncate the y-axis on the star forming plot at 5 despite a single point at ~ 25 due to a non-physical HST measurement of that galaxy.)

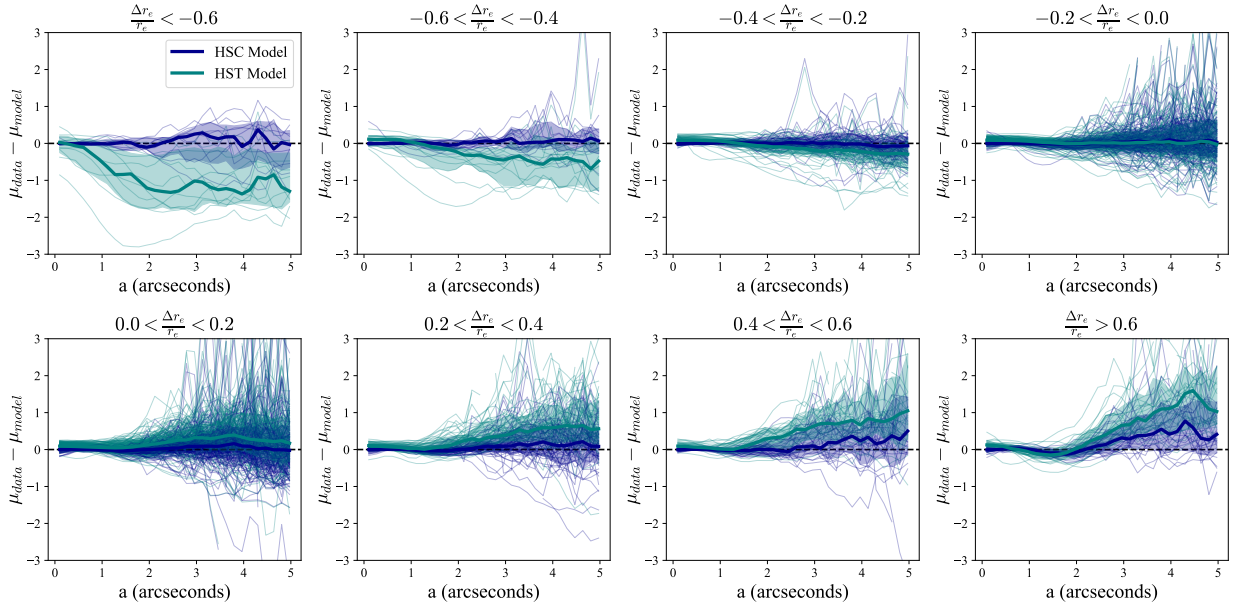

Figure 35: Individual (thin lines) and median (thick lines) residuals between the surface brightness profiles extracted from the cutouts and the best fitting models from this work (dark blue) and the fits to HST ACS images described in [215] convolved with the HSC PSF (teal). Separate panels show the galaxies binned by the agreement between the two fits in the effective radius. Profiles are only shown for galaxies where no nearby objects are simultaneously fit. In all cases, our model surface brightness profiles are consistent with no residuals. However, the HST fits which overestimate the sizes do so because they have significantly more light in the wings than our galaxies, as well as slightly more peaked cores.

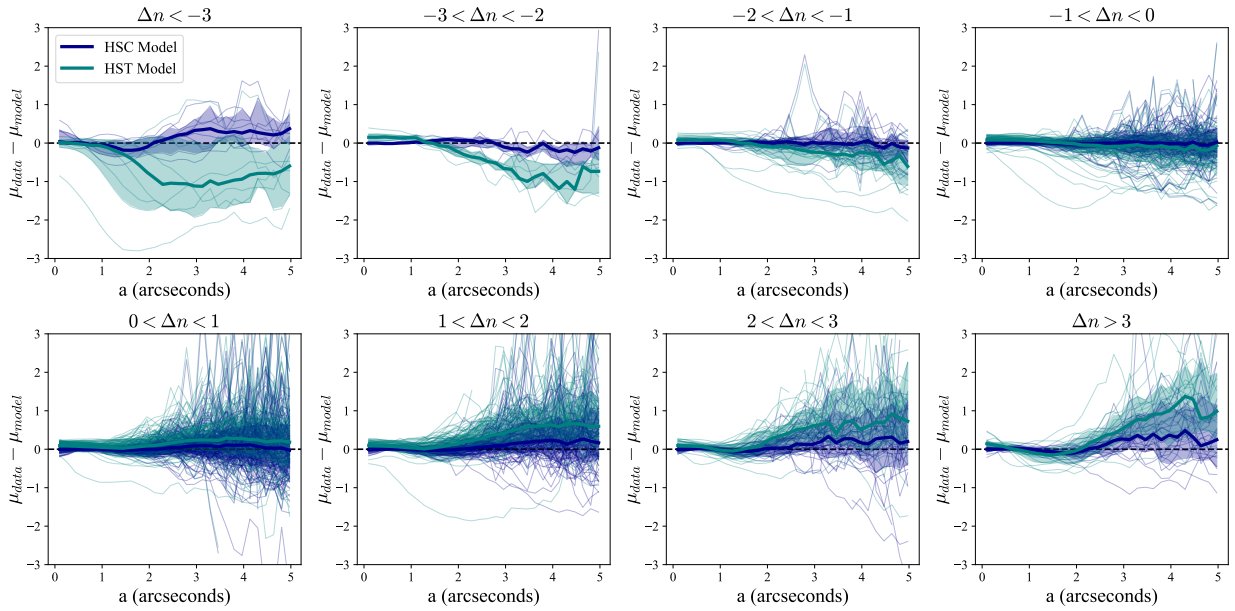

Figure 36: As in Figure 35, but this time binned by the agreement between the Sérsic indices of the fits. As with the sizes, the differences in Sérsic indices result from significant failures to successfully fit the low surface brightness wings in the HST images.

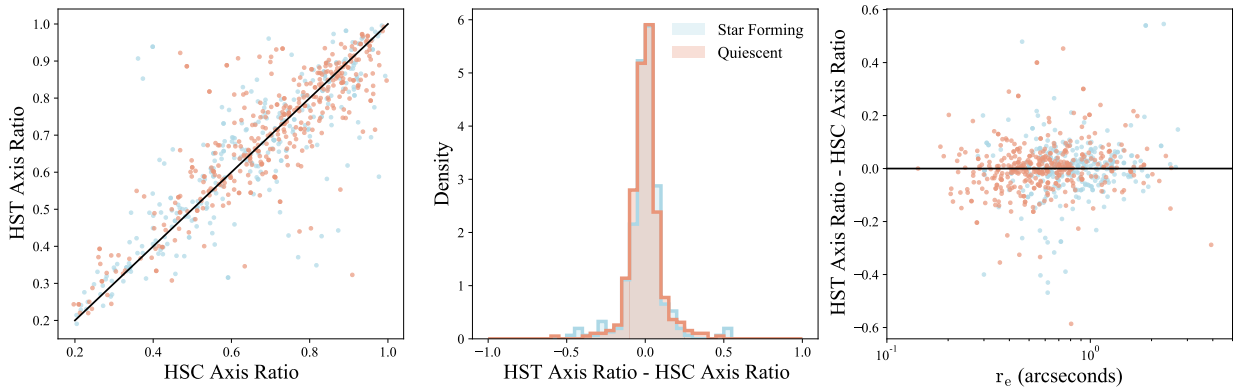

Figure 37: (Right) The axis ratio we measure using HSC data for quiescent (red) and star-forming (blue) LEGA-C galaxies versus the same parameter measured using HST data. A 1:1 correspondence is shown in black. (Center) The difference in the measurements of the axis ratios. The median deviation is consistent with zero and the scatter is very small. (Right) The difference between the axis ratios as a function of the size in arcseconds. The smallest galaxies are as well recovered as the largest ones, indicating that even the smallest galaxies in SQuIGG$\vec{L}$E which are resolved have axis ratio measurements that can be trusted.

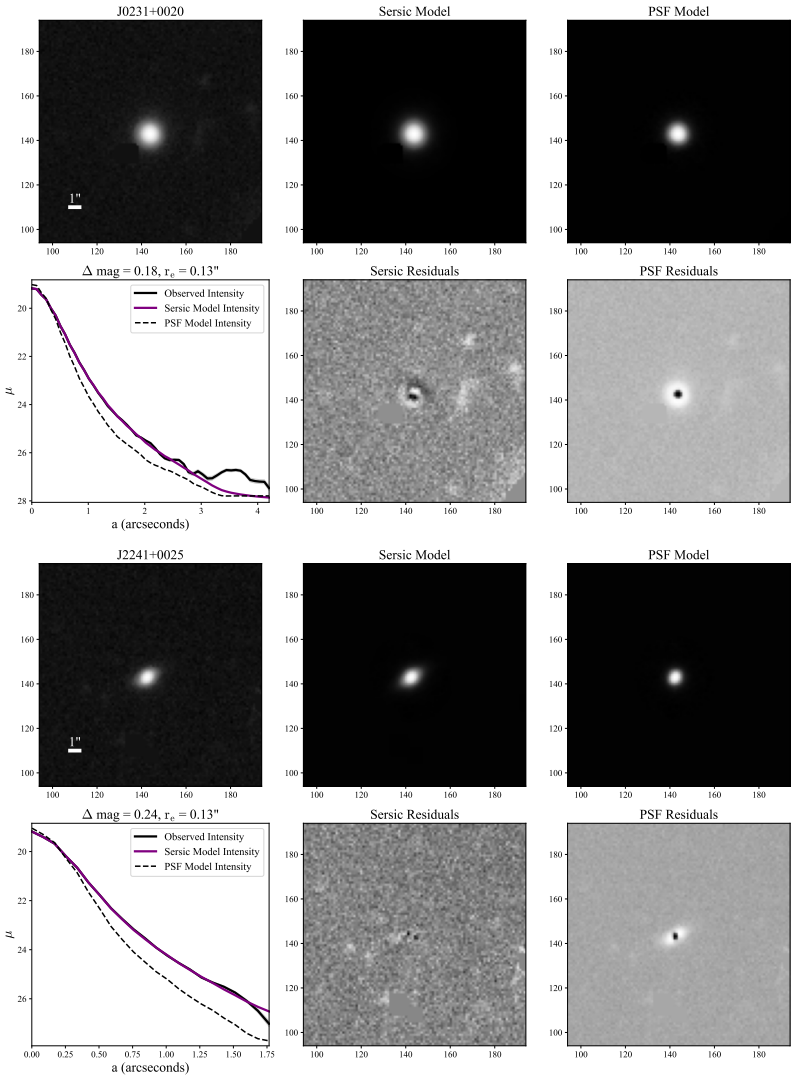

Figure 38: In the top row, ∼17x17" cutouts of the image (left), best fitting Sérsic model (center), and best fitting point source model (right) generated with `GALFIT` for the two smallest galaxies in SQuIGG$\vec{L}$E with no neighbors which required simultaneous fitting. Below each of the models, we show the residuals, with masked pixels greyed out. In the bottom left, we show the 1D surface brightness profiles for the data (blue), the Sérsic model (red), and the point source (black). Profiles are truncated when the signal to noise drops below 3. It is clear that even for $r_e \sim 0.1$" galaxies, the best fitting point source model will result in a galaxy which is too centrally peaked and which does not properly capture the galaxy wings seen in the data.

Bibliography

[1] Bela Abolfathi, D. S. Aguado, Gabriela Aguilar, Carlos Allende Prieto, Andres Almeida, Tonima Tasnim Ananna, Friedrich Anders, Scott F. Anderson, Brett H. Andrews, Borja Anguiano, Alfonso Aragón-Salamanca, Maria Argudo-Fernández, Eric Armengaud, Metin Ata, Eric Aubourg, Vladimir Avila-Reese, Carles Badenes, Stephen Bailey, Christophe Balland, Kathleen A. Barger, Jorge Barrera-Ballesteros, Curtis Bartosz, Fabienne Bastien, Dominic Bates, Falk Baumgarten, Julian Bautista, Rachael Beaton, Timothy C. Beers, Francesco Belfiore, Chad F. Bender, Mariangela Bernardi, Matthew A. Bershady, Florian Beutler, Jonathan C. Bird, Dmitry Bizyaev, Guillermo A. Blanc, Michael R. Blanton, Michael Blomqvist, Adam S. Bolton, Médéric Boquien, Jura Borissova, Jo Bovy, Christian Andres Bradna Diaz, William Nielsen Brandt, Jonathan Brinkmann, Joel R. Brownstein, Kevin Bundy, Adam J. Burgasser, Etienne Burtin, Nicolás G. Busca, Caleb I. Cañas, Mariana Cano-Díaz, Michele Cappellari, Ricardo Carrera, Andrew R. Casey, Bernardo Cervantes Sodi, Yanping Chen, Brian Cherinka, Cristina Chiappini, Peter Doohyun Choi, Drew Chojnowski, Chia-Hsun Chuang, Haeun Chung, Nicolas Clerc, Roger E. Cohen, Julia M. Comerford, Johan Comparat, Janaina Correa do Nascimento, Luiz da Costa, Marie-Claude Cousinou, Kevin Covey, Jeffrey D. Crane, Irene Cruz-Gonzalez, Katia Cunha, Gabriele da Silva Ilha, Guillermo J. Damke, Jeremy Darling, Jr. Davidson, James W., Kyle Dawson, Miguel Angel C. de Icaza Lizaola, Axel de la Macorra, Sylvain de la Torre, Nathan De Lee, Victoria de Sainte Agathe, Alice Deconto Machado, Flavia Dell'Agli, Timothée Delubac, Aleksandar M. Diamond-Stanic, John Donor, Juan José Downes, Niv Drory, Hélion du Mas des Bourboux, Christopher J. Duckworth, Tom Dwelly, Jamie Dyer, Garrett Ebelke, Arthur Davis Eigenbrot, Daniel J. Eisenstein, Yvonne P. Elsworth, Eric Emsellem, Michael Eracleous, Ghazaleh Erfanianfar, Stephanie Escoffier, Xiaohui Fan, Emma Fernández Alvar, J. G. Fernandez-Trincado, Rafael Fernand o Cirolini, Diane Feuillet, Alexis Finoguenov, Scott W. Fleming, Andreu Font-Ribera, Gordon Freischlad, Peter Frinchaboy, Hai Fu, Yilen Gómez Maqueo Chew, Lluís Galbany, Ana E. García Pérez, R. Garcia-Dias, D. A. García-Hernández, Luis Alberto Garma Oehmichen, Patrick Gaulme, Joseph Gelfand , Héctor Gil-Marín, Bruce A. Gillespie, Daniel Goddard, Jonay I. González Hernández, Violeta Gonzalez-Perez, Kathleen Grabowski, Paul J. Green, Catherine J. Grier, Alain Gueguen, Hong Guo, Julien Guy, Alex Hagen, Patrick Hall, Paul Harding, Sten Hasselquist, Suzanne Hawley, Christian R. Hayes, Fred Hearty, Saskia Hekker, Jesus Hernand ez, Hector Hernandez Toledo, David W. Hogg, Kelly Holley-Bockelmann, Jon A. Holtzman, Jiamin Hou, Bau-Ching Hsieh, Jason A. S. Hunt, Timothy A. Hutchinson, Ho Seong Hwang, Camilo Eduardo Jimenez Angel, Jennifer A. Johnson, Amy Jones, Henrik Jönsson, Eric Jullo, Fahim Sakil Khan, Karen Kinemuchi, David Kirkby, IV Kirkpatrick, Charles C., Francisco-Shu Kitaura, Gillian R. Knapp, Jean-Paul Kneib, Juna A. Kollmeier, Ivan Lacerna, Richard R. Lane, Dustin Lang, David R. Law, Jean-Marc Le Goff, Young-Bae Lee, Hongyu Li, Cheng Li, Jianhui Lian, Yu Liang, Marcos Lima, Lihwai Lin, Dan Long, Sara Lucatello, Britt Lund-

gren, J. Ted Mackereth, Chelsea L. MacLeod, Suvrath Mahadevan, Marcio Antonio Geimba Maia, Steven Majewski, Arturo Manchado, Claudia Maraston, Vivek Mariappan, Rui Marques-Chaves, Thomas Masseron, Karen L. Masters, Richard M. McDermid, Ian D. McGreer, Matthew Melendez, Sofia Meneses-Goytia, Andrea Merloni, Michael R. Merrifield, Szabolcs Meszaros, Andres Meza, Ivan Minchev, Dante Minniti, Eva-Maria Mueller, Francisco Muller-Sanchez, Demitri Muna, Ricardo R. Muñoz, Adam D. Myers, Preethi Nair, Kirpal Nand ra, Melissa Ness, Jeffrey A. Newman, Robert C. Nichol, David L. Nidever, Christian Nitschelm, Pasquier Noterdaeme, Julia O'Connell, Ryan James Oelkers, Audrey Oravetz, Daniel Oravetz, Erik Aquino Ortíz, Yeisson Osorio, Zach Pace, Nelson Padilla, Nathalie Palanque-Delabrouille, Pedro Alonso Palicio, Hsi-An Pan, Kaike Pan, Taniya Parikh, Isabelle Pâris, Changbom Park, Sebastien Peirani, Marcos Pellejero-Ibanez, Samantha Penny, Will J. Percival, Ismael Perez-Fournon, Patrick Petitjean, Matthew M. Pieri, Marc Pinsonneault, Alice Pisani, Francisco Prada, Abhishek Prakash, Anna Bárbara de Andrade Queiroz, M. Jordan Raddick, Anand Raichoor, Sandro Barboza Rembold, Hannah Richstein, Rogemar A. Riffel, Rogério Riffel, Hans-Walter Rix, Annie C. Robin, Sergio Rodríguez Torres, Carlos Román-Zúñiga, Ashley J. Ross, Graziano Rossi, John Ruan, Rossana Ruggeri, Jose Ruiz, Mara Salvato, Ariel G. Sánchez, Sebastián F. Sánchez, Jorge Sanchez Almeida, José R. Sánchez-Gallego, Felipe Antonio Santana Rojas, Basílio Xavier Santiago, Ricardo P. Schiavon, Jaderson S. Schimoia, Edward Schlafly, David Schlegel, Donald P. Schneider, William J. Schuster, Axel Schwope, Hee-Jong Seo, Aldo Serenelli, Shiyin Shen, Yue Shen, Matthew Shetrone, Michael Shull, Víctor Silva Aguirre, Joshua D. Simon, Mike Skrutskie, Anže Slosar, Rebecca Smethurst, Verne Smith, Jennifer Sobeck, Garrett Somers, Barbara J. Souter, Diogo Souto, Ashley Spindler, David V. Stark, Keivan Stassun, Matthias Steinmetz, Dennis Stello, Thaisa Storchi-Bergmann, Alina Streblyanska, Guy S. Stringfellow, Genaro Suárez, Jing Sun, Laszlo Szigeti, Manuchehr Taghizadeh-Popp, Michael S. Talbot, Baitian Tang, Charling Tao, Jamie Tayar, Mita Tembe, Johanna Teske, Aniruddha R. Thakar, Daniel Thomas, Patricia Tissera, Rita Tojeiro, Christy Tremonti, Nicholas W. Troup, Meg Urry, O. Valenzuela, Remco van den Bosch, Jaime Vargas-González, Mariana Vargas-Magaña, Jose Alberto Vazquez, Sandro Villanova, Nicole Vogt, David Wake, Yuting Wang, Benjamin Alan Weaver, Anne-Marie Weijmans, David H. Weinberg, Kyle B. Westfall, David G. Whelan, Eric Wilcots, Vivienne Wild, Rob A. Williams, John Wilson, W. M. Wood-Vasey, Dominika Wylezalek, Ting Xiao, Renbin Yan, Meng Yang, Jason E. Ybarra, Christophe Yèche, Nadia Zakamska, Olga Zamora, Pauline Zarrouk, Gail Zasowski, Kai Zhang, Cheng Zhao, Gong-Bo Zhao, Zheng Zheng, Zheng Zheng, Zhi-Min Zhou, Guangtun Zhu, Joel C. Zinn, and Hu Zou. The Fourteenth Data Release of the Sloan Digital Sky Survey: First Spectroscopic Data from the Extended Baryon Oscillation Spectroscopic Survey and from the Second Phase of the Apache Point Observatory Galactic Evolution Experiment. ApJS, 235(2):42, April 2018.

[2] Roberto G. Abraham, Sidney van den Bergh, and Preethi Nair. A New Approach to Galaxy Morphology. I. Analysis of the Sloan Digital Sky Survey Early Data Release.

ApJ, 588(1):218–229, May 2003.

[3] Hiroaki Aihara, Yusra AlSayyad, Makoto Ando, Robert Armstrong, James Bosch, Eiichi Egami, Hisanori Furusawa, Junko Furusawa, Sumiko Harasawa, Yuichi Harikane, Bau-Ching Hsieh, Hiroyuki Ikeda, Kei Ito, Ikuru Iwata, Tadayuki Kodama, Michitaro Koike, Mitsuru Kokubo, Yutaka Komiyama, Xiangchong Li, Yongming Liang, Yen-Ting Lin, Robert H. Lupton, Nate B. Lust, Lauren A. MacArthur, Ken Mawatari, Sogo Mineo, Hironao Miyatake, Satoshi Miyazaki, Surhud More, Takahiro Morishima, Hitoshi Murayama, Kimihiko Nakajima, Fumiaki Nakata, Atsushi J. Nishizawa, Masamune Oguri, Nobuhiro Okabe, Yuki Okura, Yoshiaki Ono, Ken Osato, Masami Ouchi, Yen-Chen Pan, Andrés A. Plazas Malagón, Paul A. Price, Sophie L. Reed, Eli S. Rykoff, Takatoshi Shibuya, Mirko Simunovic, Michael A. Strauss, Kanako Sugimori, Yasushi Suto, Nao Suzuki, Masahiro Takada, Yuhei Takagi, Tadafumi Takata, Satoshi Takita, Masayuki Tanaka, Shenli Tang, Dan S. Taranu, Tsuyoshi Terai, Yoshiki Toba, Edwin L. Turner, Hisakazu Uchiyama, Bovornpratch Vijarnwannaluk, Christopher Z. Waters, Yoshihiko Yamada, Naoaki Yamamoto, and Takuji Yamashita. Third data release of the Hyper Suprime-Cam Subaru Strategic Program. PASJ, 74(2):247–272, April 2022.

[4] Hiroaki Aihara, Nobuo Arimoto, Robert Armstrong, Stéphane Arnouts, Neta A. Bahcall, Steven Bickerton, James Bosch, Kevin Bundy, Peter L. Capak, James H. H. Chan, Masashi Chiba, Jean Coupon, Eiichi Egami, Motohiro Enoki, Francois Finet, Hiroki Fujimori, Seiji Fujimoto, Hisanori Furusawa, Junko Furusawa, Tomotsugu Goto, Andy Goulding, Johnny P. Greco, Jenny E. Greene, James E. Gunn, Takashi Hamana, Yuichi Harikane, Yasuhiro Hashimoto, Takashi Hattori, Masao Hayashi, Yusuke Hayashi, Krzysztof G. Hełminiak, Ryo Higuchi, Chiaki Hikage, Paul T. P. Ho, Bau-Ching Hsieh, Kuiyun Huang, Song Huang, Hiroyuki Ikeda, Masatoshi Imanishi, Akio K. Inoue, Kazushi Iwasawa, Ikuru Iwata, Anton T. Jaelani, Hung-Yu Jian, Yukiko Kamata, Hiroshi Karoji, Nobunari Kashikawa, Nobuhiko Katayama, Satoshi Kawanomoto, Issha Kayo, Jin Koda, Michitaro Koike, Takashi Kojima, Yutaka Komiyama, Akira Konno, Shintaro Koshida, Yusei Koyama, Haruka Kusakabe, Alexie Leauthaud, Chien-Hsiu Lee, Lihwai Lin, Yen-Ting Lin, Robert H. Lupton, Rachel Mandelbaum, Yoshiki Matsuoka, Elinor Medezinski, Sogo Mineo, Shoken Miyama, Hironao Miyatake, Satoshi Miyazaki, Rieko Momose, Anupreeta More, Surhud More, Yuki Moritani, Takashi J. Moriya, Tomoki Morokuma, Shiro Mukae, Ryoma Murata, Hitoshi Murayama, Tohru Nagao, Fumiaki Nakata, Mana Niida, Hiroko Niikura, Atsushi J. Nishizawa, Yoshiyuki Obuchi, Masamune Oguri, Yukie Oishi, Nobuhiro Okabe, Sakurako Okamoto, Yuki Okura, Yoshiaki Ono, Masato Onodera, Masafusa Onoue, Ken Osato, Masami Ouchi, Paul A. Price, Tae-Soo Pyo, Masao Sako, Marcin Sawicki, Takatoshi Shibuya, Kazuhiro Shimasaku, Atsushi Shimono, Masato Shirasaki, John D. Silverman, Melanie Simet, Joshua Speagle, David N. Spergel, Michael A. Strauss, Yuma Sugahara, Naoshi Sugiyama, Yasushi Suto, Sherry H. Suyu, Nao Suzuki, Philip J. Tait, Masahiro Takada, Tadafumi Takata, Naoyuki Tamura, Manobu M. Tanaka, Masaomi Tanaka, Masayuki Tanaka, Yoko Tanaka, Tsuyoshi

Terai, Yuichi Terashima, Yoshiki Toba, Nozomu Tominaga, Jun Toshikawa, Edwin L. Turner, Tomohisa Uchida, Hisakazu Uchiyama, Keiichi Umetsu, Fumihiro Uraguchi, Yuji Urata, Tomonori Usuda, Yousuke Utsumi, Shiang-Yu Wang, Wei-Hao Wang, Kenneth C. Wong, Kiyoto Yabe, Yoshihiko Yamada, Hitomi Yamanoi, Naoki Yasuda, Sherry Yeh, Atsunori Yonehara, and Suraphong Yuma. The Hyper Suprime-Cam SSP Survey: Overview and survey design. PASJ, 70:S4, January 2018.

[5] Mohammad Akhshik, Katherine E. Whitaker, Gabriel Brammer, Guillaume Mahler, Keren Sharon, Joel Leja, Matthew B. Bayliss, Rachel Bezanson, Michael D. Gladders, Allison Man, Erica J. Nelson, Jane R. Rigby, Francesca Rizzo, Sune Toft, Sarah Wellons, and Christina C. Williams. REQUIEM-2D: Spatially Resolved Stellar Populations from HST 2D Grism Spectroscopy. *arXiv e-prints*, page arXiv:2008.02276, August 2020.

[6] Mohammad Akhshik, Katherine E. Whitaker, Joel Leja, Johan Richard, Justin S. Spilker, Mimi Song, Gabriel Brammer, Rachel Bezanson, Harald Ebeling, Anna R. Gallazzi, Guillaume Mahler, Lamiya A. Mowla, Erica J. Nelson, Camilla Pacifici, Keren Sharon, Sune Toft, Christina C. Williams, Lillian Wright, and Johannes Zabl. REQUIEM-2D: A Diversity of Formation Pathways in a Sample of Spatially Resolved Massive Quiescent Galaxies at z 2. ApJ, 943(2):179, February 2023.

[7] Katherine Alatalo, Sabrina L. Cales, Philip N. Appleton, Lisa J. Kewley, Mark Lacy, Ute Lisenfeld, Kristina Nyland , and Jeffrey A. Rich. Catching Quenching Galaxies: The Nature of the WISE Infrared Transition Zone. ApJ, 794(1):L13, October 2014.

[8] Katherine Alatalo, Ute Lisenfeld, Lauranne Lanz, Philip N. Appleton, Felipe Ardila, Sabrina L. Cales, Lisa J. Kewley, Mark Lacy, Anne M. Medling, Kristina Nyland , Jeffrey A. Rich, and C. Meg Urry. Shocked POststarburst Galaxy Survey. II. The Molecular Gas Content and Properties of a Subset of SPOGs. ApJ, 827(2):106, August 2016.

[9] Omar Almaini, Vivienne Wild, David T. Maltby, William G. Hartley, Chris Simpson, Nina A. Hatch, Ross J. McLure, James S. Dunlop, and Kate Rowlands. Massive post-starburst galaxies at z ¿ 1 are compact proto-spheroids. MNRAS, 472(2):1401–1412, December 2017.

[10] Astropy Collaboration, A. M. Price-Whelan, B. M. Sipőcz, H. M. Günther, P. L. Lim, S. M. Crawford, S. Conseil, D. L. Shupe, M. W. Craig, N. Dencheva, A. Ginsburg, J. T. Vand erPlas, L. D. Bradley, D. Pérez-Suárez, M. de Val-Borro, T. L. Aldcroft, K. L. Cruz, T. P. Robitaille, E. J. Tollerud, C. Ardelean, T. Babej, Y. P. Bach, M. Bachetti, A. V. Bakanov, S. P. Bamford, G. Barentsen, P. Barmby, A. Baumbach, K. L. Berry, F. Biscani, M. Boquien, K. A. Bostroem, L. G. Bouma, G. B. Brammer,

E. M. Bray, H. Breytenbach, H. Buddelmeijer, D. J. Burke, G. Calderone, J. L. Cano Rodríguez, M. Cara, J. V. M. Cardoso, S. Cheedella, Y. Copin, L. Corrales, D. Crichton, D. D'Avella, C. Deil, É. Depagne, J. P. Dietrich, A. Donath, M. Droettboom, N. Earl, T. Erben, S. Fabbro, L. A. Ferreira, T. Finethy, R. T. Fox, L. H. Garrison, S. L. J. Gibbons, D. A. Goldstein, R. Gommers, J. P. Greco, P. Greenfield, A. M. Groener, F. Grollier, A. Hagen, P. Hirst, D. Homeier, A. J. Horton, G. Hosseinzadeh, L. Hu, J. S. Hunkeler, Ž. Ivezić, A. Jain, T. Jenness, G. Kanarek, S. Kendrew, N. S. Kern, W. E. Kerzendorf, A. Khvalko, J. King, D. Kirkby, A. M. Kulkarni, A. Kumar, A. Lee, D. Lenz, S. P. Littlefair, Z. Ma, D. M. Macleod, M. Mastropietro, C. McCully, S. Montagnac, B. M. Morris, M. Mueller, S. J. Mumford, D. Muna, N. A. Murphy, S. Nelson, G. H. Nguyen, J. P. Ninan, M. Nöthe, S. Ogaz, S. Oh, J. K. Parejko, N. Parley, S. Pascual, R. Patil, A. A. Patil, A. L. Plunkett, J. X. Prochaska, T. Rastogi, V. Reddy Janga, J. Sabater, P. Sakurikar, M. Seifert, L. E. Sherbert, H. Sherwood-Taylor, A. Y. Shih, J. Sick, M. T. Silbiger, S. Singanamalla, L. P. Singer, P. H. Sladen, K. A. Sooley, S. Sornarajah, O. Streicher, P. Teuben, S. W. Thomas, G. R. Tremblay, J. E. H. Turner, V. Terrón, M. H. van Kerkwijk, A. de la Vega, L. L. Watkins, B. A. Weaver, J. B. Whitmore, J. Woillez, V. Zabalza, and Astropy Contributors. The Astropy Project: Building an Open-science Project and Status of the v2.0 Core Package. AJ, 156(3):123, September 2018.

[11] Astropy Collaboration, T. P. Robitaille, E. J. Tollerud, P. Greenfield, M. Droettboom, E. Bray, T. Aldcroft, M. Davis, A. Ginsburg, A. M. Price-Whelan, W. E. Kerzendorf, A. Conley, N. Crighton, K. Barbary, D. Muna, H. Ferguson, F. Grollier, M. M. Parikh, P. H. Nair, H. M. Unther, C. Deil, J. Woillez, S. Conseil, R. Kramer, J. E. H. Turner, L. Singer, R. Fox, B. A. Weaver, V. Zabalza, Z. I. Edwards, K. Azalee Bostroem, D. J. Burke, A. R. Casey, S. M. Crawford, N. Dencheva, J. Ely, T. Jenness, K. Labrie, P. L. Lim, F. Pierfederici, A. Pontzen, A. Ptak, B. Refsdal, M. Servillat, and O. Streicher. Astropy: A community Python package for astronomy. A&A, 558:A33, October 2013.

[12] Michael L. Balogh, Simon L. Morris, H. K. C. Yee, R. G. Carlberg, and Erica Ellingson. Differential Galaxy Evolution in Cluster and Field Galaxies at z˜0.3. ApJ, 527(1):54–79, December 1999.

[13] Dalya Baron, Hagai Netzer, Dieter Lutz, J. Xavier Prochaska, and Ric I. Davies. Multiphase outflows in post-starburst E+A galaxies - I. General sample properties and the prevalence of obscured starbursts. MNRAS, 509(3):4457–4479, January 2022.

[14] Guillermo Barro, S. M. Faber, David C. Koo, Avishai Dekel, Jerome J. Fang, Jonathan R. Trump, Pablo G. Pérez-González, Camilla Pacifici, Joel R. Primack, Rachel S. Somerville, Haojing Yan, Yicheng Guo, Fengshan Liu, Daniel Ceverino, Dale D. Kocevski, and Elizabeth McGrath. Structural and Star-forming Relations since z $\sim$ 3: Connecting Compact Star-forming and Quiescent Galaxies. ApJ, 840(1):47, May 2017.

[15] Guillermo Barro, Jonathan R. Trump, David C. Koo, Avishai Dekel, Susan A. Kassin, Dale D. Kocevski, Sandra M. Faber, Arjen van der Wel, Yicheng Guo, Pablo G. Pérez-González, Elisa Toloba, Jerome J. Fang, Camilla Pacifici, Raymond Simons, Randy D. Campbell, Daniel Ceverino, Steven L. Finkelstein, Bob Goodrich, Marc Kassis, Anton M. Koekemoer, Nicholas P. Konidaris, Rachael C. Livermore, James E. Lyke, Bahram Mobasher, Hooshang Nayyeri, Michael Peth, Joel R. Primack, Luca Rizzi, Rachel S. Somerville, Gregory D. Wirth, and Adi Zolotov. Keck-I MOSFIRE Spectroscopy of Compact Star-forming Galaxies at z ¿~2: High Velocity Dispersions in Progenitors of Compact Quiescent Galaxies. ApJ, 795(2):145, November 2014.

[16] Peter Behroozi, Risa H. Wechsler, Andrew P. Hearin, and Charlie Conroy. UNIVERSEMACHINE: The correlation between galaxy growth and dark matter halo assembly from z = 0-10. MNRAS, 488(3):3143–3194, September 2019.

[17] K. Bekki, W. J. Couch, Y. Shioya, and A. Vazdekis. Origin of E+A galaxies - I. Physical properties of E+A galaxies formed from galaxy merging and interaction. MNRAS, 359(3):949–965, May 2005.

[18] Sirio Belli, Alessandra Contursi, Reinhard Genzel, Linda J. Tacconi, Natascha M. Förster-Schreiber, Dieter Lutz, Françoise Combes, Roberto Neri, Santiago García-Burillo, Karl F. Schuster, Rodrigo Herrera-Camus, Ken-ichi Tadaki, Rebecca L. Davies, Richard I. Davies, Benjamin D. Johnson, Minju M. Lee, Joel Leja, Erica J. Nelson, Sedona H. Price, Jinyi Shangguan, T. Taro Shimizu, Sandro Tacchella, and Hannah Übler. The Diverse Molecular Gas Content of Massive Galaxies Undergoing Quenching at z $\sim$ 1. ApJ, 909(1):L11, March 2021.

[19] Sirio Belli, Andrew B. Newman, and Richard S. Ellis. MOSFIRE Spectroscopy of Quiescent Galaxies at 1.5 ¡ z ¡ 2.5. II. Star Formation Histories and Galaxy Quenching. ApJ, 874(1):17, March 2019.

[20] Rachel Bezanson, Justin S. Spilker, Katherine A. Suess, David J. Setton, Robert Feldmann, Jenny E. Greene, Mariska Kriek, Desika Narayanan, and Margaret Verrico. Now You See It, Now You Don't: Star Formation Truncation Precedes the Loss of Molecular Gas by 100 Myr in Massive Poststarburst Galaxies at z 0.6. ApJ, 925(2):153, February 2022.

[21] Rachel Bezanson, Arjen van der Wel, Caroline Straatman, Camilla Pacifici, Po-Feng Wu, Ivana Barišić, Eric F. Bell, Charlie Conroy, Francesco D'Eugenio, Marijn Franx, Anna Gallazzi, Josha van Houdt, Michael V. Maseda, Adam Muzzin, Jesse van de Sande, David Sobral, and Justin Spilker. 1D Kinematics from Stars and Ionized Gas at z 0.8 from the LEGA-C Spectroscopic Survey of Massive Galaxies. ApJ, 868(2):L36, December 2018.

[22] Rachel Bezanson, Pieter G. van Dokkum, Tomer Tal, Danilo Marchesini, Mariska Kriek, Marijn Franx, and Paolo Coppi. The Relation Between Compact, Quiescent High-redshift Galaxies and Massive Nearby Elliptical Galaxies: Evidence for Hierarchical, Inside-Out Growth. ApJ, 697(2):1290–1298, June 2009.

[23] Michael R. Blanton, David W. Hogg, Neta A. Bahcall, Ivan K. Baldry, J. Brinkmann, István Csabai, Daniel Eisenstein, Masataka Fukugita, James E. Gunn, Željko Ivezić, D. Q. Lamb, Robert H. Lupton, Jon Loveday, Jeffrey A. Munn, R. C. Nichol, Sadanori Okamura, David J. Schlegel, Kazuhiro Shimasaku, Michael A. Strauss, Michael S. Vogeley, and David H. Weinberg. The Broadband Optical Properties of Galaxies with Redshifts 0.02¡z¡0.22. ApJ, 594(1):186–207, September 2003.

[24] Asa F. L. Bluck, Roberto Maiolino, Simcha Brownson, Christopher J. Conselice, Sara L. Ellison, Joanna M. Piotrowska, and Mallory D. Thorp. The quenching of galaxies, bulges, and disks since cosmic noon. A machine learning approach for identifying causality in astronomical data. A&A, 659:A160, March 2022.

[25] Asa F. L. Bluck, Roberto Maiolino, Joanna M. Piotrowska, James Trussler, Sara L. Ellison, Sebastian F. Sánchez, Mallory D. Thorp, Hossen Teimoorinia, Jorge Moreno, and Christopher J. Conselice. How do central and satellite galaxies quench? - Insights from spatially resolved spectroscopy in the MaNGA survey. MNRAS, 499(1):230–268, November 2020.

[26] James Bosch, Robert Armstrong, Steven Bickerton, Hisanori Furusawa, Hiroyuki Ikeda, Michitaro Koike, Robert Lupton, Sogo Mineo, Paul Price, Tadafumi Takata, Masayuki Tanaka, Naoki Yasuda, Yusra AlSayyad, Andrew C. Becker, William Coulton, Jean Coupon, Jose Garmilla, Song Huang, K. Simon Krughoff, Dustin Lang, Alexie Leauthaud, Kian-Tat Lim, Nate B. Lust, Lauren A. MacArthur, Rachel Mandelbaum, Hironao Miyatake, Satoshi Miyazaki, Ryoma Murata, Surhud More, Yuki Okura, Russell Owen, John D. Swinbank, Michael A. Strauss, Yoshihiko Yamada, and Hitomi Yamanoi. The Hyper Suprime-Cam software pipeline. PASJ, 70:S5, January 2018.

[27] Larry Bradley, Brigitta Sipocz, Thomas Robitaille, Erik Tollerud, Zé Vinícius, Christoph Deil, Kyle Barbary, Hans Moritz Günther, Mihai Cara, Ivo Busko, Simon Conseil, Michael Droettboom, Azalee Bostroem, E. M. Bray, Lars Andersen Bratholm, Tom Wilson, Matt Craig, Geert Barentsen, Sergio Pascual, Axel Donath, Johnny Greco, Gabriel Perren, P. L. Lim, and Wolfgang Kerzendorf. astropy/photutils: v0.6, January 2019.

[28] G. Bruzual and S. Charlot. Stellar population synthesis at the resolution of 2003. MNRAS, 344(4):1000–1028, October 2003.

[29] Kevin Bundy, Matthew A. Bershady, David R. Law, Renbin Yan, Niv Drory, Nicholas MacDonald, David A. Wake, Brian Cherinka, José R. Sánchez-Gallego, Anne-Marie Weijmans, Daniel Thomas, Christy Tremonti, Karen Masters, Lodovico Coccato, Aleksandar M. Diamond-Stanic, Alfonso Aragón-Salamanca, Vladimir Avila-Reese, Carles Badenes, Jésus Falcón-Barroso, Francesco Belfiore, Dmitry Bizyaev, Guillermo A. Blanc, Joss Bland-Hawthorn, Michael R. Blanton, Joel R. Brownstein, Nell Byler, Michele Cappellari, Charlie Conroy, Aaron A. Dutton, Eric Emsellem, James Etherington, Peter M. Frinchaboy, Hai Fu, James E. Gunn, Paul Harding, Evelyn J. Johnston, Guinevere Kauffmann, Karen Kinemuchi, Mark A. Klaene, Johan H. Knapen, Alexie Leauthaud, Cheng Li, Lihwai Lin, Roberto Maiolino, Viktor Malanushenko, Elena Malanushenko, Shude Mao, Claudia Maraston, Richard M. McDermid, Michael R. Merrifield, Robert C. Nichol, Daniel Oravetz, Kaike Pan, John K. Parejko, Sebastian F. Sanchez, David Schlegel, Audrey Simmons, Oliver Steele, Matthias Steinmetz, Karun Thanjavur, Benjamin A. Thompson, Jeremy L. Tinker, Remco C. E. van den Bosch, Kyle B. Westfall, David Wilkinson, Shelley Wright, Ting Xiao, and Kai Zhang. Overview of the SDSS-IV MaNGA Survey: Mapping nearby Galaxies at Apache Point Observatory. ApJ, 798(1):7, January 2015.

[30] Daniela Calzetti. Reddening and Star Formation in Starburst Galaxies. AJ, 113:162–184, January 1997.

[31] Michele Cappellari. Voronoi binning: Optimal adaptive tessellations of multi-dimensional data. page arXiv:0912.1303, December 2009.

[32] Michele Cappellari and Yannick Copin. Adaptive spatial binning of integral-field spectroscopic data using Voronoi tessellations. MNRAS, 342(2):345–354, June 2003.

[33] Michele Cappellari and Eric Emsellem. Parametric Recovery of Line-of-Sight Velocity Distributions from Absorption-Line Spectra of Galaxies via Penalized Likelihood. PASP, 116(816):138–147, February 2004.

[34] A. C. Carnall, D. J. McLeod, R. J. McLure, J. S. Dunlop, R. Begley, F. Cullen, C. T. Donnan, M. L. Hamadouche, S. M. Jewell, E. W. Jones, C. L. Pollock, and V. Wild. A surprising abundance of massive quiescent galaxies at 3 ¡ z ¡ 5 in the first data from JWST CEERS. MNRAS, 520(3):3974–3985, April 2023.

[35] A. C. Carnall, R. J. McLure, J. S. Dunlop, F. Cullen, D. J. McLeod, V. Wild, B. D. Johnson, S. Appleby, R. Davé, R. Amorin, M. Bolzonella, M. Castellano, A. Cimatti, O. Cucciati, A. Gargiulo, B. Garilli, F. Marchi, L. Pentericci, L. Pozzetti, C. Schreiber, M. Talia, and G. Zamorani. The VANDELS survey: the star-formation histories of massive quiescent galaxies at 1.0 ¡ z ¡ 1.3. MNRAS, 490(1):417–439, November 2019.

[36] A. C. Carnall, R. J. McLure, J. S. Dunlop, and R. Davé. Inferring the star formation histories of massive quiescent galaxies with BAGPIPES: evidence for multiple quenching mechanisms. MNRAS, 480(4):4379–4401, November 2018.

[37] A. C. Carnall, R. J. McLure, J. S. Dunlop, D. J. McLeod, V. Wild, F. Cullen, D. Magee, R. Begley, A. Cimatti, C. T. Donnan, M. L. Hamadouche, S. M. Jewell, and S. Walker. A massive quiescent galaxy at redshift 4.658. *arXiv e-prints*, page arXiv:2301.11413, January 2023.

[38] Gilles Chabrier. Galactic Stellar and Substellar Initial Mass Function. PASP, 115(809):763–795, July 2003.

[39] Yan-Mei Chen, Yong Shi, Vivienne Wild, Christy Tremonti, Kate Rowlands, Dmitry Bizyaev, Renbin Yan, Lihwai Lin, and Rogério Riffel. Post-starburst galaxies in SDSS-IV MaNGA. MNRAS, 489(4):5709–5722, November 2019.

[40] Jieun Choi, Aaron Dotter, Charlie Conroy, Matteo Cantiello, Bill Paxton, and Benjamin D. Johnson. Mesa Isochrones and Stellar Tracks (MIST). I. Solar-scaled Models. ApJ, 823(2):102, June 2016.

[41] Charlie Conroy. Modeling the Panchromatic Spectral Energy Distributions of Galaxies. ARA&A, 51(1):393–455, August 2013.

[42] Charlie Conroy and James E. Gunn. The Propagation of Uncertainties in Stellar Population Synthesis Modeling. III. Model Calibration, Comparison, and Evaluation. ApJ, 712(2):833–857, April 2010.

[43] Charlie Conroy, James E. Gunn, and Martin White. The Propagation of Uncertainties in Stellar Population Synthesis Modeling. I. The Relevance of Uncertain Aspects of Stellar Evolution and the Initial Mass Function to the Derived Physical Properties of Galaxies. ApJ, 699(1):486–506, July 2009.

[44] Christopher J. Conselice. The Relationship between Stellar Light Distributions of Galaxies and Their Formation Histories. ApJS, 147(1):1–28, July 2003.

[45] Warrick J. Couch, Amy J. Barger, Ian Smail, Richard S. Ellis, and Ray M. Sharples. Morphological Studies of the Galaxy Populations in Distant "Butcher-Oemler" Clusters with the Hubble Space Telescope. II. AC 103, AC 118, and AC 114 at Z = 0.31. ApJ, 497(1):188–211, April 1998.

[46] Warrick J. Couch, Richard S. Ellis, Ray M. Sharples, and Ian Smail. Morphological Studies of the Galaxy Populations in Distant "Butcher-Oemler" Clusters with HST. I. AC 114 at Z = 0.31 and Abell 370 at Z = 0.37. ApJ, 430:121, July 1994.

[47] Darren J. Croton, Volker Springel, Simon D. M. White, G. De Lucia, C. S. Frenk, L. Gao, A. Jenkins, G. Kauffmann, J. F. Navarro, and N. Yoshida. The many lives of active galactic nuclei: cooling flows, black holes and the luminosities and colours of galaxies. MNRAS, 365(1):11–28, January 2006.

[48] E. Daddi, A. Renzini, N. Pirzkal, A. Cimatti, S. Malhotra, M. Stiavelli, C. Xu, A. Pasquali, J. E. Rhoads, M. Brusa, S. di Serego Alighieri, H. C. Ferguson, A. M. Koekemoer, L. A. Moustakas, N. Panagia, and R. A. Windhorst. Passively Evolving Early-Type Galaxies at 1.4 ¡~z ¡~2.5 in the Hubble Ultra Deep Field. ApJ, 626(2):680–697, June 2005.

[49] I. Davidzon, O. Ilbert, C. Laigle, J. Coupon, H. J. McCracken, I. Delvecchio, D. Masters, P. Capak, B. C. Hsieh, O. Le Fèvre, L. Tresse, M. Bethermin, Y. Y. Chang, A. L. Faisst, E. Le Floc'h, C. Steinhardt, S. Toft, H. Aussel, C. Dubois, G. Hasinger, M. Salvato, D. B. Sanders, N. Scoville, and J. D. Silverman. The COSMOS2015 galaxy stellar mass function . Thirteen billion years of stellar mass assembly in ten snapshots. A&A, 605:A70, September 2017.

[50] L. J. M. Davies, C. del P. Lagos, A. Katsianis, A. S. G. Robotham, L. Cortese, S. P. Driver, M. N. Bremer, M. J. I. Brown, S. Brough, M. E. Cluver, M. W. Grootes, B. W. Holwerda, M. Owers, and S. Phillipps. Galaxy And Mass Assembly (GAMA): The sSFR-M_* relation part I - σ_{sSFR}-M_* as a function of sample, SFR indicator, and environment. MNRAS, 483(2):1881–1900, February 2019.

[51] Timothy A. Davis, Jenny Greene, Chung-Pei Ma, Viraj Pandya, John P. Blakeslee, Nicholas McConnell, and Jens Thomas. The MASSIVE survey - III. Molecular gas and a broken Tully-Fisher relation in the most massive early-type galaxies. MNRAS, 455(1):214–226, January 2016.

[52] Kyle S. Dawson, Jean-Paul Kneib, Will J. Percival, Shadab Alam, Franco D. Albareti, Scott F. Anderson, Eric Armengaud, Éric Aubourg, Stephen Bailey, Julian E. Bautista, Andreas A. Berlind, Matthew A. Bershady, Florian Beutler, Dmitry Bizyaev, Michael R. Blanton, Michael Blomqvist, Adam S. Bolton, Jo Bovy, W. N. Brandt, Jon Brinkmann, Joel R. Brownstein, Etienne Burtin, N. G. Busca, Zheng Cai, Chia-Hsun Chuang, Nicolas Clerc, Johan Comparat, Frances Cope, Rupert A. C. Croft, Irene Cruz-Gonzalez, Luiz N. da Costa, Marie-Claude Cousinou, Jeremy Darling, Axel de la Macorra, Sylvain de la Torre, Timothée Delubac, Hélion du Mas des Bourboux, Tom Dwelly, Anne Ealet, Daniel J. Eisenstein, Michael Eracleous,

S. Escoffier, Xiaohui Fan, Alexis Finoguenov, Andreu Font-Ribera, Peter Frinchaboy, Patrick Gaulme, Antonis Georgakakis, Paul Green, Hong Guo, Julien Guy, Shirley Ho, Diana Holder, Joe Huehnerhoff, Timothy Hutchinson, Yipeng Jing, Eric Jullo, Vikrant Kamble, Karen Kinemuchi, David Kirkby, Francisco-Shu Kitaura, Mark A. Klaene, Russ R. Laher, Dustin Lang, Pierre Laurent, Jean-Marc Le Goff, Cheng Li, Yu Liang, Marcos Lima, Qiufan Lin, Weipeng Lin, Yen-Ting Lin, Daniel C. Long, Britt Lundgren, Nicholas MacDonald, Marcio Antonio Geimba Maia, Elena Malanushenko, Viktor Malanushenko, Vivek Mariappan, Cameron K. McBride, Ian D. McGreer, Brice Ménard, Andrea Merloni, Andres Meza, Antonio D. Montero-Dorta, Demitri Muna, Adam D. Myers, Kirpal Nandra, Tracy Naugle, Jeffrey A. Newman, Pasquier Noterdaeme, Peter Nugent, Ricardo Ogando, Matthew D. Olmstead, Audrey Oravetz, Daniel J. Oravetz, Nikhil Padmanabhan, Nathalie Palanque-Delabrouille, Kaike Pan, John K. Parejko, Isabelle Pâris, John A. Peacock, Patrick Petitjean, Matthew M. Pieri, Alice Pisani, Francisco Prada, Abhishek Prakash, Anand Raichoor, Beth Reid, James Rich, Jethro Ridl, Sergio Rodriguez-Torres, Aurelio Carnero Rosell, Ashley J. Ross, Graziano Rossi, John Ruan, Mara Salvato, Conor Sayres, Donald P. Schneider, David J. Schlegel, Uros Seljak, Hee-Jong Seo, Branimir Sesar, Sarah Shandera, Yiping Shu, Anže Slosar, Flavia Sobreira, Alina Streblyanska, Nao Suzuki, Donna Taylor, Charling Tao, Jeremy L. Tinker, Rita Tojeiro, Mariana Vargas-Magaña, Yuting Wang, Benjamin A. Weaver, David H. Weinberg, Martin White, W. M. Wood-Vasey, Christophe Yeche, Zhongxu Zhai, Cheng Zhao, Gong-bo Zhao, Zheng Zheng, Guangtun Ben Zhu, and Hu Zou. The SDSS-IV Extended Baryon Oscillation Spectroscopic Survey: Overview and Early Data. AJ, 151(2):44, February 2016.

[53] Kyle S. Dawson, David J. Schlegel, Christopher P. Ahn, Scott F. Anderson, Éric Aubourg, Stephen Bailey, Robert H. Barkhouser, Julian E. Bautista, Alessandra Beifiori, Andreas A. Berlind, Vaishali Bhardwaj, Dmitry Bizyaev, Cullen H. Blake, Michael R. Blanton, Michael Blomqvist, Adam S. Bolton, Arnaud Borde, Jo Bovy, W. N. Brandt, Howard Brewington, Jon Brinkmann, Peter J. Brown, Joel R. Brownstein, Kevin Bundy, N. G. Busca, William Carithers, Aurelio R. Carnero, Michael A. Carr, Yanmei Chen, Johan Comparat, Natalia Connolly, Frances Cope, Rupert A. C. Croft, Antonio J. Cuesta, Luiz N. da Costa, James R. A. Davenport, Timothée Delubac, Roland de Putter, Saurav Dhital, Anne Ealet, Garrett L. Ebelke, Daniel J. Eisenstein, S. Escoffier, Xiaohui Fan, N. Filiz Ak, Hayley Finley, Andreu Font-Ribera, R. Génova-Santos, James E. Gunn, Hong Guo, Daryl Haggard, Patrick B. Hall, Jean-Christophe Hamilton, Ben Harris, David W. Harris, Shirley Ho, David W. Hogg, Diana Holder, Klaus Honscheid, Joe Huehnerhoff, Beatrice Jordan, Wendell P. Jordan, Guinevere Kauffmann, Eyal A. Kazin, David Kirkby, Mark A. Klaene, Jean-Paul Kneib, Jean-Marc Le Goff, Khee-Gan Lee, Daniel C. Long, Craig P. Loomis, Britt Lundgren, Robert H. Lupton, Marcio A. G. Maia, Martin Makler, Elena Malanushenko, Viktor Malanushenko, Rachel Mandelbaum, Marc Manera, Claudia Maraston, Daniel Margala, Karen L. Masters, Cameron K. McBride, Patrick McDonald, Ian D. McGreer, Richard G. McMahon, Olga Mena, Jordi Miralda-Escudé, Antonio D. Montero-Dorta, Francesco Montesano, Demitri Muna, Adam D. Myers, Tracy Naugle, Robert C.

Nichol, Pasquier Noterdaeme, Sebastián E. Nuza, Matthew D. Olmstead, Audrey Oravetz, Daniel J. Oravetz, Russell Owen, Nikhil Padmanabhan, Nathalie Palanque-Delabrouille, Kaike Pan, John K. Parejko, Isabelle Pâris, Will J. Percival, Ismael Pérez-Fournon, Ignasi Pérez-Ràfols, Patrick Petitjean, Robert Pfaffenberger, Janine Pforr, Matthew M. Pieri, Francisco Prada, Adrian M. Price-Whelan, M. Jordan Raddick, Rafael Rebolo, James Rich, Gordon T. Richards, Constance M. Rockosi, Natalie A. Roe, Ashley J. Ross, Nicholas P. Ross, Graziano Rossi, J. A. Rubiño-Martin, Lado Samushia, Ariel G. Sánchez, Conor Sayres, Sarah J. Schmidt, Donald P. Schneider, C. G. Scóccola, Hee-Jong Seo, Alaina Shelden, Erin Sheldon, Yue Shen, Yiping Shu, Anže Slosar, Stephen A. Smee, Stephanie A. Snedden, Fritz Stauffer, Oliver Steele, Michael A. Strauss, Alina Streblyanska, Nao Suzuki, Molly E. C. Swanson, Tomer Tal, Masayuki Tanaka, Daniel Thomas, Jeremy L. Tinker, Rita Tojeiro, Christy A. Tremonti, M. Vargas Magaña, Licia Verde, Matteo Viel, David A. Wake, Mike Watson, Benjamin A. Weaver, David H. Weinberg, Benjamin J. Weiner, Andrew A. West, Martin White, W. M. Wood-Vasey, Christophe Yeche, Idit Zehavi, Gong-Bo Zhao, and Zheng Zheng. The Baryon Oscillation Spectroscopic Survey of SDSS-III. AJ, 145(1):10, January 2013.

[54] Gerard de Vaucouleurs. Integrated Colors of Bright Galaxies in the u, b, V System. ApJS, 5:233, January 1961.

[55] A. Dekel and A. Burkert. Wet disc contraction to galactic blue nuggets and quenching to red nuggets. MNRAS, 438(2):1870–1879, February 2014.

[56] DESI Collaboration, Amir Aghamousa, Jessica Aguilar, Steve Ahlen, Shadab Alam, Lori E. Allen, Carlos Allende Prieto, James Annis, Stephen Bailey, Christophe Balland, Otger Ballester, Charles Baltay, Lucas Beaufore, Chris Bebek, Timothy C. Beers, Eric F. Bell, José Luis Bernal, Robert Besuner, Florian Beutler, Chris Blake, Hannes Bleuler, Michael Blomqvist, Robert Blum, Adam S. Bolton, Cesar Briceno, David Brooks, Joel R. Brownstein, Elizabeth Buckley-Geer, Angela Burden, Etienne Burtin, Nicolas G. Busca, Robert N. Cahn, Yan-Chuan Cai, Laia Cardiel-Sas, Raymond G. Carlberg, Pierre-Henri Carton, Ricard Casas, Francisco J. Castander, Jorge L. Cervantes-Cota, Todd M. Claybaugh, Madeline Close, Carl T. Coker, Shaun Cole, Johan Comparat, Andrew P. Cooper, M. C. Cousinou, Martin Crocce, Jean-Gabriel Cuby, Daniel P. Cunningham, Tamara M. Davis, Kyle S. Dawson, Axel de la Macorra, Juan De Vicente, Timothée Delubac, Mark Derwent, Arjun Dey, Govinda Dhungana, Zhejie Ding, Peter Doel, Yutong T. Duan, Anne Ealet, Jerry Edelstein, Sarah Eftekharzadeh, Daniel J. Eisenstein, Ann Elliott, Stéphanie Escoffier, Matthew Evatt, Parker Fagrelius, Xiaohui Fan, Kevin Fanning, Arya Farahi, Jay Farihi, Ginevra Favole, Yu Feng, Enrique Fernandez, Joseph R. Findlay, Douglas P. Finkbeiner, Michael J. Fitzpatrick, Brenna Flaugher, Samuel Flender, Andreu Font-Ribera, Jaime E. Forero-Romero, Pablo Fosalba, Carlos S. Frenk, Michele Fumagalli, Boris T. Gaensicke, Giuseppe Gallo, Juan Garcia-Bellido, Enrique Gaztanaga,

Nicola Pietro Gentile Fusillo, Terry Gerard, Irena Gershkovich, Tommaso Giannantonio, Denis Gillet, Guillermo Gonzalez-de-Rivera, Violeta Gonzalez-Perez, Shelby Gott, Or Graur, Gaston Gutierrez, Julien Guy, Salman Habib, Henry Heetderks, Ian Heetderks, Katrin Heitmann, Wojciech A. Hellwing, David A. Herrera, Shirley Ho, Stephen Holland, Klaus Honscheid, Eric Huff, Timothy A. Hutchinson, Dragan Huterer, Ho Seong Hwang, Joseph Maria Illa Laguna, Yuzo Ishikawa, Dianna Jacobs, Niall Jeffrey, Patrick Jelinsky, Elise Jennings, Linhua Jiang, Jorge Jimenez, Jennifer Johnson, Richard Joyce, Eric Jullo, Stéphanie Juneau, Sami Kama, Armin Karcher, Sonia Karkar, Robert Kehoe, Noble Kennamer, Stephen Kent, Martin Kilbinger, Alex G. Kim, David Kirkby, Theodore Kisner, Ellie Kitanidis, Jean-Paul Kneib, Sergey Koposov, Eve Kovacs, Kazuya Koyama, Anthony Kremin, Richard Kron, Luzius Kronig, Andrea Kueter-Young, Cedric G. Lacey, Robin Lafever, Ofer Lahav, Andrew Lambert, Michael Lampton, Martin Landriau, Dustin Lang, Tod R. Lauer, Jean-Marc Le Goff, Laurent Le Guillou, Auguste Le Van Suu, Jae Hyeon Lee, Su-Jeong Lee, Daniela Leitner, Michael Lesser, Michael E. Levi, Benjamin L'Huillier, Baojiu Li, Ming Liang, Huan Lin, Eric Linder, Sarah R. Loebman, Zarija Lukić, Jun Ma, Niall MacCrann, Christophe Magneville, Laleh Makarem, Marc Manera, Christopher J. Manser, Robert Marshall, Paul Martini, Richard Massey, Thomas Matheson, Jeremy McCauley, Patrick McDonald, Ian D. McGreer, Aaron Meisner, Nigel Metcalfe, Timothy N. Miller, Ramon Miquel, John Moustakas, Adam Myers, Milind Naik, Jeffrey A. Newman, Robert C. Nichol, Andrina Nicola, Luiz Nicolati da Costa, Jundan Nie, Gustavo Niz, Peder Norberg, Brian Nord, Dara Norman, Peter Nugent, Thomas O'Brien, Minji Oh, Knut A. G. Olsen, Cristobal Padilla, Hamsa Padmanabhan, Nikhil Padmanabhan, Nathalie Palanque-Delabrouille, Antonella Palmese, Daniel Pappalardo, Isabelle Pâris, Changbom Park, Anna Patej, John A. Peacock, Hiranya V. Peiris, Xiyan Peng, Will J. Percival, Sandrine Perruchot, Matthew M. Pieri, Richard Pogge, Jennifer E. Pollack, Claire Poppett, Francisco Prada, Abhishek Prakash, Ronald G. Probst, David Rabinowitz, Anand Raichoor, Chang Hee Ree, Alexandre Refregier, Xavier Regal, Beth Reid, Kevin Reil, Mehdi Rezaie, Constance M. Rockosi, Natalie Roe, Samuel Ronayette, Aaron Roodman, Ashley J. Ross, Nicholas P. Ross, Graziano Rossi, Eduardo Rozo, Vanina Ruhlmann-Kleider, Eli S. Rykoff, Cristiano Sabiu, Lado Samushia, Eusebio Sanchez, Javier Sanchez, David J. Schlegel, Michael Schneider, Michael Schubnell, Aurélia Secroun, Uros Seljak, Hee-Jong Seo, Santiago Serrano, Arman Shafieloo, Huanyuan Shan, Ray Sharples, Michael J. Sholl, William V. Shourt, Joseph H. Silber, David R. Silva, Martin M. Sirk, Anze Slosar, Alex Smith, George F. Smoot, Debopam Som, Yong-Seon Song, David Sprayberry, Ryan Staten, Andy Stefanik, Gregory Tarle, Suk Sien Tie, Jeremy L. Tinker, Rita Tojeiro, Francisco Valdes, Octavio Valenzuela, Monica Valluri, Mariana Vargas-Magana, Licia Verde, Alistair R. Walker, Jiali Wang, Yuting Wang, Benjamin A. Weaver, Curtis Weaverdyck, Risa H. Wechsler, David H. Weinberg, Martin White, Qian Yang, Christophe Yeche, Tianmeng Zhang, Gong-Bo Zhao, Yi Zheng, Xu Zhou, Zhimin Zhou, Yaling Zhu, Hu Zou, and Ying Zu. The DESI Experiment Part I: Science,Targeting, and Survey Design. *arXiv e-prints*, page arXiv:1611.00036, October 2016.

[57] DESI Collaboration, Amir Aghamousa, Jessica Aguilar, Steve Ahlen, Shadab Alam, Lori E. Allen, Carlos Allende Prieto, James Annis, Stephen Bailey, Christophe Balland, Otger Ballester, Charles Baltay, Lucas Beaufore, Chris Bebek, Timothy C. Beers, Eric F. Bell, José Luis Bernal, Robert Besuner, Florian Beutler, Chris Blake, Hannes Bleuler, Michael Blomqvist, Robert Blum, Adam S. Bolton, Cesar Briceno, David Brooks, Joel R. Brownstein, Elizabeth Buckley-Geer, Angela Burden, Etienne Burtin, Nicolas G. Busca, Robert N. Cahn, Yan-Chuan Cai, Laia Cardiel-Sas, Raymond G. Carlberg, Pierre-Henri Carton, Ricard Casas, Francisco J. Castander, Jorge L. Cervantes-Cota, Todd M. Claybaugh, Madeline Close, Carl T. Coker, Shaun Cole, Johan Comparat, Andrew P. Cooper, M. C. Cousinou, Martin Crocce, Jean-Gabriel Cuby, Daniel P. Cunningham, Tamara M. Davis, Kyle S. Dawson, Axel de la Macorra, Juan De Vicente, Timothée Delubac, Mark Derwent, Arjun Dey, Govinda Dhungana, Zhejie Ding, Peter Doel, Yutong T. Duan, Anne Ealet, Jerry Edelstein, Sarah Eftekharzadeh, Daniel J. Eisenstein, Ann Elliott, Stéphanie Escoffier, Matthew Evatt, Parker Fagrelius, Xiaohui Fan, Kevin Fanning, Arya Farahi, Jay Farihi, Ginevra Favole, Yu Feng, Enrique Fernandez, Joseph R. Findlay, Douglas P. Finkbeiner, Michael J. Fitzpatrick, Brenna Flaugher, Samuel Flender, Andreu Font-Ribera, Jaime E. Forero-Romero, Pablo Fosalba, Carlos S. Frenk, Michele Fumagalli, Boris T. Gaensicke, Giuseppe Gallo, Juan Garcia-Bellido, Enrique Gaztanaga, Nicola Pietro Gentile Fusillo, Terry Gerard, Irena Gershkovich, Tommaso Giannantonio, Denis Gillet, Guillermo Gonzalez-de-Rivera, Violeta Gonzalez-Perez, Shelby Gott, Or Graur, Gaston Gutierrez, Julien Guy, Salman Habib, Henry Heetderks, Ian Heetderks, Katrin Heitmann, Wojciech A. Hellwing, David A. Herrera, Shirley Ho, Stephen Holland, Klaus Honscheid, Eric Huff, Timothy A. Hutchinson, Dragan Huterer, Ho Seong Hwang, Joseph Maria Illa Laguna, Yuzo Ishikawa, Dianna Jacobs, Niall Jeffrey, Patrick Jelinsky, Elise Jennings, Linhua Jiang, Jorge Jimenez, Jennifer Johnson, Richard Joyce, Eric Jullo, Stéphanie Juneau, Sami Kama, Armin Karcher, Sonia Karkar, Robert Kehoe, Noble Kennamer, Stephen Kent, Martin Kilbinger, Alex G. Kim, David Kirkby, Theodore Kisner, Ellie Kitanidis, Jean-Paul Kneib, Sergey Koposov, Eve Kovacs, Kazuya Koyama, Anthony Kremin, Richard Kron, Luzius Kronig, Andrea Kueter-Young, Cedric G. Lacey, Robin Lafever, Ofer Lahav, Andrew Lambert, Michael Lampton, Martin Landriau, Dustin Lang, Tod R. Lauer, Jean-Marc Le Goff, Laurent Le Guillou, Auguste Le Van Suu, Jae Hyeon Lee, Su-Jeong Lee, Daniela Leitner, Michael Lesser, Michael E. Levi, Benjamin L'Huillier, Baojiu Li, Ming Liang, Huan Lin, Eric Linder, Sarah R. Loebman, Zarija Lukić, Jun Ma, Niall MacCrann, Christophe Magneville, Laleh Makarem, Marc Manera, Christopher J. Manser, Robert Marshall, Paul Martini, Richard Massey, Thomas Matheson, Jeremy McCauley, Patrick McDonald, Ian D. McGreer, Aaron Meisner, Nigel Metcalfe, Timothy N. Miller, Ramon Miquel, John Moustakas, Adam Myers, Milind Naik, Jeffrey A. Newman, Robert C. Nichol, Andrina Nicola, Luiz Nicolati da Costa, Jundan Nie, Gustavo Niz, Peder Norberg, Brian Nord, Dara Norman, Peter Nugent, Thomas O'Brien, Minji Oh, Knut A. G. Olsen, Cristobal Padilla, Hamsa Padmanabhan, Nikhil Padmanabhan, Nathalie Palanque-Delabrouille, Antonella Palmese, Daniel Pappalardo, Isabelle Pâris, Changbom Park, Anna Patej, John A. Peacock, Hiranya V. Peiris, Xiyan Peng, Will J. Percival, Sandrine Perruchot, Matthew M. Pieri, Richard Pogge,

Jennifer E. Pollack, Claire Poppett, Francisco Prada, Abhishek Prakash, Ronald G. Probst, David Rabinowitz, Anand Raichoor, Chang Hee Ree, Alexandre Refregier, Xavier Regal, Beth Reid, Kevin Reil, Mehdi Rezaie, Constance M. Rockosi, Natalie Roe, Samuel Ronayette, Aaron Roodman, Ashley J. Ross, Nicholas P. Ross, Graziano Rossi, Eduardo Rozo, Vanina Ruhlmann-Kleider, Eli S. Rykoff, Cristiano Sabiu, Lado Samushia, Eusebio Sanchez, Javier Sanchez, David J. Schlegel, Michael Schneider, Michael Schubnell, Aurélia Secroun, Uros Seljak, Hee-Jong Seo, Santiago Serrano, Arman Shafieloo, Huanyuan Shan, Ray Sharples, Michael J. Sholl, William V. Shourt, Joseph H. Silber, David R. Silva, Martin M. Sirk, Anze Slosar, Alex Smith, George F. Smoot, Debopam Som, Yong-Seon Song, David Sprayberry, Ryan Staten, Andy Stefanik, Gregory Tarle, Suk Sien Tie, Jeremy L. Tinker, Rita Tojeiro, Francisco Valdes, Octavio Valenzuela, Monica Valluri, Mariana Vargas-Magana, Licia Verde, Alistair R. Walker, Jiali Wang, Yuting Wang, Benjamin A. Weaver, Curtis Weaverdyck, Risa H. Wechsler, David H. Weinberg, Martin White, Qian Yang, Christophe Yeche, Tianmeng Zhang, Gong-Bo Zhao, Yi Zheng, Xu Zhou, Zhimin Zhou, Yaling Zhu, Hu Zou, and Ying Zu. The DESI Experiment Part II: Instrument Design. *arXiv e-prints*, page arXiv:1611.00037, October 2016.

[58] C. D'Eugenio, E. Daddi, R. Gobat, V. Strazzullo, P. Lustig, I. Delvecchio, S. Jin, A. Puglisi, A. Calabró, C. Mancini, M. Dickinson, A. Cimatti, and M. Onodera. The Typical Massive Quiescent Galaxy at z $\sim$ 3 is a Post-starburst. ApJ, 892(1):L2, March 2020.

[59] Francesco D'Eugenio, Arjen van der Wel, Po-Feng Wu, Tania M. Barone, Josha van Houdt, Rachel Bezanson, Caroline M. S. Straatman, Camilla Pacifici, Adam Muzzin, Anna Gallazzi, Vivienne Wild, David Sobral, Eric F. Bell, Stefano Zibetti, Lamiya Mowla, and Marijn Franx. Inverse stellar population age gradients of post-starburst galaxies at z = 0.8 with LEGA-C. MNRAS, 497(1):389–404, July 2020.

[60] Arjun Dey, David J. Schlegel, Dustin Lang, Robert Blum, Kaylan Burleigh, Xiaohui Fan, Joseph R. Findlay, Doug Finkbeiner, David Herrera, Stéphanie Juneau, Martin Landriau, Michael Levi, Ian McGreer, Aaron Meisner, Adam D. Myers, John Moustakas, Peter Nugent, Anna Patej, Edward F. Schlafly, Alistair R. Walker, Francisco Valdes, Benjamin A. Weaver, Christophe Yèche, Hu Zou, Xu Zhou, Behzad Abareshi, T. M. C. Abbott, Bela Abolfathi, C. Aguilera, Shadab Alam, Lori Allen, A. Alvarez, James Annis, Behzad Ansarinejad, Marie Aubert, Jacqueline Beechert, Eric F. Bell, Segev Y. BenZvi, Florian Beutler, Richard M. Bielby, Adam S. Bolton, César Briceño, Elizabeth J. Buckley-Geer, Karen Butler, Annalisa Calamida, Raymond G. Carlberg, Paul Carter, Ricard Casas, Francisco J. Castander, Yumi Choi, Johan Comparat, Elena Cukanovaite, Timothée Delubac, Kaitlin DeVries, Sharmila Dey, Govinda Dhungana, Mark Dickinson, Zhejie Ding, John B. Donaldson, Yutong Duan, Christopher J. Duckworth, Sarah Eftekharzadeh, Daniel J. Eisenstein, Thomas Etourneau, Parker A. Fagrelius, Jay Farihi, Mike Fitzpatrick, Andreu Font-

Ribera, Leah Fulmer, Boris T. Gänsicke, Enrique Gaztanaga, Koshy George, David W. Gerdes, Satya Gontcho A. Gontcho, Claudio Gorgoni, Gregory Green, Julien Guy, Diane Harmer, M. Hernandez, Klaus Honscheid, Lijuan Wendy Huang, David J. James, Buell T. Jannuzi, Linhua Jiang, Richard Joyce, Armin Karcher, Sonia Karkar, Robert Kehoe, Jean-Paul Kneib, Andrea Kueter-Young, Ting-Wen Lan, Tod R. Lauer, Laurent Le Guillou, Auguste Le Van Suu, Jae Hyeon Lee, Michael Lesser, Laurence Perreault Levasseur, Ting S. Li, Justin L. Mann, Robert Marshall, C. E. Martínez-Vázquez, Paul Martini, Hélion du Mas des Bourboux, Sean McManus, Tobias Gabriel Meier, Brice Ménard, Nigel Metcalfe, Andrea Muñoz-Gutiérrez, Joan Najita, Kevin Napier, Gautham Narayan, Jeffrey A. Newman, Jundan Nie, Brian Nord, Dara J. Norman, Knut A. G. Olsen, Anthony Paat, Nathalie Palanque-Delabrouille, Xiyan Peng, Claire L. Poppett, Megan R. Poremba, Abhishek Prakash, David Rabinowitz, Anand Raichoor, Mehdi Rezaie, A. N. Robertson, Natalie A. Roe, Ashley J. Ross, Nicholas P. Ross, Gregory Rudnick, Sasha Safonova, Abhijit Saha, F. Javier Sánchez, Elodie Savary, Heidi Schweiker, Adam Scott, Hee-Jong Seo, Huanyuan Shan, David R. Silva, Zachary Slepian, Christian Soto, David Sprayberry, Ryan Staten, Coley M. Stillman, Robert J. Stupak, David L. Summers, Suk Sien Tie, H. Tirado, Mariana Vargas-Magaña, A. Katherina Vivas, Risa H. Wechsler, Doug Williams, Jinyi Yang, Qian Yang, Tolga Yapici, Dennis Zaritsky, A. Zenteno, Kai Zhang, Tianmeng Zhang, Rongpu Zhou, and Zhimin Zhou. Overview of the DESI Legacy Imaging Surveys. AJ, 157(5):168, May 2019.

[61] Tiziana Di Matteo, Volker Springel, and Lars Hernquist. Energy input from quasars regulates the growth and activity of black holes and their host galaxies. Nature, 433(7026):604–607, February 2005.

[62] Aleksandar M. Diamond-Stanic, John Moustakas, Paul H. Sell, Christy A. Tremonti, Alison L. Coil, Julie D. Davis, James E. Geach, Sophia C. W. Gottlieb, Ryan C. Hickox, Amanda Kepley, Charles Lipscomb, Joshua Rines, Gregory H. Rudnick, Cristopher Thompson, Kingdell Valdez, Christian Bradna, Jordan Camarillo, Eve Cinquino, Senyo Ohene, Serena Perrotta, Grayson C. Petter, David S. N. Rupke, Chidubem Umeh, and Kelly E. Whalen. Compact Starburst Galaxies with Fast Outflows: Central Escape Velocities and Stellar Mass Surface Densities from Multiband Hubble Space Telescope Imaging. ApJ, 912(1):11, May 2021.

[63] L. A. Díaz-García, A. J. Cenarro, C. López-Sanjuan, I. Ferreras, A. Fernández-Soto, R. M. González Delgado, I. Márquez, J. Masegosa, I. San Roman, K. Viironen, S. Bonoli, M. Cerviño, M. Moles, D. Cristóbal-Hornillos, E. Alfaro, T. Aparicio-Villegas, N. Benítez, T. Broadhurst, J. Cabrera-Caño, F. J. Castander, J. Cepa, C. Husillos, L. Infante, J. A. L. Aguerri, V. J. Martínez, A. Molino, A. del Olmo, J. Perea, F. Prada, and J. M. Quintana. Stellar populations of galaxies in the ALHAMBRA survey up to z $\sim$ 1. III. The stellar content of the quiescent galaxy population during the last 8 Gyr. A&A, 631:A157, November 2019.

[64] Martina Donnari, Annalisa Pillepich, Dylan Nelson, Mark Vogelsberger, Shy Genel, Rainer Weinberger, Federico Marinacci, Volker Springel, and Lars Hernquist. The star formation activity of IllustrisTNG galaxies: main sequence, UVJ diagram, quenched fractions, and systematics. MNRAS, 485(4):4817–4840, June 2019.

[65] Aaron Dotter. MESA Isochrones and Stellar Tracks (MIST) 0: Methods for the Construction of Stellar Isochrones. ApJS, 222(1):8, January 2016.

[66] B. T. Draine, D. A. Dale, G. Bendo, K. D. Gordon, J. D. T. Smith, L. Armus, C. W. Engelbracht, G. Helou, Jr. Kennicutt, R. C., A. Li, H. Roussel, F. Walter, D. Calzetti, J. Moustakas, E. J. Murphy, G. H. Rieke, C. Bot, D. J. Hollenbach, K. Sheth, and H. I. Teplitz. Dust Masses, PAH Abundances, and Starlight Intensities in the SINGS Galaxy Sample. ApJ, 663(2):866–894, July 2007.

[67] A. Dressler and J. E. Gunn. Spectroscopy of galaxies in distant clusters. II. The population of the 3C 295 cluster. ApJ, 270:7–19, July 1983.

[68] Alan Dressler, Daniel D. Kelson, and Louis E. Abramson. Late Bloomer Galaxies: Growing Up in Cosmic Autumn. ApJ, 869(2):152, December 2018.

[69] Alan Dressler, Daniel D. Kelson, Louis E. Abramson, Michael D. Gladders, Jr. Oemler, Augustus, Bianca M. Poggianti, John S. Mulchaey, Benedetta Vulcani, Stephen A. Shectman, Rik J. Williams, and Patrick J. McCarthy. Demonstrating Diversity in Star-formation Histories with the CSI Survey. ApJ, 833(2):251, December 2016.

[70] Alan Dressler, Jr. Oemler, Augustus, Bianca M. Poggianti, Ian Smail, Scott Trager, Stephen A. Shectman, Warrick J. Couch, and Richard S. Ellis. Studying the Star Formation Histories of Galaxies in Clusters from Composite Spectra. ApJ, 617(2):867–878, December 2004.

[71] J. L. E. Dreyer. A New General Catalogue of Nebulæ and Clusters of Stars, being the Catalogue of the late Sir John F. W. Herschel, Bart, revised, corrected, and enlarged. MmRAS, 49:1, January 1888.

[72] Stephen A. Eales, Maarten Baes, Nathan Bourne, Malcolm Bremer, Michael J. I. Brown, Christopher Clark, David Clements, Pieter de Vis, Simon Driver, Loretta Dunne, Simon Dye, Cristina Furlanetto, Benne Holwerda, R. J. Ivison, L. S. Kelvin, Maritza Lara-Lopez, Lerothodi Leeuw, Jon Loveday, Steve Maddox, Michał J. Michałowski, Steven Phillipps, Aaron Robotham, Dan Smith, Matthew Smith, Elisabetta Valiante, Paul van der Werf, and Angus Wright. The causes of the red sequence,

the blue cloud, the green valley, and the green mountain. MNRAS, 481(1):1183–1194, November 2018.

[73] Daniel J. Eisenstein, James Annis, James E. Gunn, Alexander S. Szalay, Andrew J. Connolly, R. C. Nichol, Neta A. Bahcall, Mariangela Bernardi, Scott Burles, Francisco J. Castander, Masataka Fukugita, David W. Hogg, Željko Ivezić, G. R. Knapp, Robert H. Lupton, Vijay Narayanan, Marc Postman, Daniel E. Reichart, Michael Richmond, Donald P. Schneider, David J. Schlegel, Michael A. Strauss, Mark SubbaRao, Douglas L. Tucker, Daniel Vanden Berk, Michael S. Vogeley, David H. Weinberg, and Brian Yanny. Spectroscopic Target Selection for the Sloan Digital Sky Survey: The Luminous Red Galaxy Sample. AJ, 122(5):2267–2280, November 2001.

[74] Sara L. Ellison, Mallory D. Thorp, Hsi-An Pan, Lihwai Lin, Jillian M. Scudder, Asa F. L. Bluck, Sebastian F. Sánchez, and Mark Sargent. The ALMaQUEST Survey - II. What drives central starbursts at z $\sim$ 0? MNRAS, 492(4):6027–6041, March 2020.

[75] Sara L. Ellison, Scott Wilkinson, Joanna Woo, Ho-Hin Leung, Vivienne Wild, Robert W. Bickley, David R. Patton, Salvatore Quai, and Stephen Gwyn. Galaxy mergers can rapidly shut down star formation. *arXiv e-prints*, page arXiv:2209.07613, September 2022.

[76] Vicente Estrada-Carpenter, Casey Papovich, Ivelina Momcheva, Gabriel Brammer, James Long, Ryan F. Quadri, Joanna Bridge, Mark Dickinson, Henry Ferguson, Steven Finkelstein, Mauro Giavalisco, Catherine M. Gosmeyer, Jennifer Lotz, Brett Salmon, Rosalind E. Skelton, Jonathan R. Trump, and Benjamin Weiner. CLEAR. I. Ages and Metallicities of Quiescent Galaxies at 1.0 ¡ z ¡ 1.8 Derived from Deep Hubble Space Telescope Grism Data. ApJ, 870(2):133, January 2019.

[77] S. M. Faber. Quadratic programming applied to the problem of galaxy population synthesis. A&A, 20:361, September 1972.

[78] J. Falcón-Barroso, P. Sánchez-Blázquez, A. Vazdekis, E. Ricciardelli, N. Cardiel, A. J. Cenarro, J. Gorgas, and R. F. Peletier. An updated MILES stellar library and stellar population models. A&A, 532:A95, August 2011.

[79] Jerome J. Fang, S. M. Faber, David C. Koo, and Avishai Dekel. A Link between Star Formation Quenching and Inner Stellar Mass Density in Sloan Digital Sky Survey Central Galaxies. ApJ, 776(1):63, October 2013.

[80] G. Fasano and A. Franceschini. A multidimensional version of the Kolmogorov-Smirnov test. MNRAS, 225:155–170, March 1987.

[81] Robert Feldmann and Lucio Mayer. The Argo simulation - I. Quenching of massive galaxies at high redshift as a result of cosmological starvation. MNRAS, 446(2):1939–1956, January 2015.

[82] Laura Ferrarese and David Merritt. A Fundamental Relation between Supermassive Black Holes and Their Host Galaxies. ApJ, 539(1):L9–L12, August 2000.

[83] Dan Foreman-Mackey, Jonathan Sick, and Ben Johnson. python-fsps: Python bindings to fsps (v0.1.1), October 2014.

[84] Daniel Foreman-Mackey, David W. Hogg, Dustin Lang, and Jonathan Goodman. emcee: The MCMC Hammer. PASP, 125(925):306, March 2013.

[85] Ben Forrest, Z. Cemile Marsan, Marianna Annunziatella, Gillian Wilson, Adam Muzzin, Danilo Marchesini, M. C. Cooper, Jeffrey C. C. Chan, Ian McConachie, Percy Gomez, Erin Kado-Fong, Francesco La Barbera, Daniel Lange-Vagle, Julie Nantais, Mario Nonino, Paolo Saracco, Mauro Stefanon, and Remco F. J. van der Burg. The Massive Ancient Galaxies at z ¿ 3 NEar-infrared (MAGAZ3NE) Survey: Confirmation of Extremely Rapid Star Formation and Quenching Timescales for Massive Galaxies in the Early Universe. ApJ, 903(1):47, November 2020.

[86] P. E. Freeman, I. Kim, and A. B. Lee. Local two-sample testing: a new tool for analysing high-dimensional astronomical data. MNRAS, 471(3):3273–3282, November 2017.

[87] K. Decker French. Evolution Through the Post-starburst Phase: Using Post-starburst Galaxies as Laboratories for Understanding the Processes that Drive Galaxy Evolution. PASP, 133(1025):072001, July 2021.

[88] K. Decker French, Adam Smercina, Kate Rowlands, Akshat Tripathi, Ann I. Zabludoff, John-David T. Smith, Desika Narayanan, Yujin Yang, Yancy Shirley, and Katey Alatalo. The State of the Molecular Gas in Post-starburst Galaxies. ApJ, 942(1):25, January 2023.

[89] K. Decker French, Yujin Yang, Ann Zabludoff, Desika Narayanan, Yancy Shirley, Fabian Walter, John-David Smith, and Christy A. Tremonti. Discovery of Large Molecular Gas Reservoirs in Post-starburst Galaxies. ApJ, 801(1):1, March 2015.

[90] K. Decker French, Yujin Yang, Ann I. Zabludoff, and Christy A. Tremonti. Clocking the Evolution of Post-starburst Galaxies: Methods and First Results. ApJ, 862(1):2, July 2018.

[91] Mattia Fumagalli, Marijn Franx, Pieter van Dokkum, Katherine E. Whitaker, Rosalind E. Skelton, Gabriel Brammer, Erica Nelson, Michael Maseda, Ivelina Momcheva, Mariska Kriek, Ivo Labbé, Britt Lundgren, and Hans-Walter Rix. Ages of Massive Galaxies at 0.5 ¿ z ¿ 2.0 from 3D-HST Rest-frame Optical Spectroscopy. ApJ, 822(1):1, May 2016.

[92] Anna Gallazzi, Eric F. Bell, Stefano Zibetti, Jarle Brinchmann, and Daniel D. Kelson. Charting the Evolution of the Ages and Metallicities of Massive Galaxies since z = 0.7. ApJ, 788(1):72, June 2014.

[93] Anna Gallazzi, Stéphane Charlot, Jarle Brinchmann, Simon D. M. White, and Christy A. Tremonti. The ages and metallicities of galaxies in the local universe. MNRAS, 362(1):41–58, September 2005.

[94] Karl Glazebrook, Corentin Schreiber, Ivo Labbé, Themiya Nanayakkara, Glenn G. Kacprzak, Pascal A. Oesch, Casey Papovich, Lee R. Spitler, Caroline M. S. Straatman, Kim-Vy H. Tran, and Tiantian Yuan. A massive, quiescent galaxy at a redshift of 3.717. Nature, 544(7648):71–74, April 2017.

[95] C. Gómez-Guijarro, D. Elbaz, M. Xiao, M. Béthermin, M. Franco, B. Magnelli, E. Daddi, M. Dickinson, R. Demarco, H. Inami, W. Rujopakarn, G. E. Magdis, X. Shu, R. Chary, L. Zhou, D. M. Alexander, F. Bournaud, L. Ciesla, H. C. Ferguson, S. L. Finkelstein, M. Giavalisco, D. Iono, S. Juneau, J. S. Kartaltepe, G. Lagache, E. Le Floc'h, R. Leiton, L. Lin, K. Motohara, J. Mullaney, K. Okumura, M. Pannella, C. Papovich, A. Pope, M. T. Sargent, J. D. Silverman, E. Treister, and T. Wang. GOODS-ALMA 2.0: Source catalog, number counts, and prevailing compact sizes in 1.1 mm galaxies. A&A, 658:A43, February 2022.

[96] Jenny Greene, Rachel Bezanson, Masami Ouchi, John Silverman, and the PFS Galaxy Evolution Working Group. The Prime Focus Spectrograph Galaxy Evolution Survey. *arXiv e-prints*, page arXiv:2206.14908, June 2022.

[97] Jenny E. Greene, David Setton, Rachel Bezanson, Katherine A. Suess, Mariska Kriek, Justin S. Spilker, Andy D. Goulding, and Robert Feldmann. The Role of Active Galactic Nuclei in the Quenching of Massive Galaxies in the SQuIGG ěc{L} E Survey. ApJ, 899(1):L9, August 2020.

[98] J. Guy, S. Bailey, A. Kremin, Shadab Alam, C. Allende Prieto, S. BenZvi, A. S. Bolton, D. Brooks, E. Chaussidon, A. P. Cooper, K. Dawson, A. de la Macorra, A. Dey, Biprateep Dey, G. Dhungana, D. J. Eisenstein, A. Font-Ribera, J. E. Forero-Romero, E. Gaztañaga, S. Gontcho A Gontcho, D. Green, K. Honscheid, M. Ishak, R. Kehoe, D. Kirkby, T. Kisner, Sergey E. Koposov, Ting-Wen Lan, M. Landriau, L. Le Guillou, Michael E. Levi, C. Magneville, Christopher J. Manser, P. Martini, Aaron M. Meisner, R. Miquel, J. Moustakas, Adam D. Myers, Jeffrey A. Newman, Jundan Nie, N. Palanque-Delabrouille, W. J. Percival, C. Poppett, F. Prada, A. Raichoor, C. Ravoux, A. J. Ross, E. F. Schlafly, D. Schlegel, M. Schubnell, Ray M. Sharples, Gregory Tarlé, B. A. Weaver, Christophe Yèche, Rongpu Zhou, Zhimin Zhou, and H. Zou. The Spectroscopic Data Processing Pipeline for the Dark Energy Spectroscopic Instrument. *arXiv e-prints*, page arXiv:2209.14482, September 2022.

[99] J. F. Helmboldt, R. A. M. Walterbos, and T. Goto. Current star formation in early-type galaxies and the K+A phenomenon. MNRAS, 387(4):1537–1553, July 2008.

[100] Philip F. Hopkins, Kevin Bundy, Norman Murray, Eliot Quataert, Tod R. Lauer, and Chung-Pei Ma. Compact high-redshift galaxies are the cores of the most massive present-day spheroids. MNRAS, 398(2):898–910, September 2009.

[101] Philip F. Hopkins, Thomas J. Cox, Dušan Kereš, and Lars Hernquist. A Cosmological Framework for the Co-Evolution of Quasars, Supermassive Black Holes, and Elliptical Galaxies. II. Formation of Red Ellipticals. ApJS, 175(2):390–422, April 2008.

[102] Philip F. Hopkins, Rachel S. Somerville, Lars Hernquist, Thomas J. Cox, Brant Robertson, and Yuexing Li. The Relation between Quasar and Merging Galaxy Luminosity Functions and the Merger-driven Star Formation History of the Universe. ApJ, 652(2):864–888, December 2006.

[103] Song Huang, Alexie Leauthaud, Jenny E. Greene, Kevin Bundy, Yen-Ting Lin, Masayuki Tanaka, Satoshi Miyazaki, and Yutaka Komiyama. Individual stellar haloes of massive galaxies measured to 100 kpc at 0.3 ¡ z ¡ 0.5 using Hyper Suprime-Cam. MNRAS, 475(3):3348–3368, April 2018.

[104] E. P. Hubble. Extragalactic nebulae. ApJ, 64:321–369, December 1926.

[105] Qiana Hunt, Rachel Bezanson, Jenny E. Greene, Justin S. Spilker, Katherine A. Suess, Mariska Kriek, Desika Narayanan, Robert Feldmann, Arjen van der Wel, and Petchara Pattarakijwanich. Stellar and Molecular Gas Rotation in a Recently Quenched Massive Galaxy at z $\sim$ 0.7. ApJ, 860(2):L18, June 2018.

[106] Icko Iben. Stellar evolution within and off the main sequence. *Annual Review of Astronomy and Astrophysics*, 5(1):571–626, 1967.

[107] Marziye Jafariyazani, Andrew B. Newman, Bahram Mobasher, Sirio Belli, Richard S. Ellis, and Shannon G. Patel. Resolved Multi-element Stellar Chemical Abundances in the Brightest Quiescent Galaxy at z $\sim$ 2. ApJ, 897(2):L42, July 2020.

[108] Shuo-Wen Jin, Qiusheng Gu, Song Huang, Yong Shi, and Long-Long Feng. Color-Magnitude Distribution of Face-on nearby Galaxies in Sloan Digital Sky Survey DR7. ApJ, 787(1):63, May 2014.

[109] Ben Johnson, Dan Foreman-Mackey, Jonathan Sick, Joel Leja, Nell Byler, Mike Walmsley, Erik Tollerud, Henry Leung, and Spencer Scott. dfm/python-fsps: python-fsps v0.4.0, March 2021.

[110] Ben Johnson and Joel Leja. Bd-J/Prospector: Initial Release, December 2017.

[111] Stéphanie Juneau, Karl Glazebrook, David Crampton, Patrick J. McCarthy, Sandra Savaglio, Roberto Abraham, Raymond G. Carlberg, Hsiao-Wen Chen, Damien Le Borgne, Ronald O. Marzke, Kathy Roth, Inger Jørgensen, Isobel Hook, and Richard Murowinski. Cosmic Star Formation History and Its Dependence on Galaxy Stellar Mass. ApJ, 619(2):L135–L138, February 2005.

[112] Boris S. Kalita, Emanuele Daddi, Chiara D'Eugenio, Francesco Valentino, R. Michael Rich, Carlos Gómez-Guijarro, Rosemary T. Coogan, Ivan Delvecchio, David Elbaz, James D. Neill, Annagrazia Puglisi, and Veronica Strazzullo. An Ancient Massive Quiescent Galaxy Found in a Gas-rich z 3 Group. ApJ, 917(2):L17, August 2021.

[113] Guinevere Kauffmann, Timothy M. Heckman, Simon D. M. White, Stéphane Charlot, Christy Tremonti, Jarle Brinchmann, Gustavo Bruzual, Eric W. Peng, Mark Seibert, Mariangela Bernardi, Michael Blanton, Jon Brinkmann, Francisco Castander, Istvan Csábai, Masataka Fukugita, Zeljko Ivezic, Jeffrey A. Munn, Robert C. Nichol, Nikhil Padmanabhan, Aniruddha R. Thakar, David H. Weinberg, and Donald York. Stellar masses and star formation histories for 10^5 galaxies from the Sloan Digital Sky Survey. MNRAS, 341(1):33–53, May 2003.

[114] Guinevere Kauffmann, Timothy M. Heckman, Simon D. M. White, Stéphane Charlot, Christy Tremonti, Eric W. Peng, Mark Seibert, Jon Brinkmann, Robert C. Nichol, Mark SubbaRao, and Don York. The dependence of star formation history and internal structure on stellar mass for 10^5 low-redshift galaxies. MNRAS, 341(1):54–69, May 2003.

[115] Satoshi Kawanomoto, Fumihiro Uraguchi, Yutaka Komiyama, Satoshi Miyazaki, Hisanori Furusawa, François Finet, Takashi Hattori, Shiang-Yu Wang, Naoki Yasuda, and Naotaka Suzuki. Hyper Suprime-Cam: Filters. PASJ, 70(4):66, August 2018.

[116] Lalitwadee Kawinwanichakij, John D. Silverman, Xuheng Ding, Angelo George, Ivana Damjanov, Marcin Sawicki, Masayuki Tanaka, Dan S. Taranu, Simon Birrer, Song Huang, Junyao Li, Masato Onodera, Takatoshi Shibuya, and Naoki Yasuda. Hyper Suprime-Cam Subaru Strategic Program: A Mass-dependent Slope of the Galaxy Size-Mass Relation at z ¡ 1. ApJ, 921(1):38, November 2021.

[117] Jr. Kennicutt, Robert C. The Global Schmidt Law in Star-forming Galaxies. ApJ, 498(2):541–552, May 1998.

[118] Dušan Kereš, Neal Katz, David H. Weinberg, and Romeel Davé. How do galaxies get their gas? MNRAS, 363(1):2–28, October 2005.

[119] Gourav Khullar, Matthew B. Bayliss, Michael D. Gladders, Keunho J. Kim, Michael S. Calzadilla, Veronica Strazzullo, Lindsey E. Bleem, Guillaume Mahler, Michael McDonald, Benjamin Floyd, Christian L. Reichardt, Florian Ruppin, Alexandro Saro, Keren Sharon, Taweewat Somboonpanyakul, Brian Stalder, and Antony A. Stark. Synthesizing Stellar Populations in South Pole Telescope Galaxy Clusters. I. Ages of Quiescent Member Galaxies at 0.3 ¡ z ¡ 1.4. ApJ, 934(2):177, August 2022.

[120] John Kormendy and Luis C. Ho. Coevolution (Or Not) of Supermassive Black Holes and Host Galaxies. ARA&A, 51(1):511–653, August 2013.

[121] Mariska Kriek and Charlie Conroy. The Dust Attenuation Law in Distant Galaxies: Evidence for Variation with Spectral Type. ApJ, 775(1):L16, September 2013.

[122] Mariska Kriek, Ivo Labbé, Charlie Conroy, Katherine E. Whitaker, Pieter G. van Dokkum, Gabriel B. Brammer, Marijn Franx, Garth D. Illingworth, Danilo Marchesini, Adam Muzzin, Ryan F. Quadri, and Gregory Rudnick. The Spectral Energy Distribution of Post-starburst Galaxies in the NEWFIRM Medium-band Survey: A Low Contribution from TP-AGB Stars. ApJ, 722(1):L64–L69, October 2010.

[123] Mariska Kriek, Pieter G. van Dokkum, Ivo Labbé, Marijn Franx, Garth D. Illingworth, Danilo Marchesini, and Ryan F. Quadri. An Ultra-Deep Near-Infrared Spectrum of a Compact Quiescent Galaxy at z = 2.2. ApJ, 700(1):221–231, July 2009.

[124] Joel Leja, Benjamin D. Johnson, Charlie Conroy, Pieter van Dokkum, Joshua S. Speagle, Gabriel Brammer, Ivelina Momcheva, Rosalind Skelton, Katherine E. Whitaker, Marijn Franx, and Erica J. Nelson. An Older, More Quiescent Universe from Panchromatic SED Fitting of the 3D-HST Survey. ApJ, 877(2):140, June 2019.

[125] Joel Leja, Benjamin D. Johnson, Charlie Conroy, Pieter G. van Dokkum, and Nell Byler. Deriving Physical Properties from Broadband Photometry with Prospector: Description of the Model and a Demonstration of its Accuracy Using 129 Galaxies in the Local Universe. ApJ, 837(2):170, March 2017.

[126] Joel Leja, Joshua S. Speagle, Benjamin D. Johnson, Charlie Conroy, Pieter van Dokkum, and Marijn Franx. A New Census of the 0.2 ¡ z ¡ 3.0 Universe. I. The Stellar Mass Function. ApJ, 893(2):111, April 2020.

[127] Joel Leja, Joshua S. Speagle, Yuan-Sen Ting, Benjamin D. Johnson, Charlie Conroy, Katherine E. Whitaker, Erica J. Nelson, Pieter van Dokkum, and Marijn Franx. A New Census of the 0.2¡ z ¡3.0 Universe, Part II: The Star-Forming Sequence. *arXiv e-prints*, page arXiv:2110.04314, October 2021.

[128] Davide Lena. Reduction of Integral Field Spectroscopic Data from the Gemini Multi-Object Spectrograph (a commented example). page arXiv:1409.8264, September 2014.

[129] Michael Levi, Chris Bebek, Timothy Beers, Robert Blum, Robert Cahn, Daniel Eisenstein, Brenna Flaugher, Klaus Honscheid, Richard Kron, Ofer Lahav, Patrick McDonald, Natalie Roe, David Schlegel, and representing the DESI collaboration. The DESI Experiment, a whitepaper for Snowmass 2013. *arXiv e-prints*, page arXiv:1308.0847, August 2013.

[130] Chris Lintott, Kevin Schawinski, Steven Bamford, Anå¾e Slosar, Kate Land, Daniel Thomas, Edd Edmondson, Karen Masters, Robert C. Nichol, M. Jordan Raddick, Alex Szalay, Dan Andreescu, Phil Murray, and Jan Vandenberg. Galaxy Zoo 1: data release of morphological classifications for nearly 900 000 galaxies. MNRAS, 410(1):166–178, January 2011.

[131] Chris J. Lintott, Kevin Schawinski, Anže Slosar, Kate Land, Steven Bamford, Daniel Thomas, M. Jordan Raddick, Robert C. Nichol, Alex Szalay, Dan Andreescu, Phil Murray, and Jan Vandenberg. Galaxy Zoo: morphologies derived from visual inspection of galaxies from the Sloan Digital Sky Survey. MNRAS, 389(3):1179–1189, September 2008.

[132] Sidney Lower, Desika Narayanan, Joel Leja, Benjamin D. Johnson, Charlie Conroy, and Romeel Davé. How Well Can We Measure the Stellar Mass of a Galaxy: The Impact of the Assumed Star Formation History Model in SED Fitting. ApJ, 904(1):33, November 2020.

[133] Piero Madau and Mark Dickinson. Cosmic Star-Formation History. ARA&A, 52:415–486, August 2014.

[134] R. Maiolino, M. Cirasuolo, J. Afonso, F. E. Bauer, R. Bowler, O. Cucciati, E. Daddi, G. De Lucia, C. Evans, H. Flores, A. Gargiulo, B. Garilli, P. Jablonka, M. Jarvis, J. P. Kneib, S. Lilly, T. Looser, M. Magliocchetti, Z. Man, F. Mannucci, S. Maurogordato, R. J. McLure, P. Norberg, P. Oesch, E. Oliva, S. Paltani, C. Pappalardo, Y. Peng, L. Pentericci, L. Pozzetti, A. Renzini, M. Rodrigues, F. Royer, S. Serjeant, L. Vanzi, V. Wild, and G. Zamorani. MOONRISE: The Main MOONS GTO Extragalactic Survey. *The Messenger*, 180:24–29, June 2020.

[135] David T. Maltby, Omar Almaini, Vivienne Wild, Nina A. Hatch, William G. Hartley, Chris Simpson, Kate Rowlands, and Miguel Socolovsky. The structure of post-starburst galaxies at 0.5 ¡ z ¡ 2: evidence for two distinct quenching routes at different epochs. MNRAS, 480(1):381–401, October 2018.

[136] Allison W. S. Man, Johannes Zabl, Gabriel B. Brammer, Johan Richard, Sune Toft, Mikkel Stockmann, Anna R. Gallazzi, Stefano Zibetti, and Harald Ebeling. An exquisitely deep view of quenching galaxies through the gravitational lens: Stellar population, morphology, and ionized gas. *arXiv e-prints*, page arXiv:2106.08338, June 2021.

[137] S. Alwin Mao and Eve C. Ostriker. Galactic Disk Winds Driven by Cosmic Ray Pressure. ApJ, 854(2):89, February 2018.

[138] J. Matharu, A. Muzzin, G. B. Brammer, R. F. J. van der Burg, M. W. Auger, P. C. Hewett, J. C. C. Chan, R. Demarco, P. van Dokkum, D. Marchesini, E. J. Nelson, A. G. Noble, and G. Wilson. HST/WFC3 grism observations of z $\sim$ 1 clusters: evidence for evolution in the mass-size relation of quiescent galaxies from post-starburst galaxies. MNRAS, 493(4):6011–6032, April 2020.

[139] Jasleen Matharu, Adam Muzzin, Gabriel B. Brammer, Erica J. Nelson, Matthew W. Auger, Paul C. Hewett, Remco van der Burg, Michael Balogh, Ricardo Demarco, Danilo Marchesini, Allison G. Noble, Gregory Rudnick, Arjen van der Wel, Gillian Wilson, and Howard K. C. Yee. HST/WFC3 Grism Observations of z 1 Clusters:

Evidence for Rapid Outside-in Environmental Quenching from Spatially Resolved Hα Maps. ApJ, 923(2):222, December 2021.

[140] Richard M. McDermid, Katherine Alatalo, Leo Blitz, Frédéric Bournaud, Martin Bureau, Michele Cappellari, Alison F. Crocker, Roger L. Davies, Timothy A. Davis, P. T. de Zeeuw, Pierre-Alain Duc, Eric Emsellem, Sadegh Khochfar, Davor Krajnović, Harald Kuntschner, Raffaella Morganti, Thorsten Naab, Tom Oosterloo, Marc Sarzi, Nicholas Scott, Paolo Serra, Anne-Marie Weijmans, and Lisa M. Young. The ATLAS^{3D} Project - XXX. Star formation histories and stellar population scaling relations of early-type galaxies. MNRAS, 448(4):3484–3513, April 2015.

[141] D. J. McLeod, R. J. McLure, J. S. Dunlop, F. Cullen, A. C. Carnall, and K. Duncan. The evolution of the galaxy stellar-mass function over the last 12 billion years from a combination of ground-based and HST surveys. MNRAS, 503(3):4413–4435, May 2021.

[142] R. J. McLure, L. Pentericci, A. Cimatti, J. S. Dunlop, D. Elbaz, A. Fontana, K. Nandra, R. Amorin, M. Bolzonella, A. Bongiorno, A. C. Carnall, M. Castellano, M. Cirasuolo, O. Cucciati, F. Cullen, S. De Barros, S. L. Finkelstein, F. Fontanot, P. Franzetti, M. Fumana, A. Gargiulo, B. Garilli, L. Guaita, W. G. Hartley, A. Iovino, M. J. Jarvis, S. Juneau, W. Karman, D. Maccagni, F. Marchi, E. Mármol-Queraltó, E. Pompei, L. Pozzetti, M. Scodeggio, V. Sommariva, M. Talia, O. Almaini, I. Balestra, S. Bardelli, E. F. Bell, N. Bourne, R. A. A. Bowler, M. Brusa, F. Buitrago, K. I. Caputi, P. Cassata, S. Charlot, A. Citro, G. Cresci, S. Cristiani, E. Curtis-Lake, M. Dickinson, G. G. Fazio, H. C. Ferguson, F. Fiore, M. Franco, J. P. U. Fynbo, A. Galametz, A. Georgakakis, M. Giavalisco, A. Grazian, N. P. Hathi, I. Jung, S. Kim, A. M. Koekemoer, Y. Khusanova, O. Le Fèvre, J. M. Lotz, F. Mannucci, D. T. Maltby, K. Matsuoka, D. J. McLeod, H. Mendez-Hernandez, J. Mendez-Abreu, M. Mignoli, M. Moresco, A. Mortlock, M. Nonino, M. Pannella, C. Papovich, P. Popesso, D. P. Rosario, M. Salvato, P. Santini, D. Schaerer, C. Schreiber, D. P. Stark, L. A. M. Tasca, R. Thomas, T. Treu, E. Vanzella, V. Wild, C. C. Williams, G. Zamorani, and E. Zucca. The VANDELS ESO public spectroscopic survey. MNRAS, 479(1):25–42, September 2018.

[143] Moein Mosleh, Sandro Tacchella, Alvio Renzini, C. Marcella Carollo, Alireza Molaeinezhad, Masato Onodera, Habib G. Khosroshahi, and Simon Lilly. Connection between Stellar Mass Distributions within Galaxies and Quenching Since z = 2. ApJ, 837(1):2, March 2017.

[144] Lamiya A. Mowla, Pieter van Dokkum, Gabriel B. Brammer, Ivelina Momcheva, Arjen van der Wel, Katherine Whitaker, Erica Nelson, Rachel Bezanson, Adam Muzzin, Marijn Franx, John MacKenty, Joel Leja, Mariska Kriek, and Danilo Marchesini.

COSMOS-DASH: The Evolution of the Galaxy Size-Mass Relation since z $\sim$ 3 from New Wide-field WFC3 Imaging Combined with CANDELS/3D-HST. ApJ, 880(1):57, July 2019.

[145] Adam Muzzin, Danilo Marchesini, Mauro Stefanon, Marijn Franx, Henry J. McCracken, Bo Milvang-Jensen, James S. Dunlop, J. P. U. Fynbo, Gabriel Brammer, Ivo Labbé, and Pieter G. van Dokkum. The Evolution of the Stellar Mass Functions of Star-forming and Quiescent Galaxies to z = 4 from the COSMOS/UltraVISTA Survey. ApJ, 777(1):18, November 2013.

[146] Thorsten Naab, Peter H. Johansson, and Jeremiah P. Ostriker. Minor Mergers and the Size Evolution of Elliptical Galaxies. ApJ, 699(2):L178–L182, July 2009.

[147] Erica June Nelson, Pieter G. van Dokkum, Natascha M. Förster Schreiber, Marijn Franx, Gabriel B. Brammer, Ivelina G. Momcheva, Stijn Wuyts, Katherine E. Whitaker, Rosalind E. Skelton, Mattia Fumagalli, Christopher C. Hayward, Mariska Kriek, Ivo Labbé, Joel Leja, Hans-Walter Rix, Linda J. Tacconi, Arjen van der Wel, Frank C. van den Bosch, Pascal A. Oesch, Claire Dickey, and Johannes Ulf Lange. Where Stars Form: Inside-out Growth and Coherent Star Formation from HST Hα Maps of 3200 Galaxies across the Main Sequence at 0.7 ¡ z ¡ 1.5. ApJ, 828(1):27, September 2016.

[148] K. G. Noeske, B. J. Weiner, S. M. Faber, C. Papovich, D. C. Koo, R. S. Somerville, K. Bundy, C. J. Conselice, J. A. Newman, D. Schiminovich, E. Le Floc'h, A. L. Coil, G. H. Rieke, J. M. Lotz, J. R. Primack, P. Barmby, M. C. Cooper, M. Davis, R. S. Ellis, G. G. Fazio, P. Guhathakurta, J. Huang, S. A. Kassin, D. C. Martin, A. C. Phillips, R. M. Rich, T. A. Small, C. N. A. Willmer, and G. Wilson. Star Formation in AEGIS Field Galaxies since z=1.1: The Dominance of Gradually Declining Star Formation, and the Main Sequence of Star-forming Galaxies. ApJ, 660(1):L43–L46, May 2007.

[149] Camilla Pacifici, Kartheik G. Iyer, Bahram Mobasher, Elisabete da Cunha, Viviana Acquaviva, Denis Burgarella, Gabriela Calistro Rivera, Adam C. Carnall, Yu-Yen Chang, Nima Chartab, Kevin C. Cooke, Ciaran Fairhurst, Jeyhan Kartaltepe, Joel Leja, Katarzyna Małek, Brett Salmon, Marianna Torelli, Alba Vidal-García, Médéric Boquien, Gabriel G. Brammer, Michael J. I. Brown, Peter L. Capak, Jacopo Chevallard, Chiara Circosta, Darren Croton, Iary Davidzon, Mark Dickinson, Kenneth J. Duncan, Sandra M. Faber, Harry C. Ferguson, Adriano Fontana, Yicheng Guo, Boris Haeussler, Shoubaneh Hemmati, Marziye Jafariyazani, Susan A. Kassin, Rebecca L. Larson, Bomee Lee, Kameswara Bharadwaj Mantha, Francesca Marchi, Hooshang Nayyeri, Jeffrey A. Newman, Viraj Pandya, Janine Pforr, Naveen Reddy, Ryan Sanders, Ekta Shah, Abtin Shahidi, Matthew L. Stevans, Dian Puspita Triani, Krys-

tal D. Tyler, Brittany N. Vanderhoof, Alexander de la Vega, Weichen Wang, and Madalyn E. Weston. The Art of Measuring Physical Parameters in Galaxies: A Critical Assessment of Spectral Energy Distribution Fitting Techniques. ApJ, 944(2):141, February 2023.

[150] Camilla Pacifici, Susan A. Kassin, Benjamin J. Weiner, Bradford Holden, Jonathan P. Gardner, Sandra M. Faber, Henry C. Ferguson, David C. Koo, Joel R. Primack, Eric F. Bell, Avishai Dekel, Eric Gawiser, Mauro Giavalisco, Marc Rafelski, Raymond C. Simons, Guillermo Barro, Darren J. Croton, Romeel Davé, Adriano Fontana, Norman A. Grogin, Anton M. Koekemoer, Seong-Kook Lee, Brett Salmon, Rachel Somerville, and Peter Behroozi. The Evolution of Star Formation Histories of Quiescent Galaxies. ApJ, 832(1):79, November 2016.

[151] Casey Papovich, Mark Dickinson, and Henry C. Ferguson. The Stellar Populations and Evolution of Lyman Break Galaxies. ApJ, 559(2):620–653, October 2001.

[152] Minjung Park, Sirio Belli, Charlie Conroy, Sandro Tacchella, Joel Leja, Sam E. Cutler, Benjamin D. Johnson, Erica J. Nelson, and Razieh Emami. Rapid Quenching of Galaxies at Cosmic Noon. *arXiv e-prints*, page arXiv:2210.03747, October 2022.

[153] Minjung Park, Sandro Tacchella, Erica J. Nelson, Lars Hernquist, Rainer Weinberger, Benedikt Diemer, Dylan Nelson, Annalisa Pillepich, Federico Marinacci, and Mark Vogelsberger. On the formation of massive quiescent galaxies with diverse morphologies in the TNG50 simulation. *arXiv e-prints*, page arXiv:2112.07679, December 2021.

[154] Shannon G. Patel, Daniel D. Kelson, Bradford P. Holden, Marijn Franx, and Garth D. Illingworth. The Star-formation-rate-Density Relation at 0.6 ¡ z ¡ 0.9 and the Role of Star-forming Galaxies. ApJ, 735(1):53, July 2011.

[155] Debosmita Pathak, Sirio Belli, and Rainer Weinberger. Quenching, Mergers, and Age Profiles for z = 2 Galaxies in IllustrisTNG. ApJ, 916(2):L23, August 2021.

[156] Petchara Pattarakijwanich, Michael A. Strauss, Shirley Ho, and Nicholas P. Ross. The Evolution of Post-starburst Galaxies from z ~1 to the Present. ApJ, 833(1):19, December 2016.

[157] M. M. Pawlik, V. Wild, C. J. Walcher, P. H. Johansson, C. Villforth, K. Rowlands, J. Mendez-Abreu, and T. Hewlett. Shape asymmetry: a morphological indicator for automatic detection of galaxies in the post-coalescence merger stages. MNRAS, 456(3):3032–3052, March 2016.

[158] J. A. Peacock. Two-dimensional goodness-of-fit testing in astronomy. MNRAS, 202:615–627, February 1983.

[159] Chien Y. Peng, Luis C. Ho, Chris D. Impey, and Hans-Walter Rix. Detailed Decomposition of Galaxy Images. II. Beyond Axisymmetric Models. AJ, 139(6):2097–2129, June 2010.

[160] Michael B. Pracy, Warrick J. Couch, Chris Blake, Kenji Bekki, Craig Harrison, Matthew Colless, Harald Kuntschner, and Roberto de Propris. Spatially resolved spectroscopy of the E+A galaxies in the z= 0.32 cluster AC 114. MNRAS, 359(4):1421–1432, June 2005.

[161] Salvatore Quai, Maan H. Hani, Sara L. Ellison, David R. Patton, and Joanna Woo. Interacting galaxies in the IllustrisTNG simulations - III. (The rarity of) quenching in post-merger galaxies. MNRAS, 504(2):1888–1901, June 2021.

[162] K. Rowlands, T. Heckman, V. Wild, N. L. Zakamska, V. Rodriguez-Gomez, J. Barrera-Ballesteros, J. Lotz, D. Thilker, B. H. Andrews, M. Boquien, J. Brinkmann, J. R. Brownstein, H. C. Hwang, and R. Smethurst. SDSS-IV MaNGA: spatially resolved star formation histories and the connection to galaxy physical properties. MNRAS, 480(2):2544–2561, October 2018.

[163] K. Rowlands, V. Wild, N. Bourne, M. Bremer, S. Brough, S. P. Driver, A. M. Hopkins, M. S. Owers, S. Phillipps, K. Pimbblet, A. E. Sansom, L. Wang, M. Alpaslan, J. Bland-Hawthorn, M. Colless, B. W. Holwerda, and E. N. Taylor. Galaxy And Mass Assembly (GAMA): The mechanisms for quiescent galaxy formation at z ¡ 1. MNRAS, 473(1):1168–1185, January 2018.

[164] Amélie Saintonge, Guinevere Kauffmann, Carsten Kramer, Linda J. Tacconi, Christof Buchbender, Barbara Catinella, Silvia Fabello, Javier Graciá-Carpio, Jing Wang, Luca Cortese, Jian Fu, Reinhard Genzel, Riccardo Giovanelli, Qi Guo, Martha P. Haynes, Timothy M. Heckman, Mark R. Krumholz, Jenna Lemonias, Cheng Li, Sean Moran, Nemesio Rodriguez-Fernandez, David Schiminovich, Karl Schuster, and Albrecht Sievers. COLD GASS, an IRAM legacy survey of molecular gas in massive galaxies - I. Relations between H_2, H I, stellar content and structural properties. MNRAS, 415(1):32–60, July 2011.

[165] P. Sánchez-Blázquez, R. F. Peletier, J. Jiménez-Vicente, N. Cardiel, A. J. Cenarro, J. Falcón-Barroso, J. Gorgas, S. Selam, and A. Vazdekis. Medium-resolution Isaac Newton Telescope library of empirical spectra. MNRAS, 371(2):703–718, September 2006.

[166] Marcin Sawicki and H. K. C. Yee. Optical-Infrared Spectral Energy Distributions of Z ¿ 2 Lyman Break Galaxies. AJ, 115(4):1329–1339, April 1998.

[167] Elizaveta Sazonova, Katherine Alatalo, Kate Rowlands, Susana E. Deustua, K. Decker French, Timothy Heckman, Lauranne Lanz, Ute Lisenfeld, Yuanze Luo, Anne Medling, Kristina Nyland, Justin A. Otter, Andreea O. Petric, Gregory F. Snyder, and Claudia Megan Urry. Are All Post-starbursts Mergers? HST Reveals Hidden Disturbances in the Majority of PSBs. ApJ, 919(2):134, October 2021.

[168] Kevin Schawinski, C. Megan Urry, Brooke D. Simmons, Lucy Fortson, Sugata Kaviraj, William C. Keel, Chris J. Lintott, Karen L. Masters, Robert C. Nichol, Marc Sarzi, Ramin Skibba, Ezequiel Treister, Kyle W. Willett, O. Ivy Wong, and Sukyoung K. Yi. The green valley is a red herring: Galaxy Zoo reveals two evolutionary pathways towards quenching of star formation in early- and late-type galaxies. MNRAS, 440(1):889–907, May 2014.

[169] Joop Schaye, Robert A. Crain, Richard G. Bower, Michelle Furlong, Matthieu Schaller, Tom Theuns, Claudio Dalla Vecchia, Carlos S. Frenk, I. G. McCarthy, John C. Helly, Adrian Jenkins, Y. M. Rosas-Guevara, Simon D. M. White, Maarten Baes, C. M. Booth, Peter Camps, Julio F. Navarro, Yan Qu, Alireza Rahmati, Till Sawala, Peter A. Thomas, and James Trayford. The EAGLE project: simulating the evolution and assembly of galaxies and their environments. MNRAS, 446(1):521–554, January 2015.

[170] David J. Schlegel, Douglas P. Finkbeiner, and Marc Davis. Maps of Dust Infrared Emission for Use in Estimation of Reddening and Cosmic Microwave Background Radiation Foregrounds. ApJ, 500(2):525–553, June 1998.

[171] Maarten Schmidt. The Rate of Star Formation. ApJ, 129:243, March 1959.

[172] A. Schnorr-Müller, M. Trevisan, R. Riffel, A. L. Chies-Santos, C. Furlanetto, T. V. Ricci, F. S. Lohmann, R. Flores-Freitas, N. D. Mallmann, and K. A. Alamo-Martínez. The puzzling origin of massive compact galaxies in MaNGA. MNRAS, 507(1):300–317, October 2021.

[173] P. H. Sell, C. A. Tremonti, R. C. Hickox, A. M. Diamond-Stanic, J. Moustakas, A. Coil, A. Williams, G. Rudnick, A. Robaina, J. E. Geach, S. Heinz, and E. M. Wilcots. Massive compact galaxies with high-velocity outflows: morphological analysis and constraints on AGN activity. MNRAS, 441(4):3417–3443, July 2014.

[174] David J. Setton, Rachel Bezanson, Katherine A. Suess, Qiana Hunt, Jenny E. Greene, Mariska Kriek, Justin S. Spilker, Robert Feldmann, and Desika Narayanan. SQuIGG ěc{L} E Survey: Massive z $\sim$ 0.6 Post-starburst Galaxies Exhibit Flat Age Gradients. ApJ, 905(1):79, December 2020.

[175] David J. Setton, Biprateep Dey, Gourav Khullar, Rachel Bezanson, Jeffrey A. Newman, Jessica N. Aguilar, Steven Ahlen, Brett H. Andrews, David Brooks, Axel de la Macorra, Arjun Dey, Sarah Eftekharzadeh, Andreu Font-Ribera, Satya Gontcho A Gontcho, Anthony Kremin, Stephanie Juneau, Martin Landriau, Aaron Meisner, Ramon Miquel, John Moustakas, Alan Pearl, Francisco Prada, Gregory Tarlé, Małgorzata Siudek, Benjamin Alan Weaver, Zhimin Zhou, and Hu Zou. DESI Survey Validation Spectra Reveal an Increasing Fraction of Recently Quenched Galaxies at z 1. ApJ, 947(2):L31, April 2023.

[176] David J. Setton, Margaret Verrico, Rachel Bezanson, Jenny E. Greene, Katherine A. Suess, Andy D. Goulding, Justin S. Spilker, Mariska Kriek, Robert Feldmann, Desika Narayanan, Khalil Hall-Hooper, and Erin Kado-Fong. The Compact Structures of Massive z $\sim$ 0.7 Post-starburst Galaxies in the SQuIGG$\vec{L}$E Sample. ApJ, 931(1):51, May 2022.

[177] Stephen A. Shectman, Stephen D. Landy, Augustus Oemler, Douglas L. Tucker, Huan Lin, Robert P. Kirshner, and Paul L. Schechter. The Las Campanas Redshift Survey. ApJ, 470:172, October 1996.

[178] Shiyin Shen, H. J. Mo, Simon D. M. White, Michael R. Blanton, Guinevere Kauffmann, Wolfgang Voges, J. Brinkmann, and Istvan Csabai. The size distribution of galaxies in the Sloan Digital Sky Survey. MNRAS, 343(3):978–994, August 2003.

[179] Debora Sijacki, Mark Vogelsberger, Shy Genel, Volker Springel, Paul Torrey, Gregory F. Snyder, Dylan Nelson, and Lars Hernquist. The Illustris simulation: the evolving population of black holes across cosmic time. MNRAS, 452(1):575–596, September 2015.

[180] Joseph Harry Silber, Parker Fagrelius, Kevin Fanning, Michael Schubnell, Jessica Nicole Aguilar, Steven Ahlen, Jon Ameel, Otger Ballester, Charles Baltay, Chris Bebek, Dominic Benton Beard, Robert Besuner, Laia Cardiel-Sas, Ricard Casas, Francisco Javier Castander, Todd Claybaugh, Carl Dobson, Yutong Duan, Patrick Dunlop, Jerry Edelstein, William T. Emmet, Ann Elliott, Matthew Evatt, Irena Gershkovich, Julien Guy, Stu Harris, Henry Heetderks, Ian Heetderks, Klaus Honscheid, Jose Maria Illa, Patrick Jelinsky, Sharon R. Jelinsky, Jorge Jimenez, Armin Karcher, Stephen Kent, David Kirkby, Jean-Paul Kneib, Andrew Lambert, Mike Lampton, Daniela Leitner, Michael Levi, Jeremy McCauley, Aaron Meisner, Timothy N. Miller,

Ramon Miquel, Juliá Mundet, Claire Poppett, David Rabinowitz, Kevin Reil, David Roman, David Schlegel, Santiago Serrano, William Van Shourt, David Sprayberry, Gregory Tarlé, Suk Sien Tie, Curtis Weaverdyck, Kai Zhang, Marco Azzaro, Stephen Bailey, Santiago Becerril, Tami Blackwell, Mohamed Bouri, David Brooks, Elizabeth Buckley-Geer, Jose Peñate Castro, Mark Derwent, Arjun Dey, Govinda Dhungana, Peter Doel, Daniel J. Eisenstein, Nasib Fahim, Juan Garcia-Bellido, Enrique Gaztañaga, Satya Gontcho A Gontcho, Gaston Gutierrez, Philipp Hörler, Robert Kehoe, Theodore Kisner, Anthony Kremin, Luzius Kronig, Martin Landriau, Laurent Le Guillou, Paul Martini, John Moustakas, Nathalie Palanque-Delabrouille, Xiyan Peng, Will Percival, Francisco Prada, Carlos Allende Prieto, Guillermo Gonzalez de Rivera, Eusebio Sanchez, Justo Sanchez, Ray Sharples, Marcelle Soares-Santos, Edward Schlafly, Benjamin Alan Weaver, Zhimin Zhou, Yaling Zhu, and Hu Zou. The Robotic Multi-Object Focal Plane System of the Dark Energy Spectroscopic Instrument (DESI). *arXiv e-prints*, page arXiv:2205.09014, May 2022.

[181] Adam Smercina, John-David T. Smith, K. Decker French, Eric F. Bell, Daniel A. Dale, Anne M. Medling, Kristina Nyland, George C. Privon, Kate Rowlands, Fabian Walter, and Ann I. Zabludoff. After The Fall: Resolving the Molecular Gas in Post-Starburst Galaxies. *arXiv e-prints*, page arXiv:2108.03231, August 2021.

[182] Gregory F. Snyder, Thomas J. Cox, Christopher C. Hayward, Lars Hernquist, and Patrik Jonsson. K+A Galaxies as the Aftermath of Gas-rich Mergers: Simulating the Evolution of Galaxies as Seen by Spectroscopic Surveys. ApJ, 741(2):77, November 2011.

[183] Joshua S. Speagle. DYNESTY: a dynamic nested sampling package for estimating Bayesian posteriors and evidences. MNRAS, 493(3):3132–3158, April 2020.

[184] Justin Spilker, Rachel Bezanson, Ivana Barišić, Eric Bell, Claudia del P. Lagos, Michael Maseda, Adam Muzzin, Camilla Pacifici, David Sobral, Caroline Straatman, Arjen van der Wel, Pieter van Dokkum, Benjamin Weiner, Katherine Whitaker, Christina C. Williams, and Po-Feng Wu. Molecular Gas Contents and Scaling Relations for Massive, Passive Galaxies at Intermediate Redshifts from the LEGA-C Survey. ApJ, 860(2):103, June 2018.

[185] Justin S. Spilker, Manuel Aravena, Kedar A. Phadke, Matthieu Béthermin, Scott C. Chapman, Chenxing Dong, Anthony H. Gonzalez, Christopher C. Hayward, Yashar D. Hezaveh, Katrina C. Litke, Matthew A. Malkan, Daniel P. Marrone, Desika Narayanan, Cassie Reuter, Joaquin D. Vieira, and Axel Weiß. Ubiquitous Molecular Outflows in z ¿ 4 Massive, Dusty Galaxies. II. Momentum-driven Winds Powered by Star Formation in the Early Universe. ApJ, 905(2):86, December 2020.

[186] Justin S. Spilker, Kedar A. Phadke, Manuel Aravena, Matthieu Béthermin, Scott C. Chapman, Chenxing Dong, Anthony H. Gonzalez, Christopher C. Hayward, Yashar D. Hezaveh, Sreevani Jarugula, Katrina C. Litke, Matthew A. Malkan, Daniel P. Marrone, Desika Narayanan, Cassie Reuter, Joaquin D. Vieira, and Axel Weiss. Ubiquitous Molecular Outflows in z ¿ 4 Massive, Dusty Galaxies. I. Sample Overview and Clumpy Structure in Molecular Outflows on 500 pc Scales. ApJ, 905(2):85, December 2020.

[187] Justin S. Spilker, Katherine A. Suess, David J. Setton, Rachel Bezanson, Robert Feldmann, Jenny E. Greene, Mariska Kriek, Sidney Lower, Desika Narayanan, and Margaret Verrico. Star Formation Suppression by Tidal Removal of Cold Molecular Gas from an Intermediate-redshift Massive Post-starburst Galaxy. ApJ, 936(1):L11, September 2022.

[188] Volker Springel, Tiziana Di Matteo, and Lars Hernquist. Black Holes in Galaxy Mergers: The Formation of Red Elliptical Galaxies. ApJ, 620(2):L79–L82, February 2005.

[189] Caroline M. S. Straatman, Ivo Labbé, Lee R. Spitler, Rebecca Allen, Bruno Altieri, Gabriel B. Brammer, Mark Dickinson, Pieter van Dokkum, Hanae Inami, Karl Glazebrook, Glenn G. Kacprzak, Lalit Kawinwanichakij, Daniel D. Kelson, Patrick J. McCarthy, Nicola Mehrtens, Andy Monson, David Murphy, Casey Papovich, S. Eric Persson, Ryan Quadri, Glen Rees, Adam Tomczak, Kim-Vy H. Tran, and Vithal Tilvi. A Substantial Population of Massive Quiescent Galaxies at z ~4 from ZFOURGE. ApJ, 783(1):L14, March 2014.

[190] Katherine A. Suess, Rachel Bezanson, Justin S. Spilker, Mariska Kriek, Jenny E. Greene, Robert Feldmann, Qiana Hunt, and Desika Narayanan. Massive Quenched Galaxies at z 0.7 Retain Large Molecular Gas Reservoirs. ApJ, 846(2):L14, September 2017.

[191] Katherine A. Suess, Mariska Kriek, Rachel Bezanson, Jenny E. Greene, David Setton, Justin S. Spilker, Robert Feldmann, Andy D. Goulding, Benjamin D. Johnson, Joel Leja, Desika Narayanan, Khalil Hall-Hooper, Qiana Hunt, Sidney Lower, and Margaret Verrico. {SQuIGG}ěc{L}{E} : Studying Quenching in Intermediate-z Galaxies-Gas, {Angu}ěc{L}{ar} Momentum, and Evolution. ApJ, 926(1):89, February 2022.

[192] Katherine A. Suess, Mariska Kriek, Sedona H. Price, and Guillermo Barro. Half-mass Radii for 7000 Galaxies at $1.0 \leq z \leq 2.5$: Most of the Evolution in the Mass-Size Relation Is Due to Color Gradients. ApJ, 877(2):103, June 2019.

[193] Katherine A. Suess, Mariska Kriek, Sedona H. Price, and Guillermo Barro. Half-mass Radii of Quiescent and Star-forming Galaxies Evolve Slowly from $0 \lesssim z \leq 2.5$: Implications for Galaxy Assembly Histories. ApJ, 885(1):L22, November 2019.

[194] Katherine A. Suess, Mariska Kriek, Sedona H. Price, and Guillermo Barro. Color Gradients along the Quiescent Galaxy Sequence: Clues to Quenching and Structural Growth. ApJ, 899(2):L26, August 2020.

[195] Katherine A. Suess, Mariska Kriek, Sedona H. Price, and Guillermo Barro. Dissecting the Size-Mass and Σ_1-Mass Relations at 1.0 ¡ z ¡ 2.5: Galaxy Mass Profiles and Color Gradients as a Function of Spectral Shape. ApJ, 915(2):87, July 2021.

[196] Katherine A. Suess, Joel Leja, Benjamin D. Johnson, Rachel Bezanson, Jenny E. Greene, Mariska Kriek, Sidney Lower, Desika Narayanan, David J. Setton, and Justin S. Spilker. Recovering the Star Formation Histories of Recently Quenched Galaxies: The Impact of Model and Prior Choices. ApJ, 935(2):146, August 2022.

[197] Daniel Szomoru, Marijn Franx, and Pieter G. van Dokkum. Sizes and Surface Brightness Profiles of Quiescent Galaxies at z ~2. ApJ, 749(2):121, April 2012.

[198] S. Tacchella, C. M. Carollo, A. Renzini, N. M. Förster Schreiber, P. Lang, S. Wuyts, G. Cresci, A. Dekel, R. Genzel, S. J. Lilly, C. Mancini, S. Newman, M. Onodera, A. Shapley, L. Tacconi, J. Woo, and G. Zamorani. Evidence for mature bulges and an inside-out quenching phase 3 billion years after the Big Bang. *Science*, 348(6232):314–317, April 2015.

[199] Sandro Tacchella, Charlie Conroy, S. M. Faber, Benjamin D. Johnson, Joel Leja, Guillermo Barro, Emily C. Cunningham, Alis J. Deason, Puragra Guhathakurta, Yicheng Guo, Lars Hernquist, David C. Koo, Kevin McKinnon, Constance M. Rockosi, Joshua S. Speagle, Pieter van Dokkum, and Hassen M. Yesuf. Fast, Slow, Early, Late: Quenching Massive Galaxies at $z \sim 0.8$. ApJ, 926(2):134, February 2022.

[200] Sandro Tacchella, Avishai Dekel, C. Marcella Carollo, Daniel Ceverino, Colin DeGraf, Sharon Lapiner, Nir Mand elker, and Joel R. Primack. Evolution of density profiles in high-z galaxies: compaction and quenching inside-out. MNRAS, 458(1):242–263, May 2016.

[201] L. J. Tacconi, R. Genzel, A. Saintonge, F. Combes, S. García-Burillo, R. Neri, A. Bolatto, T. Contini, N. M. Förster Schreiber, S. Lilly, D. Lutz, S. Wuyts, G. Accurso, J. Boissier, F. Boone, N. Bouché, F. Bournaud, A. Burkert, M. Carollo, M. Cooper, P. Cox, C. Feruglio, J. Freundlich, R. Herrera-Camus, S. Juneau, M. Lippa, T. Naab,

A. Renzini, P. Salome, A. Sternberg, K. Tadaki, H. Übler, F. Walter, B. Weiner, and A. Weiss. PHIBSS: Unified Scaling Relations of Gas Depletion Time and Molecular Gas Fractions. ApJ, 853(2):179, February 2018.

[202] Ken-ichi Tadaki, Sirio Belli, Andreas Burkert, Avishai Dekel, Natascha M. Förster Schreiber, Reinhard Genzel, Masao Hayashi, Rodrigo Herrera-Camus, Tadayuki Kodama, Kotaro Kohno, Yusei Koyama, Minju M. Lee, Dieter Lutz, Lamiya Mowla, Erica J. Nelson, Alvio Renzini, Tomoko L. Suzuki, Linda J. Tacconi, Hannah Übler, Emily Wisnioski, and Stijn Wuyts. Structural Evolution in Massive Galaxies at z $\sim$ 2. ApJ, 901(1):74, September 2020.

[203] Masahiro Takada, Richard S. Ellis, Masashi Chiba, Jenny E. Greene, Hiroaki Aihara, Nobuo Arimoto, Kevin Bundy, Judith Cohen, Olivier Doré, Genevieve Graves, James E. Gunn, Timothy Heckman, Christopher M. Hirata, Paul Ho, Jean-Paul Kneib, Olivier Le Fèvre, Lihwai Lin, Surhud More, Hitoshi Murayama, Tohru Nagao, Masami Ouchi, Michael Seiffert, John D. Silverman, Laerte Sodré, David N. Spergel, Michael A. Strauss, Hajime Sugai, Yasushi Suto, Hideki Takami, and Rosemary Wyse. Extragalactic science, cosmology, and Galactic archaeology with the Subaru Prime Focus Spectrograph. PASJ, 66(1):R1, February 2014.

[204] Masayuki Tanaka, Francesco Valentino, Sune Toft, Masato Onodera, Rhythm Shimakawa, Daniel Ceverino, Andreas L. Faisst, Anna Gallazzi, Carlos Gómez-Guijarro, Mariko Kubo, Georgios E. Magdis, Charles L. Steinhardt, Mikkel Stockmann, Kiyoto Yabe, and Johannes Zabl. Stellar Velocity Dispersion of a Massive Quenching Galaxy at z = 4.01. ApJ, 885(2):L34, November 2019.

[205] Daniel Thomas, Claudia Maraston, Ralf Bender, and Claudia Mendes de Oliveira. The Epochs of Early-Type Galaxy Formation as a Function of Environment. ApJ, 621(2):673–694, March 2005.

[206] Daniel Thomas, Claudia Maraston, Kevin Schawinski, Marc Sarzi, and Joseph Silk. Environment and self-regulation in galaxy formation. MNRAS, 404(4):1775–1789, June 2010.

[207] Mallory D. Thorp, Sara L. Ellison, Luc Simard, Sebastian F. Sánchez, and Braulio Antonio. Spatially resolved star formation and metallicity profiles in post-merger galaxies from MaNGA. MNRAS, 482(1):L55–L59, January 2019.

[208] B. M. Tinsley and J. E. Gunn. Evolutionary synthesis of the stellar population in elliptical galaxies. I. Ingredients, broad-band colors, and infrared features. ApJ, 203:52–62, January 1976.

[209] S. Toft, A. Gallazzi, A. Zirm, M. Wold, S. Zibetti, C. Grillo, and A. Man. Deep Absorption Line Studies of Quiescent Galaxies at z ~2: The Dynamical-mass-Size Relation and First Constraints on the Fundamental Plane. ApJ, 754(1):3, July 2012.

[210] S. Toft, V. Smolčić, B. Magnelli, A. Karim, A. Zirm, M. Michalowski, P. Capak, K. Sheth, K. Schawinski, J. K. Krogager, S. Wuyts, D. Sanders, A. W. S. Man, D. Lutz, J. Staguhn, S. Berta, H. Mccracken, J. Krpan, and D. Riechers. Submillimeter Galaxies as Progenitors of Compact Quiescent Galaxies. ApJ, 782(2):68, February 2014.

[211] Christy A. Tremonti, John Moustakas, and Aleksandar M. Diamond-Stanic. The Discovery of 1000 km s^{-1} Outflows in Massive Poststarburst Galaxies at z=0.6. ApJ, 663(2):L77–L80, July 2007.

[212] Francesco Valentino, Masayuki Tanaka, Iary Davidzon, Sune Toft, Carlos Gómez-Guijarro, Mikkel Stockmann, Masato Onodera, Gabriel Brammer, Daniel Ceverino, Andreas L. Faisst, Anna Gallazzi, Christopher C. Hayward, Olivier Ilbert, Mariko Kubo, Georgios E. Magdis, Jonatan Selsing, Rhythm Shimakawa, Martin Sparre, Charles Steinhardt, Kiyoto Yabe, and Johannes Zabl. Quiescent Galaxies 1.5 Billion Years after the Big Bang and Their Progenitors. ApJ, 889(2):93, February 2020.

[213] A. van der Wel, E. F. Bell, B. Häussler, E. J. McGrath, Yu-Yen Chang, Yicheng Guo, D. H. McIntosh, H. W. Rix, M. Barden, E. Cheung, S. M. Faber, H. C. Ferguson, A. Galametz, N. A. Grogin, W. Hartley, J. S. Kartaltepe, D. D. Kocevski, A. M. Koekemoer, J. Lotz, M. Mozena, M. A. Peth, and Chien Y. Peng. Structural Parameters of Galaxies in CANDELS. ApJS, 203(2):24, December 2012.

[214] A. van der Wel, M. Franx, P. G. van Dokkum, R. E. Skelton, I. G. Momcheva, K. E. Whitaker, G. B. Brammer, E. F. Bell, H. W. Rix, S. Wuyts, H. C. Ferguson, B. P. Holden, G. Barro, A. M. Koekemoer, Yu-Yen Chang, E. J. McGrath, B. Häussler, A. Dekel, P. Behroozi, M. Fumagalli, J. Leja, B. F. Lundgren, M. V. Maseda, E. J. Nelson, D. A. Wake, S. G. Patel, I. Labbé, S. M. Faber, N. A. Grogin, and D. D. Kocevski. 3D-HST+CANDELS: The Evolution of the Galaxy Size-Mass Distribution since z = 3. ApJ, 788(1):28, June 2014.

[215] A. van der Wel, K. Noeske, R. Bezanson, C. Pacifici, A. Gallazzi, M. Franx, J. C. Muñoz-Mateos, E. F. Bell, G. Brammer, S. Charlot, P. Chauké, I. Labbé, M. V. Maseda, A. Muzzin, H. W. Rix, D. Sobral, J. van de Sande, P. G. van Dokkum, V. Wild, and C. Wolf. The VLT LEGA-C Spectroscopic Survey: The Physics of Galaxies at a Lookback Time of 7 Gyr. ApJS, 223(2):29, April 2016.

[216] Arjen van der Wel, Rachel Bezanson, Francesco D'Eugenio, Caroline Straatman, Marijn Franx, Josha van Houdt, Michael V. Maseda, Anna Gallazzi, Po-Feng Wu, Camilla Pacifici, Ivana Barisic, Gabriel B. Brammer, Juan Carlos Munoz-Mateos, Sarah Vervalcke, Stefano Zibetti, David Sobral, Anna de Graaff, Joao Calhau, Yasha Kaushal, Adam Muzzin, Eric F. Bell, and Pieter G. van Dokkum. The Large Early Galaxy Astrophysics Census (LEGA-C) Data Release 3: 3000 High-quality Spectra of K_s-selected Galaxies at z ¿ 0.6. ApJS, 256(2):44, October 2021.

[217] Pieter G. van Dokkum, Erica June Nelson, Marijn Franx, Pascal Oesch, Ivelina Momcheva, Gabriel Brammer, Natascha M. Förster Schreiber, Rosalind E. Skelton, Katherine E. Whitaker, Arjen van der Wel, Rachel Bezanson, Mattia Fumagalli, Garth D. Illingworth, Mariska Kriek, Joel Leja, and Stijn Wuyts. Forming Compact Massive Galaxies. ApJ, 813(1):23, November 2015.

[218] Pieter G. van Dokkum, Katherine E. Whitaker, Gabriel Brammer, Marijn Franx, Mariska Kriek, Ivo Labbé, Danilo Marchesini, Ryan Quadri, Rachel Bezanson, Garth D. Illingworth, Adam Muzzin, Gregory Rudnick, Tomer Tal, and David Wake. The Growth of Massive Galaxies Since z = 2. ApJ, 709(2):1018–1041, February 2010.

[219] Margaret Verrico, David J. Setton, Rachel Bezanson, Jenny E. Greene, Katherine A. Suess, Andy D. Goulding, Justin S. Spilker, Mariska Kriek, Robert Feldmann, Desika Narayanan, Vincenzo Donofrio, and Gourav Khullar. Merger Signatures are Common, but not Universal, In Massive, Recently-Quenched Galaxies at z~0.7. *arXiv e-prints*, page arXiv:2211.16532, November 2022.

[220] J. R. Weaver, I. Davidzon, S. Toft, O. Ilbert, H. J. McCracken, K. M. L. Gould, C. K. Jespersen, C. Steinhardt, C. D. P. Lagos, P. L. Capak, C. M. Casey, N. Chartab, A. L. Faisst, C. C. Hayward, J. S. Kartaltepe, O. B. Kauffmann, A. M. Koekemoer, V. Kokorev, C. Laigle, D. Liu, A. Long, G. E. Magdis, C. J. R. McPartland, B. Milvang-Jensen, B. Mobasher, A. Moneti, Y. Peng, D. B. Sanders, M. Shuntov, A. Sneppen, F. Valentino, L. Zalesky, and G. Zamorani. COSMOS2020: The Galaxy Stellar Mass Function: On the assembly and star formation cessation of galaxies at $0.2z \leq 7.5$. *arXiv e-prints*, page arXiv:2212.02512, December 2022.

[221] Kristi Webb, Michael L. Balogh, Joel Leja, Remco F. J. van der Burg, Gregory Rudnick, Adam Muzzin, Kevin Boak, Pierluigi Cerulo, David Gilbank, Chris Lidman, Lyndsay J. Old, Irene Pintos-Castro, Sean McGee, Heath Shipley, Andrea Biviano, Jeffrey C. C. Chan, Michael Cooper, Gabriella De Lucia, Ricardo Demarco, Ben Forrest, Pascale Jablonka, Egidijus Kukstas, Ian G. McCarthy, Karen McNab, Julie Nantais, Allison Noble, Bianca Poggianti, Andrew M. M. Reeves, Benedetta Vulcani, Gillian Wilson, Howard K. C. Yee, and Dennis Zaritsky. The GOGREEN survey: post-infall environmental quenching fails to predict the observed age difference

between quiescent field and cluster galaxies at z ¿ 1. MNRAS, 498(4):5317–5342, November 2020.

[222] Sarah Wellons, Paul Torrey, Chung-Pei Ma, Vicente Rodriguez-Gomez, Mark Vogelsberger, Mariska Kriek, Pieter van Dokkum, Erica Nelson, Shy Genel, Annalisa Pillepich, Volker Springel, Debora Sijacki, Gregory Snyder, Dylan Nelson, Laura Sales, and Lars Hernquist. The formation of massive, compact galaxies at z = 2 in the Illustris simulation. MNRAS, 449(1):361–372, May 2015.

[223] Ariel Werle, Bianca Poggianti, Alessia Moretti, Callum Bellhouse, Benedetta Vulcani, Marco Gullieuszik, Mario Radovich, Jacopo Fritz, Alessandro Ignesti, Johan Richard, Geneviève Soucail, Gustavo Bruzual, Stephane Charlot, Matilde Mingozzi, Cecilia Bacchini, Neven Tomicic, Rory Smith, Andrea Kulier, Giorgia Peluso, and Andrea Franchetto. Post-starburst galaxies in the centers of intermediate redshift clusters. *arXiv e-prints*, page arXiv:2203.08862, March 2022.

[224] Kelly E. Whalen, Ryan C. Hickox, Alison L. Coil, Aleksandar M. Diamond-Stanic, James E. Geach, John Moustakas, Gregory H. Rudnick, David S. N. Rupke, Paul H. Sell, Christy A. Tremonti, Julie D. Davis, Serena Perrotta, and Grayson C. Petter. The Space Density of Intermediate Redshift, Extremely Compact, Massive Starburst Galaxies. *arXiv e-prints*, page arXiv:2209.13632, September 2022.

[225] Katherine E. Whitaker, Rachel Bezanson, Pieter G. van Dokkum, Marijn Franx, Arjen van der Wel, Gabriel Brammer, Natascha M. Förster-Schreiber, Mauro Giavalisco, Ivo Labbé, Ivelina G. Momcheva, Erica J. Nelson, and Rosalind Skelton. Predicting Quiescence: The Dependence of Specific Star Formation Rate on Galaxy Size and Central Density at 0.5 ¡ z ¡ 2.5. ApJ, 838(1):19, March 2017.

[226] Katherine E. Whitaker, Mariska Kriek, Pieter G. van Dokkum, Rachel Bezanson, Gabriel Brammer, Marijn Franx, and Ivo Labbé. A Large Population of Massive Compact Post-starburst Galaxies at z ¿ 1: Implications for the Size Evolution and Quenching Mechanism of Quiescent Galaxies. ApJ, 745(2):179, February 2012.

[227] Katherine E. Whitaker, Pieter G. van Dokkum, Gabriel Brammer, and Marijn Franx. The Star Formation Mass Sequence Out to z = 2.5. ApJ, 754(2):L29, August 2012.

[228] Katherine E. Whitaker, Christina C. Williams, Lamiya Mowla, Justin S. Spilker, Sune Toft, Desika Narayanan, Alexandra Pope, Georgios E. Magdis, Pieter G. van Dokkum, Mohammad Akhshik, Rachel Bezanson, Gabriel B. Brammer, Joel Leja, Allison Man, Erica J. Nelson, Johan Richard, Camilla Pacifici, Keren Sharon, and

Francesco Valentino. Quenching of star formation from a lack of inflowing gas to galaxies. Nature, 597(7877):485–488, September 2021.

[229] Vivienne Wild, Omar Almaini, Michele Cirasuolo, Jim Dunlop, Ross McLure, Rebecca Bowler, Joao Ferreira, Emma Bradshaw, Robert Chuter, and Will Hartley. A new method for classifying galaxy SEDs from multiwavelength photometry. MNRAS, 440(2):1880–1898, May 2014.

[230] Vivienne Wild, Omar Almaini, Jim Dunlop, Chris Simpson, Kate Rowlands, Rebecca Bowler, David Maltby, and Ross McLure. The evolution of post-starburst galaxies from z=2 to 0.5. MNRAS, 463(1):832–844, November 2016.

[231] Vivienne Wild, Laith Taj Aldeen, Adam Carnall, David Maltby, Omar Almaini, Ariel Werle, Aaron Wilkinson, Kate Rowlands, Micol Bolzonella, Marco Castellano, Adriana Gargiulo, Ross McLure, Laura Pentericci, and Lucia Pozzetti. The star formation histories of z $\sim$ 1 post-starburst galaxies. MNRAS, 494(1):529–548, March 2020.

[232] Aaron Wilkinson, Omar Almaini, Vivienne Wild, David Maltby, William G. Hartley, Chris Simpson, and Kate Rowlands. From starburst to quiescence: post-starburst galaxies and their large-scale clustering over cosmic time. MNRAS, 504(3):4533–4550, July 2021.

[233] Scott Wilkinson, Sara L. Ellison, Connor Bottrell, Robert W. Bickley, Stephen Gwyn, Jean-Charles Cuillandre, and Vivienne Wild. The merger fraction of post-starburst galaxies in UNIONS. *arXiv e-prints*, page arXiv:2207.04152, July 2022.

[234] Christina C. Williams, Justin S. Spilker, Katherine E. Whitaker, Romeel Davé, Charity Woodrum, Gabriel Brammer, Rachel Bezanson, Desika Narayanan, and Benjamin Weiner. ALMA Measures Rapidly Depleted Molecular Gas Reservoirs in Massive Quiescent Galaxies at z $\sim$ 1.5. ApJ, 908(1):54, February 2021.

[235] Joanna Woo and Sara L. Ellison. Two growing modes and the morphology-quiescence relation in isolated galaxies. MNRAS, 487(2):1927–1945, August 2019.

[236] Guy Worthey and D. L. Ottaviani. Hγ and Hδ Absorption Features in Stars and Stellar Populations. ApJS, 111(2):377–386, August 1997.

[237] Po-Feng Wu. Searching for Local Counterparts of High-redshift Poststarburst Galaxies in Integral Field Unit Spectroscopic Surveys of Nearby Galaxies. ApJ, 913(1):44, May 2021.

[238] Po-Feng Wu, Arjen van der Wel, Rachel Bezanson, Anna Gallazzi, Camilla Pacifici, Caroline M. S. Straatman, Ivana Barišić, Eric F. Bell, Priscilla Chauke, Francesco D'Eugenio, Marijn Franx, Adam Muzzin, David Sobral, and Josha van Houdt. The Colors and Sizes of Recently Quenched Galaxies: A Result of Compact Starburst before Quenching. ApJ, 888(2):77, January 2020.

[239] Po-Feng Wu, Arjen van der Wel, Rachel Bezanson, Anna Gallazzi, Camilla Pacifici, Caroline M. S. Straatman, Ivana Barišić, Eric F. Bell, Priscilla Chauke, Josha van Houdt, Marijn Franx, Adam Muzzin, David Sobral, and Vivienne Wild. Fast and Slow Paths to Quiescence: Ages and Sizes of 400 Quiescent Galaxies from the LEGA-C Survey. ApJ, 868(1):37, November 2018.

[240] Masafumi Yagi and Tomotsugu Goto. The Spatial Distribution of Poststarburst Signatures in E+A Galaxies. AJ, 131(4):2050–2055, April 2006.

[241] Michael Yano, Mariska Kriek, Arjen van der Wel, and Katherine E. Whitaker. The Relation between Galaxy Structure and Spectral Type: Implications for the Buildup of the Quiescent Galaxy Population at 0.5 ¡ z ¡ 2.0. ApJ, 817(2):L21, February 2016.

[242] Hassen M. Yesuf. Quenching in the Right Place at the Right Time: Tracing the Shared History of Starbursts, AGNs, and Post-starburst Galaxies Using Their Structures and Multiscale Environments. *arXiv e-prints*, page arXiv:2207.12844, July 2022.

[243] Donald G. York, J. Adelman, Jr. Anderson, John E., Scott F. Anderson, James Annis, Neta A. Bahcall, J. A. Bakken, Robert Barkhouser, Steven Bastian, Eileen Berman, William N. Boroski, Steve Bracker, Charlie Briegel, John W. Briggs, J. Brinkmann, Robert Brunner, Scott Burles, Larry Carey, Michael A. Carr, Francisco J. Castander, Bing Chen, Patrick L. Colestock, A. J. Connolly, J. H. Crocker, István Csabai, Paul C. Czarapata, John Eric Davis, Mamoru Doi, Tom Dombeck, Daniel Eisenstein, Nancy Ellman, Brian R. Elms, Michael L. Evans, Xiaohui Fan, Glenn R. Federwitz, Larry Fiscelli, Scott Friedman, Joshua A. Frieman, Masataka Fukugita, Bruce Gillespie, James E. Gunn, Vijay K. Gurbani, Ernst de Haas, Merle Haldeman, Frederick H. Harris, J. Hayes, Timothy M. Heckman, G. S. Hennessy, Robert B. Hindsley, Scott Holm, Donald J. Holmgren, Chi-hao Huang, Charles Hull, Don Husby, Shin-Ichi Ichikawa, Takashi Ichikawa, Željko Ivezić, Stephen Kent, Rita S. J. Kim, E. Kinney, Mark Klaene, A. N. Kleinman, S. Kleinman, G. R. Knapp, John Korienek, Richard G. Kron, Peter Z. Kunszt, D. Q. Lamb, B. Lee, R. French Leger, Siriluk Limmongkol, Carl Lindenmeyer, Daniel C. Long, Craig Loomis, Jon Loveday, Rich Lucinio, Robert H. Lupton, Bryan MacKinnon, Edward J. Mannery, P. M. Mantsch, Bruce Margon, Peregrine McGehee, Timothy A. McKay, Avery Meiksin, Aronne Merelli, David G. Monet, Jeffrey A. Munn, Vijay K. Narayanan, Thomas Nash, Eric Neilsen, Rich Neswold, Heidi Jo Newberg, R. C. Nichol, Tom Nicinski,

Mario Nonino, Norio Okada, Sadanori Okamura, Jeremiah P. Ostriker, Russell Owen, A. George Pauls, John Peoples, R. L. Peterson, Donald Petravick, Jeffrey R. Pier, Adrian Pope, Ruth Pordes, Angela Prosapio, Ron Rechenmacher, Thomas R. Quinn, Gordon T. Richards, Michael W. Richmond, Claudio H. Rivetta, Constance M. Rockosi, Kurt Ruthmansdorfer, Dale Sandford, David J. Schlegel, Donald P. Schneider, Maki Sekiguchi, Gary Sergey, Kazuhiro Shimasaku, Walter A. Siegmund, Stephen Smee, J. Allyn Smith, S. Snedden, R. Stone, Chris Stoughton, Michael A. Strauss, Christopher Stubbs, Mark SubbaRao, Alexander S. Szalay, Istvan Szapudi, Gyula P. Szokoly, Anirudda R. Thakar, Christy Tremonti, Douglas L. Tucker, Alan Uomoto, Dan Vanden Berk, Michael S. Vogeley, Patrick Waddell, Shu-i. Wang, Masaru Watanabe, David H. Weinberg, Brian Yanny, Naoki Yasuda, and SDSS Collaboration. The Sloan Digital Sky Survey: Technical Summary. AJ, 120(3):1579–1587, September 2000.

[244] Lisa M. Young, Martin Bureau, Timothy A. Davis, Francoise Combes, Richard M. McDermid, Katherine Alatalo, Leo Blitz, Maxime Bois, Frédéric Bournaud, Michele Cappellari, Roger L. Davies, P. T. de Zeeuw, Eric Emsellem, Sadegh Khochfar, Davor Krajnović, Harald Kuntschner, Pierre-Yves Lablanche, Raffaella Morganti, Thorsten Naab, Tom Oosterloo, Marc Sarzi, Nicholas Scott, Paolo Serra, and Anne-Marie Weijmans. The ATLAS^{3D} project - IV. The molecular gas content of early-type galaxies. MNRAS, 414(2):940–967, June 2011.

[245] Ann I. Zabludoff and Dennis Zaritsky. A Collision of Subclusters in Abell 754. ApJ, 447:L21, July 1995.

[246] Ann I. Zabludoff, Dennis Zaritsky, Huan Lin, Douglas Tucker, Yasuhiro Hashimoto, Stephen A. Shectman, Augustus Oemler, and Robert P. Kirshner. The Environment of "E+A" Galaxies. ApJ, 466:104, July 1996.

[247] Yirui Zheng, Vivienne Wild, Natalia Lahén, Peter H. Johansson, David Law, John R. Weaver, and Noelia Jimenez. Comparison of stellar populations in simulated and real post-starburst galaxies in MaNGA. MNRAS, 498(1):1259–1277, October 2020.

[248] Rongpu Zhou, Biprateep Dey, Jeffrey A. Newman, Daniel J. Eisenstein, K. Dawson, S. Bailey, A. Berti, J. Guy, Ting-Wen Lan, H. Zou, J. Aguilar, S. Ahlen, Shadab Alam, D. Brooks, A. de la Macorra, A. Dey, G. Dhungana, K. Fanning, A. Font-Ribera, S. Gontcho A Gontcho, K. Honscheid, Mustapha Ishak, T. Kisner, A. Kovács, A. Kremin, M. Landriau, Michael E. Levi, C. Magneville, P. Martini, Aaron M. Meisner, R. Miquel, J. Moustakas, Adam D. Myers, Jundan Nie, N. Palanque-Delabrouille, W. J. Percival, C. Poppett, F. Prada, A. Raichoor, A. J. Ross, E. Schlafly, D. Schlegel, M. Schubnell, Gregory Tarlé, B. A. Weaver, R. H. Wechsler, Christophe Yèche, and

Zhimin Zhou. Target Selection and Validation of DESI Luminous Red Galaxies. *arXiv e-prints*, page arXiv:2208.08515, August 2022.

[249] Rongpu Zhou, Jeffrey A. Newman, Kyle S. Dawson, Daniel J. Eisenstein, David D. Brooks, Arjun Dey, Biprateep Dey, Yutong Duan, Sarah Eftekharzadeh, Enrique Gaztañaga, Robert Kehoe, Martin Landriau, Michael E. Levi, Timothy C. Licquia, Aaron M. Meisner, John Moustakas, Adam D. Myers, Nathalie Palanque-Delabrouille, Claire Poppett, Francisco Prada, Anand Raichoor, David J. Schlegel, Michael Schubnell, Ryan Staten, Gregory Tarlé, and Christophe Yèche. Preliminary Target Selection for the DESI Luminous Red Galaxy (LRG) Sample. *Research Notes of the American Astronomical Society*, 4(10):181, October 2020.

[250] Adi Zolotov, Avishai Dekel, Nir Mandelker, Dylan Tweed, Shigeki Inoue, Colin DeGraf, Daniel Ceverino, Joel R. Primack, Guillermo Barro, and Sandra M. Faber. Compaction and quenching of high-z galaxies in cosmological simulations: blue and red nuggets. MNRAS, 450(3):2327–2353, July 2015.

[251] Hu Zou, Xu Zhou, Xiaohui Fan, Tianmeng Zhang, Zhimin Zhou, Jundan Nie, Xiyan Peng, Ian McGreer, Linhua Jiang, Arjun Dey, Dongwei Fan, Boliang He, Zhaoji Jiang, Dustin Lang, Michael Lesser, Jun Ma, Shude Mao, David Schlegel, and Jiali Wang. Project Overview of the Beijing-Arizona Sky Survey. PASP, 129(976):064101, June 2017.